Title
Heterogeneous Catalytic Conversion of Biomass-Derived Platform Molecules to Fuels and Specialty Chemicals

Author
Rorrer, Julie

Publication Date
2019

Peer reviewed|Thesis/dissertation

Heterogeneous Catalytic Conversion of Biomass-Derived Platform Molecules to Fuels and Specialty Chemicals

By

Julie E. Rorrer

A dissertation submitted in partial satisfaction of the

requirements for the degree of

Doctor of Philosophy

in

Chemical Engineering

in the

Graduate Division

of the

University of California, Berkeley

Committee in charge:

Professor Alexis T. Bell, Chair
Professor F. Dean Toste
Professor Alexander Katz

Summer 2019

Heterogeneous Catalytic Conversion of Biomass-Derived Platform Molecules to Fuels and Specialty Chemicals

Julie E. Rorrer

Abstract

Heterogeneous Catalytic Conversion of Biomass-Derived Platform Molecules to Fuels and Specialty Chemicals

By
Julie E. Rorrer
Doctor of Philosophy in Chemical Engineering
University of California, Berkeley
Professor Alexis T. Bell, Chair

The increasing global consumption of petroleum-derived fuels and chemicals has resulted in rapid generation of atmospheric CO_2, the accumulation of which has adverse effects on the global climate. One strategy for lowering the overall emission of CO_2 from the combustion of petroleum-derived fuels and lubricants is to replace them with similar products derived from renewable sources. This approach has the potential to be both environmentally responsible and economical, particularly if policy changes incentivize the use of non-fossil energy resources in the future.

Biomass, such as agricultural waste, is a readily available source of renewable carbon for producing fuels and chemicals that does not compete with the demand for food. Efforts in biological fermentation of biomass-derived sugars via ABE fermentation have enabled the attainment of renewable butanol, acetone, and ethanol with the molar ratio of 6:3:1. These so-called platform molecules can be upgraded to produce higher carbon number fuels and chemicals using heterogeneous catalysts. This thesis is focused on developing an understanding of several heterogeneous catalytic pathways towards producing fuels and specialty chemicals from renewable platform molecules; specifically, acetone, ethanol, and other biomass-derived alcohols.

The first three chapters of this thesis are centered around understanding the etherification of biomass-derived alcohols and other platform molecules to produce ethers for use as fuels and lubricants. Ethers have attracted recent interest as diesel additives and specialty chemicals due to their high cetane numbers and excellent lubricant properties, and they can be produced via direct etherification of biomass-derived alcohols in the liquid phase. The competing reaction for alcohol dehydration over an acid catalyst is unimolecular dehydration to form alkenes, which is thermodynamically favored above approximately 350 K. To improve the activity and selectivity towards direct etherification of long chain alcohols in the liquid phase, it is necessary to develop an understanding of the mechanism and kinetics of etherification and dehydration reactions. In the first study of this dissertation, tungstated zirconia was identified as a selective solid acid catalyst for the liquid phase etherification of 1-dodecanol. Through kinetic modeling and mechanistic probing, this study suggested that a cooperative effect between Brønsted and Lewis acid sites on tungstated zirconia enhances the selectivity to ether by increasing the surface concentration of adsorbed alcohol molecules, promoting bi-molecular etherification over unimolecular dehydration. Kinetic isotope effects for linear alcohol dehydration were measured to elucidate the rate limiting steps in the mechanism. Effects of alcohol concentration and product inhibition were measured and fit to kinetic models consistent with the proposed mechanisms. In addition, acid site characterization and selective poisoning experiments were used to probe the role of the acid sites and support the proposed mechanism.

In the second study, the scope of alcohols for the synthesis of ethers via direct etherification over tungstated zirconia was expanded to include a variety of biomass-derived alcohols ranging from C_6-C_{24} with varying degrees of carbon chain branches and substitution. The effects of alcohol length, position of carbon chain branches, and length of carbon chain branches were studied for etherification and dehydration reactions. Trends in the effects of alcohol structure on selectivity were consistent with the proposed mechanisms for etherification and dehydration and elucidated possible pathways to selectively form ethers from biomass-derived alcohols. In the third chapter of this thesis, these studies of direct etherification were explored within in the greater context of the etherification literature. Tradeoffs between catalyst selectivity, activity, stability, and reaction conditions required to achieve the most economically and environmentally favorable routes to biomass-derived ethers were discussed with the goal of identifying the combination of catalyst properties required to achieve high ether selectivity for a specified class of synthons.

Continuing the investigation of the valorization of alcohols via heterogeneous catalysis, the next study focused on the valorization of ethanol through oxidation reactions over Ag, Au, and Cu nanoparticles on Li_2O/Al_2O_3. The interest in studying the oxidation of ethanol over arose from striking reports in the literature that identified Ag and Ag, Au, and Cu nanoparticles on Li_2O/Al_2O_3 as highly selective catalysts for the single-step conversion of ethanol to ethylene oxide, a valuable precursor for the synthesis of many polymers and specialty chemicals. Motivated by these reports, a systematic study of the effects of catalyst support, Li_2O loading, and various nanoparticle synthesis procedures was performed to provide an understanding of the unexpected selectivity reported in the literature. Systematic kinetic measurements and product characterization revealed that the primary product of this reaction is acetaldehyde, not ethylene oxide, and that errors in previous reports in the literature could be attributed to mis-identification of products with gas chromatography and mass spectrometry.

The last study in this thesis is centered around the valorization of bio-ethanol and acetone via conversion to isobutene. Isobutene is a valuable specialty chemical used in the production of fuel additives, polymers, and other high-value products. Isobutene is normally produced via steam cracking of petroleum naptha, thus the use of renewable platform molecules such as ethanol and acetone to synthesize isobutene has received increasing interest. Recent work in the literature has shown that zinc-zirconia mixed oxides selectively catalyze the production of isobutene from ethanol and acetone in the presence of water at 723 K. While this reaction is stable and selective, little is known about the mechanism, kinetics, and reaction pathway. In this study, a thorough investigation into the mechanism and kinetics of the acetone and ethanol conversion to isobutene was performed with the aim of elucidating the reaction pathway, the roles of active acidic and basic sites, and the role of water in promoting stability and selectivity. A reaction sequence for the conversion of ethanol to isobutene was proposed and supporting using a combination of catalyst synthesis, characterization, and kinetic measurements. The 5-step sequence starts with the dehydrogenation of ethanol to acetaldehyde, followed by oxidation to acetic acid, ketonization to acetone, and then dimerization to diacetone alcohol which then either undergoes decomposition or dehydration to mesityl oxide and subsequent hydrolysis to produce isobutene and acetic acid, which undergoes further ketonization to acetone. The dispersion of zinc oxide on zirconia was found to produce a balance between Lewis acidic and basic sites that promotes the cascade reactions of ethanol and acetone to isobutene.

Overall, this thesis brings together fundamental studies of the mechanisms and kinetics of these heterogeneous catalytic reactions to create a broader picture of the catalyst properties and reaction conditions necessary to enable the selective conversion of biomass-derived platform

molecules to fuels and specialty chemicals. Bifunctional catalysts with cooperative Brønsted and Lewis acid sites, as well as Lewis acid and base sites, have emerged as versatile systems to study C-O and C-C bond forming reactions. This thesis also demonstrates the versatility of the zirconia support and various promoters in producing catalytic materials with tunable acid and base properties, and thus tunable catalytic activity and selectivity. By providing extensive catalyst characterization as well as kinetic and mechanistic probing, this thesis elucidates the catalytic properties and reaction conditions that favor the effective production of fuels and specialty chemicals from renewable platform molecules, specifically concentrating on the synthesis of ethers and isobutene. While this thesis focuses on the fundamental understanding of these reactions, the insights gained are part of a larger effort by the scientific community to develop creative solutions to the growing global energy demands in the dawn of an era when continuing to burn fossil fuels is triggering devastating effects on the health of the planet and its inhabitants.

Table of Contents

List of Figures

List of Tables

List of Schemes

Acknowledgements

To do justice to how grateful I am for all the people who have helped me prepare this dissertation is a more insurmountable task than figuring out how to organize the mechanistic discussion of the multi-step cascade reaction presented in Chapter 6. Nevertheless, I will do my best to acknowledge many of the mentors, friends, and colleagues throughout my formative years that have brought me to this point.

First, I'd like to thank my advisers, Professor Alexis Bell and Professor Dean Toste, for their thoughtful guidance throughout this PhD. It only took me one short meeting with Professor Toste to know that he would be a great source of creativity and wisdom for developing a chemical intuition about the systems I would study. His enthusiasm for science and collaborative spirit inspire me to think outside the box and stay excited about my research. Professor Bell has been an incredible mentor. From day one, he treated me like a colleague in training, always with respect and with honest advice. It has been a pleasure to grow as a researcher with him and to learn how to tell science as a story, and it speaks to his character that he has graduated so many students over the years with diverse learning styles that have gone on to find success in their careers. I am truly lucky to have had two mentors that have been so supportive, and I take pride in the skills I have gained with their guidance.

Next, I'd like to thank the collaborators and colleagues that have helped me through the years. I thank Ying He and Suresh Pindi for their synthesis contributions to the etherification work, and for being thorough, timely, and responsive. I'd like to thank the rest of my co-workers at the Energy Biosciences Building: Kostas Goulas, who was not only a wonderful mentor to help me get started in the lab, but who has now become a lifelong friend; Lin Louie for asking me what types of acid sites were present on my catalyst, and for generally being such a positive force of energy in the first few years of my PhD; and Adam Grippo for holding the lab together and for keeping lab fun. I am also grateful to Alex Wang, George Arab, Deepak Jadhav, and Shylesh Pillai for being great lab-mates at EBI and to Amit Gokhale and Jessica Fahey for great discussion with BP. I thank rest of the brilliant chemists in the Toste group as well for their great discussions and for welcoming me onto the Toste Salad baseball team despite my being a chemical engineer. And I thank Germany for sharing Miriam Eulers with us during her master's degree. It was a pleasure to work with her and develop a friendship. I would also like to acknowledge the undergraduate students I have mentored over the years: Alan Liu, Francesca Tinga, and Jennifer Grannen.

After making the move to Tan Hall, I was yet again surrounded my incredible mentors and friends. I thank Chris Ho for helping me with everything under the sun, and under the hood of my GC, and for being such a good friend that we had to create a cardboard cutout of him after he left because we missed him so much. I thank Neelay Phadke for all his guidance getting started in Tan Hall and for his kind friendship. I thank Darinka Primc, Jeroen Van der Mynbrugge, Christianna Lininger, and Liang Qi for being excellent office and lab-mates, and I appreciate Paul Kim and Danna Nozik for always going with me to get coffee (even though they don't drink coffee) and for the excellent lab-related memes. I also gratefully acknowledge many other Bell choir members past and present: Gregory Johnson, Erum Mansoor, Philomena Weng, Lance Bettinson, Oyinkansola Romiluyi, Kun Jiang, Ezra Clark, Jaoquin Resasco, James Dombroski, Alice Yeh, and Rachel Licht. I thank Julie Fornaciari for becoming a close friend and for becoming a voice for the students in the department, and I thank Natalie Lefton and Branden Leonhardt for reminding me of the excitement of starting a PhD and for bringing fun into the lab. It is a tragedy that we didn't overlap at Berkeley longer.

I'd like to thank the Graduate Student Advisory Committee (GSAC) and the Department of Chemical Engineering at UC Berkeley. I thank Professor Alexander Katz for serving as my qualifying exam chair as well as on my thesis committee, and Enrique Iglesia, Wenjun Zhang, and Robert Bergman for serving on my qualifying exam committee. I am grateful for Carlet Altamirano, Kim Eastman, Jeff King, and all the other administrators in the department who work tirelessly so that we can focus on science. I also thank Colin Cerretani, Markita Landry, Esayas Kelkile, and Marjorie Went for helping me have a great Graduate Student Instructor experience.

I am grateful for mentorship throughout my undergraduate years that solidified my desire to pursue a PhD. I particularly thank Professor Candace Chan for being my undergraduate research advisor throughout my time at Arizona State University, Dr. Matthew Yung for introducing me to biofuel-related catalysis at NREL, Professor Erik Johansson for being my REU mentor at Portland State University, and Professor Christine Kelly at Oregon State University for introducing me to my first undergraduate research experience.

I couldn't have made it through this experience without the beautiful friendships I have developed with my classmates and roommates during my time at Berkeley. Thank you to Sudi Jawahery, Sondre Schnell, Kristen Colwell, Clay Batton, Jon Allen, and Danielle Devlin for being the best fellow inhabitants of the "Hearst Castle." Thank you to the Alligator House (Pete Dudenas, Parry Grewal, Matt Witman, Andrew Crothers, Rebecca Pinals, Sarah Berlinger, Tammy Hsu, and Constance Visser-Witman) for being honorary roommates and culinary buddies, and for being a community of people that make Berkeley feel like home. Thank you to the rest of the incoming class of 2014, especially Marc Martin-Casas, Eddy Zaia, Jamie Lincoff, Leslie Chan, Monica Neugebauer, Dogan Gidon, Lisa Burdette, and Nicolas Grosso-Giordano, for sharing this experience with me. I am honored to have been part of this inspiring and brilliant group of people who each have bright futures ahead of them.

I am fortunate to have made incredible friends at ASU who have been such a big part of my journey in chemical engineering. I thank Taylor Dolberg and Noelle Rabiah for being supportive and loving and for taking the plunge into the PhD with me, despite going to Northwestern and Stanford. I also thank Jacqueline Sanchez, Tyler Sherman, John Rabiah, Brendan Marozas, Kiri Olsen, and many others for their support in my college years. Thank you to Erin Shear and Carly DeMeo for being two of the best lifelong friends, and to Amanda Schupp, Kayla Reiman, Victoria Harkins, and all my other close friends who have shown me endless love and support. If I listed you all, these acknowledgements would be longer than this dissertation.

Berkeley has provided me with a rich local community during my PhD. I especially thank Community Resources for Science and the Bay Area Scientists in Schools (BASIS) program, as well as the Expanding Your Horizons (EYH) Program at UC Berkeley for the opportunity to engage in outreach. And I'd also like to thank all the scientists and artists who have contributed to and supported my outreach project ColorMePhD. I would be remiss not to thank Bangkok Thai on University, Monte Cristo Taqueria, and Berkeley Espresso for being there for me as well.

Finally, I'd like to thank my family. Thank you to my mom and dad, who introduced me to science. If it weren't for their support, advice, nurturing, and unconditional love, I wouldn't be here today. Thank you to my brother Chris, who knows my spirit better than any other and is a constant source of humor, music, and love. Thank you to Grandma and Grandpa Rorrer and the entire Barden family. I know that Grandma Mary and Grandpa Richard would be so proud of me, and I thank them for all their love while they were here with us. And, thank you to Kyle Diederichsen, for being the most supportive and loving partner. You have made this journey into an incredible experience and I couldn't imagine doing it without you.

The work in this dissertation was funded by the following sources: The Energy Biosciences Institute (EBI) funded by British Petroleum (BP), the National Science Foundation (NSF) Graduate Research Fellowship Program (GRFP), and the Lawrence Berkeley National Lab (LBNL) Chemical Sciences Division through the Director, Office of Science, Office of Basic Energy Sciences of the U.S. Department of Energy.

1. Introduction[†]

I. Motivation

Anthropogenic climate change is widely accepted as one of the greatest threats to the global population. The increasing consumption of fossil fuels has led to a vast buildup of atmospheric CO_2, which contributes to the greenhouse gas effect, thus warming the planet.[1] The increasing temperatures contribute to rising sea levels and coastal displacement,[2] food and water shortages,[3] species decline,[4] and numerous disruptions to the ecosystem that will have lasting devastating environmental, economic, political, and social effects. Combating climate change is a multifaceted effort that will require the implementation of clean energy technologies, policy changes,[5] and a shift in social attitudes regarding the severity of the situation. One method of lowering global CO_2 emissions is to replace petroleum-derived fuels and specialty chemicals with renewable alternatives.[6] While this is just one part of a greater effort to combat climate change, the market for petroleum-derived chemicals and transportation fuels is vast and continues to expand, necessitating efficient and cost-effective methods of meeting these demands. An attractive feedstock for producing sustainable fuels and specialty chemicals is lignocellulosic biomass, because it does not compete with food feedstocks and would otherwise be considered waste.[7]

There have been many recent developments in the production of fuels and specialty chemicals from biomass.[6,8–10] Recent investigations of ABE fermentation of biomass-derived glucose using *clostridium acetobutylicum* have shown that a mixture of butanol, acetone, and ethanol can be produced with the molar ratio of 6:3:1.[11,12] Various heterogeneous catalytic pathways involving condensation, reduction, acetalization, and dehydration have been identified for producing liquid fuels from biomass-derived platform chemicals.[10,13,14] Among the promising methods of utilizing biomass-derived platform molecules such as alcohols and ketones are the direct etherification of alcohols to produce ethers and the conversion of ethanol and acetone to isobutene, as shown in Scheme 1.1, which are the primary focus of this dissertation.

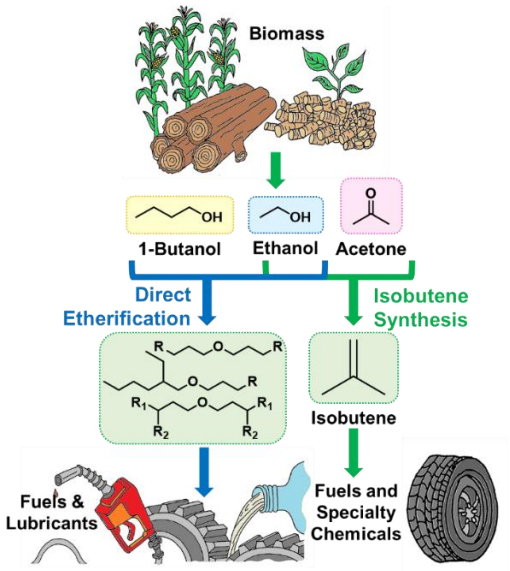

Scheme 1.1. Valorization of biomass-derived platform molecules acetone, butanol, and ethanol to produce ethers as fuels and lubricants as well as isobutene for the synthesis of fuels and specialty chemicals.

[†] Portions of this chapter were originally published in a Review in *ChemSusChem*.[233]

II. Synthesis of Ethers from Biomass-Derived Alcohols

Ethers have emerged as a class of molecules with excellent properties that can be used to meet the growing demands for gasoline additives,[15–18] cetane enhancers for diesel fuel,[19–21] automotive lubricants,[22,23] and other valuable products.[24–26] What makes ethers attractive for meeting these applications is that they can be produced from biomass-derived platform molecules with a minimum consumption of molecular hydrogen, unlike the synthesis of fuels from the hydrogenation of furan-containing condensation products or aldol condensation products derived from biomass. This latter characteristic is important since currently nearly all hydrogen is produced by steam reforming of methane, a process that produces a mole of fossil-based CO_2 per four moles of H_2. Ethers can be synthesized from the bimolecular dehydration of alcohols over an acid catalyst; but, under acidic conditions unimolecular dehydration to produce olefins can also occur. Understanding how to selectively produce ethers from biomass-derived alcohols requires an understanding of the mechanism and kinetics of etherification and dehydration reactions, as well as the catalyst properties and active sites required to promote selective etherification.

While unimolecular dehydration of small alcohols such as ethanol has been studied over solid acid catalysts in the gas phase, the etherification and dehydration of diesel and lubricant-range molecules in the liquid phase is not well understood. In this dissertation, a comprehensive investigation of the effect of alcohol structure on the mechanism and kinetics of liquid phase etherification and unimolecular dehydration reactions over tungstated zirconia was performed. In addition, studies of kinetic isotope effects and kinetic models were used to probe the rate limiting steps and the role of Lewis and Brønsted acid sites in the proposed mechanisms. The etherification studies presented in this dissertation provide an understanding of the mechanism, kinetics, and effect of alcohol structure on the liquid-phase etherification of long-chain biomass-derived alcohols, illuminating new routes to producing ethers suitable as fuels and lubricants.

III. Synthesis of Isobutene from Biomass-Derived Platform Molecules

Ethanol is an attractive biomass-derived platform molecule for the production of fuels and specialty chemicals such as 1,3-butadiene,[27–30] diethyl ether,[31] ethylene,[32] propene and other olefins,[33–35] and butanol.[36,37] Acetone is also a useful biomass-derived platform molecule for the synthesis of fuels and specialty chemicals such as methyl isobutyl ketone.[13,38,39] Acetic acid can be produced from biomass by fermentation by yeast, or from waste gases using *clostridium liungdahlii*,[40] and is thus also a useful platform molecule for various condensation and ketonization reactions to produce fuels and specialty chemicals.[41] Some valorization pathways for the upgrading of ethanol, acetone, and acetic acid are shown in Scheme 1.2.

One promising avenue for the valorization of bio-ethanol and acetone is the synthesis of isobutene. Isobutene is a valuable specialty chemical used in the production of fuel additives, polymers, and other high-value products. Reports in the literature have identified zinc-zirconium mixed oxides ($Zn_xZr_yO_z$) as effective and selective catalysts for the production of isobutene from ethanol at 723 K.[42,43] It has been proposed that the balanced acid/base properties of $Zn_xZr_yO_z$ are responsible for the selective conversion of ethanol to isobutene; however, there are many unanswered questions concerning the reaction pathway, mechanism, and roles of acid and base sites.

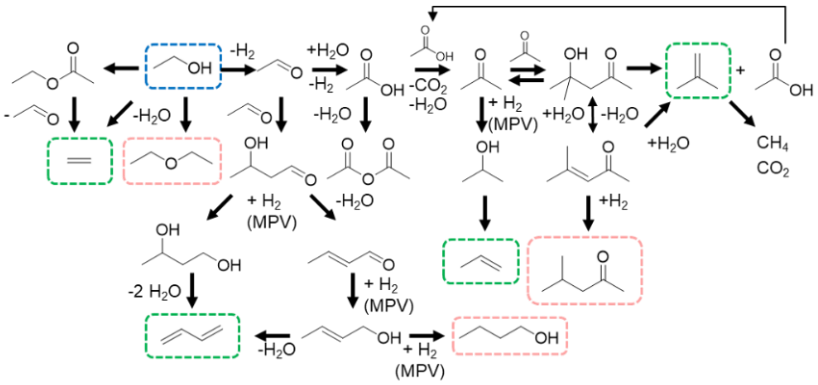

Scheme 1.2. Ethanol valorization pathways over metal oxide catalysts.

The addition of zinc oxide to the zirconia surface passivates strong acid sites and introduces basicity which suppresses the undesired unimolecular dehydration of ethanol to ethylene. But, it is unclear if the zirconia offers any role beyond providing a high surface area support. In addition, the role of water in this reaction pathway and mechanism is unclear. Understanding the role of water and the mechanism of catalyst deactivation in the absence of water is critical for maximizing catalyst activity and understanding the optimal feed conditions for this reaction. In this dissertation, the mechanism and kinetics of the acetone and ethanol to isobutene reactions were studied in order to elucidate the reaction pathway, the roles of active acidic and basic sites, and the role of water in promoting stability and selectivity. Understanding the reaction pathway, mechanism, and roles of the acidic and basic sites can help to define the catalyst properties required to selectively produce isobutene from a variety of sustainably-derived platform molecules such as ethanol, acetone, and acetic acid, enabling more effective production of renewable fuels and specialty chemicals.

IV. Outline of Dissertation

This dissertation examines the valorization of biomass-derived platform molecules via the etherification of alcohols, oxidation of ethanol, and the conversion of ethanol and acetone to isobutene. Chapters 2, 3, and 4 are centered around the synthesis of biomass-derived ethers. Chapter 2 begins by investigating the mechanism and kinetics of the etherification and unimolecular dehydration of 1-dodecanol over tungstated zirconia in the liquid phase. Building from the mechanistic studies in Chapter 2, Chapter 3 probes the mechanism and kinetics of the etherification and dehydration of a broader range of biomass-derived alcohols to elucidate the relationship between alcohol structure and reactivity and selectivity for etherification and dehydration over tungstated zirconia. In Chapter 4, the etherification of biomass-derived alcohols is examined in the greater context of the recent literature, identifying the tradeoffs between catalyst selectivity, activity, stability, and reaction conditions required to achieve the most economically and environmentally favorable routes to biomass-derived ethers. Chapter 5 presents a brief study of the oxidation of ethanol over alumina-supported catalysts with various promoters with the aim of clarifying discrepancies in selectivities reported in the literature. This dissertation closes with Chapter 6, an experimental study on the mechanism and kinetics of the conversion of ethanol and acetone to isobutene over zinc-zirconia mixed oxide catalysts. Overall, this work provides a deeper understanding of the valorization of biomass-derived platform molecules and how kinetic and mechanistic probing, characterization of acid and base sites, and the roles of zirconia and other supports can be tuned to promote high selectivity towards the desired products.

2. Mechanism and Kinetics of 1-Dodecanol Etherification over Tungstated Zirconia‡

I. Abstract

Growing interest in finding renewable alternatives to conventional fossil fuels and petroleum-derived specialty chemicals has motivated the investigation of biomass-derived alcohols to make ethers as diesel additives or lubricants. To optimize the direct etherification of long chain alcohols in the liquid phase, it is necessary to develop an understanding of the kinetics and mechanism of etherification and dehydration reactions. In this study, tungstated zirconia was identified as a selective solid-acid catalyst for the liquid-phase etherification of 1-dodecanol. Investigations of the mechanism and kinetics of this reaction suggest that cooperation between Brønsted- and Lewis-acid sites on tungstated zirconia enhances the selectivity to ether by increasing the surface concentration of adsorbed alcohol, thereby promoting bi-molecular ether formation relative to unimolecular alcohol dehydration. The suggested rate limiting step for etherification is the formation of a C-O bond between two adsorbed alcohol molecules, and the suggested rate-limiting step for dehydration is the cleavage of the C-H bond of the β-carbon atom in an adsorbed alcohol. Measurements of the kinetic isotope effects for etherification and dehydration support the proposed mechanism. A microkinetic model based on the proposed mechanism for 1-dodecanol etherification and dehydration over tungstated zirconia accurately describes the observed effects of alcohol concentration and product inhibition.

II. Introduction

Continued use of fossil energy resources to produce fuels contributes to an increase in atmospheric CO_2 and in turn to changes in the global climate.[1] This concern has motivated the exploration of biomass as a possible source of renewable carbon for the production of fuels and lubricants.[6] A central question is how to convert biomass into synthons that could be used to produce fuels and lubricants. One of the appealing approaches is to ferment the sugars derived by hydrolysis of cellulose and hemicellulose into alcohols such as ethanol and butanol. The condensation of furfural with acetone under hydrogen can also produce 1-octanol.[44] Other longer-chain alcohols such as 1-dodecanol can be produced by hydrolysis of triglycerides and fatty acids. These linear alcohols can also be converted to higher carbon-number alcohols with branched carbon chains via the Guerbet reaction, and the corresponding Guerbet alcohols can be converted to ethers.[45]

Ethers are attractive products because they can be used as diesel additives and automotive lubricant base oils. Diesel-range linear ethers produced from biomass are of interest because they have high cetane numbers as well as high energy density.[19,21,46,47] Shorter chain branched ethers have high octane numbers and can be added to gasoline.[16] Ethers are also of interest as lubricants. For example, alkylated di-phenyl ether and glyceryl ethers have excellent properties,[48,49] and branching in the alkyl portions of ethers lowers the pour points and raises the viscosity of the ether.[22,50] Therefore, ether-based lubricants sourced from biomass provide a stable, tunable, and renewable alternative to poly-alpha-olefins produced from petroleum.[51,52]

Ethers can be prepared either by direct, acid-catalyzed etherification of alcohols, or by reductive etherification of an alcohol and an aldehyde or ketone. Direct etherification of alcohols is advantageous because it does not require the use of hydrogen and precious metal catalysts for

‡ This chapter was originally published in the *Journal of Catalysis,* and is adapted with permission from co-author Y. He. [99]

reduction.[53] The competing reaction in the presence of an acid catalyst is alcohol dehydration to produce the corresponding alkene, a process that is favored thermodynamically at temperatures above approximately 350 K. Since higher temperatures are desirable for increasing reaction rates, this raises the question of how one can favor etherification over alkene formation.

Selective etherification has been reported for the liquid-phase reactions of 1-octanol, 1-hexanol, and 1-pentanol over acid catalysts such as Amberlyst 70,[54,55] Nafion NR-50,[55,56] and H-BEA zeolite.[57] While polymeric resins are selective to ether, they are not as thermally stable as metal oxides.[55,58] Zeolites, on the other hand, are thermally stable, but catalyze unwanted side products and deactivate due to coking.[59]

In this study, a series of solid-acid catalysts were screened for the direct etherification of 1-dodecanol and identified tungstated zirconia as a highly active and selective catalyst. Tungstated zirconia has been employed previously for acid-catalyzed reactions including gas-phase isomerization of n-butane,[60] gas-phase dehydration of alcohols to alkenes,[61] and liquid-phase reactions, such as esterification, transesterification, and alkylation.[61–63] Investigations of the gas-phase kinetics for the dehydration of short-chain, linear alcohols over tungstated zirconia indicate that dehydration occurs via a unimolecular mechanism but that these alcohols are not converted to ethers.[64,65] By contrast, we found that the etherification of dodecanol in the liquid phase is highly selective over tungstated zirconia. Motivated by this finding, we undertook an investigation of the mechanism and kinetics of the etherification and dehydration of 1-dodecanol over tungstated zirconia with the objective of developing an explanation for the high selectivity of this catalyst for etherification in the liquid phase.

III. Materials and Methods

i. Materials

All chemicals obtained commercially were used without further purification. The following compounds were obtained from Sigma-Aldrich: 1-hexanol (>98%), 1-dodecanol (>98%), decane (>95%), dodecane (>99%), hexane (>99%), 1-hexene (>99%), and pyridine (99.8%). N-tetradecane was obtained from Spectrum Chemical (>99%), and was used as an internal standard for analytical purposes. Di-dodecyl ether (>95%) and 1-dodecene (>95%) were obtained from TCI. Di-n-hexyl ether (>98%), and 2,6-di-tert-butyl-pyridine (97%) were obtained from Alpha Aesar. Hexan-1,1-d_2-1-ol (>99%) was obtained from CDN Isotopes Inc. Hexan-2,2-d_2-1-ol was synthesized and purified to >98% according to Ref.[66] Amberlyst 15 (hydrogen form, dry), and Amberlyst 36 were obtained from Sigma-Aldrich. Amberlyst 70 was obtained from Dow Chemical, and was dried at 368 K and stored in a desiccator before use. Zeolite BEA was obtained from Alpha Aesar, and was calcined at 873 K for 6 h before use. Gamma-alumina was obtained from Strem Chemicals. Mesostructured silica (MCM-41 hexagonal type), Nafion NR-50, and mesostructured aluminosilicate (MCM-41, hexagonal) were obtained from Sigma-Aldrich. Para-toluene sulfonic acid was obtained from Spectrum Chemical.

ii. Synthesis of Deuterated Substrate

2,2-D_2-hexan-1-ol was prepared according literature.[66] Methyl hexanoate (1.0g, 3.85 mmol) was dissolved in MeOH-*d*3 (10 mL) and sodium methoxide (0.324g, 6.0 mmol) was added. The mixture was heated under reflux for 1 hr, and then cooled to room temperature. Then the mixture was then combined with 30 mL of pentane and extracted with D_2O. The organic layer was dried over anhydrous Na_2SO_4 and the solvent was evaporated under reduced pressure. The

procedure was repeated twice to give 2,2-D_2-methyl hexanoate. 2,2-D_2-methyl hexanoate was then dissolved in Et_2O (15 mL). The mixture was added dropwise to a suspension of $LiAlH_4$ (250 mg, 6.25 mmol) in Et_2O (10 mL) at 0°C. The reaction mixture was warmed to room temperature and stirred for 2 hr. Workup provided 2,2-D_2-hexan-1-ol as a colorless oil. The product was purified by flash column chromatography when necessary.

iii. Synthesis of Zirconia and Tungstated Zirconia

Porous amorphous zirconia, monoclinic zirconia, and tungstated zirconia were synthesized using previously reported methods.[60,67,68] Amorphous zirconium oxyhydroxide ($ZrO_x(OH)_{4-2x}$) was formed by adding ammonium hydroxide (Spectrum, 28-30%) dropwise to a stirred solution of 0.5 M zirconyl chloride octahydrate (Sigma Aldrich, 98%) at 298 K. The precipitate was filtered and rinsed with 10% ammonium hydroxide and dried at 383 K for 24 h. Tungstated zirconia (4.1, 7.7, 10.2, 12.6, 15.4, 22.3 wt% W) was prepared via incipient wetness impregnation of amorphous zirconium oxyhydroxide with aqueous ammonium metatungstate hydrate (Spectrum). After impregnation, all catalysts were heated at 10 K/min and treated in air at 1073 K for 3 h, then cooled to room temperature. To prepare pure zirconia, amorphous zirconium oxyhydroxide was calcined at 1073 K under the same incipient wetness impregnation conditions but without the addition of ammonium metatungstate. Each catalyst was then crushed to < 250 micron mesh using a mortar and pestle.

iv. Catalyst Characterization

Powder X-ray diffraction (XRD) patterns for WO_x/ZrO_2 (0-22 wt% W) were taken with a Bruker D8 GADDS diffractometer equipped with a Cu−Kα source (40 kV, 40 mA). Raman spectra were obtained with a LabRAM HR Horiba Scientific Raman spectrometer equipped with a 633 nm^{-1} laser. BET surface area measurements were performed with a Micrometrics TriStar BET and pretreated with a Micrometrics FlowPrep 060. Brønsted- and Lewis-acid sites were identified and the ratio of these sites was determined from IR spectra of adsorbed pyridine. Spectra were acquired using a Thermo Scientific Nicolet 6700 Fourier Transform Infrared Spectrometer (FT-IR) equipped with a Diffuse Reflectance Infrared Fourier Transform Spectrometer (DRIFTS) cell. A mixture of catalyst (50 mg) diluted with KBr (250 mg) was added to the DRIFTS cell and pretreated at 573 K for 2 h under helium. Background scans of the catalyst were taken at 393 K, 423 K, 473 K, 523 K, and 573 K. Pyridine was introduced into the He flow at 393 K, and spectral data was taken after stabilization of adsorbed pyridine at 393 K. The temperature was then raised to measure the amount of pyridine that remained adsorbed at 423 K, 473 K, 523 K, and 573 K. Spectral intensities were calculated using the Kubelka-Munk function. The concentration of Brønsted-acid sites was determined by titration with NH_4OH. The protons on the catalysts were first exchanged for Na^+ cations by placing the catalyst in a 1M NaCl solution overnight, and then the solution was titrated with NH_4OH until the pH was neutral, using phenolphthalein as an indicator. The moles of base added was used as a metric for the number of H^+ ions in solution.[69] ICP Elemental analysis was performed by Galbraith Laboratories, Inc. in order to determine tungsten weight loadings.

v. Isotopic Labeling and NMR

Isotopic labeling of the alpha and beta hydrogen atoms in 1-hexanol was used to support the proposed mechanisms of etherification and dehydration. Hexan-2,2-d_2-1-ol was prepared

according to literature and the structure was confirmed using ^{1}H NMR.[66] Kinetic isotope effects (k_H/k_D) were determined by measuring the initial rates of alkene and ether formation for 1-hexanol, hexan-1,1-d_2-1-ol, and hexan-2,2-d_2-1-ol. NMR spectra of the reaction products were recorded with a Bruker AVQ-400 spectrometer.

vi. Batch Reactions

All reactions were carried out in sealed 12 mL Q-Tube batch reaction vessels with magnetic stirring at 600 RPM using an IKA C-MAG HS 10 digital hot plate with temperature control accurate to within +/- 1 K. For determination of the reaction kinetics, a separate batch reaction was carried out for each time point to insure consistency of volume and concentration of each sample. All reactions over tungstated zirconia were carried out either in the absence of solvent or in decane with 100 mg of catalyst and 250 µL of dodecanol (unless otherwise noted). N-tetradecane (100 µL) was added post-reaction as a standard for analysis. The reactants and catalyst were added to the Q-Tube in the pre-heated hot plate with an aluminum heating block, and after the specified reaction time, the vials were removed from the hot plate and placed in an ice bath to stop the reaction. Products were diluted with 5 mL of acetone then centrifuged at 4000 RPM for 8 min to remove the catalyst. A 200 µL aliquot of this solution was then diluted with another 1.3 mL of acetone and added to a GC vial for analysis with gas chromatography and mass spectroscopy.

vii. Product Analysis

Product analysis was carried out using a Varian CP-3800 Gas Chromatograph/Mass Spectrometer (GC/MS). The products were detected using a flame ionization detector (FID) to ensure high a signal to noise ratio and were identified using the Varian 320 triple quadrupole mass spectrometer (MS). N-tetradecane was used as an internal standard to ensure accurate product quantification. FID response factors were determined using commercially purified compounds. For all reactions, the main products observed were ether, alkenes, and water. At longer reaction times, trace amounts of branched ether and oligomerized olefins were detected but were considered to be negligible. Mass balances for all reactions were achieved to within ± 5%, with the assumption that one mole of water is formed for every mole of ether or alkene formed.

viii. Analysis of Reaction Kinetics

Initial rates of etherification and dehydration of 1-dodecanol were determined by measuring the initial rates of formation of ether and alkene. Individual batch reactions for each time point were carried out at each temperature over the temperature range of 388 – 403 K. Mass transfer limitations for linear alcohols were found to be negligible at 600 RPM for catalyst particle sizes less than 250 µm in diameter, as shown in Figure 2.1.

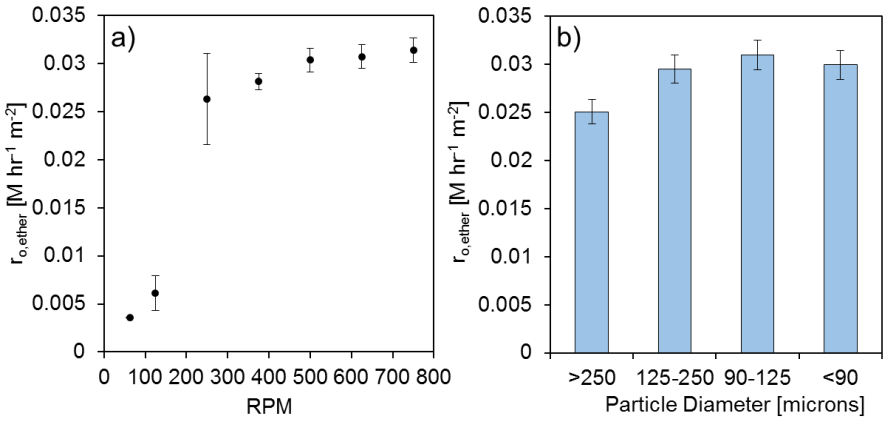

Figure 2.1. a) Initial rate of ether formation [M h^{-1} m^{-2}] with varying stir speeds for particles <250 microns in diameter, b) initial rate of ether formation [M h^{-1} m^{-2}] for varying particle diameters [microns] separated by mesh. Reaction conditions: 402 K, 100 mg WO_x/ZrO_2 (12.6 wt% W), 200 mg dodecanol, 73.5 mg n-tetradecane.

IV. Results and Discussion

i. Catalyst Selection

A number of solid-acid catalysts were screened for the liquid-phase etherification of 1-dodecanol because of their excellent stability and recoverability. Table 2.1 summarizes the results of these experiments, which were carried out at 393 K and low alcohol conversions (<15%), for which the inhibiting effects of products on catalytic activity and selectivity are negligible.[65] Amberlyst 70, Nafion NR-50, and WO_x/ZrO_2 (12.6 wt% W) exhibited the highest ether selectivities (97%, 98%, and 94%, respectively). Amberlyst 70 is a Brønsted-acidic styrene-divinylbenzene resin with a high density of sulfonic acid groups, and Nafion NR-50 has Brønsted-acidic sulfonic acid groups enhanced by an electron-withdrawing polyfluorocarbon backbone.[55,58] While Amberlyst 70 and Nafion NR-50 are highly selective to ether, they are unstable above 463 K.[55,58] The high thermal stability of tungstated zirconia is advantageous since the catalyst can be readily regenerated through re-calcination in air, eliminating the need for solvents such as toluene required for resin regeneration.[70] In addition, resins such as Nafion NR-50 are known to swell in the reaction medium, thereby introducing inconsistent mass transfer limitations due to variation in the number of accessible acid sites with time.[70] Because of its high activity, thermal stability, and selectivity, WO_x/ZrO_2 (12.6 wt% W) was selected for further investigation.

Table 2.1. Screening of acid catalysts for the etherification of 1-dodecanol to di-n-dodecyl ether.

Entry	Acid Catalyst	Dodecanol Conversion (%)	Sel. to Ether (%)	Sel. to Alkenes/ Other (%)
1	Zeolite Beta	5	61	39
2	Para-Toluene Sulfonic Acid	3	40	60
3	Amberlyst 15	4	46	54
4	Amberlyst 36	6	65	35
5	Amberlyst 70	11	97	3
6	Nafion NR-50	10	98	2
7	WO_x/ZrO_2 (12.6 wt% W)	14	94	6
8	ZrO_2, Amorphous	0	0	0
9	ZrO_2, Monoclinic	0	0	0
10	Gamma-Alumina	0	0	0
11	Mesostructured Silica	0	0	0
12	Mesostructured Aluminosilicate	0	0	0

Reaction Conditions: 393 K, 4 h, 600 RPM, 500 mg 1-dodecanol, 150 mg n-tetradecane as internal standard. Entry 1: $3.3*10^{-5}$ mol eq. H+ acid sites, entries 2-5: $1*10^{-4}$ mol eq. H+ acid sites, entry 6: 0.043 g. cat, entry 7: $9.1*10^{-6}$ mol eq. H+ sites, entries 8-12: 100 mg catalyst.

ii. Catalyst Characterization

Figure 2.2a and b show X-Ray Diffraction (XRD) and Raman spectra for different weight loadings of WO_x/ZrO_2. For low weight loadings of tungstated zirconia, the zirconia exists primarily in the monoclinic phase. From the XRD in Figure 2.2a, the 0 wt% W sample (i) has peaks at 2θ angles of 24, 28, 32, and 56°, which are characteristic of monoclinic zirconia.[63,67,71] These peaks can also be observed for the 4 wt% W sample (ii). As the weight loading increases, features for tetragonal zirconia become predominant, as evidenced by the XRD peaks at 2θ angles of approximately 30, 35, 50, and 59° for the 4-22 wt% catalysts.[67,71,72] The presence of tetragonal zirconia has been attributed to tungsten oxide inhibition of zirconia sintering and transformation to the monoclinic phase during calcination.[61,73] When the weight loading of tungsten oxide becomes high enough to completely cover the surface of the zirconia (v-vii), bulk tungsten oxide is formed, as evidenced by the presence of XRD peaks at 2θ angles between 23-25°.[74]

The Raman spectra for the catalysts are shown in Figure 2.2b. Spectrum (i) exhibits bands at 178-220, 307-379, and at 635 cm^{-1}, which confirm that the zirconia is monoclinic.[75] As the tungsten oxide weight loading increases, a small band appears at 1020 cm^{-1}. This band has been attributed to terminal W=O bonds, characteristic of oligomeric tungsten oxide species.[63] At weight loadings above 10.2 wt% W (spectrum (iv)), bands at 274, 715, and 807 cm^{-1} appear that are characteristic of the W-O bond stretches for bulk WO_3.[76] For the 12.6 wt% tungstated zirconia, it is estimated that the Lewis-acid sites on the surface are predominantly due to W because the exposed Zr has been covered.

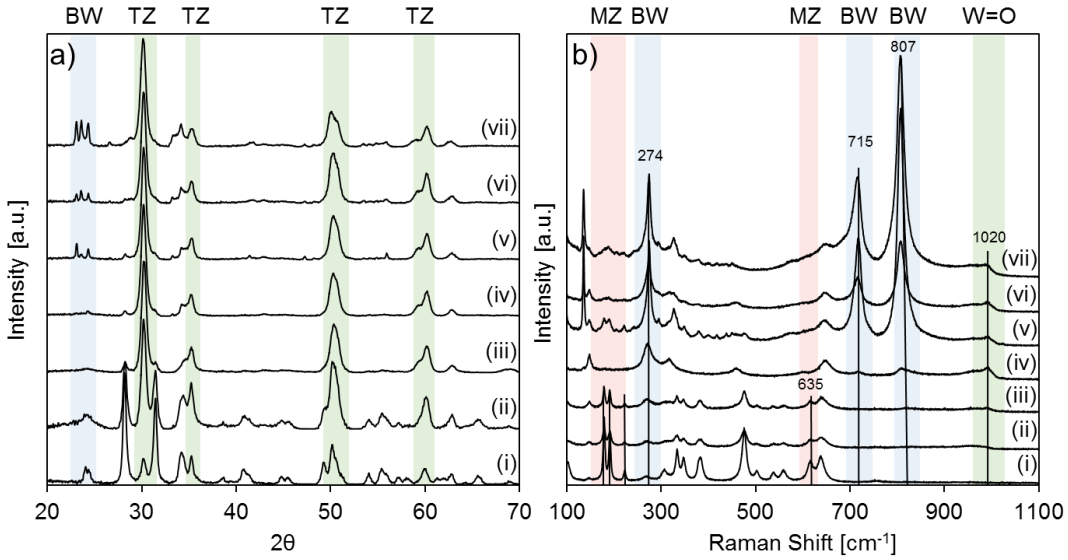

Figure 2.2. a) X-ray diffraction spectra of catalysts with tungsten weight loadings of i) 0% ii) 4.1%, iii) 7.7%, iv) 10.2%, v) 12.6%, vi) 15.4%, and vii) 22.3%. b) Raman spectra of catalysts with tungsten weight loadings of i) 0% ii) 4.1%, iii) 7.7%, iv) 10.2%, v) 12.6%, vi) 15.4%, and vii) 22.3%. Abbreviations: monoclinic zirconia (MZ), bulk WO_3 (BW), tetragonal zirconia (TZ).

Figure 2.3a shows the relationship between W weight loading and Brønsted-acid site density. The surface concentration of Brønsted-acid sites rises to a maximum at about 12.6 wt% and then declines. This pattern is very similar to previously reported studies, in which the appearance of a maximum in the surface concentration of Brønsted-acid sites at a tungsten weight

loading of 12.6 wt% was attributed to the formation of a polytungstate monolayer.[65,68,77] Figure 2.3b demonstrates that the surface area also reaches a maximum at a tungsten weight loading of 12.6%. This effect is attributed to the fact that the addition of tungsten oxide inhibits the sintering of zirconia to the denser monoclinic phase, resulting in a higher surface area.[78,79] However, once the monolayer of polymeric tungsten oxide is exceeded, the formation of bulk WO_3 increases the mass of the catalyst but does not provide any additional active surface area, and is thus responsible for the decrease in surface area per mass of catalyst for the 15 and 22% W catalysts. The BET surface area, the concentration of Brønsted-acid sites, and the ratio of Brønsted- to Lewis-acid sites as functions of W weight loading are given in Table 2.2. The DRIFTS spectra of adsorbed pyridine used to determine the ratio of Brønsted- to Lewis-acid sites on the 4-22 wt% catalysts are provided in Figure 2.4.

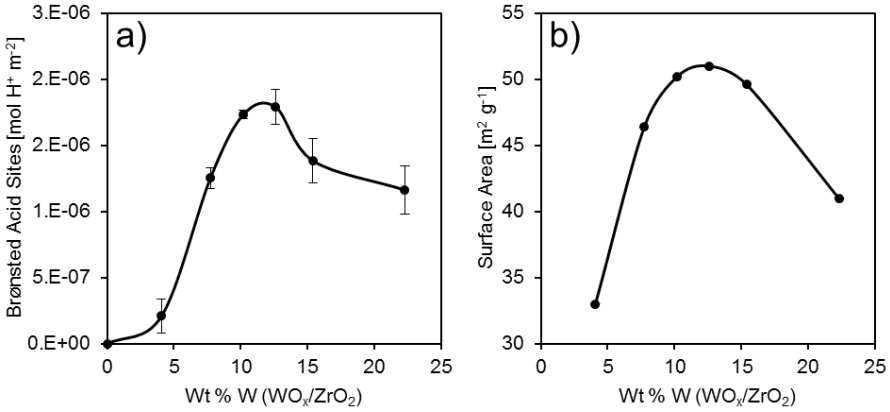

Figure 2.3. a) Brønsted-acid site density [mol H^+ m^{-2}] versus W weight loading [%], b) Surface area [m^2 g^{-1}] versus W weight loading.

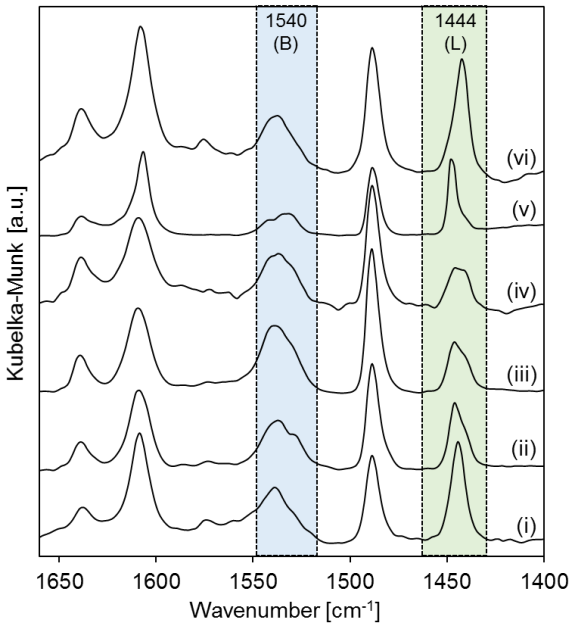

Figure 2.4. a) DRIFTS spectra for the adsorption of pyridine at 393 K onto Brønsted (B) and Lewis (L) acid sites of tungstated zirconia with W weight loadings of i) 4.1%, ii) 7.7%, iii) 10.2%, iv) 12.6%, v) 15.4%, and vi) 22.3%. Intensities normalized by the Kubelka-Munk function. Brønsted- to Lewis-acid site ratios calculated using extinction coefficients from Emeis.

Table 2.2. Characterization of 4-22 wt% W/ WO_x/ZrO_2.

Weight loading of W (wt% W, WO_x/ZrO_2)	BET Surface Area ($m^2\ g^{-1}$)	Brønsted Acid Sites (mol eq. $H^+\ m^{-2}$)	Ratio of Brønsted / Lewis Acid Sites (393 K)
4.1	33	$2.09*10^{-7} \pm 1.2*10^{-7}$	0.33 ± 0.01
7.7	46	$1.26*10^{-7} \pm 6.5*10^{-8}$	0.57 ± 0.24
10.2	50	$1.74*10^{-6} \pm 4.0*10^{-8}$	0.92 ± 0.05
12.6	51	$1.78*10^{-6} \pm 1.4*10^{-7}$	0.90 ± 0.02
15.4	50	$1.38*10^{-6} \pm 1.6*10^{-7}$	0.30 ± 0.11
22.3	41	$1.17*10^{-6} \pm 1.7*10^{-7}$	0.28 ± 0.04

The surface concentrations of active Brønsted- and Lewis-acid sites can be determined by poisoning them with a strongly bound adsorbate. DRIFTS spectra of adsorbed pyridine were obtained and used to determine the ratio of Brønsted- to Lewis-acid sites for the 4-22 wt% catalysts. As observed in Figure 2.4, bands at 1609 and 1444 cm^{-1} indicate the presence of Lewis-acid sites, and bands at 1639 and 1540 cm^{-1} indicate the presence of Brønsted acid sites upon addition of pyridine.[67,80] Extinction coefficients published by Emeis were used to determine the ratio of Brønsted- to Lewis-acid sites from the intensities of the bands at 1444 cm^{-1} and 1540 cm^{-1}.[81] As shown in Table 2.2, the ratio of Brønsted- to Lewis-acid sites increases with increasing weight loading of W until 12.6 wt%, beyond which the ratio decreases. Below 12.6 wt% W the Lewis-acid sites come from both tungsten and zirconia, but above 12.6 wt% W the Lewis-acid sites are predominately from tungsten. The decrease in the ratio of Brønsted- to Lewis-acid sites above 12.6 wt% is attributed to the formation of bulk tungsten oxide, as suggested by the structural characterization.

Pyridine poisons both Brønsted- and Lewis-acid sites, whereas 2,6-di-tert-butyl pyridine, a hindered base, will only poison Brønsted-acid sites.[82] Figure 2.5 shows the diffuse reflectance infrared spectra for 2,6-di-tert-butyl pyridine adsorbed on the 12.6 wt% W catalyst. The spectrum of adsorbed pyridine in Figure 2.5a exhibits bands at 1540 cm^{-1} and 1444 cm^{-1}, attributable to pyridine interacting with Brønsted- and Lewis-acid sites, respectively. By contrast, the spectrum for adsorbed 2,6-di-tert-butyl pyridine, shown in Figure 2.5b, only exhibits a band at 1540 cm^{-1} for pyridine adsorption onto Brønsted-acid sites, but the band at 1444 cm^{-1} for pyridine adsorption onto Lewis-acid sites is absent.

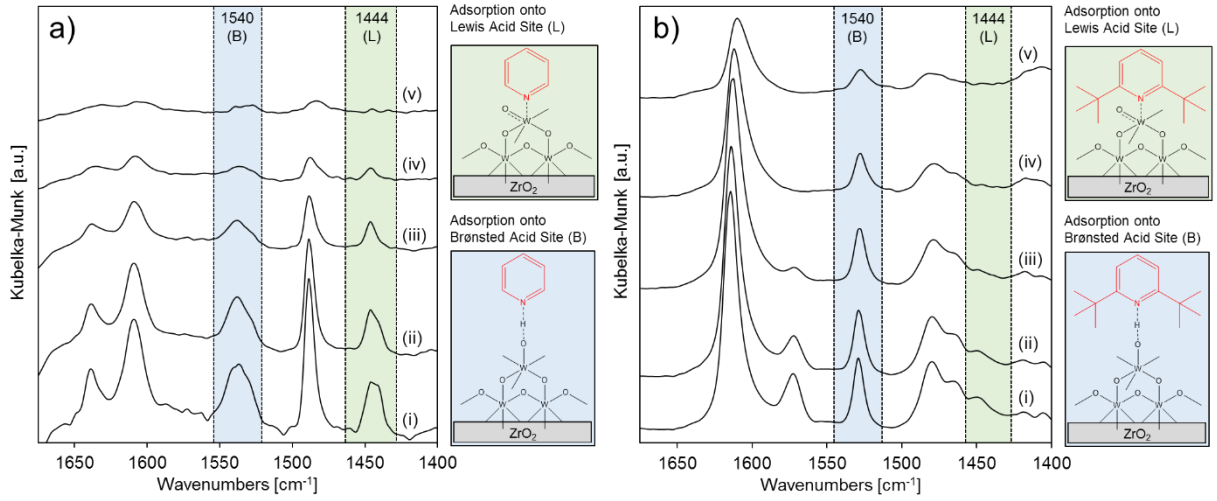

Figure 2.5. a) DRIFTS spectra for the adsorption of pyridine onto WO_x/ZrO_2 (12.6 wt% W) at i) 393 K, ii) 423 K, iii) 473 K, iv) 523 K, and v) 573 K. b) DRIFTS spectra for the adsorption of 2,6-di-tert-butyl-pyridine onto WO_x/ZrO_2 (12.6 wt% W) at i) 393 K, ii) 423 K, iii) 473 K, iv) 523 K, and v) 573 K. Intensities normalized by the Kubelka-Munk function.

iii. Mechanisms and Kinetics of Dodecanol Etherification and Dehydration

A number of mechanisms have been proposed to explain the etherification and dehydration of alcohols over heterogeneous acid catalysts; these include dual-site Langmuir-Hinshelwood type mechanisms, Eley-Rideal type mechanisms with only one adsorbed alcohol, and mechanisms with more complex dimers and trimers of adsorbed reactants and products. Cunill et al. have proposed a modified Eley-Rideal model for the Brønsted-acid catalyzed liquid-phase etherification of 1-hexanol over Amberlyst 70 in which water remains adsorbed on the catalyst surface and, therefore, competes with the alcohol for acid sites.[54] The Bhan group has proposed that the gas-phase etherification of ethanol over the Lewis-acidic γ-Al_2O_3 is inhibited by alcohol-water dimers on the catalyst surface.[32] Iglesia and coworkers have proposed that the gas-phase dehydration of ethanol over polyoxometalates involves adsorbed dimer and trimer species.[83] In the case of tungstated zirconia, different authors have claimed that the active centers for alcohol dehydration are Lewis- or Brønsted-acid sites. Larsen et al. have proposed that the dehydration of 1-propanol, 2-propanol, and tert-butanol over tungstated zirconia proceeds solely over Lewis-acid sites,[64] whereas Iglesia and coworkers have proposed that 2-butanol dehydration occurs only over Brønsted-acid sites.[65] Theoretical and experimental evidence for synergistic effects between Lewis- and Brønsted-acid sites have also been suggested for metal oxide catalysis in the etherification of glycerol and other biomass-derived alcohols.[84,85] As discussed below, we propose that the mechanism for liquid-phase dodecanol etherification over tungstated zirconia that is most consistent with the kinetics reported here involves both Brønsted- and Lewis-acid sites and that the mechanism of dodecanol dehydration involves only Brønsted-acid sites.

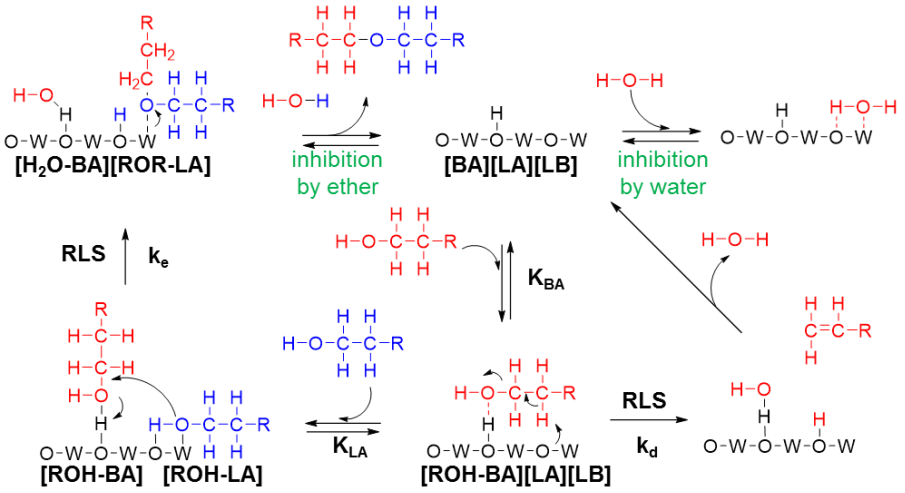

Scheme 2.1. Proposed mechanism for liquid phase primary linear alcohol etherification and unimolecular dehydration over tungstated zirconia.

The proposed mechanisms for etherification and dehydration of dodecanol over tungstated zirconia are shown in Scheme 2.1. We envision that the first step for both etherification and dehydration is the reversible adsorption of the alcohol onto a Brønsted-acid site. While the alcohol in Scheme 2.1 is shown as molecularly adsorbed, it is possible that it may adsorb dissociatively to form alkoxide species and adsorbed water;[32,86] however, the differentiation between associative and dissociative adsorption was not considered in the present study. For etherification, the second alcohol molecule is assumed to adsorb onto an adjacent Lewis-acid site, and the rate-limiting step (RLS) is taken to be the reaction of the two adsorbed species to form adsorbed water and ether,

which then desorb in the final step. The rate-limiting step for dehydration is the reaction of an alcohol molecule adsorbed at a Brønsted-acid site with a vacant basic site adjacent to the Brønsted-acid site, resulting in the abstraction of a hydrogen atom from the β-carbon of the adsorbed alcohol. The final step in the dehydration pathway is the desorption of water. As will be discussed below, ether and water can inhibit the rates of dodecanol etherification and dehydration.

To identify the rate-limiting steps for the liquid-phase etherification and dehydration of dodecanol, experiments were carried out using deuterium-labeled alcohols. The catalyst for these experiments was WO_x/ZrO_2 (12.6 wt% W). NMR was used to identify which H(D) atoms are involved in each reaction. Dehydration and etherification reactions of deuterium-labeled 1-hexanol (hexan-1,1-d_2-1-ol and hexan-2,2-d_2-1-ol) were used to probe the movement of hydrogen atoms on the α and β carbons of the alcohol. ^{1}H NMR of the ether and alkene products of the hexan-2,2-d_2-1-ol reaction showed no evidence of hydrogen on the β-carbon of the alkene, and no hydrogen present on either of the β-carbons of the ether. These results indicate that the hydrogens on the β-carbon are not involved in etherification but are involved in the irreversible dehydration step. Also, the ^{1}H NMR of the products from the reaction of hexan-1,1-d_2-1-ol showed no change in the position of deuterium atoms on the α-carbon. In both deuterated alcohols, the lack of D/H scrambling indicates that etherification and dehydration are irreversible under the conditions of the experiment. The NMR spectra are provided in Figure 2.12 - Figure 2.17 in the Supporting Information section.

Measurement of kinetic isotope effects was used to confirm that the rate-limiting step for 1-hexanol dehydration is cleavage of the β-carbon C-H bond. Table 2.3 shows that there is a kinetic isotope effect for unimolecular dehydration of hexan-2,2-d_2-1-ol to form hexene (k_H/k_D = 1.64 ± 0.09), but there is no kinetic isotope effect for bimolecular etherification to form di-hexyl ether (k_H/k_D = 1.03 ± 0.08), confirming that the rate limiting step for alkene formation is β-carbon hydrogen bond cleavage. No kinetic isotope effect was observed for etherification or unimolecular dehydration reactions over hexan-1,1-d_2-ol, confirming that the α carbon-hydrogen bond is not involved in the rate limiting step. Therefore, the rate limiting step for etherification must involve either formation of the C-O bond or desorption of the ether from the acid site. This finding is in agreement with the results of the Bhan group, who used kinetic isotope effects to confirm that the β-carbon hydrogen bond cleavage was the rate limiting step for unimolecular dehydration of propanol over γ-Al_2O_3.[31]

Table 2.3. Measured kinetic isotope effects for hexene and di-n-hexyl ether synthesis at 418 K for the dehydration of hexan-1,1-d_2-1-ol and hexan-2,2-d_2-1-ol.

Product	Reactant	
	hexan-1,1-d_2-1-ol	hexan-2,2-d_2-1-ol
Di-n-Hexyl Ether KIE (k_H/k_D)	1.00 ± 0.09	1.03 ± 0.08
Hexene KIE (k_H/k_D)	1.01 ± 0.09	1.64 ± 0.09

The kinetics of dodecanol etherification and dehydration based on Scheme 2.1 involve the equilibrium adsorption of alcohol on Brønsted- and Lewis-acid sites and the rates of the reactions leading to alcohol etherification and dehydration. These relationships are given by Equations 2.1-2.4:

$$[ROH] + [BA] \overset{K_{BA}}{\longleftrightarrow} [ROH - BA] \quad 2.1$$

$$[ROH] + [LA] \overset{K_{LA}}{\longleftrightarrow} [ROH - LA] \quad 2.2$$

$$r_e = k_e[ROH - LA][ROH - BA] \quad 2.3$$

$$r_d = k_d[ROH - BA][LB] \quad 2.4$$

Substitution of Equations 2.1 and 2.22 into Equations 2.3 and 2.4 gives:

$$r_e = k_e K_{LA} K_{BA}[ROH]^2[LA][BA] \quad 2.5$$

$$r_d = k_d K_{BA}[ROH][BA][LB] \quad 2.6$$

The overall rates of etherification and dehydration based on this set of elementary steps and site balances on the Brønsted-acid sites [BA], Lewis-acid sites [LA], and Lewis-base sites [LB] are given by the following expressions (see Supporting Information for the derivation of these expressions):

$$r_e = \frac{k_e K_{LA} K_{BA}[ROH]^2}{(1 + K_{BA}[ROH] + K_{ROR-BA}[ROR] + K_{H2O-BA}[H_2O])(1 + K_{LA}[ROH] + K_{ROR-LA}[ROR] + K_{H2O-LA}[H_2O])} \quad 2.7$$

$$r_d = \frac{k_d K_{BA}[ROH]}{(1 + K_{BA}[ROH] + K_{ROR-BA}[ROR] + K_{H2O-BA}[H_2O])(1 + K_{LB}[ROH] + K_{ROR-LB}[ROR] + K_{H2O-LB}[H_2O])} \quad 2.8$$

In Equations 2.7 and 2.8, k_e is the rate coefficient for the rate-limiting step of etherification, K_{LA} is the equilibrium constant for adsorption of an alcohol onto a Lewis-acid site, K_{BA} is the equilibrium constant for adsorption of an alcohol onto a Brønsted-acid site, $K_{ROR\text{-}BA}$ is the equilibrium constant for ether adsorption onto a Brønsted-acid site, $K_{H2O\text{-}BA}$ is the equilibrium constant for water adsorption onto a Brønsted-acid site, $K_{ROR\text{-}LA}$ is the equilibrium constant for ether adsorption onto a Lewis-acid site, $K_{H2O\text{-}LA}$ is the equilibrium constant for water adsorption onto a Lewis-acid site, k_d is the rate constant for the rate-limiting step of dehydration, K_{LB} is the equilibrium constant for adsorption of an alcohol onto a basic site, $K_{ROR\text{-}LB}$ is the equilibrium constant for adsorption of an ether onto a basic site, and $K_{H2O\text{-}LB}$ is the equilibrium constant for adsorption of water onto a basic site. For low conversions where [ROR] and [H_2O] are negligible, and with the assumption that the Brønsted-acid sites are saturated with reactant ($K_{BA}[ROR] >> 1$), Equations 2.7 and 2.8 simplify to:

$$r_e = \frac{k_e K_{LA}[ROH]}{1 + K_{LA}[ROH]} \quad 2.9$$

$$r_d = \frac{k_d}{1 + K_{LB}[ROH]} \quad 2.10$$

iv. Rates of Dodecanol Etherification and Dehydration

The effect of alcohol concentration on the initial rates of etherification and dehydration was determined by measuring the initial rates of di-dodecyl ether and dodecene formation at varying initial concentrations of dodecanol in decane over a temperature range of 388-403 K, and

the results are shown in Figure 2.6. The solid curves in these figures represent a fit to the data by Equations 2.9 and 2.10. The rate coefficients and equilibrium constants required to achieve these fits are given in Table 2.4. It is clear from Figure 2.6a and b, and from the parity plots shown in Figure 2.6c and d, that there is good agreement between the predicted and observed rates for ether and alkene formation for temperatures between 388 and 403 K.

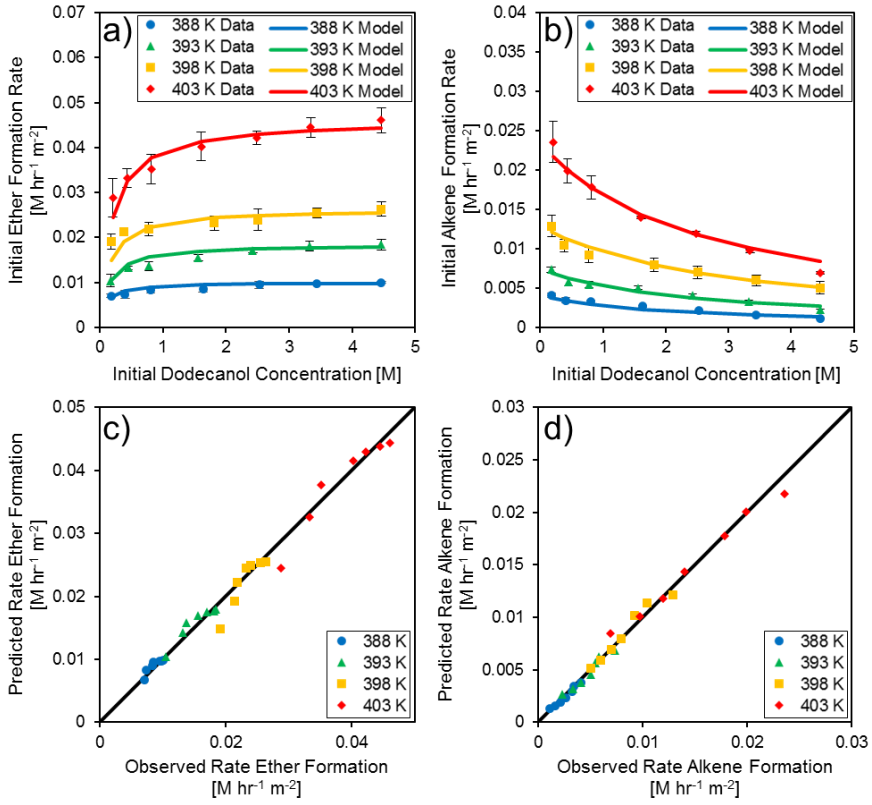

Figure 2.6. a) Effect of initial dodecanol concentration in decane [M] on initial rates of di-dodecyl ether formation [M h^{-1} m^{-2}], b) Effect of initial dodecanol concentration in decane [M] on initial rates of dodecene formation [M h^{-1} m^{-2}] for reactions from 388-403 K with 100 mg WO_x/ZrO_2 (12.6 wt% W) and a reaction volume of $2.4*10^4$ L. c) Parity plot for ether formation, d) Parity plot for alkene formation.

The rate coefficients and equilibrium constants k_e, k_d, K_{LA}, and K_{LB} and the respective activation energies and enthalpies of adsorption were determined from Arrhenius and Van't Hoff plots, as shown in Figure 2.7, and the values of these parameters are given in Table 2.1. The apparent activation energy for etherification (128 kJ mol^{-1}), is significantly lower than the activation energy for unimolecular dehydration (152 kJ mol^{-1}). The value of the apparent activation energy for etherification lies in the range of values reported for liquid-phase etherification of 1-hexanol and 1-octanol over other solid acid catalysts such as H-BEA, Amberlyst 70, and Nafion NR-50, which range from 118-150 kJ mol^{-1}.[54,56,57] The unimolecular dehydration activation barrier also falls within the range of values reported for the dehydration of linear alcohols over solid acids such as TiO_2, ZrO_2, and γ-Al_2O_3, which range from 141-171 kJ mol^{-1}.[87,88] The relatively high activation barrier for unimolecular dehydration compared to etherification observed in this study over tungstated zirconia explains the higher selectivity to ether in the liquid phase than the gas phase.

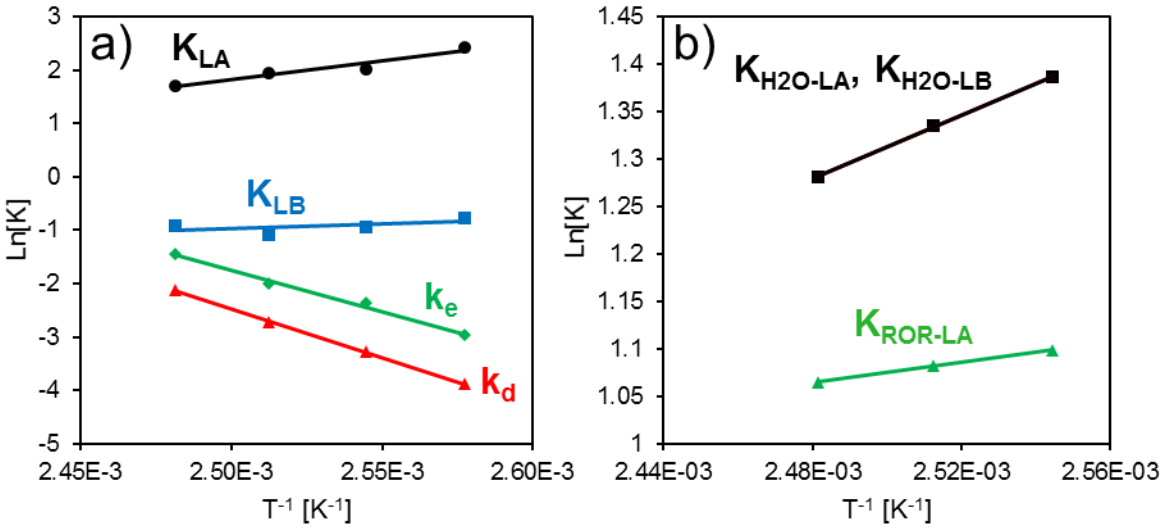

Figure 2.7. Arrhenius and Van't Hoff plots for k_e, k_d, K_{LA}, K_{LB}, K_{H2O-LA}, K_{H2O-LB}, and K_{ROR-LA} used to obtain activation energies and adsorption enthalpies obtained from model fitting.

Table 2.4. Kinetic Parameters.

Temperature [K]	k_e [M h^{-1} m^{-2}]	k_d [M h^{-1} m^{-2}]	K_{LA} [M^{-1}]	K_{LB} [M^{-1}]
388	0.010	0.004	11.5	0.459
393	0.018	0.007	7.50	0.391
398	0.026	0.013	7.06	0.341
403	0.046	0.024	5.53	0.400
E_a [kJ mol^{-1}]	128 ± 8	152 ± 2		
ln[A] [M h^{-1} m^{-2}]	35 ± 3	42 ± 1		
ΔH_{ads} [kJ mol^{-1}]			-59 ± 12	-15 ± 14
ΔS [J mol^{-1} K^{-1}]			-132 ± 31	-44 ± 35

v. Inhibition of Dodecanol Etherification and Dehydration by Water and Ether

Water has been shown to inhibit Brønsted-acid sites during the liquid-phase etherification of 1-hexanol over Amberlyst 70,[54] and it is reasonable to expect that ether may have a similar inhibitory effect. To assess the influence of water and ether on the rates of etherification and dehydration of dodecanol, the initial rates of ether and alkene formation were measured at 393 K with varying initial concentrations of water and ether added to the reactor. To distinguish between ether added initially and ether formed, di-decyl ether was used for ether inhibition experiments instead of di-dodecyl ether. The results indicate that water inhibits both ether and alkene formation, while the di-decyl ether only inhibits ether formation and not dehydration, as demonstrated by Figure 2.8.

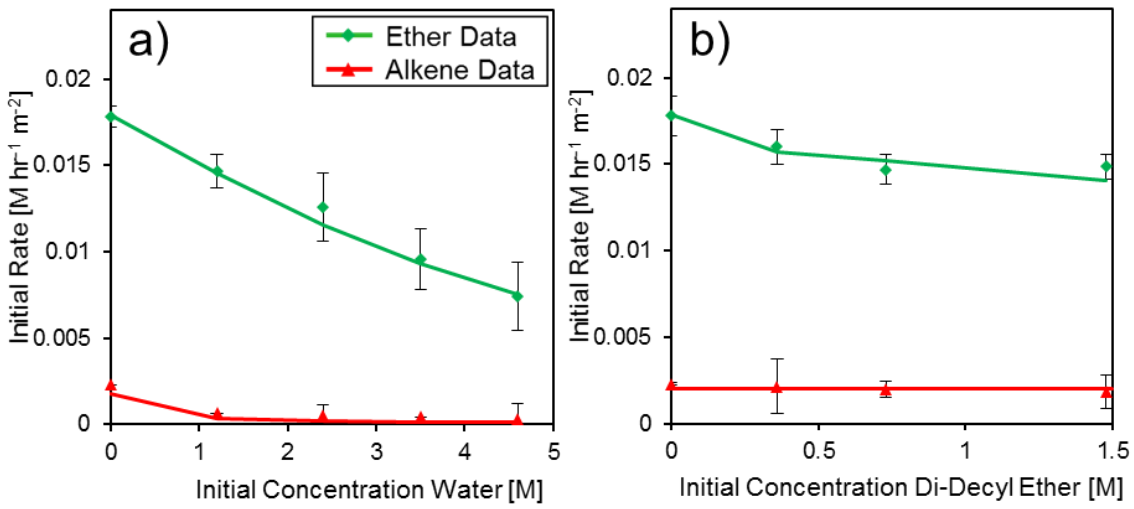

Figure 2.8. a) Initial rates of ether (diamond), and alkene (triangle) formation [M h^{-1} m^{-2}] as a function of initial water concentration [M], b) Initial rates of ether (diamond), and alkene (triangle) formation [M h^{-1} m^{-2}] as a function of initial di-decyl-ether concentration [M]. Reaction conditions: 100 mg WO_x/ZrO_2 (12.6 wt% W), 393 K.

With the assumption that saturation of Brønsted-acid sites is unaffected by the presence of water and ether, but ether and water inhibit adsorption on Lewis-acid and base sites, the rate expressions for etherification and dehydration now become:

$$r_e = \frac{k_e K_{LA}[ROH]}{(1 + K_{LA}[ROH] + K_{ROR-LA}[ROR] + K_{H2O-LA}[H_2O])} \quad 2.11$$

$$r_d = \frac{k_d}{(1 + K_{LB}[ROH] + K_{ROR-LB}[ROR] + K_{H2O-LB}[H_2O])} \quad 2.12$$

The values of the rate coefficients and equilibrium constants appearing in Equations 2.11 and 2.12, k_e, k_d, K_{LA}, and K_{LB}, were fixed at the values given in Table 2.4 and the equilibrium constants K_{ROR-LA}, K_{H2O-LA}, K_{ROR-LB}, and K_{H2O-LB} were then fitted to the data using the following constraints: First, the value of K_{ROR-LB} was taken to be approximately equal to 0 based on ether-inhibition experiments indicating that ether only inhibits the rate of etherification. Second, when considering acid site balances over both Lewis-acid sites and Lewis-base sites, it was assumed that water adsorbs onto an acid-base pair; therefore, K_{H2O-LA} must be equal to K_{H2O-LB}. Finally, inhibition studies suggested that water has a greater inhibiting effect on both reactions, implying that $K_{ROR-LA} < K_{H2O-LA}$ and K_{H2O-LB}. Using these constraints, data for the complete conversion of pure dodecanol at 393 K, 398 K, and 403 K was used to estimate values for K_{ROR-LA}, K_{H2O-LA}, and K_{H2O-LB}. The experimental curves for concentration of reactants and products versus time and the fits of the model to these data are shown in Figure 2.9. The equilibrium constants and adsorption energies obtained in this manner are shown in Table 2.5.

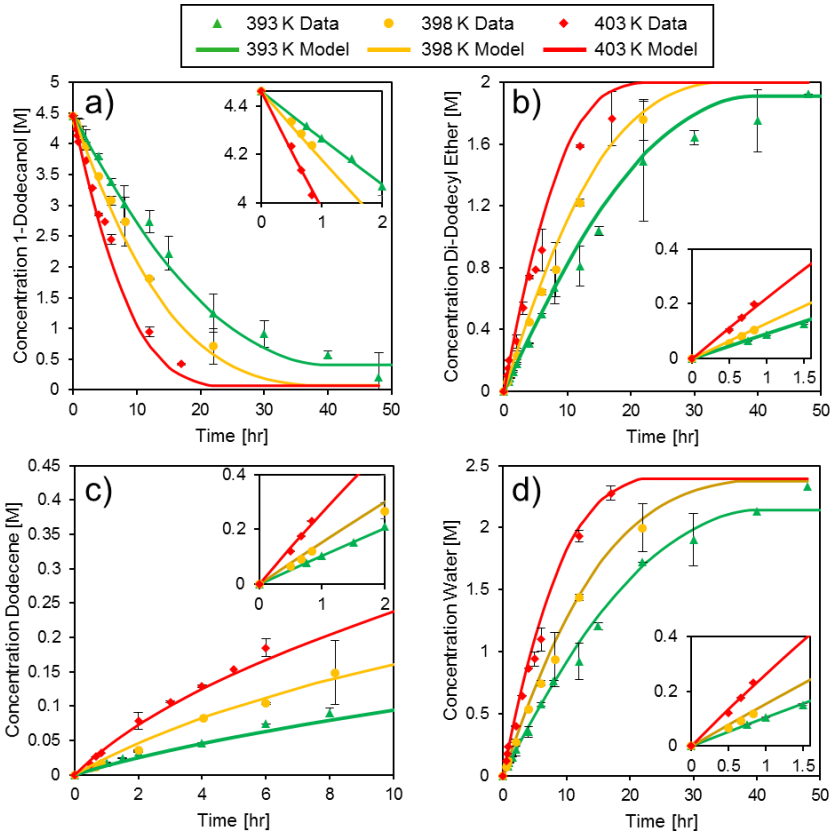

Figure 2.9. Concentration [M] versus time [hr] for experimental data and model from 393 K – 403 K for a) 1-dodecanol, b) di-dodecyl ether, c) dodecene, and d) water over WO_x/ZrO_2 (12.6 wt% W). Linear portions of the time-course curves for low conversions are shown in the insets.

Table 2.5. Kinetic Parameters for Water and Ether Inhibition.

Temperature [K]	$K_{ROR\text{-}LA}$ [M^{-1}]	$K_{H2O\text{-}LA}$ [M^{-1}]	$K_{H2O\text{-}LB}$ [M^{-1}]
393	3	4	4
398	2.95	3.8	3.8
403	2.9	3.6	3.6
ΔH [kJ mol^{-1}]	-4	-14	-14
ΔS [J mol^{-1} K^{-1}]	-2.2 ± 0.14	-44 ± 35	-24 ± 0.78

vi. Role of Brønsted- and Lewis-Acid Sites

The role of the Brønsted-acid sites was probed by examining the relationship between reaction rates and Brønsted-acid site density, whereas poisoning experiments were used to probe the roles of both Brønsted- and Lewis-acid sites.

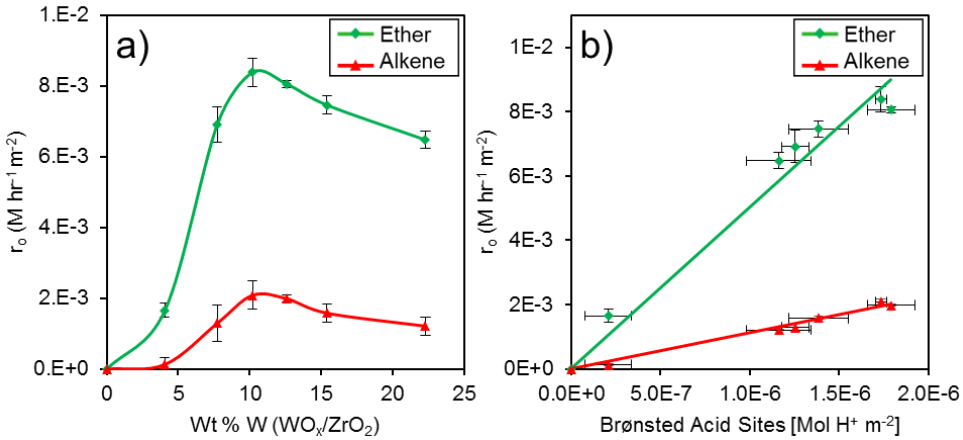

Figure 2.10. a) Initial rates of ether and alkene formation [M h^{-1} m^{-2}] versus W weight loading, b) Brønsted-acid site density [mol H^+ m^{-2}] versus rates of ether and alkene formation [M h^{-1} m^{-2}]. Reaction conditions: 393 K, 100 mg WO_x/ZrO_2 (12.6 wt% W), 600 RPM.

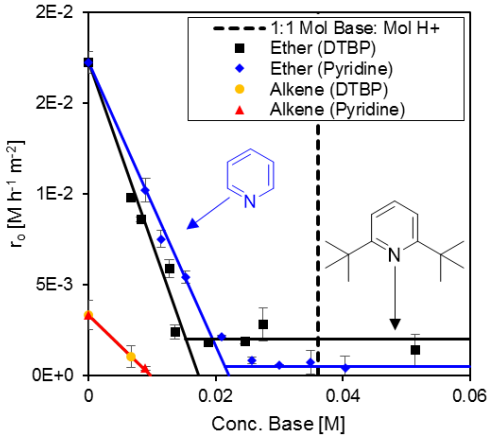

Figure 2.11. Initial rates of ether formation [M h^{-1} m^{-2}] with varying initial concentrations [M] of 2,6-di-tert-butyl pyridine (DTBP) (black square) and pyridine (blue diamond), and initial rates of alkene formation with varying initial concentration.

Initial rates of etherification and dehydration were measured over tungstated zirconia with varying Brønsted-acid site densities. The initial rates of etherification and dehydration across the 4-22 wt% catalysts are shown in Figure 2.10a. The rates of etherification and dehydration peak between 10.2 and 12.6 wt% W, where the Brønsted acid site density reaches a maximum. It is clear from Figure 2.10b that the initial rates of 1-dodecanol etherification and dehydration have a nearly linear relationship with Brønsted-acid site density and that the selectivity to ether does not change significantly with Brønsted-acid site density. Characterization of the catalysts (see Table 2.2) indicates that the ratio of Brønsted- to Lewis-acid sites changes with weight loading of tungsten, suggesting that the selectivity to ether is independent of the ratio of Brønsted- to Lewis-acid sites. However, as the Brønsted-acid site density increases, so does the fraction of Lewis-acid sites attributed to W, thus the rate of reaction may also increase with increasing W Lewis-acid site density.

As demonstrated from the DRIFTS characterization in Figure 2.5a and b, pyridine poisons both Brønsted- and Lewis-acid sites, whereas 2,6-di-tert-butyl pyridine poisons only Brønsted acid

sites. To test the effects of acid-site poisoning on the rates of ether and alkene formation, the initial rates of etherification and dehydration were measured for reactions with different initial concentrations of pyridine or 2,6-di-tert-butyl pyridine added to the reaction mixture. These results are shown in Figure 2.11. The rate of ether formation is observed to decrease as the concentration of the base increases, with the decrease in the rate being somewhat smaller for pyridine than for 2,6-di-tert-butyl pyridine poisoning. These results clearly demonstrate that both poisons are effective in blocking the adsorption of alcohol onto Brønsted-acid sites, a critical initial step for etherification.

Because the Brønsted- to Lewis-acid site ratio for WO_x/ZrO_2 (12.6 wt% W) is approximately 0.9, if Lewis-acid sites were not at all active in the etherification reaction, we would predict that approximately 1.8 moles of pyridine would be necessary to achieve the same decrease in rate as 1 mole of 2,6-di-tert-butyl pyridine. However, for this reaction, the decrease in the etherification rate is nearly the same for pyridine and hindered pyridine. This observation is consistent with the proposed mechanism, indicating that both Brønsted- and Lewis-acid sites play a role in the etherification reaction. Upon poisoning both Brønsted- and Lewis-acid sites with pyridine, the rate of ether formation reaches zero; however, after poisoning only the Brønsted-acid sites on the surface with hindered pyridine, some ether formation can still occur. This suggests that the Lewis-acid sites may be active for etherification on their own. The fact that Lewis-acid sites are still active supports the hypothesis that the surface is dominated by W Lewis-acid sites as opposed to Zr Lewis-acid sites because zirconia itself is not active for etherification (Table 2.1, entries 8-9). We also note that no alkene is formed once all of the Brønsted-acid sites are poisoned, consistent with the proposed mechanism. Based on the proposed mechanism and the resulting expressions for the reaction rates, we anticipate that the overall selectivity to ether would decrease if the tungsten Lewis-acid sites could be poisoned without altering the Brønsted-acid site density.

The dotted vertical line in Figure 2.11 represents the concentration of base equal to the measured concentration of Brønsted-acid sites determined by base titration. There are several possible reasons why the concentration of Brønsted-acid sites measured by ion exchange and titration is not equal to the concentration of hindered pyridine at which the rate becomes zero. First, given that there is a distribution in acid site strength, there may be some acid sites that are not active for etherification or dehydration. Second, the presence of a base on a Brønsted- or Lewis-acid site may alter the acidity of adjacent Lewis- or Brønsted-acid sites, respectively. Finally, there may be steric factors responsible for the enhanced decrease in rate. Bond lengths for W-O are on the order of 2 angstroms, and O-H bonds are on the order of 0.8 angstroms,[89] while the width of pyridine is on the order of 2.8 angstroms,[90] making it possible that a single pyridine molecule could inhibit multiple acid sites.

V. Conclusions

Tungstated zirconia is shown to be active and highly selective for the etherification of 1-dodecanol. It is proposed that the mechanism for liquid-phase etherification of 1-dodecanol over this catalyst involves a cooperation between Brønsted- and Lewis-acid sites that facilitates the bi-molecular etherification reaction. Isotopic labeling studies suggest that the rate-limiting step for etherification involves the formation of a carbon oxygen bond between two adsorbed alcohol molecules, and that the rate-limiting step for dehydration is the cleavage of the bond between the β-carbon and a hydrogen atom in an adsorbed alcohol. The proposed mechanism suggests that both etherification and dehydration require alcohol adsorption onto a Brønsted-acid site and that etherification requires an additional alcohol adsorbed onto an adjacent W Lewis-acid site, while

dehydration requires an open Lewis base site. A kinetic model based on the proposed mechanism (Scheme 2.1) was developed and fitted to initial reaction rate data for etherification and dehydration. This model was then modified to include the inhibiting effects of ether and water on both reactions. It was found that the rates of etherification and dehydration correlate linearly with Brønsted-acid site density, supporting the hypothesis that both reactions require Brønsted-acid sites. Due to the absence of activity for etherification over pure zirconia, and the relationship between tungsten oxide weight loading and reaction rate, it was concluded that the active Lewis-acid sites are associated with the dispersed tungsten oxide as opposed to zirconia. Poisoning of the catalyst with pyridine and hindered pyridine indicates that Lewis-acid sites are active for etherification but not dehydration, which is consistent with the proposed mechanism.

VI. Supporting Information

i. Kinetic Model Derivation

Based on the mechanism in Scheme 2.1, the elementary steps up to the kinetically-relevant steps for etherification and dehydration are shown, where ROH=dodecanol, BA=Brønsted-Acid Site, LA =Lewis-Acid Site, LB=Lewis-Base site, and RA=dodecane:

$$[ROH] + [BA] \overset{K_{BA}}{\longleftrightarrow} [ROH - BA] \quad \text{S2.1}$$

$$[ROH] + [LA] \overset{K_{LA}}{\longleftrightarrow} [ROH - LA] \quad \text{S2.2}$$

$$[ROH - LA] + [ROH - BA] \overset{k_e}{\rightarrow} [ROR - LA] + [BA] \quad \text{S2.3}$$

$$[ROH - BA] + [LB] \overset{k_d}{\rightarrow} [RA] + [BA] + [LB] \quad \text{S2.4}$$

In addition, inhibition of Brønsted-Acid Sites, Lewis-Acid Sites, and Lewis-Base Sites with Water and Ether are shown, where $K_{H2O\text{-}BA}$, $K_{H2O\text{-}LA}$, and $K_{H2O\text{-}LB}$ are inhibition by water of a Brønsted-acid site, Lewis-acid site, and Lewis-base site, respectively, and $K_{ROR\text{-}BA}$, $K_{ROR\text{-}LA}$, and $K_{ROR\text{-}LB}$ are inhibition by ether of a Brønsted-acid site, Lewis-acid site, and Lewis-base site, respectively:

$$[H_2O] + [BA] \overset{K_{H2O-BA}}{\longleftrightarrow} [H_2O - BA] \quad \text{S2.5}$$

$$[H_2O] + [LA] \overset{K_{H2O-LA}}{\longleftrightarrow} [H_2O - LA] \quad \text{S2.6}$$

$$[H_2O] + [LB] \overset{K_{H2O-LB}}{\longleftrightarrow} [H_2O - LB] \quad \text{S2.7}$$

$$[ROR] + [BA] \overset{K_{ROR-BA}}{\longleftrightarrow} [ROR - BA] \quad \text{S2.8}$$

$$[ROR] + [LA] \overset{K_{ROR-LA}}{\longleftrightarrow} [ROR - LA] \quad \text{S2.9}$$

$$[ROR] + [LB] \overset{K_{ROR-LB}}{\longleftrightarrow} [ROR - LB] \quad \text{S2.10}$$

Assuming steps S2.3 and S2.4 are the kinetically relevant steps for etherification and dehydration, respectively, the rate equations become:

$$r_e = k_e[ROH - LA][ROH - BA] \quad \text{S2.11}$$

$$r_d = k_d[ROH - BA][LB] \quad \text{S2.12}$$

Assuming steps S2.1-S2.2 and S2.5-S2.10 are quasi-equilibrated, the following site balances can used to determine the fraction of Brønsted-acid sites [BA], Lewis-Acid Sites [LA], and Lewis-Base Sites [LB]:

Brønsted-Acid Site Balance:

$$1 = [BA] + [ROH - BA] + [ROR - BA] + [H_2O - BA]$$
$$1 = [BA] + K_{BA}[ROH][BA] + K_{ROR-BA}[ROR][BA] + K_{H2O-BA}[H_2O][BA]$$
$$1 = [BA](1 + K_{BA}[ROH] + K_{ROR-BA}[ROR] + K_{H2O-BA}[H_2O])$$
$$[BA] = \frac{1}{1 + K_{BA}[ROH] + K_{ROR-BA}[ROR] + K_{H2O-BA}[H_2O]} \quad \text{S2.13}$$

Lewis-Acid Site Balance:

$$1 = [LA] + [ROH - LA] + [ROR - LA] + [H_2O - LA]$$
$$1 = [LA] + K_{LA}[ROH][LA] + K_{ROR-LA}[ROR][LA] + K_{H2O-LA}[H_2O][LA]$$
$$1 = [LA](1 + K_{LA}[ROH] + K_{ROR-LA}[ROR] + K_{H2O-LA}[H_2O])$$
$$[LA] = \frac{1}{1 + K_{LA}[ROH] + K_{ROR-LA}[ROR] + K_{H2O-LA}[H_2O]} \quad \text{S2.14}$$

Lewis-Base Site Balance:

$$1 = [LB] + [ROH - LB] + [ROR - LB] + [H_2O - LB]$$
$$1 = [LB] + K_{LB}[ROH][LB] + K_{ROR-LB}[ROR][LB] + K_{H2O-LB}[H_2O][LB]$$
$$1 = [LB](1 + K_{LB}[ROH] + K_{ROR-LB}[ROR] + K_{H2O-LB}[H_2O]$$
$$[LB] = \frac{1}{1 + K_{LB}[ROH] + K_{ROR-LB}[ROR] + K_{H2O-LB}[H_2O]} \quad \text{S2.15}$$

Substituting the site balances S2.13 and S2.14 into equation S2.11 yields the rate expression for etherification (Equation 2.7):

$$r_e = k_e[ROH - LA][ROH - BA]$$
$$r_e = k_e K_{LA} K_{BA}[ROH]^2[LA][BA]$$
$$r_e = \frac{k_e K_{LA} K_{BA}[ROH]^2}{(1 + K_{BA}[ROH] + K_{ROR-BA}[ROR] + K_{H2O-BA}[H_2O])(1 + K_{LA}[ROH] + K_{ROR-LA}[ROR] + K_{H2O-LA}[H_2O])} \quad 2.7$$

Substituting the site balances S2.13 and S2.15 into Equation S2.12 yields the rate expression for dehydration (Equation 2.8):

$$r_d = k_d[ROH - BA][LB]$$
$$r_d = k_d K_{BA}[ROH][BA][LB]$$
$$r_d = \frac{k_d K_{BA}[ROH]}{(1 + K_{BA}[ROH] + K_{ROR-BA}[ROR] + K_{H2O-BA}[H_2O])(1 + K_{LB}[ROH] + K_{ROR-LB}[ROR] + K_{H2O-LB}[H_2O])} \quad 2.8$$

ii. NMR of Reactants, Deuterated Reactants, and Products

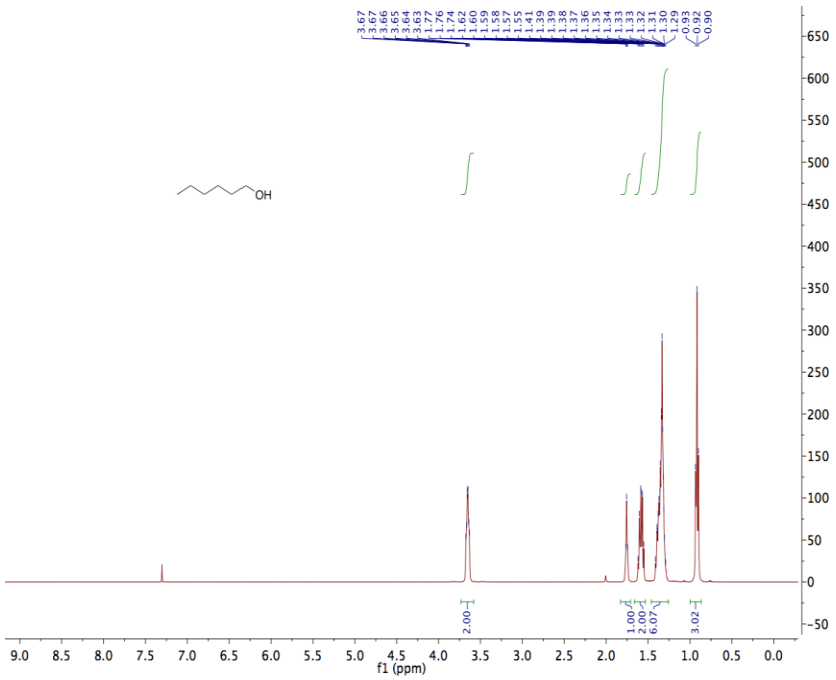

Figure 2.12. Hydrogen NMR spectrum of 1-Hexanol.

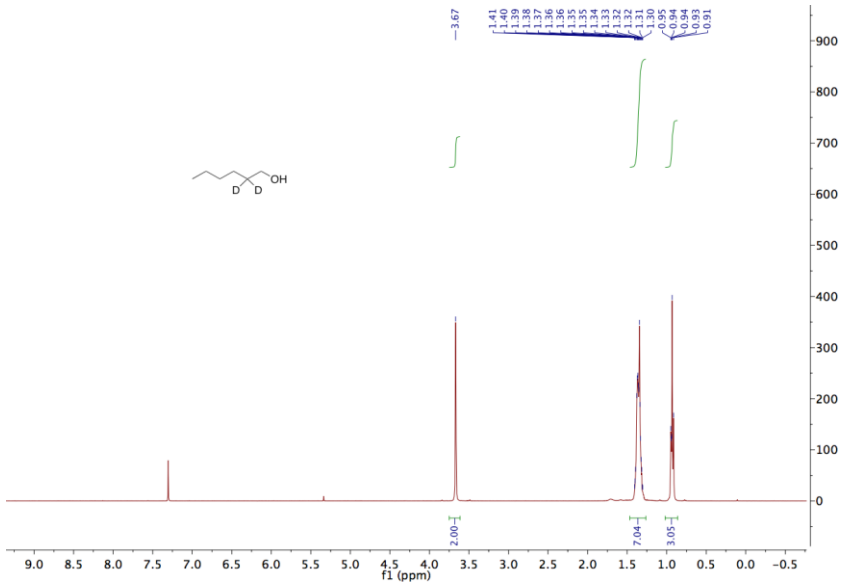

Figure 2.13. Hydrogen NMR spectra of hexan-2,2-d_2-1-ol. Lack of peaks between 1.5-2 ppm indicates the presence of deuterium labeled atoms on the second carbon from the –OH group.

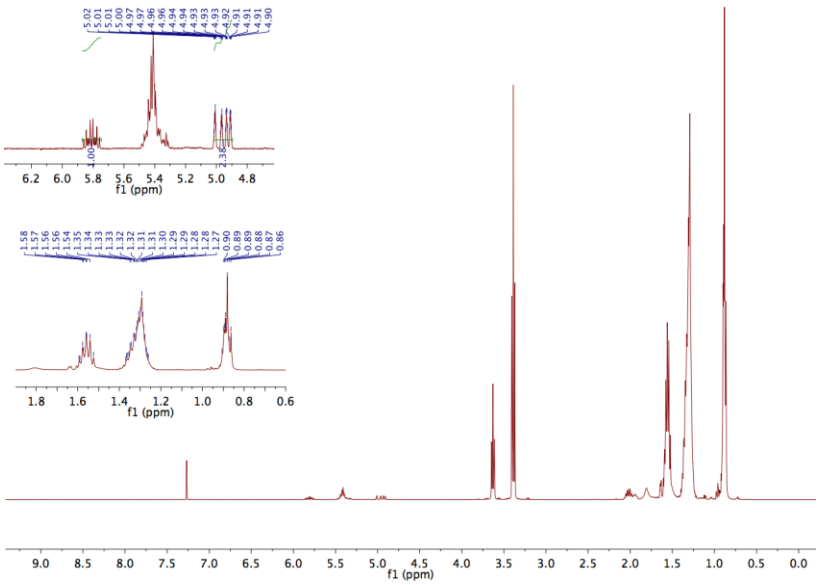

Figure 2.14. Hydrogen NMR spectra of reaction products from 1-hexanol reaction over WO_x/ZrO_2 (12.6 wt% W) to produce hexenes (hex-1-ene, hex-2-ene) and di-n-hexyl ether.

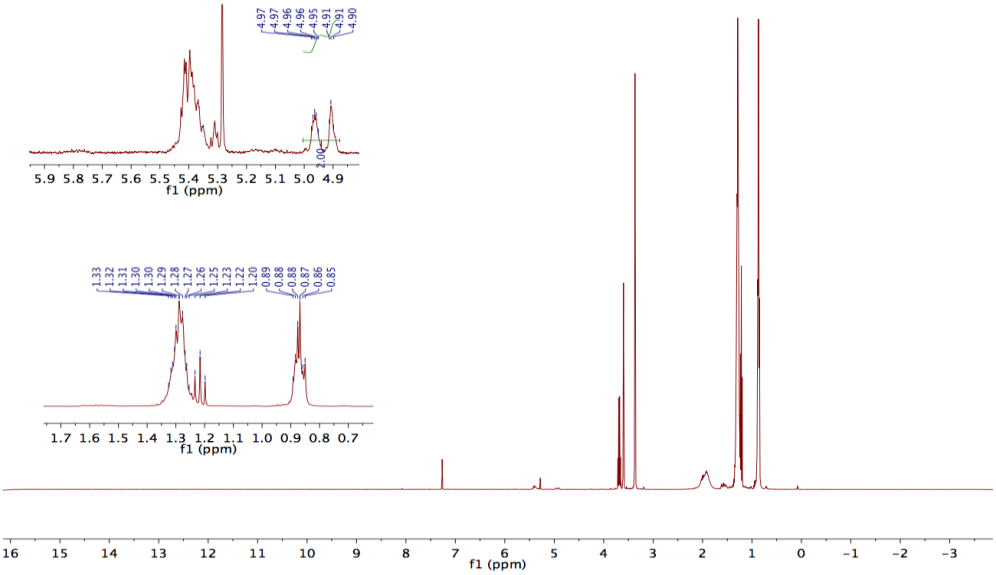

Figure 2.15. Hydrogen NMR spectra of reaction products from hexan-2,2-d_2-1-ol reaction over WO_x/ZrO_2 (12.6 wt% W) to produce labeled hexenes (hex-1-ene-2-d, hex-2-ene-2-d) and 1-((hexyl-2,2-d_2)oxy)hexane-2,2-d_2.

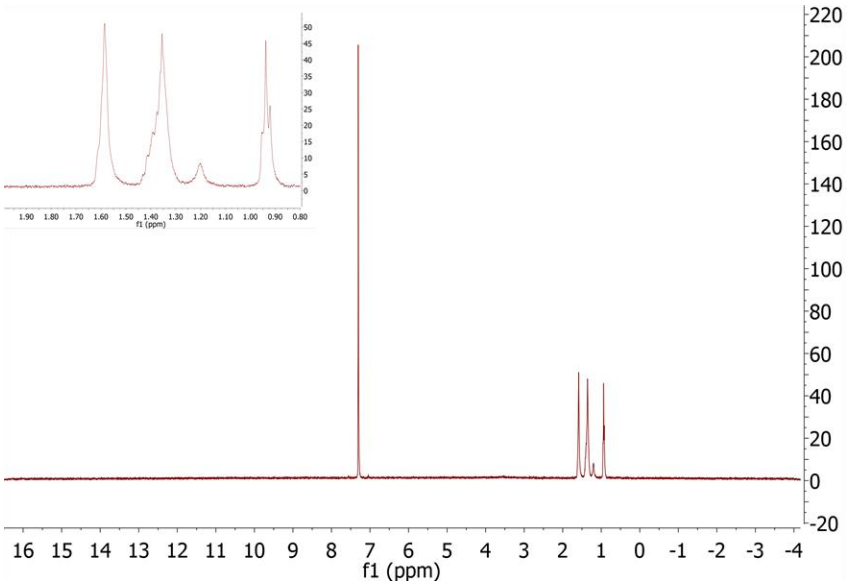

Figure 2.16. Hydrogen NMR spectra of hexan-1,1-d_2-1-ol obtained from CDN Isotopes, Inc.

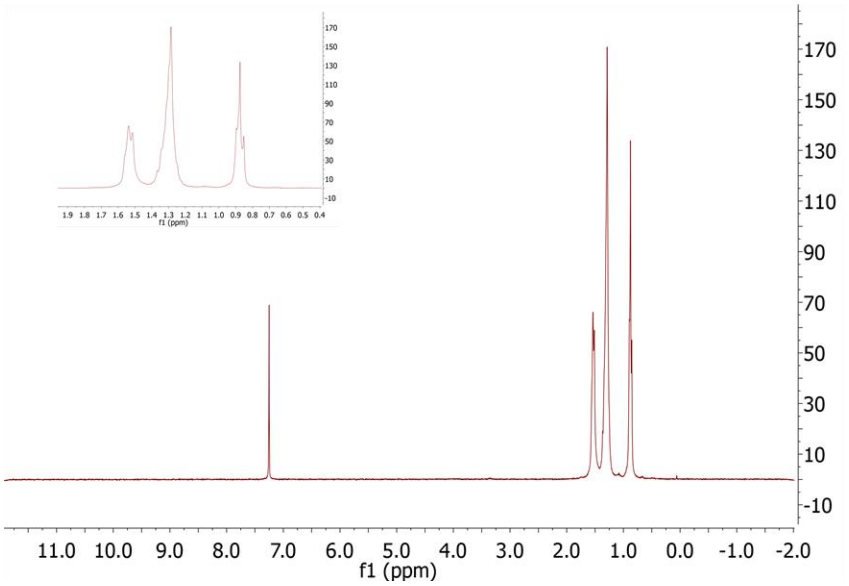

Figure 2.17. Hydrogen NMR spectra of reaction products from hexan-1,1-d_2-1-ol reaction over WO_x/ZrO_2 (12.6 wt% W) to produce labeled hexenes (hex-1-ene-1,1-d_2) and 1-((hexyl-1,1-d_2)oxy)hexane-1,1-d_2.

3. Effect of Alcohol Structure on the Kinetics and Mechanism of Etherification and Dehydration over Tungstated Zirconia[§]

I. Abstract

Linear and branched ether molecules have attracted recent interest as diesel additives and lubricants that can be produced from biomass-derived alcohols. In this study, tungstated zirconia was identified as a selective and green solid acid catalyst for the direct etherification of primary alcohols in the liquid phase, achieving ether selectivities of >94% for C_6-C_{12} linear alcohol coupling at 393 K. The length of linear primary alcohols (C_6-C_{12}) was shown to have a negligible effect on apparent activation energies for etherification and dehydration, demonstrating the possibility to produce both symmetrical and asymmetrical linear ethers. Reactions over a series of C_6 alcohols with varying methyl branch positions indicated that substituted alcohols (2°, 3°) and alcohols with branches on the β-carbon readily undergo dehydration, but alcohols with branches at least 3 carbons away from the –OH group are highly selective to ether. A novel model compound, 4-hexyl-1-dodecanol, was synthesized and tested in order to further demonstrate this structure-activity relationship. Trends in the effects of alcohol structure on selectivity were consistent with previously proposed mechanisms for etherification and dehydration and help to define possible pathways to selectively form ethers from biomass-derived alcohols.

II. Introduction

As the adverse effects of anthropogenic climate change continue to increase, the global need for clean and renewable energy is now larger than ever before. One method of lowering net atmospheric CO_2 emissions is to replace conventional fossil fuels and petroleum-derived specialty chemicals with renewable alternatives.[91] Ethers have attracted recent interest as renewable fuels and lubricants. Symmetric and asymmetric linear ethers in the C_8-C_{12} range are suitable diesel additives due to their high cetane numbers.[19,46,92,93] Branched ethers such as methyl tert-butyl ether can also be added to gasoline because of their high octane numbers.[16] Longer chain branched ethers in the C_{28}-C_{32} range have low pour points and excellent lubricant properties,[22,49,94] and could replace poly-alpha-olefin lubricants, which are produced from fossil reserves.[51,52]

Biomass-derived alcohols are promising candidates for producing renewable ethers. Ethanol and butanol can be obtained in high yields through fermentation processes such as ABE fermentation.[11,95,96] Longer chain linear alcohols like 1-octanol and 1-dodecanol can be produced from the condensation of biomass-derived furan platform molecules, and the hydrolysis of triglycerides and fatty acids, respectively,[97] and then built up into branched alcohols with higher carbon numbers through the Guerbet reaction.[45] Some general approaches to producing linear and branched alcohols from biomass-derived platform molecules are summarized in Scheme 3.1.

Direct etherification of biomass-derived alcohols over an acid catalyst is an attractive method of producing ethers because it does not require hydrogen gas and precious metal catalysts like reductive etherification.[53] The competing reaction for alcohol dehydration over an acid catalyst is unimolecular dehydration to form alkenes, which is thermodynamically favored at temperatures above approximately 350 K. Due to their high volatility, and the propensity to form gums, alkenes are not desired in fuel and lubricant blends.[98]

[§] This chapter was originally published in *ChemSusChem* and is adapted with permission from co-author S. Pindi.[159]

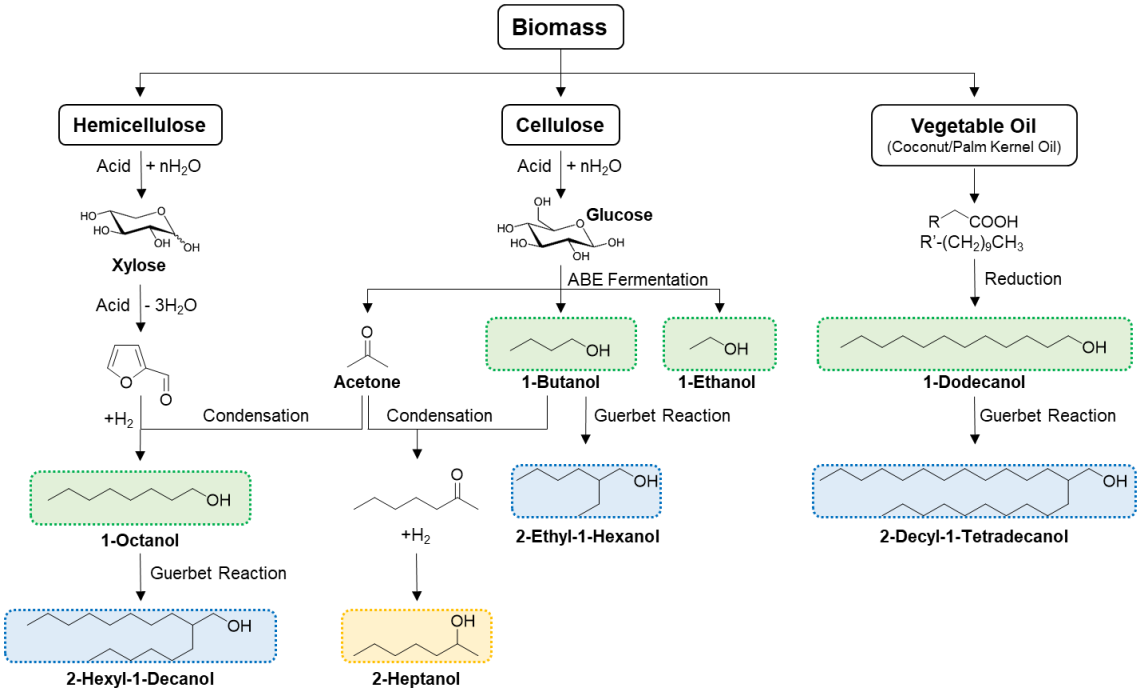

Scheme 3.1. General approach to producing linear and branched alcohols from biomass-derived platform molecules.

In the previous chapter of this dissertation, tungstated zirconia was identified as a selective catalyst for the liquid phase etherification of 1-dodecanol, with ether selectivities above 94% at moderate temperatures (393 K).[99] This study suggested that the high selectivity to ether is due to a cooperative effect between Brønsted- and Lewis-acid sites on the surface of the catalyst which promote the bi-molecular etherification reaction. This research motivates the current study, which aims to evaluate the extent to which tungstated zirconia can be used to produce a variety of symmetrical and asymmetrical ethers, and mixtures of ethers, for fuel and lubricant applications.

Kinetic studies of alcohol dehydration reactions have traditionally been centered on gas phase unimolecular dehydration.[64,87,88] Experimental and computational studies of gas phase unimolecular dehydration of alcohols over γ-Al_2O_3 have supported the theory that increasing the substitution of the alcohol increases the stability of the intermediate in the rate limiting step for dehydration, resulting in a decrease in activation barrier for dehydration with increasing substitution.[31,88]

While studying the effect of alcohol structure in the gas phase where unimolecular dehydration dominates has provided some insight into the relationship between unimolecular dehydration rates and substitution, the kinetics of etherification must also be explored in order to understand the relationship between alcohol structure and selectivity to ether. Some efforts have been made to investigate the catalytic conversion of alcohols to both symmetrical and asymmetrical ethers at moderate temperatures where etherification dominates. Various acidic resins and zeolites have been shown to be effective in the liquid phase etherification of 1-pentanol, 1-hexanol, and 1-octanol to produce symmetrical ethers.[54,56,57,100] Tejero, et. al. have demonstrated that it is also possible to produce asymmetrical ethers like ethyl-hexyl ether and ethyl-octyl ether through cross-coupling of 1-hexanol or 1-octanol with ethanol or diethylcarbonate.[93,101]

But, to our knowledge, the literature is lacking a comprehensive study of the kinetics of liquid phase etherification reactions over a large range of long-chain 1-alcohols (C_6-C_{12}), and a

more thorough investigation into the effect of branched alcohols on the formation of symmetrical and asymmetrical ethers in the lubricant range (C_{12}-C_{36}). While acidic resins such as Amberlyst 70 and Nafion NR-50 have been shown to be effective for etherification of linear alcohols in the liquid phase, measuring accurate rate data is difficult due to the swelling of these resins in the solvent, which causes changes in the number of accessible active sites over time.[70] Tungstated zirconia is thermally stable, does not deactivate or swell in the reactant media, and has been shown to be an effective catalyst for etherification of alcohols. Thus, this chapter will comprehensively study the effects of linear alcohol length, carbon chain branches, and positions of carbon chain branches on the kinetics of etherification and dehydration reactions over tungstated zirconia in the liquid phase, with the aim of understanding the relationship between ether selectivity and alcohol structure.

III. Experimental Section

i. Materials

All chemicals obtained commercially were used without further purification. The following chemicals were obtained from Sigma-Aldrich: 1-hexanol (>98%), 1-octanol (>99%), 1-decanol (>99%), 1-dodecanol (>98%), 2-hexanol (>99%), 2-methyl-1-pentanol (>99%), 3-methyl-1-pentanol (>99%), 4-methyl-1-pentanol (>97%), 2-ethyl-1-hexanol (>99%), 2-butyl-1-octanol (>95%), 2-hexyl-1-decanol (>97%), 2-octyl-1-dodecanol (>97%), 2-decyl-1-tetradecanol (97%), dodecane (>99%), hexane (>99%), 1-hexene (>99%), and pyridine (99.8%). The following chemicals were obtained from Spectrum Chemical: 1-heptanol (>98%), 1-octene (>99%), and n-tetradecane (>99%), which was used as an internal standard for analytical purposes. The following chemicals were obtained from TCI: 1-nonanol (>99%), 1-undecanol (>99%), di-n-octyl ether (>95%), di-n-decyl ether (>95%), and di-dodecyl ether (>95%), 1-decene (>95%) and 1-dodecene (>95%). Di-n-hexyl ether (>98%) was obtained from Alpha Aesar. Synthesis and characterization of 4-hexyl-1-dodecanol is provided in the Supporting Information.

ii. Synthesis and Characterization of Tungstated Zirconia

Tungstated zirconia (WO_x/ZrO_2, 12.6 wt% W) was synthesized and characterized using previously reported methods.[60,67,68,99] Powder X-ray diffraction (XRD) patterns for WO_x/ZrO_2 (0-22 wt% W) were taken with a Bruker D8 GADDS diffractometer equipped with a Cu−Kα source (40 kV, 40 mA). Raman spectra were obtained with a LabRAM HR Horiba Scientific Raman spectrometer equipped with a 633 nm^{-1} laser. BET surface area measurements were performed with a Micrometrics TriStar BET and pretreated with a Micrometrics FlowPrep 060. The ratio of Brønsted- to Lewis-acid sites was determined from IR spectra of adsorbed pyridine, using a previously reported method.[99] Spectra were acquired using a Thermo Scientific Nicolet 6700 Fourier Transform Infrared Spectrometer (FT-IR) equipped with a Diffuse Reflectance Infrared Fourier Transform Spectrometer (DRIFTS) cell. ICP Elemental analysis was performed by Galbraith Laboratories, Inc. in order to determine tungsten weight loadings.

iii. Batch Reactions

All reactions were carried out in sealed 12 mL Q-Tube batch reaction vessels with magnetic stirring at 600 RPM using an IKA C-MAG HS 10 digital hot plate with temperature control accurate to within +/- 1 K. A separate batch reaction was performed for each time point for kinetic studies in order to ensure consistency of volume and concentration of each sample. All reactions over tungstated zirconia were carried out solvent-free with 100 mg of catalyst, 100 µL of n-

tetradecane as an internal standard, and between 84-205 µL of reactant depending on the reaction conditions (unless otherwise noted). Reaction products were dissolved in acetone for analysis with GC/MS.

iv. Product Analysis

The analysis of products was carried out using a Varian CP-3800 Gas Chromatograph/ Mass Spectrometer (GC/MS). The products were quantified using the flame ionization detector (FID) and were identified using the Varian 320 triple quadrupole mass spectrometer (MS). N-tetradecane was used as an internal standard to ensure accurate product quantification. FID response factors for pure commercial compounds were obtained from linear calibration curves, and the effective carbon number method was used to predict response factors for products which are not available in high purity. This method predicts FID response to within ±1.7%.[102] Mass balances for all reactions were achieved within ± 5% unless otherwise noted.

v. Kinetic Analysis

To measure the initial rates of etherification and unimolecular dehydration of 1-hexanol, 1-heptanol, 1-octanol, 1-nonanol, 1-decanol, 1-undecanol, 1-dodecanol, 4-methyl-1-pentanol, 3-methyl-1-pentanol, 2-methyl-1-pentanol, 2-hexanol, and 2-methyl-2-pentanol, individual batch reactions for each time point were carried out at each temperature. Mass transfer limitations were found to be negligible at stirring speeds of 600 RPM for catalyst particle sizes less than 250 µm in diameter. This conclusion was determined by measuring the initial catalytic activity as a function of stirring speed and particle size.

For each experiment, conversion (X_a), selectivity to ether (S_{ether}), selectivity to alkenes ($S_{alkenes}$) were defined as follows:

$$X_a = \frac{mol\ of\ a\ reacted}{initial\ mol\ of\ a}$$

$$S_{ether} = \frac{moles\ of\ a\ reacted\ to\ form\ ether}{moles\ of\ a\ reacted}$$

$$S_{alkenes} = \frac{moles\ of\ a\ reacted\ to\ form\ alkene}{moles\ of\ a\ reacted}$$

Initial rates of ether and alkene formation (r_o) were calculated from the experimentally measured curve of moles of product formed per mass of catalyst versus time (t).

Apparent activation energies were calculated from an Arrhenius plot of the natural log of the initial rates versus the inverse temperature. At low conversions (< 25%), the reaction is pseudo-zero order in reactant, indicating that the surface of the catalyst is saturated with reactant. Under these conditions, the inhibiting effects of water and ether, and the formation of additional products such as branched ether and oligomerized alkenes are negligible.[99]

The Arrhenius relation was given by:

$$r_o = k_{app} = A_{app} exp\left(\frac{E_{a,app}}{RT}\right)$$

Where r_o is the initial rate of ether or alkene formation, k_{app} is the apparent rate constant for the reaction, A_{app} is the apparent pre-exponential factor, and $E_{a,app}$ is the apparent activation energy. For the Arrhenius fitting, the pre-exponential factor was fixed for both the etherification and dehydration plots of the C_6 alcohols and linear alcohols, based upon the assumptions that the active sites for each reaction are equivalent, and that the entropy of adsorption of the most abundant surface intermediates and the change in entropy of the transition states are both consistent across the various substrates. The pre-exponential factors were fit to minimize the standard error on the

least squares regression for each group of substrates. Error bars for activation energies were taken from the standard error of the least squares regression. Arrhenius plots, initial rates, pre-exponential factors, activation energies, and the temperature ranges for each reaction are given in the Supporting Information section.

IV. Results and Discussion

i. Catalyst Characterization

Tungstated zirconia (WO_x/ZrO_2, 12.6 wt% W) was characterized with X-ray diffraction, Raman spectroscopy, and DRIFTS FTIR with adsorbed pyridine to determine the structure and confirm the presence of Brønsted- and Lewis-acid sites. From the XRD pattern in Figure 3.1a, the peaks at 2θ angles of 30, 35, 50, and 59° (yellow) indicate the presence of tetragonal zirconia,[67,71,72] and the peaks between 23-25° (pink) represent the presence of bulk tungsten oxide.[74] From the Raman spectra in Figure 3.1b, the bands at bands at 274, 715, and 807 cm^{-1} (pink) indicate the W-O stretching of bulk tungsten oxide,[76] and the band at 1020 cm^{-1} (yellow) is indicative of polymeric tungsten oxide terminated by a tungsten oxygen double bond.[63] The DRIFTS FTIR spectra of adsorbed pyridine shown in Figure 3.1c demonstrates that both Brønsted- and Lewis- acid sites are present on the surface of the catalyst, as evidenced by bands of adsorbed pyridine at 1540 cm^{-1} (blue), and 1444 cm^{-1} (green), respectively. Additional catalyst characterization is summarized in Table 3.1.

Table 3.1. Characterization of 12.6 wt% WO_x/ZrO_2

Property	Value
Weight loading of W (%)	12.6
Zirconia Crystal Structure (XRD)	Tetragonal
BET Surface Area (m^2 g^{-1})	51
Brønsted Acid Sites (mol eq. H^+ m^{-2})	$1.78*10^{-6} \pm 1.4*10^{-7}$
Ratio of Brønsted / Lewis Acid Sites	0.90 ± 0.02 (393 K)

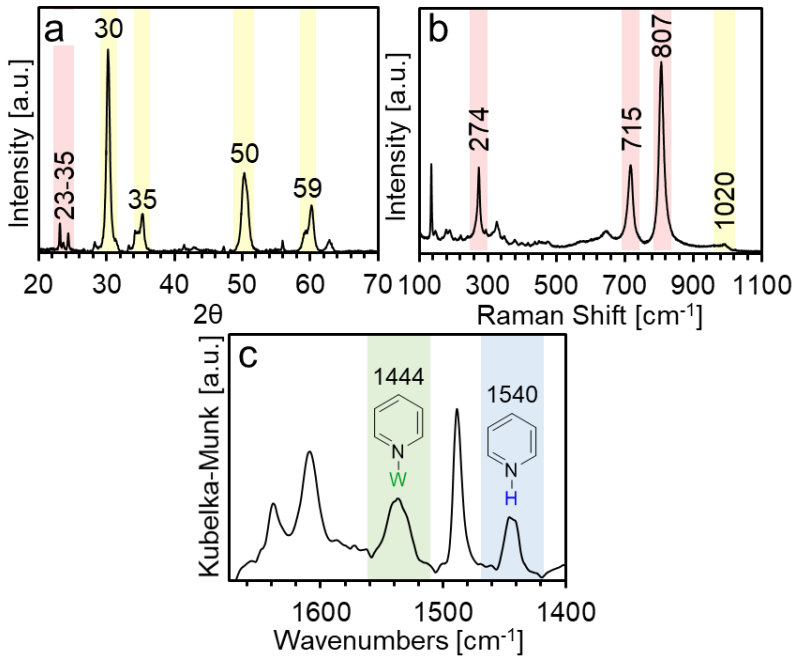

Figure 3.1. Characterization of 12.6 wt% W (WO_x/ZrO_2), a) X-ray diffraction spectrum, b) Raman spectrum, c) DRIFTS FTIR spectrum of adsorbed pyridine at 393 K.

ii. Effect of Alcohol Structure on Kinetics: Linear Primary Alcohols (C_6-C_{12})

To build symmetrical and asymmetrical linear ethers in the diesel range, it is necessary to investigate the effect of alcohol chain length on the apparent kinetics of etherification and dehydration over tungstated zirconia. The selectivity to ether for C_6-C_{12} alcohols (1-hexanol, 1-heptanol, 1-octanol, 1-nonanol, 1-decanol, 1-undecanol, and 1-dodecanol) was measured for temperatures between 393 - 418 K. The results are summarized in Table 3.2.

Table 3.2. Selectivity of primary linear alcohols (C_6-C_{12}) to symmetrical ethers (C_{12}- C_{24}) over tungstated zirconia with varying temperature.

	Selectivity to Symmetrical Ether (%) / (Conversion of Alcohol (%))					
Reactant	393 K	398 K	403 K	408 K	413 K	418 K
1-Hexanol	>99 /(4)	94 /(6)	88 /(11)	88 /(22)	89 /(27)	87 /(39)
1-Heptanol	>99 /(5)	80 /(7)	80 /(11)	82 /(26)	80 /(25)	80 /(38)
1-Octanol	>99 /(4)	92 /(6)	92 /(12)	83 /(20)	85 /(28)	80 /(33)
1-Nonanol	>99 /(4)	89 /(7)	85 /(12)	86 /(20)	81 /(28)	77 /(37)
1-Decanol	>99 /(4)	95 /(8)	94 /(11)	90 /(18)	88 /(25)	85 /(38)
1-Undecanol	>99 /(5)	92 /(6)	89 /(9)	88 /(17)	82 /(25)	78 /(42)
1-Dodecanol	94 /(6)	94 /(7)	86 /(11)	83 /(26)	80 /(30)	84 /(38)

Reaction Conditions: 1 h, 100 mg WO_x/ZrO_2 (12.6 wt% W), 600 RPM, 564 µmol reactant, 125 µmol n-tetradecane. Remaining selectivity is attributed to alkenes, and trace amounts of branched ether. Error within ±2% for data at 393 – 413 K, and within ±4% for 418 K.

For all of the linear alcohols studied, the selectivity to ether decreases with increasing temperature. However, the carbon chain length does not appear to have any significant effect on the selectivity. Nel and Klerk observed that ether selectivity of C_6-C_{12} linear alcohols decreased with increasing carbon chain length for gas phase reactions over η-alumina at 523 K.[19] The authors claimed that their system was limited by external mass transfer, which could explain why they observed a decrease in selectivity for longer chain alcohols.

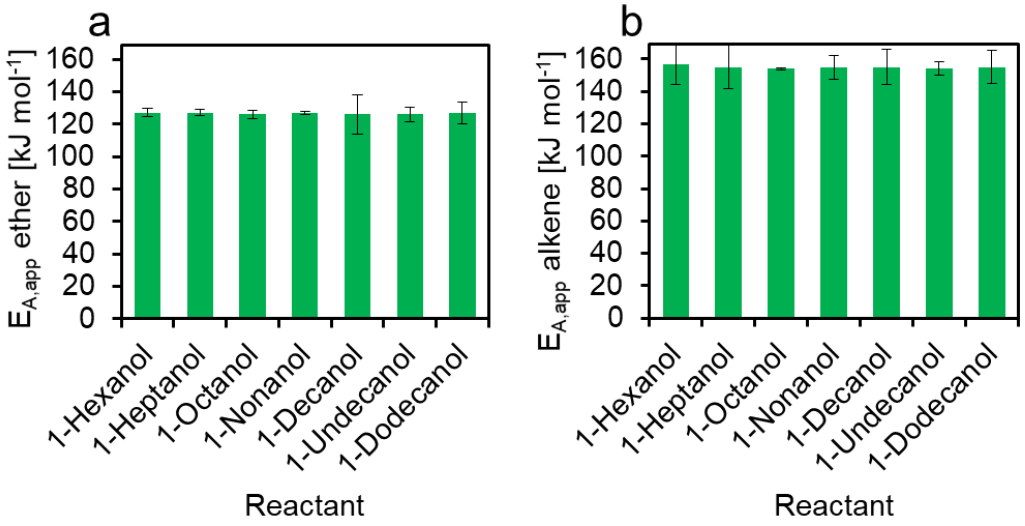

Figure 3.2. a) Apparent activation energies for etherification, b) apparent activation energies for dehydration of C_6-C_{12} primary alcohols over WO_x/ZrO_2 (12.6 wt% W).

The apparent activation energies for etherification and dehydration of linear alcohols in the liquid phase were obtained by measuring the initial rates of ether and alkene formation over a range of temperatures. A sample time-course study of 1-dodecanol etherification over WO_x/ZrO_2

(12.6 wt% W) at 393 K is shown in Figure 3.5 in the Supporting Information, which demonstrates that at conversions below approximately 25%, the kinetics are pseudo-zero order. The rates, selectivities, Arrhenius plots, and temperature ranges for which the initial rates were obtained are provided in Figure 3.6, and Table 3.6 and Table 3.7 in the Supporting Information.

Figure 3.2 shows the apparent activation energies for etherification and dehydration of primary linear alcohols 1-hexanol, 1-heptanol, 1-octanol, 1-nonanol, 1-decanol, 1-undecanol, and 1-dodecanol. Overall, the activation barriers for unimolecular dehydration in Figure 3.2b (154-157 kJ mol^{-1}) are greater than the activation barriers for etherification in Figure 3.2a (126-127 kJ mol^{-1}), which explains the decrease in selectivity to ether with increasing temperature observed in Table 3.2. The activation energies for linear alcohol etherification do not change significantly with increasing carbon chain length, implying that the length of linear alcohols has little effect on the kinetics of etherification and dehydration.

For applications in diesel fuel, mixtures of linear alcohols could be tuned in the reactant feed to create a distribution of ethers that contains a desired molecular weight distribution. A similar tuning of molecular weights has been demonstrated previously for the trimerization of ketones for diesel fuel mixtures.[103] Because the etherification activation energies and reaction rates do not vary significantly between linear alcohols in the C_6-C_{12} range, a mixture of alcohols will couple in a nearly random statistical distribution. An example distribution study is shown in Figure 3.3. Seven linear alcohols (1-hexanol, 1-heptanol, 1-octanol, 1-nonanol, 1-decanol, 1-undecanol, and 1-dodecanol) in equimolar ratios were reacted together over tungstated zirconia at 393 K. The theoretical selectivity distribution for random cross-coupling of alcohols is shown in black, and the experimental distribution of ether products is shown in green. Figure 3.3 shows that there is a slight preference for coupling of the shorter chain alcohols, which could be explained by the fact that the experiment was run at high conversion (>90%), where the inhibiting effects of water and ether are no longer negligible. Under these conditions, it is possible that the bulkier ethers such as di-dodecyl ether introduce steric effects and thus have a greater inhibiting effect on the rate of consumption of the longer chain alcohols. The observation that cross-coupling of linear alcohols is nearly statistical suggests that the distribution of linear alcohols in the feed could be tuned to produce a variety of desired ether blends.

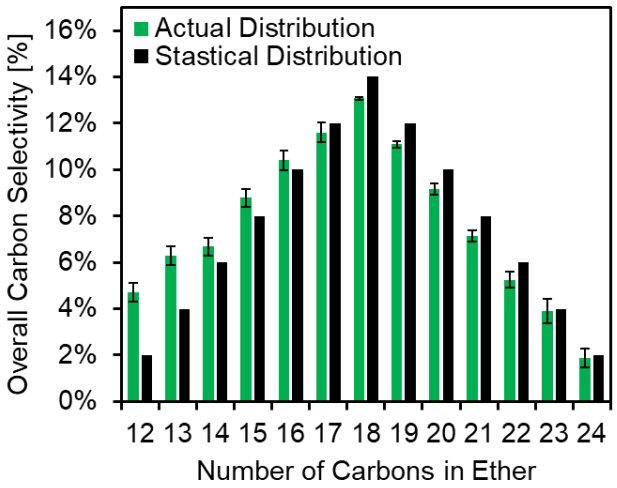

Figure 3.3. Ether Distribution for C_6-C_{12} alcohols. Reaction conditions: 393 K, 48 h, 100 mg WO_x/ZrO_2 (12.6 wt% W), 600 RPM. Equimolar ratio of 1-hexanol, 1-heptanol, 1-octanol, 1-nonanol, 1-decanol, 1-undecanol, and 1-dodecanol, with n-tetradecane as an internal standard. Conversion >90%.

iii. Effect of Alcohol Structure on Kinetics: Position of Carbon Chain Branches

To systematically study the effect of the position of carbon chain branches on etherification kinetics, a series of C_6 alcohols with varying degrees of substitution and positions of methyl groups were reacted over tungstated zirconia. Table 3.3 shows the selectivity to ether for the C_6 alcohols at 393 K. Primary C_6 alcohols with a methyl group at least 3 carbons away from the –OH group (1-hexanol, 4-methyl-1-pentanol, and 3-methyl-1-pentanol) exhibit a very high selectivity to ether. As the methyl group approaches the β-carbon (2-methyl-1-pentanol), the ether selectivity rapidly decreases. Secondary and tertiary C_6 alcohols (2-hexanol and 2-methyl-2-pentanol) rapidly dehydrated under these conditions, forming no ether.

Table 3.3. Selectivity of reactions over C_6 alcohols.

Reactant	Conversion	Selectivity to Ether	Selectivity to Alkenes/Other
1-Hexanol	11%	>99%	<1%
4-Methyl-1-Pentanol	10%	>99%	<1%
3-Methyl-1-Pentanol	10%	87%	13%
2-Methyl-1-Pentanol	14%	<1%	>99%
2-Hexanol	>99%	<1%	>99%
2-Methyl-2-Pentanol	>99%	<1%	>99%

Reaction Conditions: 393 K, 4 h, 100 mg WO_x/ZrO_2 (12.6 wt% W), 600 RPM, 168 µL reactant, 100 µL n-tetradecane as internal standard.

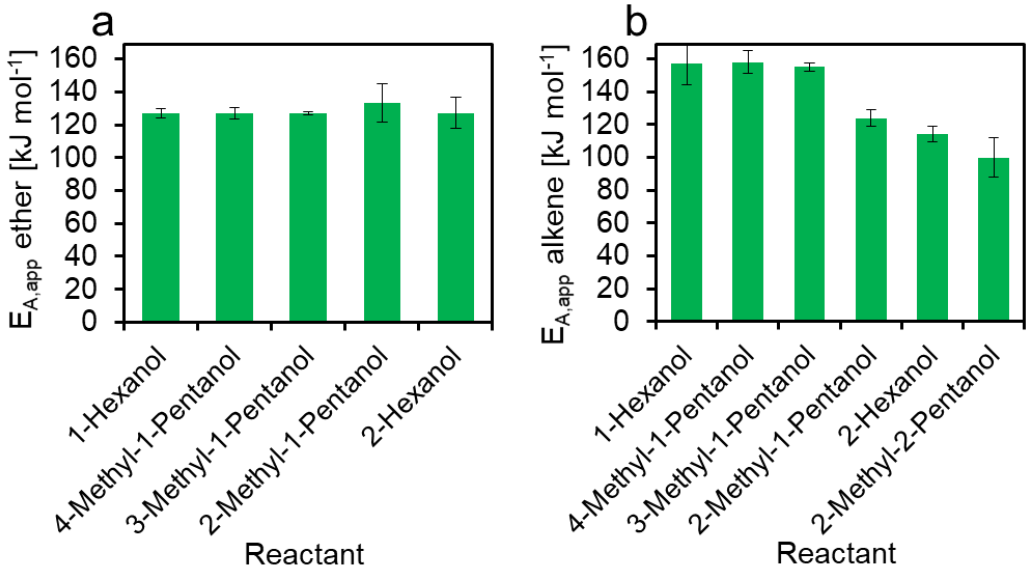

Figure 3.4. a) Apparent activation energies for etherification, b) apparent activation energies for dehydration of C_6 alcohols (1-hexanol, 4-methyl-1-pentanol, 3-methyl-1-pentanol, 2-methyl-1-pentanol, 2-hexanol, and 2-methyl-2-pentanol) over WO_x/ZrO_2 (12.6 wt% W).

To further study the relationship between branching position and kinetics, the apparent activation energies of etherification and dehydration of the C_6 alcohols were measured and are shown in Figure 3.4. Temperature ranges were selected such that initial rates of both ether and alkene could be measured, except for 2-methyl-2-pentanol, for which ether could not be detected

at any of the temperatures in the range of 333-418 K. The initial rates, Arrhenius plots, temperature ranges, and ether selectivities at selected temperatures are provided in Figure 3.7, Table 3.8, Table 3.9, and Table 3.10 in the Supporting Information.

Figure 3.4a shows that the apparent activation barrier for etherification is fairly independent of the reactant. But from Figure 3.4b, it is clear that as the substitution of the alcohol increases, the barrier for unimolecular dehydration decreases. The dehydration activation barriers for 1-hexanol, 4-methyl-1-pentanol, and 3-methyl-1-pentanol are 157 ± 13, 158 ± 10, and 155 ± 1 kJ mol^{-1}, respectively, indicating that the barriers are within error for alcohols with branching at least 3 carbons away from the –OH group. But for 2-methyl-1-pentanol, 2-hexanol, and 2-methyl-2-pentanol, the barriers are 124 ± 2, 114 ± 5, and 100 ± 12 kJ mol^{-1}, respectively, indicating that the dehydration barrier decreases with increasing substitution of the alcohol. In our previous study, measurements of kinetic isotope effects for 1-hexanol dehydration over tungstated zirconia suggested that the rate limiting step for unimolecular dehydration is the cleavage of a β-carbon hydrogen bond.[99] This is consistent with the findings in Figure 3.4, since the increased substitution of the α- and β-carbons would increase the stability of the carbocation intermediate formed during unimolecular dehydration, making dehydration more favorable. Also found in our previous study, the dehydration of 1-hexanol produced both 1-hexene and 2-hexene, as verified by NMR; however, no methyl shift was observed, as might be expected for the dehydration of a substrate such as 3,3-di-methyl-2-butanol.[99,104]

In addition, steric effects that limit α-carbon oxygen bond formation between two alcohols could explain the preference towards unimolecular dehydration for 2° and 3° alcohols.[31] Similar relationships between alcohol structure and dehydration activation barriers have been observed in the literature for other solid acid catalysts. Activation energies of 145, 141, 121, and 110 kJ mol^{-1} have been reported for gas phase unimolecular dehydration of ethanol, 1-propanol, 2-propanol, and 2-methyl-2-propanol, respectively, over γ-Al_2O_3, indicating that increasing substitution decreases the activation barrier for unimolecular dehydration.[31,88] Mpourmpakis, et. al. observed that dehydration activation barriers of ethanol, 1-propanol, 2-propanol, and 2-methyl-2-propanol also decreased with increasing substitution for dehydration reactions over γ-Al_2O_3, ZrO_2, and TiO_2.[87] The relationship between alcohol substitution and reactivity for unimolecular dehydration is in agreement with the results presented here for C_6 alcohols in the liquid phase, and the relative activation energies for etherification provide an explanation for the selectivity trends observed in Table 3.3.

iv. Effect of Alcohol Structure: Length of Carbon Chain Branches

While the kinetics of linear alcohols do not vary significantly from C_6-C_{12}, the addition of branches changes the selectivity to ether. To further investigate the effects of branch size on ether selectivity, a series of Guerbet alcohols with increasing carbon chain backbone length and branch length were reacted with 1-dodecanol in 1:1 molar ratios at low conversions to form symmetrical and asymmetrical ethers in the lubricant range (C_{16}-C_{36}). The pathways for these reactions are shown in Scheme 3.2, and the results are summarized in Table 3.4. Symmetrical branched ethers (1E) are only formed in small amounts from the coupling of small Guerbet alcohols (2-ethyl-1-hexanol and 2-butyl-1-octanol), and are not formed from the coupling of bulkier alcohols (>C_{16}). In addition, the reactivity of Guerbet alcohols decreases with increasing bulkiness.

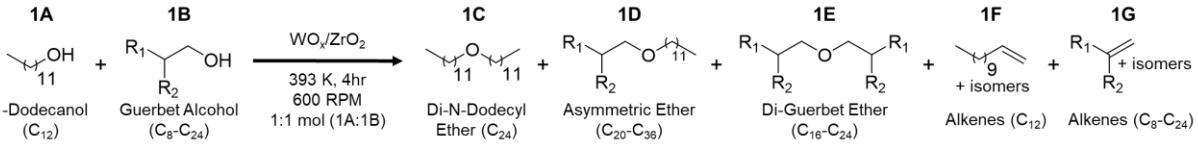

Scheme 3.2. Pathways for 1-dodecanol etherification and dehydration with varying Guerbet alcohols (C_8-C_{24}) over tungstated zirconia.

Table 3.4. Effect of branch length of Guerbet alcohols on the selectivity of ethers and alkenes in reaction with 1-dodecanol.

Guerbet Alcohol	R_1	R_2	Conversion of 1A (%)	Dodecanol Selectivity (%)			Conversion of 1B (%)	Guerbet Alcohol Selectivity (%)		
				1C	1D	1F		1D	1E	1G
2-Ethyl-1-Hexanol	4	2	14	63	20	16	33	11	3	86
2-Butyl-1-Octanol	6	4	18	69	16	15	26	11	1	89
2-Hexyl-1-Decanol	8	6	21	71	10	20	13	18	0	82
2-Octyl-1-Dodecanol	10	8	23	72	7	21	9	20	0	80
2-Decyl-1-Tetradecanol	12	10	23	72	6	22	3	17	0	83

Reaction Conditions: 393 K, 4 h, 100 mg WO_x/ZrO_2 (12.6 wt% W), 600 RPM, $5.6*10^{-4}$ mol 1-dodecanol, $5.6*10^{-4}$ mol Guerbet alcohol, $3.9*10^{-4}$ mol n-tetradecane as internal standard.

The relatively low selectivity towards branched ethers from the etherification of Guerbet alcohols is likely due to the relatively low activation barrier for unimolecular dehydration of alcohols with substitution on the β-carbon. From Table 3.3, the addition of methyl branches affected the selectivity to ether to a lesser extent when the branch was 3 carbons away from the –OH group. Thus it was hypothesized that etherification of a longer chain branched alcohol with the branch further down the carbon chain would result in higher selectivity to ether than a Guerbet alcohol of the same chain length. To test this, the model compound 4-hexyl-1-dodecanol was synthesized and reacted over tungstated zirconia at 393 K, as shown in Scheme 3.3. The synthesis and characterization of 4-hexyl-1-dodecanol is detailed in the Supporting Information.

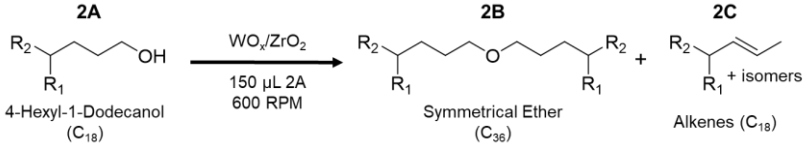

Scheme 3.3. Reaction of 4-Hexyl-1-Dodecanol over tungstated zirconia.

Table 3.5. Etherification and dehydration of 4-hexyl-1-dodecanol.

Alcohol	R_1	R_2	Temperature [K]	Reaction Time [h]	Conversion of Alcohol (%)	Selectivity (%)	
						Ether	Alkenes
4-Hexyl-1-Dodecanol	6	8	393	4	23	40	60
4-Hexyl-1-Dodecanol	6	8	383	4	11	49	51
4-Hexyl-1-Dodecanol	6	8	383	16	22	52	48

Reaction Conditions: 600 RPM, 100 mg WO_x/ZrO_2 (12.6 wt% W), 600 RPM, 150 µL 4-hexyl-1-dodecanol, $3.9*10^{-4}$ mol n-tetradecane as internal standard. Note: 10% mass balance missing for 16 h reaction.

From Table 3.5, it can be observed that there is significant improvement in selectivity to ether for the C_{18} alcohol when the branching position is further away from the –OH group, reaching 40% selectivity to ether (2B) at a conversion of 23% at 393 K. Upon lowering the temperature to 383 K, the selectivity was further increased to 49%, which is expected as etherification was shown to be more favorable at lower temperatures. The results given in Table 3.4 indicate that 2-hexyl-1-decanol (C_{16}) and 2-octyl-1-dodecanol (C_{20}) do not produce symmetrical ethers in reactions with 1-dodecanol over tungstated zirconia. For additional comparison, Guerbet alcohols 2-hexyl-1-decanol and 2-octyl-1-dodecanol were also reacted over tungstated zirconia under the same

conditions as those used for the reaction of 4-hexyl-1-dodecanol in the absence of 1-dodecanol. No ether was detected for either of these reactions (Table 3.11, Supporting Information).

Thus, placing the branch further away from the –OH group of the alcohol significantly improves the selectivity to ether. This raises the question of how branched alcohols with branches further down the carbon chain could be produced from biomass. One potential route would be to start with the condensation of biomass-derived furfural and 2-methyl-furan,[105] then selectively hydrogenate to produce 5-pentyl-1-decanol, which could further be reacted over an acid catalyst to form ether, as shown in Scheme 3.4.

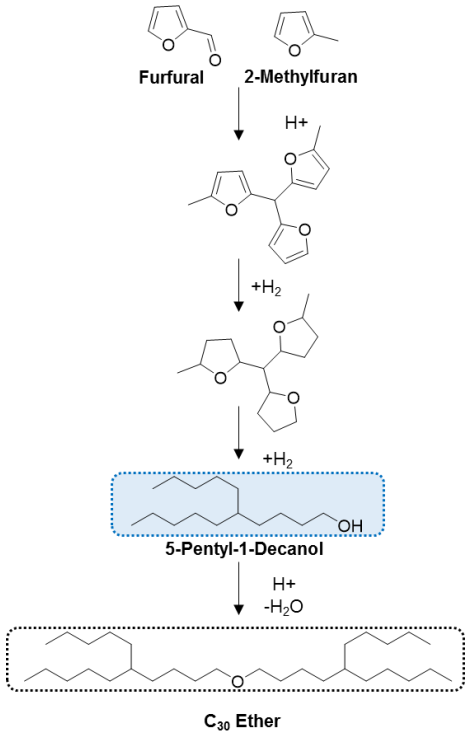

Scheme 3.4. Proposed route to produce branched lubricants from biomass-derived platform molecules.

V. Conclusions

Tungstated zirconia was identified as an effective solid acid catalyst for the direct etherification of primary linear alcohols in the liquid phase. The effect of alcohol structure on etherification and dehydration reactions was studied by investigating the effects of alcohol length, positions of carbon chain branches, and size of carbon chain branches. The rate of dehydration relative to etherification was shown to increase with increasing temperature, which is consistent with the thermodynamic preference for dehydration with increasing temperature. The positions of carbon chain branches were shown to have significant effects on ether selectivity. Addition of carbon chain branches to the α and β carbons on the alcohol were shown to increase the dehydration selectivity, which is consistent with the mechanism proposed in an earlier work. It was also demonstrated that alcohols with carbon chain branching at least 3 carbons away from the –OH group exhibit significantly higher ether selectivity than corresponding alcohols with branches on the α- or β-carbons. Activation energy trends for etherification and dehydration provided a more complete explanation for the ether selectivity trends observed over a range of alcohol structures. Understanding the effects of alcohol structure on direct etherification reactions is crucial for utilizing biomass-derived alcohols to make diesel additives, lubricants, and specialty chemicals.

VI. Supporting Information

i. Initial Rates, Selectivities, and Activation Energies

Table 3.6. Initial rates, apparent activation energies, and apparent pre-exponential factors for linear alcohol etherification reactions.

Reactant	$R_{o,ether}$ [a] [μmol kg^{-1} s^{-1}]						$E_{A,app}$ [b] [kJ mol^{-1}]
	393 K	398 K	403 K	408 K	413 K	418 K	
1-Hexanol	32	55	79	118	180	272	127 ± 1
1-Heptanol	29	46	73	199	173	264	127 ± 2
1-Octanol	35	57	96	141	219	315	126 ± 3
1-Nonanol	40	57	87	121	178	280	127 ± 1
1-Decanol	39	67	96	184	278	436	126 ± 12
1-Undecanol	38	66	92	167	255	357	126 ± 4
1-Dodecanol	35	49	66	120	168	292	127 ± 7

[a] Initial rates for 0^{th} order region ($r_o=k_{app}$), [b] apparent activation energy for ether formation fit using Arrhenius equation $r_o=k_{app}=Ae^{-EAapp/RT}$, with pre-exponential factor (A) fixed at $2.12*10^{18}$ μmol kg^{-1} s^{-1}. Reaction Conditions: 564 μmol reactant, 125 μmol n-tetradecane, 100 mg WO_x/ZrO_2 (12.6 wt% W).

Table 3.7. Initial rates, apparent activation energies, and apparent pre-exponential factors for linear alcohol dehydration reactions.

Reactant	$R_{o,alkene}$ [a] [μmol kg^{-1} s^{-1}]			$E_{A,app}$ [b] [kJ mol^{-1}]
	408 K	413 K	418 K	
1-Hexanol	38	56	97	157 ± 13
1-Heptanol	71	119	185	155 ± 11
1-Octanol	89	145	236	154 ± 1
1-Nonanol	63	109	193	155 ± 7
1-Decanol	59	102	203	155 ± 11
1-Undecanol	75	135	228	154 ± 5
1-Dodecanol	64	112	158	155 ± 10

[a] Initial rates for 0^{th} order region ($r_o=k_{app}$), [b] apparent activation energy for alkene formation fit using Arrhenius equation $r_o=k_{app}=Ae^{-EAapp/RT}$, with pre-exponential factor (A) fixed at $3.84*10^{21}$ μmol kg^{-1} s^{-1}. Reaction Conditions: 564 μmol reactant, 125 μmol n-tetradecane,100 mg WO_x/ZrO_2 (12.6 wt% W).

Table 3.8. Initial rates, apparent activation energies, and apparent pre-exponential factors for C6 alcohol etherification reactions.

Reactant	$R_{o,ether}$ [a] [μmol kg^{-1} s^{-1}] Temperature [K]												$E_{A,app}$ [b] [kJ mol^{-1}]
	333	338	343	373	378	383	393	398	403	408	413	418	
1-Hexanol	-	-	-	-	-	-	32	55	79	118	180	272	127 ± 1
4-Methyl-1-Pentanol	-	-	-	-	-	-	29	-	-	124	182	272	127 ± 3
3-Methyl-1-Pentanol	-	-	-	-	-	-	25	-	-	102	156	238	127 ± 1
2-Methyl-1-Pentanol	-	-	-	-	-	-	-	8	14	22	-	-	133 ± 11
2-Hexanol	-	-	-	11	19	36	-	-	-	-	-	-	127 ± 10
2-Methyl-2-Pentanol	0	0	0	-	-	-	-	-	-	-	-	-	-

[a] Initial rates for 0^{th} order region ($r_o=k_{app}$), [b] apparent activation energy for ether formation fit using Arrhenius equation $r_o=k_{app}=Ae^{-EAapp/RT}$, with pre-exponential factor (A) fixed at $2.12*10^{18}$ μmol kg^{-1} s^{-1}. Reaction Conditions: 564 μmol reactant, 125 μmol n-tetradecane, 100 mg WO_x/ZrO_2 (12.6 wt% W) for 1-hexanol, 4-methyl-1-pentanol, 3-methyl-1-pentanol, 50 mg WO_x/ZrO_2 (12.6 wt% W) for 2-methyl-1-pentanol, 2-hexanol, and 2-methyl-2-pentanol.

Table 3.9. Initial rates, apparent activation energies, and apparent pre-exponential factors for C6 alcohol dehydration reactions.

Reactant	$R_{o,alkene}$ [a] [µmol kg^{-1} s^{-1}] Temperature [K]												$E_{A,app}$ [b] [kJ mol^{-1}]
	333	338	343	373	378	383	393	398	403	408	413	418	
1-Hexanol	-	-	-	-	-	-	-	-	-	38	56	97	157 ± 13
4-Methyl-1-Pentanol	-	-	-	-	-	-	-	-	-	26	35	49	158 ± 10
3-Methyl-1-Pentanol	-	-	-	-	-	-	12	-	-	59	91	125	155 ± 1
2-Methyl-1-Pentanol	-	-	-	-	-	-	61	101	159	243	-	-	124 ± 2
2-Hexanol	-	-	-	205	329	487	-	-		-	-		114 ± 5
2-Methyl-2-Pentanol	393	760	1,167	-	-	-	-	-	-	-	-	-	100 ± 12

[a] Initial rates for 0^{th} order region ($r_o=k_{app}$), [b] apparent activation energy for alkene formation fit using Arrhenius equation $r_o=k_{app}=Ae^{-EAapp/RT}$, with pre-exponential factor (A) fixed at $3.84*10^{21}$ µmol kg^{-1} s^{-1} for 1-hexanol, 4-methyl-1-pentanol, and 3-methyl-1-pentanol, and at $2.12*10^{18}$ µmol kg^{-1} s^{-1} for 2-methyl-1-pentanol, 2-hexanol, and 2-methyl-2-pentanol based off of best fit of linear regression. Reaction Conditions: 564 µmol reactant, 125 µmol n-tetradecane, 100 mg WO_x/ZrO_2 (12.6 wt% W) for 1-hexanol, 4-methyl-1-pentanol, 3-methyl-1-pentanol, 50 mg WO_x/ZrO_2 (12.6 wt% W) for 2-methyl-1-pentanol, 2-hexanol, and 2-methyl-2-pentanol.

Table 3.10. Selectivity to Ether for C_6 alcohol dehydration reactions.

Reactant	Temperature [K]	Selectivity to Ether [%]
1-Hexanol	408	86
	413	87
	418	85
4-Methyl-1-Pentanol	408	91
	413	91
	418	92
3-Methyl-1-Pentanol	408	78
	413	77
	418	79
2-Methyl-1-Pentanol	398	14
	403	15
	408	15
2-Hexanol	373	10
	378	10
	383	13
2-Methyl-2-Pentanol	333	0
	338	0
	343	0

Reaction Conditions: 564 µmol reactant, 125 µmol n-tetradecane, 100 mg WO_x/ZrO_2 (12.6 wt% W) for 1-hexanol, 4-methyl-1-pentanol, 3-methyl-1-pentanol, 50 mg WO_x/ZrO_2 (12.6 wt% W) for 2-methyl-1-pentanol, 2-hexanol, and 2-methyl-2-pentanol.

ii. Reactions of Guerbet Alcohols in the Absence of Solvent

Table 3.11. Reaction of Guerbet Alcohols in Absence of Solvent

Alcohol	Temperature [K]	Reaction Time [h]	Selectivity (%)	
			Symmetrical Ether	Alkenes/ Other
2-Hexyl-Decanol	393	4	0	>99
2-Octyl-Dodecanol	393	4	0	>99

Reaction Conditions: 600 RPM, 100 mg WO_x/ZrO_2 (12.6 wt% W), 600 RPM, $5.0*10^{-4}$ mol alcohol, $3.9*10^{-4}$ mol n-tetradecane as internal standard.

iii. Sample Time Course for Dodecanol Etherification

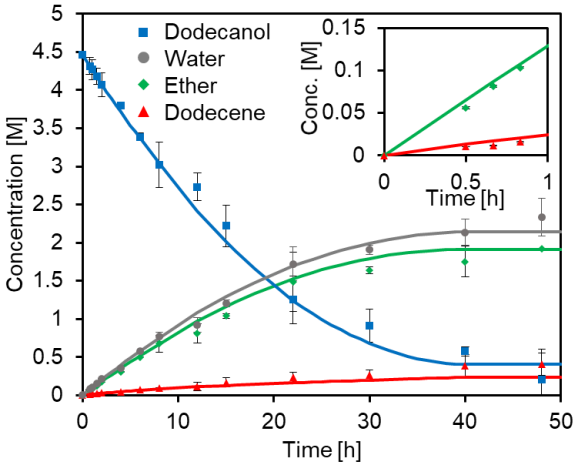

Figure 3.5. a) Time course study of 1-dodecanol reaction over WO_x/ZrO_2 (12.6 wt% W) from 0-50 hours. Reaction conditions: 393 K, 600 RPM, 100 mg catalyst, 240 mg 1-dodecanol, inset: linear portion of time course study where reaction is zero order in all species.

iv. Arrhenius Plots

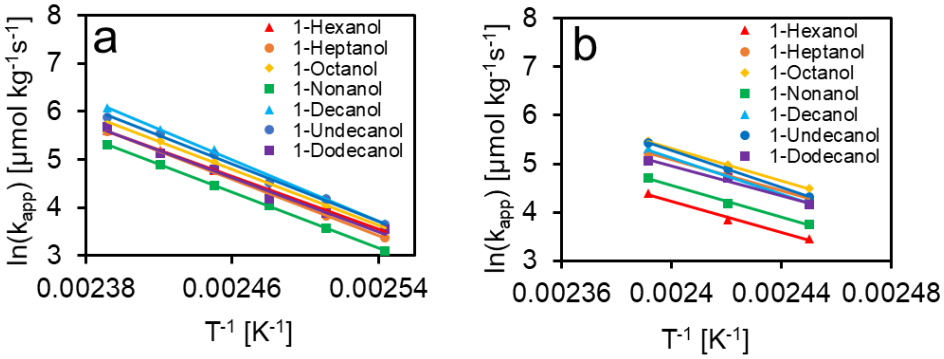

Figure 3.6. Arrhenius plots for a) etherification, and b) dehydration of linear alcohols (C_6-C_{12}) over tungstated zirconia.

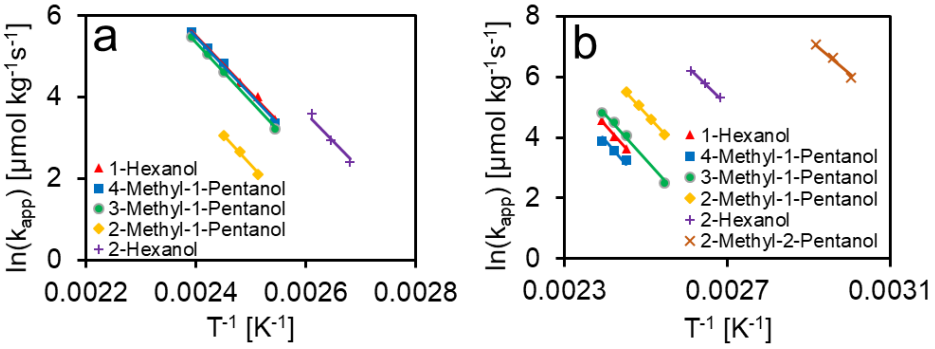

Figure 3.7. Arrhenius plots for etherification (a), and dehydration (b) of C_6 alcohols (1-hexanol, 2-methyl-1-pentanol, 3-methyl-1-pentanol, 2-methyl-1-pentanol, 2-hexanol, and 2-methyl-2-pentanol) over tungstated zirconia.

v. Synthesis and Characterization of 4-Hexyl-1-Dodecanol

Synthesis of 4-hexyldodecan-1-ol:

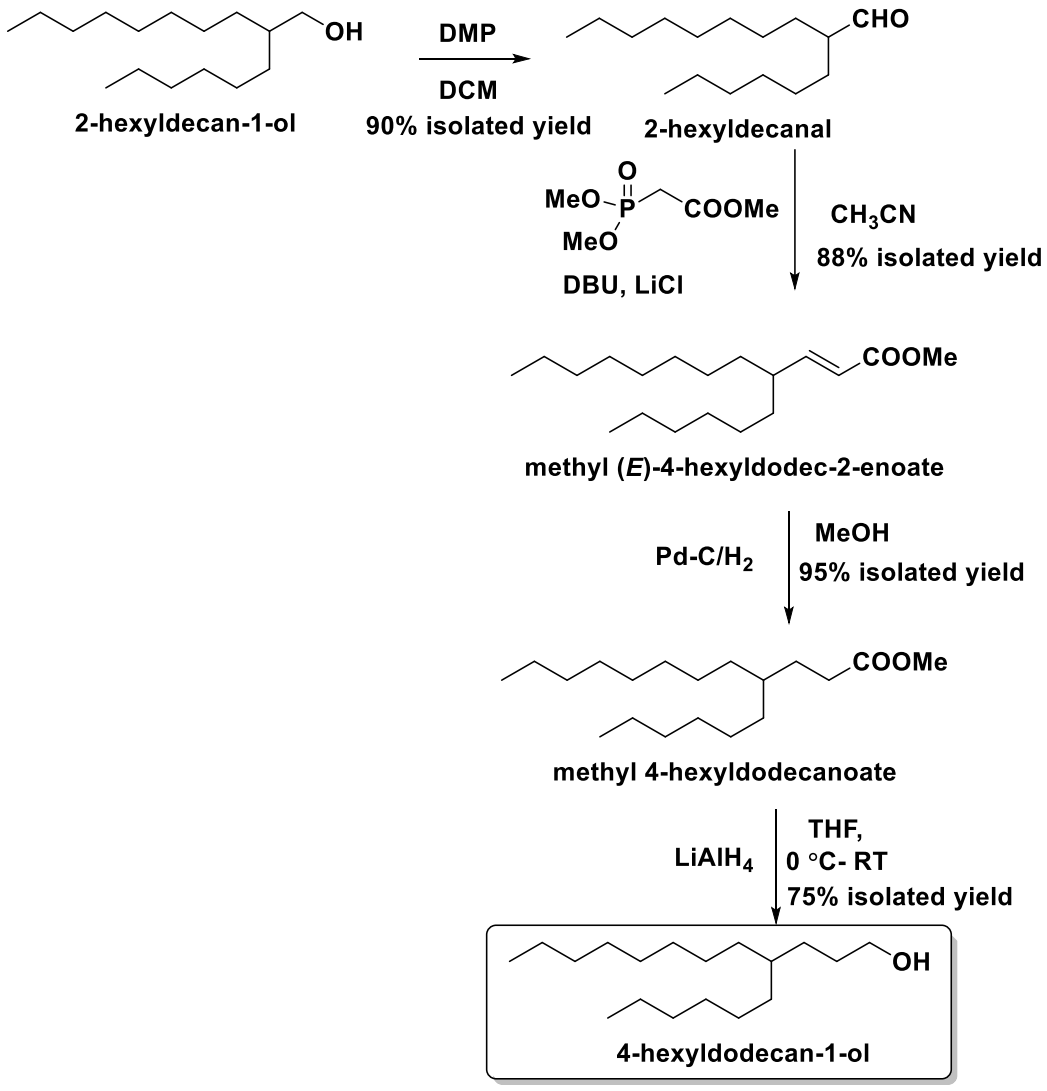

Synthesis of 2-hexyldecanal:

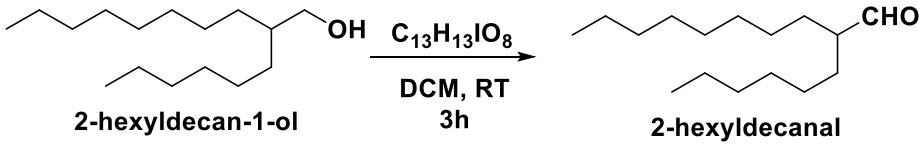

A 500 mL round bottomed flask was loaded with 2-hexyldecan-1-ol (16.5 mmol, 1.0 equiv.), Dess–Martin periodinane (DMP) (24.75 mmol, 1.5 equiv.) and DCM under argon. The reaction mixture was continuously stirred at room temperature until all of the starting material was consumed, as indicated by TLC. At this stage, the reaction mixture was diluted with ether, and washed with a 1:1 mixture of 10% $Na_2S_2O_3$ and saturated aqueous $NaHCO_3$, followed by water and brine. The organic layer was dried over anhydrous Na_2SO_4, and concentrated under vacuum. The crude mixture was purified by column chromatography with hexanes to give the desired compound in 90% yield (14.97 mmol). The NMR is in agreement with literature.[106]

Procedure for the synthesis of methyl (E)-4-hexyldodec-2-enoate:

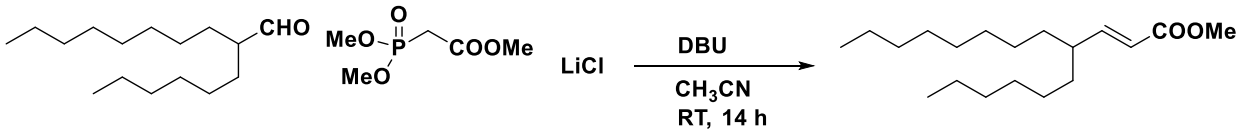

In a round bottomed flask, LiCl (19.96 mmol, 1.2 equiv.) was suspended in dry acetonitrile (50 mL), under argon at room temperature phosphonate (19.96 mmol, 1.2 equiv.), DBU (16.64 mmol, 1.0 equiv.) and aldehyde (16.64 mmol, 1.0 equiv.) were added respectively. The reaction mixture was stirred at room temperature for 14 hours; at this stage reaction mixture was diluted with ether and washed with saturated aqueous NH_4Cl and brine. The ether layer was dried over anhydrous Na_2SO_4, and concentrated under vacuum. The crude mixture was purified by column chromatography (Hexanes → 32:1 Hexanes and ethyl acetate) to give desired compound in 88% yield (14.97 mmol)

^{1}H NMR (400 MHz, $CDCl_3$) δ 6.73 (ddt, *J* = 14.8, 9.5, 2.6 Hz, 1H), 5.84 – 5.65 (m, 1H), 3.72 (q, *J* = 5.1, 3.9 Hz, 3H), 2.10 (dt, *J* = 9.7, 4.5 Hz, 1H), 1.23 (trace quantities of grease and other aliphatic hydrocarbons, m, 29H), 0.86 (d, *J* = 6.1 Hz, 6H).

Procedure for the synthesis of methyl 4-hexyldodecanoate:

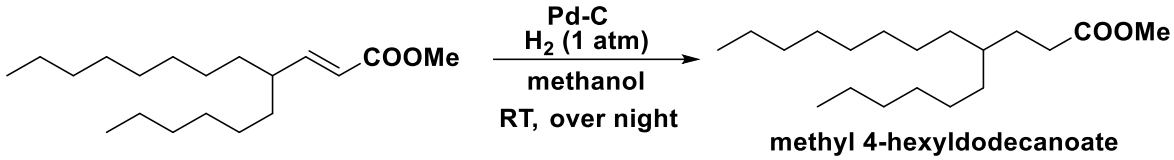

A 100 mL round bottomed flask was loaded with methyl (E)-4-hexyldodec-2-enoate (15.0 mmol), 10% Pd-C (450mg) and 45 mL methanol. The reaction mixture was purged and equipped with a hydrogen balloon and stirred at room temperature overnight. The resulted reaction mixture was passed through celite pad and the filter cake was washed with methanol. The filtrate was concentrated under vacuum to give the desired methyl 4-hexyldodecanoate in 95% yield and the product was used for next step without any further purification.

^{1}H NMR (400 MHz, $CDCl_3$) δ 3.63 (s, 3H), 2.35 – 2.12 (m, 2H), 1.66 – 1.48 (m, 2H), 1.37 – 1.08 (m, 27H), 0.85 (t, *J* = 6.8 Hz, 6H);

Procedure for the synthesis of 4-hexyldodecan-1-ol:

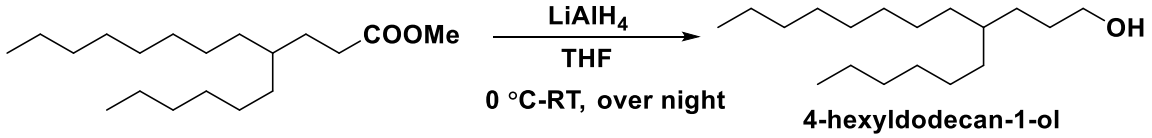

Methyl 4-hexyldodecanoate (13.4 mmol, 1 equiv.) in THF was added to a suspension of LAH (29.5 mmol, 2.2 equiv.) in THF under argon at 0 °C for 10 minutes. The reaction mixture was warmed to room temperature and stirred overnight. The reaction mixture was then poured into ice water slowly and acidified to pH=3 with 1N HCl and was then extracted with ethyl acetate. The organic layer was dried over anhydrous Na_2SO_4, and concentrated under vacuum. The crude mixture was purified by column chromatography with DCM to give the desired compound in 74% yield (9.98 mmol).

^{1}H NMR (600 MHz, $CDCl_3$) δ 3.62 (t, *J* = 6.7 Hz, 2H), 1.69 – 1.45 (m, 2H), 1.31 – 1.21 (m, 28H), 0.88 (t, *J* = 7.0 Hz, 6H); ^{13}C NMR (151 MHz, $CDCl_3$) δ 63.7, 37.4, 33.8, 32.1, 32.1, 30.3, 30.1, 29.9, 29.8, 29.7, 29.5, 26.8, 26.8, 22.9, 22.8, 14.3, 14.3.

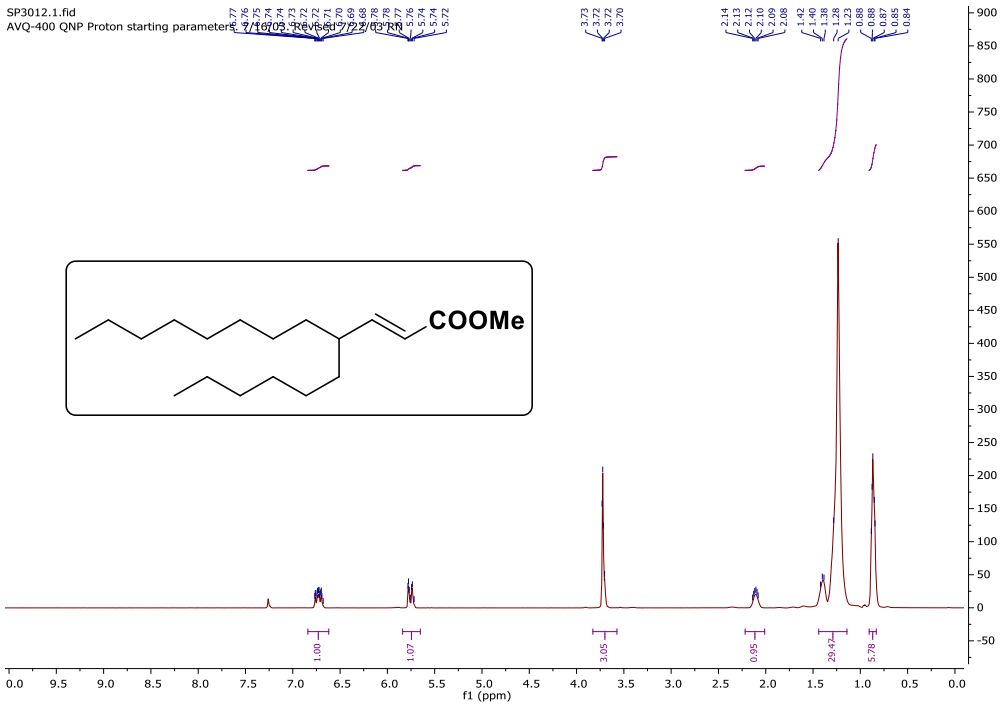

Figure 3.8. ^{1}H NMR of methyl (E)-4-hexyldodec-2-enoate.

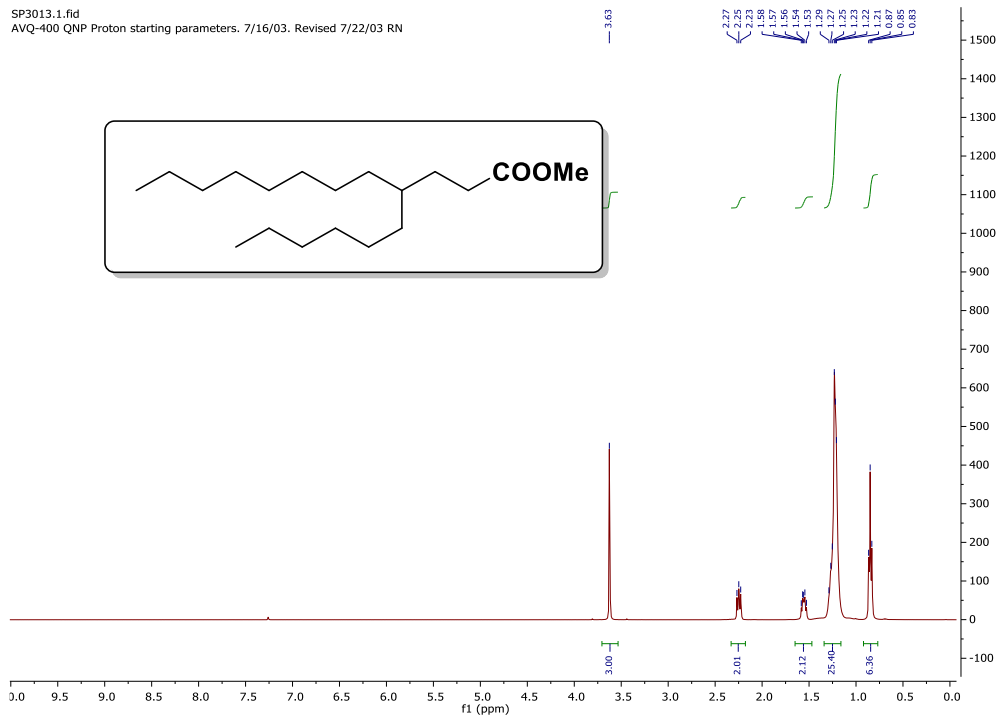

Figure 3.9. ^{1}H NMR of methyl 4-hexyldodecanoate.

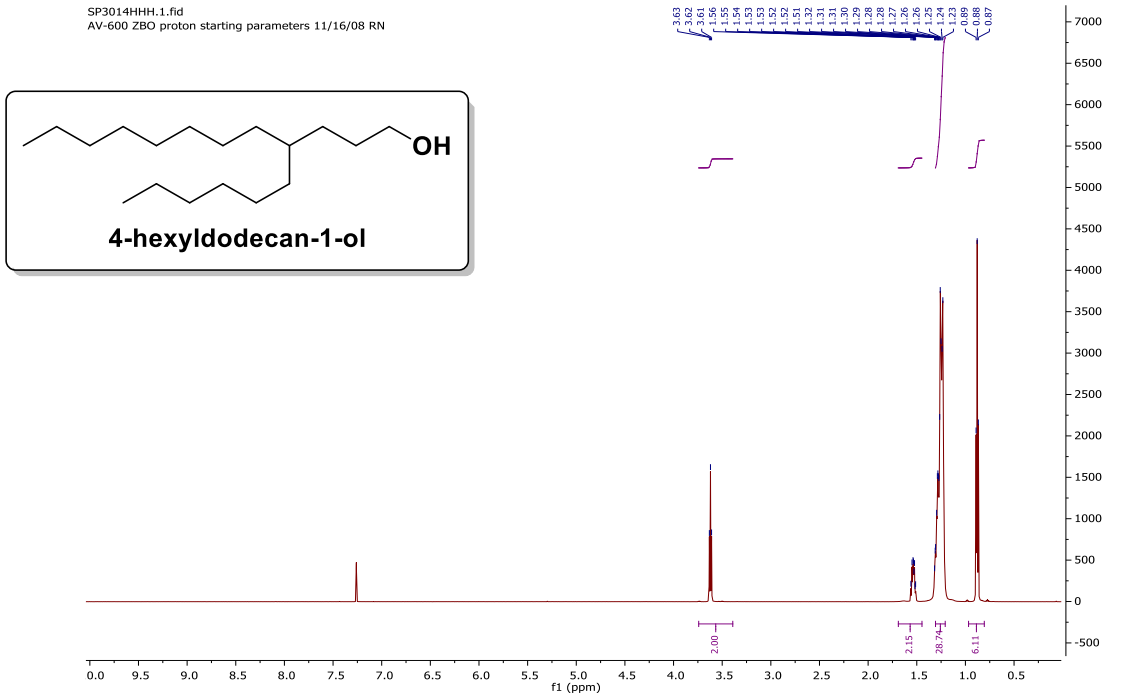

Figure 3.10. ^{1}H NMR of 4-hexyldodecan-1-ol.

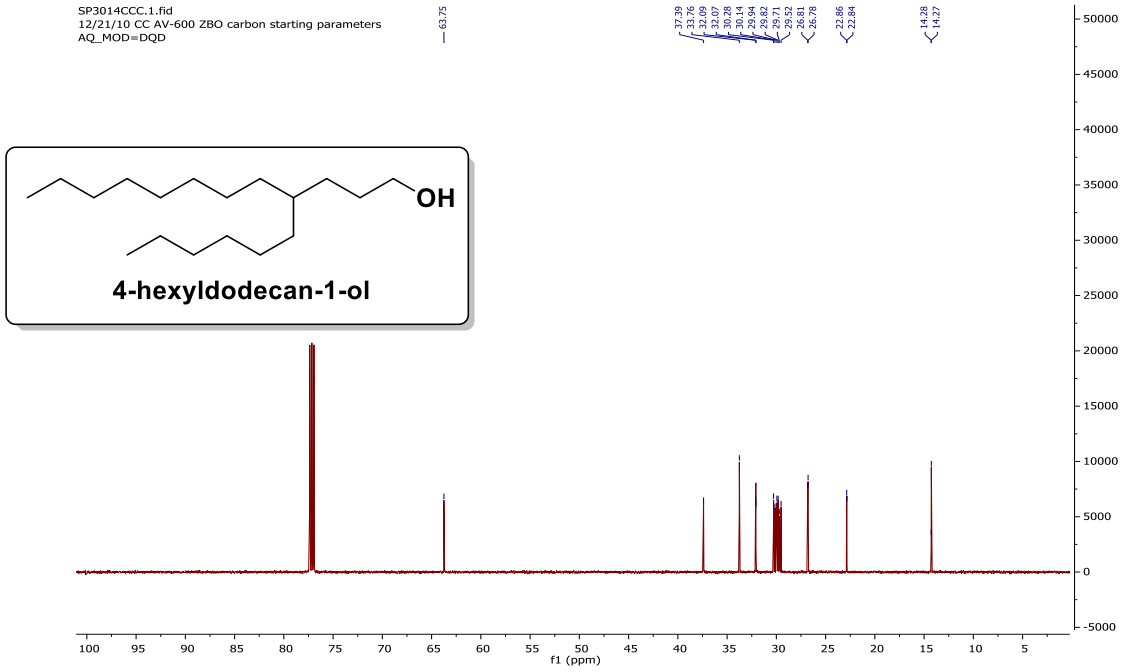

Figure 3.11. ^{13}C NMR of methyl 4-hexyldodecan-1-ol.

4. Synthesis of Biomass-Derived Ethers for Use as Fuels and Lubricants[**]

I. Abstract

Ethers synthesized from biomass-derived compounds have exceptional properties as fuels, lubricants, and specialty chemicals, and can serve as replacements for petroleum-derived products. Recent efforts have identified heterogeneous catalysts for the selective synthesis of ethers from alcohols, aldehydes, ketones, furans, esters, olefins, carboxylic acids, and other molecules derived from biomass. This chapter highlights the scope of etherification reactions and provides insights into the choice of catalysts and reaction conditions best suited for producing targeted ethers from the available starting materials. We start by noting the properties of ethers for specific applications and then discuss the methods by which synthons for ether synthesis can be obtained from biomass. We then summarize progress made on the synthesis of ethers via direct etherification of alcohols; reductive etherification of alcohols with aldehydes or ketones; etherification of furanic compounds, esters, and carboxylic acids; and the addition of alcohols to olefins. Next, we discuss the mechanisms of these reactions and catalyst properties required to promote them with the goal of understanding how reaction conditions can be tuned to optimize catalyst activity and selectivity towards desired ethers. We close by examining the tradeoffs between catalyst selectivity, activity, stability, and reaction conditions required to achieve the most economically and environmentally favorable routes to biomass-derived ethers.

II. Introduction

In Chapters 2 and 3 of this dissertation, the direct etherification of biomass-derived alcohols over tungstated zirconia was investigated. First, the mechanism and kinetics of the etherification and dehydration of 1-dodecanol was studied, followed by a comprehensive investigation of the effect of alcohol structure on the kinetics of etherification and dehydration over tungstated zirconia. The objective of this chapter is to review recent reports of ether synthesis from biomass-derived platform molecules and understand how heterogeneous catalysts promote these reactions. To this end, we examine the roles of Brønsted and Lewis acid sites on the reaction mechanism and the role of substrate composition and structure. The ultimate aim is to identify the combination of catalyst properties required to achieve high ether selectivity for a specified class of synthons. Meeting this objective is not easy since etherification can occur by direct etherification of alcohols and reductive etherification alcohols with aldehydes, furans, ketones, carboxylic acids, esters, and olefins. The etherification of glycerol is also discussed briefly, since several recent reviews have discussed glycerol conversion to ethers,[107,108] solketal,[109,110] acrolein,[111–115] propylene glycol,[116] polymers,[117,118] propanediols,[119,120] glycerol oxidation products,[121] fuel additives,[108,122] and other value-added products.[117,122–124] Williamson ether synthesis and other homogeneous routes are not discussed, since these processes require catalyst separation and produce salts.[25,125] Instead, we focus exclusively on the use of heterogeneous catalysts due to their ease of separation from products.

This chapter begins by discussing the fuel and lubricant properties of ethers obtained by the etherification of biomass-derived platform molecules, and the methods for sourcing these molecules from biomass. This is followed by a discussion of ether formation via direct etherification of alcohols, reductive etherification of alcohols and carbonyl compounds, and etherification of olefins with alcohols. Through this discussion, we describe the reaction conditions

[**] This chapter is adapted from a Review paper published in *ChemSusChem*.[233]

and catalyst properties required for selective ether synthesis, and specifically discuss the role of cooperative effects between Brønsted and Lewis acid sites in controlling ether selectivity. Finally, we offer a roadmap for producing targeted ethers from available starting materials in high selectivity by utilizing knowledge of the effects of reactant structure, catalyst properties, and reaction conditions.

III. Applications and Fuel and Lubricant Properties of Biomass-Derived Ethers

Figure 4.1 shows some example structures of ethers synthesized from biomass-derived molecules that have properties making them suitable as diesel fuels, cetane boosters, octane boosters, automotive lubricants, and other products. Ethers that could serve as diesel are shown in Table 4.1. Symmetrical, linear ethers such as di-n-hexyl ether and di-n-octyl ether have high energy density and high cetane numbers, which allows for decreased ignition delay in diesel vehicles.[19,21,46,47] Addition of di-ethyl ether to ethanol biodiesel blends also reduces the ignition delay, exhaust gas oxygen, smoke emissions, and particulate matter.[126] Linear asymmetrical ethers such as ethyl-octyl ether and butyl-hexyl ether also have high cetane numbers and can be added to diesel blends.[19,20]

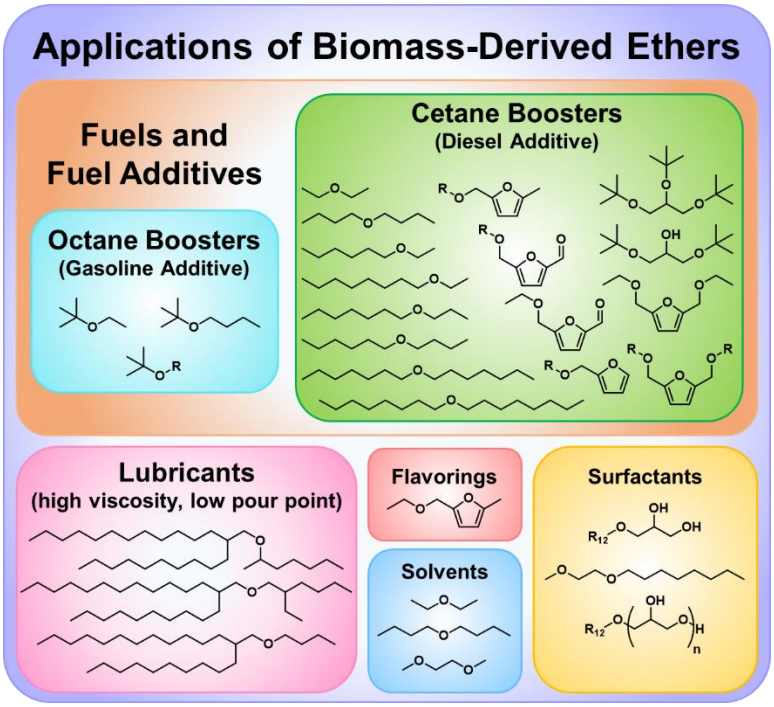

Figure 4.1. Applications of selected biomass-derived ethers.

For use as gasoline additives, shorter chain branched ethers are suitable due to their high octane numbers.[16] The increased substitution of the ether results in a higher ignition delay, allowing the fuel to be used in gasoline engines, which operate at high compression ratios. An example is ethyl-*tert*-butyl ether (ETBE), which has an octane number of 112.[15] Not only can ETBE be produced from renewable sources, but it also has a higher boiling point, a lower flash point, lower blending Reid vapor pressure, and lower solubility in water than methyl-*tert*-butyl ether.[15,127] Over the years, the global consumption of ETBE for use in gasoline has increased as ETBE has excellent gasoline additive properties but has reduced environmental toxicity and

improved biodegradability compared to MTBE, is less soluble in water, and utilizes renewable ethanol.[15,122,128]

Table 4.1. Representative linear alkyl ethers and selected diesel fuel properties.

Ether	Blending Cetane Number [BCN]	Blending Cloud Point [BCP °C]	Blending Cold Filter Plugging Point [BCFPP °C]
 di-methyl-ether	55-66[129]		
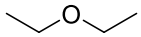 di-ethyl-ether	>125[129]		
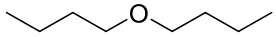 di-n-butyl ether	85[19]	-20[19]	-13[19]
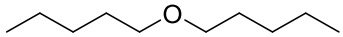 di-n-pentyl ether	109[19]	-22[19]	-20[19]
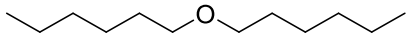 di-n-hexyl ether	117[19]	-7[19]	-5[19]
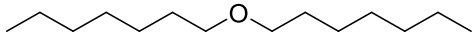 di-n-heptyl ether	117[19]	-7[19]	-5[19]
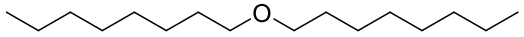 di-n-octyl ether	118[19], 119[130]	-17[19,130]	-15[19,130]
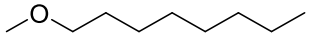 methyl-octyl ether	89 [20]		
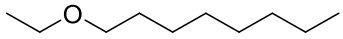 ethyl-octyl ether	100[19], 98[20]		
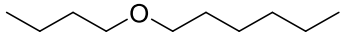 n-butyl-hexyl ether	94[19]		
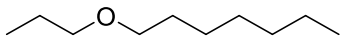 n-heptyl propyl ether	94[19]		
Reference: diesel fuel	48–51 [20,130]	-2 to 5[130]	-4 to 3 [130]

Mono-ethers and di-ethers derived from furans such as 5-(ethoxymethyl)furfural-2-carboxaldehyde (EMF) and 2,5-bis(ethoxymethyl)furan (BEMF) have excellent cetane numbers and can be added to diesel or used as a drop-in fuel.[131–133] EMF has an energy density of 8.7 kWh L^{-1}, comparable to gasoline (8.8 kWh L^{-1}) and diesel (9.7 kWh L^{-1}), and superior to that of ethanol (6.1 kWh L^{-1}).[132]

Ethers derived from biomass also have the potential to replace petroleum-derived automotive lubricants.[22,134,135] Transportation vehicles consume almost 30% of energy produced today, and of that, approximately one third is lost due to friction and wear.[136,137] This gives rise to a global demand for lubricants of around 35 million tonnes per year, with automotive lubricants accounting for about 15% of the total lubricant consumption.[138] The performance of automotive lubricants is judged by a number of criteria, including the kinematic viscosity at 40 °C and 100 °C, (KV100 and KV40, respectively), the viscosity index (VI), the pour point (PP), the oxidation stability (DSC onset T), the volatility (TGA Noack), and the cold-cranking simulator viscosity (CCS). The current synthetic automotive lubricant consists of poly-alpha-olefins (PAO), which are derived from petroleum via the oligomerization of α-olefins.[51,52] However, as shown in Table 4.2, recent reports have shown that branched ethers such as 11-(((2-ethylhexyl)oxy)methyl)-tricosane have comparable lubricant properties, and can be synthesized from renewable sources.[22] Branches in the alkyl portions of ethers lower the pour point and raise the viscosity of the ether, enhancing

the lubricant properties.[22,50] Other ethers such as alkylated di-phenyl ether and glycerol ethers have excellent lubricant properties.[48,49] Glycerol ethers and poly-ethers also have applications as surfactants[24,139] and fuel additives.[108] Monododecyl polyglyceryl ether (MAGEn) and multidodecyl polyglyceryl ethers produced from the etherification of glycerol with dodecanol have excellent surfactant properties.[139] Other monoether glyceryl ethers have been shown to have pharmaceutical applications such as anti-inflammatory, antibacterial, anti-tumor, and antifungal properties.[140–142] Di- and tri-*tert*-butyl ethers are soluble in diesel fuel, and can be added as oxygenates to decrease the viscosity and cloud points.[143–146]

Table 4.2. Comparison of Lubricant Properties of PAO and C32 Ether (Ref. 22)

	KV100 [cSt]	KV40 [cSt]	VI	PP °C	DSC oxidation onset T [8C]	TGA Noack [wt.%]	CCS [cP]
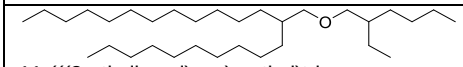 11-(((2-ethylhexyl)oxy)methyl)tricosane	3.5	12.0	145	-36	206	5.1	769
Reference: Poly-Alpha-Olefins (PAO)	4.0	17.8	126	-75	221	18.8	1276

One of the important considerations in utilizing ethers as fuels and lubricants is their propensity to form peroxides. There is a delicate balance with peroxide formation, because some peroxide formation is beneficial for ignition properties of the fuel, but too much peroxide formation can lead to stability and safety concerns. The peroxide number is a measure of a tendency for a material to form peroxides.[147,148] Compounds are classified based upon their peroxide numbers in order to ensure safe handling. For example, diethyl ether is classified as a group B compound for peroxide formation, meaning it must be discarded or used after one year of storage.[148] On the other hand, MTBE forms peroxides more slowly than tetrahydrofuran (THF), 2-methyl-THF, and 2,5-dimethyl furan.[148] Another important consideration is the fact that the addition of oxygenates to fuel blends also impacts the exhaust emissions, lowering carbon monoxide emissions and other unregulated emissions such as benzene and 1,3-butadiene.[92] A review by Di Nicola et al. provides greater detail about emissions from ethers and organic carbonate fuel additives.[92]

IV. Platform Molecules from Biomass-Derived Feedstocks

A variety of synthons derived from the carbohydrate fraction of biomass can be used to produce ethers. These include aldehydes, ketones, alcohols, and furans. Scheme 4.1 illustrates pathways for producing these synthons starting from C_5 and C_6 sugars. Recent investigations of ABE fermentation of glucose using *clostridium acetobutylicum* have shown that a mixture of butanol, acetone, and ethanol can be produced with the molar ratio of 6:3:1.[11,12] These products can be further upgraded to afford higher carbon number alcohols and ketones, such as 2-pentanone, 2-heptanone, 4-heptanone, 6-undecanone, methyl isobutyl ketone (MIBK), and others.[13,149,150] Some of these same compounds can be prepared from furfural and 5-hydroxymethyl furfural (HMF) by the dehydration of xylose and glucose, respectively.[69,151,152]

Condensation of furfural with acetone in the presence of hydrogen produces 1-octanol.[44] Other linear alcohols such as 1-hexanol and 1-dodecanol can be accessed from glucose via engineered *Escherichia coli*[153] and via hydrolysis of triglycerides and fatty acids,[149] respectively. Furfural can be converted to 1-pentanol via hydrogenation to furfuryl alcohol, followed by hydrolysis to produce levulinic acid, which can then be hydrogenated to form 1-pentanol.[154,155]

The carbon number of linear alcohols can be further increased via the Guerbet pathway, which affords branched alcohols such as 2-ethyl-1-hexanol, 2-hexyl-1-decanol, 2-decyl-1-tetradecanol, and others.[45] Olefins derived from biomass are also useful synthons for producing ethers. For example, isobutene can be selectively formed from acetone or ethanol over zinc oxide dispersed on zirconia in the presence of water,[42,43] or via fermentation of biomass-derived sugars.[156] Other olefins such as octene, decene, and 2-ethyl hexene can be prepared via unimolecular dehydration of biomass-derived alcohols.

Glycerol is another abundant and inexpensive biomass-derived platform chemical obtained as a byproduct of biodiesel production. Sources of triglycerides for the generation of biodiesel include various vegetable oils, waste oil products, and algae.[8,9]

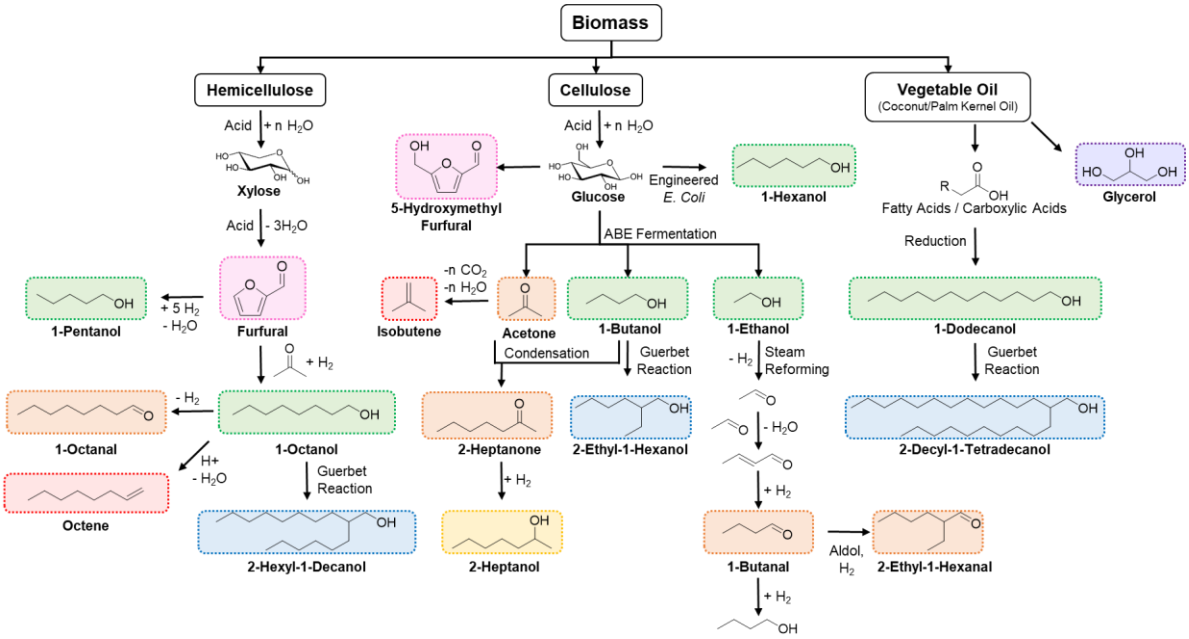

Scheme 4.1. Overview of processes for deriving alcohols, aldehydes, ketones, and furans from biomass-derived feedstocks

V. Synthesis of Ethers from Biomass-Derived Platform Chemicals

A number of different pathways are available for obtaining biomass-derived synthons for the production of ethers, as shown in Scheme 4.1. The choice of synthetic pathway depends on the composition of the feedstock and the desired final product and selectivity. In this section, we discuss the scope of direct etherification of alcohols, the reductive etherification of alcohols with aldehydes, ketones, esters, and carboxylic acids in the presence of hydrogen, direct and reductive etherification of furanic compounds, and the etherification of olefins by reaction with alcohols. For each of these methods, we examine the reaction mechanism and the activity and selectivity of known catalysts, and discuss adjustments that can be made to the reaction conditions in order to obtain the maximum product yield.

i. Direct Etherification of Alcohols

a) Direct Etherification of Linear and Branched Alcohols

Direct etherification of alcohols over a solid-acid catalyst involves the bimolecular dehydration of two alcohols in the absence of a reducing agent to produce ether and water, as

shown by the solid green arrow in Figure 4.2a. Solid-acid catalyzed etherification of alcohols in the liquid phase enables the production of ethers in a single phase, and can be performed in the presence of either a solvent, or using the alcohol as the solvent itself. One of the advantages of the latter approach is that it eliminates the need for solvent separation. Various polymeric resins, metal oxides, and other solid acid catalysts are effective for the direct etherification of linear alcohols. The competing reaction in the presence of an acid catalyst is unimolecular dehydration of the alcohol to form an olefin, a product that is thermodynamically favored over ether formation at elevated temperatures. For example, Figure 4.2b shows that the unimolecular dehydration of 1-dodecanol is thermodynamically favored over formation of di-dodecyl ether at temperatures above ~ 350 K.[99] Other linear and branched alcohols such as 1-hexanol, 2-hexanol, and 3-hexanol follow the same trend of increasing thermodynamic preference for unimolecular dehydration with increasing temperature.[157] Olefins are not desired in fuel and lubricant blends because they tend to form gums.[98] Moreover, as shown in Figure 4.2a, primary olefins can rehydrate to form secondary alcohols, which can result in the formation of branched ethers, which change fuel properties such as the cetane number.[158] Olefins can also oligomerize to form larger olefins and coke, resulting in catalyst deactivation. Other challenges with direct etherification are associated with the inhibiting effects of water and ether on reaction rates and ether selectivity.[32,99]

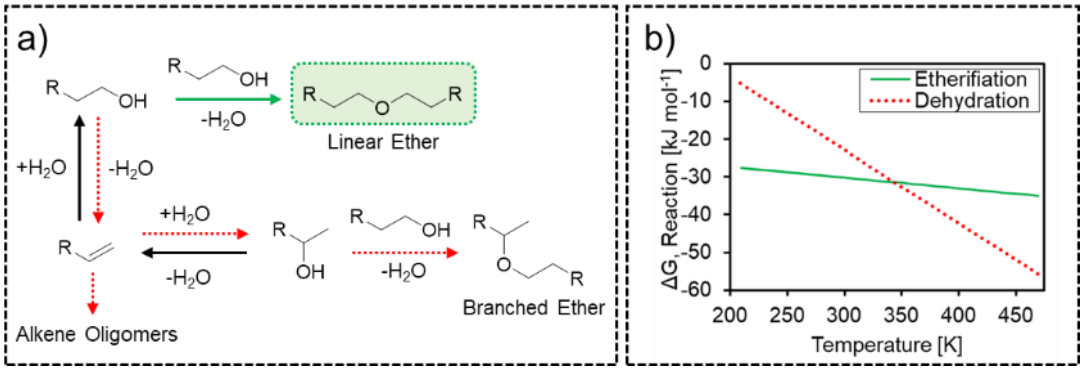

Figure 4.2. a) Reaction pathway for acid catalyzed direct etherification of alcohols (solid green arrow) and side product formation (dashed red arrows), b) Gibbs free energies of formation for 1-dodecanol etherification (green, solid) and unimolecular dehydration (red, dashed).

To achieve high ether selectivity, the catalyst must either operate at temperatures below the temperature at which unimolecular dehydration becomes thermodynamically preferred or have an intrinsic selectivity for etherification versus dehydration. The most desirable catalyst has high activity (turnover number), low activation energy for etherification, high selectivity for etherification, high thermal stability, and reusability. Table 4.3 lists several heterogeneous catalysts and reaction conditions that are effective for the direct liquid-phase etherification of linear alcohols to symmetrical ethers. The reported solid-acid catalysts employed for direct etherification include Brønsted acid catalysts, Lewis acid catalysts, and catalysts with both Brønsted and Lewis acid sites. Among these are acidic resins, metal oxides, and other solid-acid catalysts. The desired acid strength for etherification is not clearly defined, with some studies suggesting that etherification requires high acid site density and low acid strength,[19] and others suggesting that acid strength only affects rates but not selectivity.[83] Published studies suggest that bimolecular etherification of alcohols requires that two alcohol molecules interact favorably with one another. This condition can be achieved either by using a catalyst with strong acid sites located within large pores that provide a high local concentration of alcohol, or by using a catalyst with two proximate active sites for adsorption of both alcohols.

Table 4.3. Synthesis of symmetrical ethers via direct etherification of aliphatic alcohols catalyzed by solid acids.

Entry	Reactant	Catalyst	Temp. [K]	Sel. to di-Ether	TON *	E_A, Etherification [kJ/ mol]	E_A, Dehydration [kJ/mol]	Ref
1	1-pentanol	Amberlyst 70	423	98	2.7	114.7±5.4		[55]
2	1-pentanol	NR50	423	98	6.5	109.3±3.4		
3	1-pentanol	H-BEA 25	423	89	1.5	121.2±1.7		
4	1-pentanol	Amberlyst 36	423	86	3.9	110.1±2.1		
			393	92	0.4			
5	1-pentanol	CT- 224	423	97	3.1	119.1±4.3		
			393	97	0.2			
6	1-pentanol	DL-H/03	423	96	3.2	110.6±2.6		
7	1-pentanol	DL-I/03	423	83	3.4	113.4±6.5		
8	1-pentanol	Dow 50	423	98	2.7	114.7±1.5		
			393	100	0.3			
9	1-hexanol	Amberlyst 70	423	97.7		108 ±7		[56]
10	1-hexanol	Amberlyst 70	463	86.9				
11	1-hexanol	Nafion NR50	423	97.9		118 ±6		
12	1-hexanol	Nafion NR50	463	93.4				
13	1-hexanol	Zeolite H-BEA-25	463	88.8		148 ±11		
14	1-hexanol	Amberlyst 70	423–463 K			125 ± 3**,121 ± 3***		[54]
15	1-octanol	Zeolite BEA SiO_2:Al_2O_3 75:1	390-430 K			149.8		[57]
16	1-hexanol	WO_x/ZrO_2	393	>99	1.3	127 ± 1	157 ± 13	[159]
17	4-methyl-1-pentanol	WO_x/ZrO_2	393	>99	1.2	127 ± 3	158 ± 10	
18	3-methyl-1-pentanol	WO_x/ZrO_2	393	87	1.0	127 ± 1	155 ± 1	
19	2-methyl-1-pentanol	WO_x/ZrO_2	393	<1		133 ± 11	124 ± 2	
20	2-hexanol	WO_x/ZrO_2	393	<1		127 ± 10	114 ± 5	
21	2-methyl-2-pentanol	WO_x/ZrO_2	393	<1		--	100 ± 12	
22	1-heptanol	WO_x/ZrO_2	393	>99	1.2	127 ± 2	155 ± 11	
23	1-octanol	WO_x/ZrO_2	393	>99	1.4	126 ± 3	154 ± 1	
24	1-nonanol	WO_x/ZrO_2	393	>99	1.6	127 ± 1	155 ± 7	
25	1-decanol	WO_x/ZrO_2	393	>99	1.6	126 ± 12	155 ± 11	
26	1-undecanol	WO_x/ZrO_2	393	>99	1.5	126 ± 4	154 ± 5	
27	1-dodecanol	WO_x/ZrO_2	393	94	1.4	127 ± 7	155 ± 10	[99,159]
28	1-dodecanol	Amberlyst 70	393	97	0.7			[99]
29	1-dodecanol	Nafion NR50	393	98	1.9			
30	1-dodecanol	Zeolite BEA	393	61	0.2			
31	1-dodecanol	Amberlyst 15	393	46	0.1			
32	1-dodecanol	Amberlyst 36	393	65	0.3			
33	1-hexanol	η-Alumina	523	61 ± 3				[19]
34	1-heptanol	η-Alumina	523	71 ± 3				
35	1-octanol	η-Alumina	523	65 ± 3				
36	1-nonanol	η-Alumina	523	73 ± 1				
37	1-decanol	η-Alumina	523	66 ± 3				
38	1-dodecanol	η-Alumina	548	50 ± 6				

* Turnover Number [$r_{0,\ ether,\ eq.}$ (mol/(h eq H^+)], **Fit using a Langmuir-Hinshelwood model, *** Fit using a modified Eley-Rideal model.

Brønsted acid catalysts involve proton donor sites. Polymeric resins such as Amberlyst and Nafion contain Brønsted-acidic H atoms attached to sulfonic acid groups. Amberlyst 70 is a macroporous sulfonic styrene-di-vinyl benzene (DVB) resin catalyst with a surface area of 36 m^2 g^{-1} and an acid site concentration of 3 eq H^+ kg^{-1}.[160] Nafion NR-50 is a sulfonated Brønsted-acidic catalyst that has a fluorinated backbone, as shown in Figure 4.3b. Amberlyst 70 and Nafion NR-50 stand out as active and selective Brønsted acid catalysts for the direct etherification of linear primary alcohols 1-octanol, 1-hexanol, and 1-pentanol.[54–56] Table 4.3, entries 1-2, 5-6, 8-9, and

11, show that Amberlyst 70, Nafion NR-50, as well as resins Purolite CT-224, Amberlyst DL-H/03, and Dow 50 are highly selective for the synthesis of symmetrical ethers from linear alcohols at 423 K, which is above the critical temperature at which unimolecular dehydration is thermodynamically favored. Nevertheless, as the temperature increases, the rates increase but the ether selectivity decreases for many of the catalysts.[19,56,99]

Polymeric resins are limited by intraparticle mass transfer, thermal stability, and ease of regeneration. For example, Amberlyst 70 and Nafion NR50 are unstable above 463 K,[55,58] and other resins such as Amberlyst 15 are even less thermally stable and are not recommended for use above 393 K. Moreover, regeneration of resin catalysts requires solvents and separation processes that consume energy and generate additional waste.

In a study of octanol etherification over gel-type and macroreticular polymeric resins, the best selectivity to di-n-octyl ether was observed for catalysts with a low degree of crosslinking.[130] Resins with low crosslinking degree (Amberlyst 39 and Amberlyst 70) were also found to be more selective for the etherification of 1-hexanol and 1-pentanol than catalysts with higher degrees of crosslinking with DVB.[100] As shown in Figure 4.3a, a high degree of DVB crosslinking (pink) results in more confined pore volumes and thus less accessibility to the active sites by long chain alcohols. Solvent effects on polymer swelling are also important, as they introduce mass transfer limitations due to variation in the number of accessible acid sites with time.[70] Cooley et al. have examined the microscopic and bulk swelling behavior of Nafion in mixtures of water and ethanol using small angle X-ray diffraction and optical microscopy.[161] While the microscopic swelling decreased with increasing ethanol content, the bulk swelling increased dramatically with increasing ethanol content. The authors concluded that the ethanol plasticizes the fluorocarbon matrix in Nafion, which allows the ionic material to form numerous smaller clusters compared to membranes swollen solely with water.[161] A lower degree of crosslinking generally results in greater swelling of the resins, and as a result, improved accessibility of the active centers for etherification.

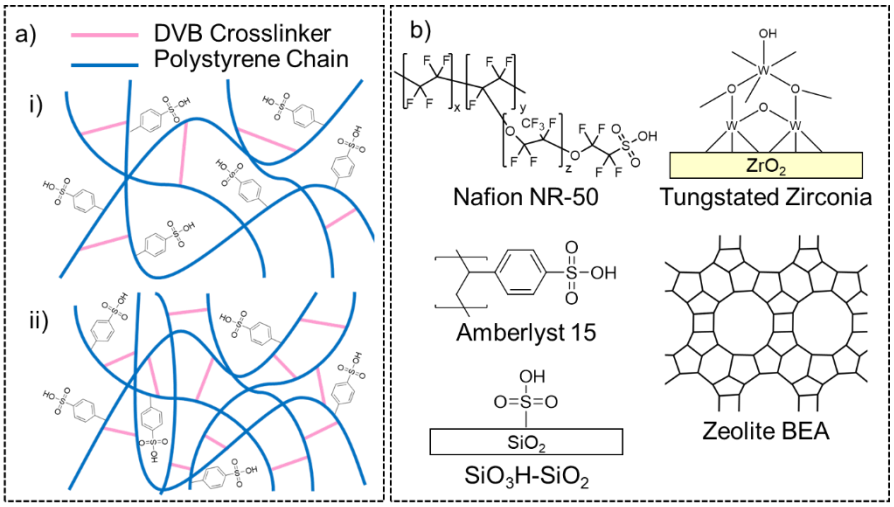

Figure 4.3. a) Sulfonated polystyrene resin catalysts with low (i) and high (ii) crosslinking degree, b) Solid-acid catalysts of interest for etherification and dehydration.

Zeolites, such as H-BEA pictured in Figure 4.3b, are also strong acids, but have superior thermal stability to resins, and can be regenerated easily by calcination. The Brønsted acid site in zeolites is generated when a silicon atom (4^+) in the framework structure is replaced by an aluminum atom (3^+), requiring a proton to balance the charge; thus, the higher the Al/Si ratio, the

higher the Brønsted acid site density. However, zeolites tend to catalyze undesired side reactions, such as unimolecular dehydration, more rapidly than etherification, and produce coke, which results in catalyst deactivation.[59] Table 4.3 shows that the selectivity to di-dodecyl ether for dodecanol etherification over H-BEA at 393 K is only 61%, compared to 97% and 98% for Amberlyst 70 and Nafion NR-50, respectively. Moreover, while Amberlyst 70, Nafion NR-50, and tungstated zirconia exhibit similar activation energies for 1-hexanol etherification (108 - 127 kJ mol^{-1}) the activation energy for the H-BEA-25 is significantly higher (148 ± 11 kJ mol^{-1}).[54,56,159] A study of HUSY suggests that its higher surface hydrophilicity leads to the retention of a portion of the byproduct water inside the pores, thereby reducing its etherification activity at low temperatures.[46,162] If high reaction temperatures and ease of catalyst regeneration are desired at the expense of selectivity, then zeolites such as H-BEA could be employed as solid Brønsted acids.

Another class of solid acids are Lewis-acidic catalysts such as zirconia, alumina, silica, and aluminosilicates. At 393 K, Lewis-acidic zirconia, gamma-alumina, mesostructured silica, and mesostructured aluminosilicate, have all been shown to be inactive for the liquid phase etherification of 1-dodecanol.[99] While η-alumina has been shown to be active for etherification of C_6-C_{12} linear alcohols at 523 K (Table 4.3, entries 33-38), it is not highly selective.[19] We have shown that tungstated zirconia, a solid acid catalyst containing both Brønsted and Lewis acid sites, promotes the direct etherification of primary linear alcohols ranging from hexanol to dodecanol, with ether selectivities of over 94% at 393 K.[99,159] Tungstated zirconia is also highly active. The turnover frequency (TOF) normalized per Brønsted acid site at 393 K for 1-hexanol etherification sites is 1.3 s^{-1}, which is significantly higher than the TOFs for the etherification of 1-pentanol over Amberlyst 70, Nafion NR50, Zeolite HBEA 25, Amberlyst 36, CT-224, DL-H/03, DL-I/03, and Dow 50 (0-0.4 s^{-1}) at the same temperature and reactant concentration.[55] We hypothesize that tungstated zirconia is an effective catalyst for the etherification of alcohols because Brønsted and Lewis acid sites on the surface of the catalyst work cooperatively to promote bimolecular etherification over unimolecular dehydration, as illustrated in Figure 4.4.[99] In contrast to acidic resins, tungstated zirconia exhibits high thermal stability and facile catalyst regeneration, making it an excellent choice of catalyst for the synthesis of symmetrical linear ethers.

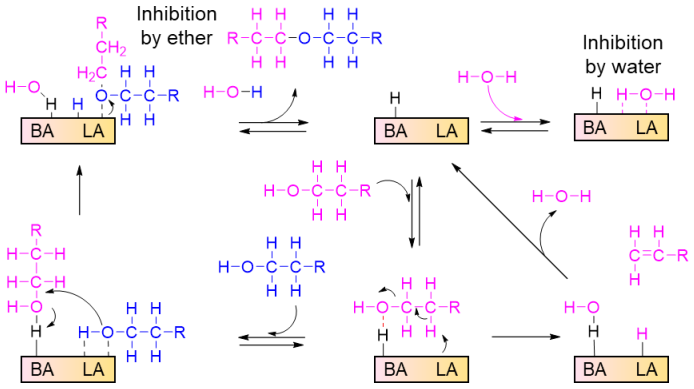

Figure 4.4. Mechanism of direct etherification and dehydration of linear alcohols over cooperative Brønsted (BA) and Lewis (LA) acid sites of tungstated zirconia (adapted from [99]).

In addition to forming linear symmetrical ethers, direct etherification of alcohols can be used to synthesize asymmetrical ethers such as ethyl-octyl ether. As shown in Table 4.4, Amberlyst 121, Dowex 50Wx2, and CT244 are most selective for producing ethyl-octyl ether from equimolar feed ratios of ethanol and octanol,[20,163] although symmetrical ethers are still formed. As shown in Table 4.3, the alkyl chain length of the alcohols does not have a significant effect on the ether

selectivity nor the activation energies for etherification and dehydration over tungstated zirconia (entries 22-27) and Amberlyst 70 (entries 1, 9, and 28). Because of the negligible changes in kinetics with increasing linear alcohol length, mixtures of linear alcohols couple in a nearly statistical manner. Our study of alcohol etherification over tungstated zirconia presented in Chapter 3 showed that equimolar mixtures of 1-hexanol, 1-heptanol, 1-octanol, 1-nonanol, 1-decanol, 1-undecanol, and 1-dodecanol produce a nearly statistical distribution of C_{12}-C_{24} ethers at 393 K.[159] In another study, Walsh et al. demonstrated that short-chain (C_1-C_5) alcohols couple to form a nearly statistical distribution of ethers over Nafion SAC-13 and Purolite CT-175 in the presence of supercritical CO_2.[164] Thus, the cross-coupling of alcohols is desirable for producing mixtures of ethers for diesel blends, but not when pure asymmetrical ether products are desired because homocoupling of alcohols will also occur.

Table 4.4. Synthesis of ethyl-octyl ether via direct etherification of ethanol and octanol catalyzed by solid acids.

Entry	Mol. Octanol: Ethanol	Catalyst	Temperature [K]	Selectivity to Ethyl Octyl Ether	Ref.
1	1:1	Amb 15	423	17.1*	[163]
2	1:1	Amb 35	423	15.2*	
3	1:1	Amb 16	423	21.9*	
4	1:1	Amb 36	423	20.6*	
5	1:1	Amb 39	423	35.1*	
6	1:1	Amb 70	423	42.8*	
7	1:1	CT-224	423	39.3*	
8	1:1	Amb 31	423	36.8*	
9	1:1	Dowex 50Wx4-50	423	40.8*	
10	1:1	Amb 121	423	45.7*	
11	1:1	Amb 121	423	30.3 from EtOH, 69.0 from Octanol	[20]
12	1:1	Amb 70	423	25.5 from EtOH, 69.4 from Octanol	
13	1:1	CT-224	423	26.2 from EtOH, 72.4 from Octanol	
14	1:1	Dowex 50Wx2	423	26.1 from EtOH, 73.7 from Octanol	

*(Moles of ethanol reacted to form ethyl octyl ether + moles of octanol reacted to form ethyl octyl ether)/moles of ethanol and octanol reacted*100%

The synthesis of ethyl-hexyl ether and ethyl-octyl ether has also been investigated using diethyl carbonate as an ethylating agent, where two moles of alcohols are added to one mole of diethyl carbonate to produce two moles of asymmetrical ethers, one mole of H_2O, and one mole of CO_2.[93,101,165] Carbonates such as dimethyl and diethyl carbonate are now considered "green reagents" because they be prepared from the catalytic oxidative carbonylation of methanol or ethanol with CO_2 rather than from phosgene.[18,166] But, Tejero et al. compared ethyl-octyl ether synthesis via etherification of octanol with diethyl carbonate and via direct etherification of ethanol and octanol, and concluded that direct etherification was the most effective method of producing ethyl-octyl-ether over acidic ion-exchange resins.[101] The authors found that at long reaction times, the yields of ethyl-octyl ether were similar for the two synthesis methods, but at early reaction times, direct etherification of ethanol and octanol resulted in higher rates of ethyl-octyl ether formation. Furthermore, they suggest that direct etherification is preferable to etherification of alcohol with a carbonate because it does not produce CO_2.[101]

Direct etherification of branched alcohols in the absence of solvent has also been investigated over tungstated zirconia. Our studies concluded that primary alcohols with carbon branches at least three carbons away from hydroxyl group are highly selective to ether formation, but as the carbon branch approaches the alpha and beta carbons of the alcohol, the selectivity to

ether drastically drops, as shown in Table 4.3 (entries 16-21) and illustrated in Figure 4.5.[159] Other studies have also shown that substituted alcohols, such as 2-butanol, readily undergo unimolecular dehydration over tungsten oxide catalysts, while etherification is negligible.[82]

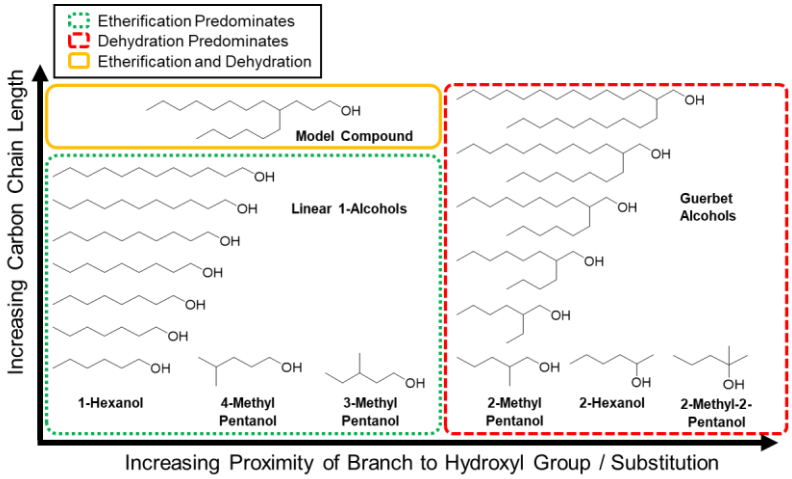

Figure 4.5. Various alcohols and their tendencies to undergo etherification or dehydration over tungstated zirconia at 393 K from ref.[159]

In our previous study of the kinetics and mechanism of etherification and dehydration over tungstated zirconia discussed in Chapter 2, measurements of kinetic isotope effects revealed that the rate-limiting step for unimolecular dehydration of 1-alcohols is the cleavage of a β-carbon hydrogen bond of the alcohol.[99] Kinetic isotope studies of ethanol dehydration over γ-Al_2O_3 have also suggested that this is the rate-limiting step.[31,167] The addition of alkyl branches to the alpha and beta carbons of the alcohol enhances the stability of the carbocation intermediate involved in the unimolecular dehydration, thereby promoting olefin formation. This evidence, coupled with the fact that activation barriers for dehydration decrease with increasing substitution of the alcohol,[31,99] suggests that direct etherification is limited to primary alcohols with no branches or with branches located a sufficient distance from the hydroxyl group.

Measurements of the kinetics of ethanol dehydration and etherification in the gas phase have also revealed important considerations concerning the inhibition by ethanol-water dimers, as well as more complicated dimer and trimer species.[32,167–170] The inhibition by water was observed for primary linear alcohol etherification over tungstated zirconia, as shown in Figure 4.4;[99] but, it was also observed for 1-octanol etherification over BEA,[57] and for 1-pentanol etherification over Amberlyst 70.[160] The removal of water is thus an important consideration for improving selectivity towards ethers across a variety of catalysts, particularly if the reaction is operated in a batch process at high conversions. In this connection, we note that Tejero et al. have found that water removal during the etherification of 1-pentanol over Purolite CT-224 by distillation improved ether selectivity.[171]

Ether selectivity can also be improved by eliminating both external and internal mass transfer limitations. In addition to considering the molecular size of adsorbing species and swelling of pore sizes caused by alcohols and solvent (if the solvent is different than the alcohol), external mass transfer can be improved by operating at high stirring rates, whereas small particle sizes reduce the effects of internal mass transfer. Improper mixing hinders bimolecular interactions of alcohols, especially for alcohols with long chain lengths, such as 4-hexyl-dodecanol (Figure 4.5),

resulting in a decreased selectivity with increasing chain length due to external mass-transfer limitations.[19,159]

The preceding discussion suggests that catalysts with both large pore volumes and small particle sizes enable selective ether synthesis via direct etherification from a wide variety of alcohols. Consistent with this conclusion, a recent study of ethanol dehydration over the metal organic framework MOF UIO-66, which contains nodes in the form of a Zr_6O_8 cluster, demonstrated that the catalyst exhibits 100% selectivity to diethyl ether at 473-523 K.[169] The authors suggest that the key to achieving high ether selectivity is the breaking of node-linker bonds, which forms defect sites proximate to open sites that facilitate effective bond formation between the alcohols. The authors found that the rate of etherification was three times greater for MOF UiO-66 (200 nm particle diameter) than for MOF UiO-67 (800 nm particle diameter), suggesting that transport limitations in the pores are significant.[169] In practice, though, this catalyst may not be suitable for selective ether formation because while vacancy sites produce more catalytically active sites, they contribute to a loss of crystallinity and, thus, stability.[169]

In summary, in order to achieve high yields of ethers from alcohols via direct etherification, a balance must be struck between catalyst selectivity, activity, and thermal stability. Moreover, the reactor in which etherification is carried out must be well mixed and water produced by the reaction should be separated from the reactant mixture. Catalysts with confined spaces such as zeolites and resins with a high degree of crosslinking exhibit lower selectivity to ether, suggesting that pore confinement isolates alcohols and facilitates unimolecular dehydration. Achieving a high local concentration of alcohols at the catalyst surface is necessary to promote bimolecular etherification. This can be achieved either using Brønsted acid catalysts with large pores that swell up in the presence of the solvent, such as Amberlyst 70, or through adsorption of alcohols onto catalysts containing proximate Brønsted and Lewis acid sites that facilitate the cross-coupling reaction, as occurs for tungstated zirconia. Still, the method of direct etherification is only applicable for producing symmetrical ethers from linear alcohols or blends of asymmetrical and symmetrical ethers from a feed composed of a mixture of linear alcohols. If high selectivities of linear asymmetrical ethers or ethers with branches closer than three carbons away from the hydroxyl group are desired, the method of reductive etherification of an alcohol and an aldehyde or ketone is preferred. This method is discussed in Section 4.V.ii.

b) Synthesis of mono-, di-, and tri- ethers via the direct etherification of glycerol and polyols with alcohols

Glycerol is an inexpensive byproduct of biodiesel production and has emerged as an attractive platform molecule for the production of fuels and specialty chemicals. The valorization of glycerol through acetalization, dehydration to acrolein, conversion to 1,3-propanediol, and other methods has been studied and reviewed extensively; therefore, we will only highlight a few examples of glycerol valorization to fuels and lubricants via direct etherification using solid-acid catalysts.

Brønsted acid catalysts such as Amberlyst 70, Amberlyst 15, Amberlyst 35, sulfated zirconia, sulfonated silica, and zeolite H-BEA are effective for catalyzing the etherification of glycerol with a variety of alcohols in the liquid phase.[24,140,172–177] Table 4.5 illustrates a number of examples of solid-acid catalyzed direct etherification of glycerol with alcohols. In general, the major product for the mono-ether is 1a, whereas 1b is the minor product formed by the more sterically difficult etherification of the middle hydroxyl group of the glycerol. Similarly, 2b is the minor product for the di-ethers. The tri-ether (3) is a result of etherification of each of the hydroxyl groups of glycerol

with alcohols. The bimolecular etherification of two alcohols (4) as well as the oligomerization of glycerol (5) also occurs. Notably, in the case of ethanol etherification with glycerol, the side reaction of diethyl ether formation did not have a significant effect on the rates of formation of the desired products.[178] In order to maximize yields of mono-, di-, and tri-glycerol ethers, it is important to consider the effects of the catalyst properties, alcohol structure, temperature, and water removal in order to optimize the kinetics.

Table 4.5. Ethers produced by direct etherification of glycerol with alcohols.

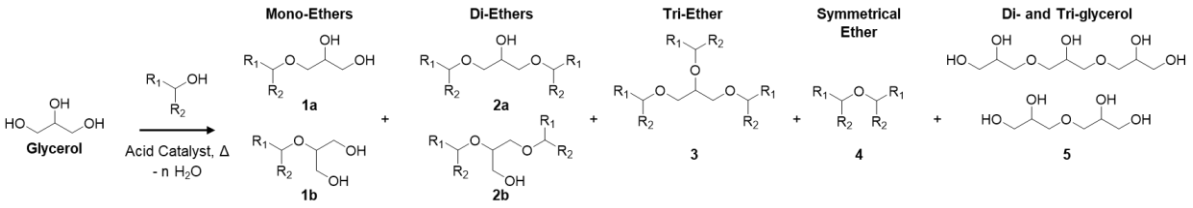

Ent	Catalyst	Temp. [K]	Time [h]	Alcohol [A]	Gly:A [mol]	Conversion [%]		Yield [%]					Ref
						Gly.	A	1a + 1b	2a +2b	3	4	5	
1	Amb. 70 (10 wt%)	403	24	1-dodecanol	1	57	0	0	-	-	-	25	[24]
2	Amb. 70 (10 wt%)	403	24	1-dodecanol	4	36	5	5	-	-	-	25	[24]
3	Amb. 70 (10 wt%)	403	24	1-butanol	4	17	26	26	-	-	-	4	[24]
4	Amb. 70 (10 wt%)	403	24	1-pentanol	4	13	22	22	-	-	-	4	[24]
5	Amb. 70 (10 wt%)	403	24	1-hexanol	4	11	13	13	-	-	-	4	[24]
6	Amb. 70 (10 wt%)	403	24	1-octanol	4	36	5	5	-	-	-	6	[24]
7	SiO_2–SO_3H (1.7 mol%)	353	7	1-phenyl-propan-1-ol	1	88	NA	76	12	-	NA	-	[140]
8	SiO_2–SO_3H (1.7 mol%)	353	48	1-dodecanol	NA	0	0	-	-	-	-	-	[140]
9	SiO_2–SO_3H (2.5 mol%)	353	39	oct-2-en-1-ol	NA	NA	NA	61	-	-	-	-	[140]
10	SiO_2–SO_3H (1.7 mol%)	353	19	benzyl alcohol	NA	NA	NA	76	-	-	-	-	[140]
11	Amberlyst 35	383	2	benzyl alcohol	~0.33	100	NA	~40	~20	~2	~30	-	[172]
12	K-10 montmorillonite	383	2	benzyl alcohol	~0.33	100	NA	~40	~3	~0	~55	-	[172]
13	Zeolite Beta	383	2	benzyl alcohol	~0.33	100	NA	~55	~2	~0	~40	-	[172]
14	Sulfated Zirconia	413	6	benzyl alcohol	1	NA	~70	~25	~25		~20	-	[173]
15	Amb.15 (1.2 wt%)	343	6	*tert*-butanol	4	NA	NA	36.6 [b]	13.7 [b]	0	4.9 [a,b]	-	[174]
16	Amb. 15	343	6	isobutanol	0.25	100	NA	8.3	60.4	31.3			[175]
17	Amb. 15	343	6	*tert*-butanol	0.25	78.9	NA	56.5	21.9	0.4			[176]
18	Amb. 15	343	6	1-butanol	0.25	0	NA	0	0	0	-	-	[177]
19	Amb. 15	433	6	1-butanol	0.25	85.1	NA	70.0	0.4	0.09	-	-	[177]
20	Amb. 15	393	6	ethanol	~0.1	0	NA	-	-	-	-	-	[178]
21	Amb. 15	413	6	ethanol	~0.1	0	NA	-	-	-	-	-	[178]
22	Amb. 15	433	6	ethanol	~0.1	32	NA	32	0	0	-	-	[178]
23	DBSA	403	24	1-dodecanol	4	26	72	10	9	-	62	-	[24]

[a] selectivity to isobutene, [b] product distribution (wt%), with remainder 28.6 wt% *tert*-butanol and 6.4 wt% glycerol

To synthesize mono-, di-, and tri- ethers of glycerol with linear alcohols, one must consider the tradeoff between etherification activity and selectivity. For the etherification of glycerol with ethanol over Amberlyst 15 shown in Table 4.5, entries 20-22, no reaction occurred below 433 K.[178] While this reaction is highly selective to the mono-ether, the catalyst is not reusable, as Amberlyst 15 is unstable above 393 K. Similarly, the etherification of glycerol with butanol over Amberlyst 15 is active at 433 K, reaching a mono-ether yield of up to 70% at a glycerol conversion of 85.1%, but is not active at 343 K, as shown in Table 4.5, entries 18-19.[177] Therefore, for these reactions, it is recommended that a more thermally stable catalyst such as Amberlyst 70 or a metal oxide is used, since high temperatures are required.

For the synthesis of glycerol ethers using alcohols such as 1-dodecanol and 1-octanol, there are additional challenges due to mass transfer limitations introduced by the poor solubility of long chain alcohols in glycerol. As shown in Table 4.5, entry 8, a temperature of 353 K is insufficient for etherification of dodecanol with glycerol over sulfonated silica, a catalyst that is active under the same conditions for the etherification of glycerol with benzyl alcohol to produce mono-ether (entry 10).[140] Adding a surfactant promotes etherification of glycerol with long-chain alcohols such as dodecanol in the liquid phase to improve solubility. For example, Jérôme et al. have used dodecylbenzene sulfonic acid (DBSA) to enable emulsification of the reaction medium, which resulted in yields of monododecyl glycerol ethers of 30% at 403 K, as shown in Table 4.5, entry 23.[24] De Campo et al. have also demonstrated that using a well-tuned amphiphilic copolymer PSt-PSSA, a surfactant acid catalyst grafted on silica, significantly increased ether formation from dodecanol and glycerol by facilitating better contact between the two reactants.[139]

Amberlyst 70 and sulfonic acid supported on silica are effective for the synthesis of mono-ethers from linear and benzyl alcohols, as demonstrated by Table 4.5, entries 2-7, 9, and 10.[24,140] Amberlyst 15 is effective for producing di- and tri-ethers from the reaction of glycerol with isobutanol to produce diesel additives, as demonstrated by Table 4.5 entry 16. [175] If high yields of di- and tri-ethers are desired, the water must be removed during the synthesis to increase the conversion. Frusteri et al. used a membrane to selectively remove water and shift the equilibrium of the reaction towards the formation of poly-ethers for the etherification of glycerol with *tert*-butyl alcohol[174,176] as well as butanol.[177] De Campo et al. have also used a water removal process to increase selectivity of alkyl-poly-gylceryl ether (AGEM) during the etherification of dodecanol and glycerol over sulfonated silica catalysts, leading to yields of AGEM > 80 % at 423 K.[139]

The effectiveness of strong solid Brønsted acids for glycerol etherification reactions depends on several catalyst properties including hydrophilicity, accessibility, and thermal and mechanical stability. In a study of glycerol etherification with ethanol over solid acid catalysts, Fajula et al. suggested that the hydrophobicity of the catalyst is an important factor in determining etherification activity. The authors found that strongly hydrophobic catalysts were less effective for glycerol etherification because they were unable to allow for the adsorption of glycerol; however, hydrophilic catalysts that adsorb glycerol too strongly also resulted in lower etherification rates.[178] For example, Nafion NR50, a hydrophobic strong Brønsted-acidic fluorinated sulfonated polystyrene resin, did not catalyze the etherification of glycerol but it did

catalyze bimolecular etherification of the alcohol.[178] The authors also studied the etherification of glycerol with ethanol over a series of zeolites with varying silica to alumina ratios and found that there is a tradeoff between the silica to alumina ratio and the etherification activity. As the aluminum content was increased, a higher density of acid sites were generated, which contributed to an increase in the etherification rate; however, the surface also became more polar, thus decreasing the glycerol etherification rate due to the increased hydrophobicity. The authors found that a compromise could be achieved with zeolites with intermediate aluminum contents (Si/Al ratios around 25), which were the most effective for glycerol etherification. Amberlyst resins 15 and 35 were also effective for glycerol etherification at 433 K, with selectivities towards mono-ethoxy glyceryl ethers of 100% and 90% (remainder di-ethers) at glycerol conversions of 32% and 52%, respectively. While the zeolites were found to be active at 473 K and are more thermally stable, they also exhibited lower selectivity. The tradeoff between selectivity and thermal stability of the catalyst is thus a concern for direct etherification of glycerol, as well as for primary alcohols as discussed earlier, since higher temperatures not only increase rates of alcohol but also catalyze the unimolecular dehydration of alcohols to olefins, especially for substituted alcohols like isobutanol, 2-propanol, and for Guerbet alcohols.

The accessibility of acid sites also plays a fundamental role in promoting catalyst activity, as it has been found that catalysts with larger pore volumes are more active.[174] The kinetics of glycerol etherification with alcohols depends greatly on the reactant concentration and temperature. For example, Frusteri et al. found that the molar ratio of alcohol to glycerol for *tert*-butanol etherification with glycerol over Amberlyst 15 does not affect the product distribution.[174] However, Jaworski et al. reported that for the etherification of benzyl alcohol with glycerol over sulfated zirconia, mono-ether and di-ether formation rates were first order in benzyl alcohol concentration, but benzyl alcohol self-condensation was second order with respect to benzyl alcohol.[173] They also found that benzyl-alcohol self-condensation had a higher activation energy than mono- and di-ether formation, suggesting an explanation for the higher selectivity towards cross-etherification at lower temperatures.[173]

Several approaches can be considered to address the tradeoff between activity and selectivity that occurs with increasing temperature of etherification. Batch reactors coupled with water permselective membranes can enhance ether selectivity by removing water. As temperature is increased, membrane effectiveness increases, but unimolecular dehydration of alcohols also increases.[177] Therefore, developing stable membrane separators that are effective at lower temperatures could improve ether selectivity. Further modification of the acid-base properties of the catalysts could also enable tuning of product distributions for glycerol etherification. For example, Weckhuysen et al. have found that the rates of etherification of glycerol to produce di- and tri-glycerols over CaO, SrO, and BaO at 533 K increase with increasing basicity of the catalyst.[179] Understanding the role of Lewis acidity and basicity could enable the development of catalysts that optimize glycerol adsorption and reaction to form ethers.[85]

ii. Reductive Etherification of Alcohols with Aldehydes, Ketones, Esters, and Carboxylic Acids

Asymmetrical ethers with and without branching are desirable as cetane boosters and as automotive lubricant base oils. As noted above, direct etherification of a branched alcohol and a linear alcohol is ineffective for the synthesis of asymmetrical branched ethers, because substituted alcohols and alcohols with carbon chain branches on the alpha and beta carbons readily undergo dehydration. This method is also relatively ineffective for the synthesis of asymmetrical linear ethers because the alcohols will self-couple to generate symmetrical ethers. Reductive etherification of alcohols with aldehydes and ketones provides an alternative approach for producing high yields of symmetrical and asymmetrical ethers with a variety of structures and degrees of carbon chain branches.[22,25,180]

Scheme 4.2a shows a general scheme for the reductive etherification of a carbonyl compound with an alcohol to produce an asymmetrical ether. The overall reductive etherification reaction of an alcohol with an aldehyde or ketone to produce an ether and water occurs in the presence of H_2, a catalyst for H_2 activation, such as carbon-supported palladium, and an acid catalyst.

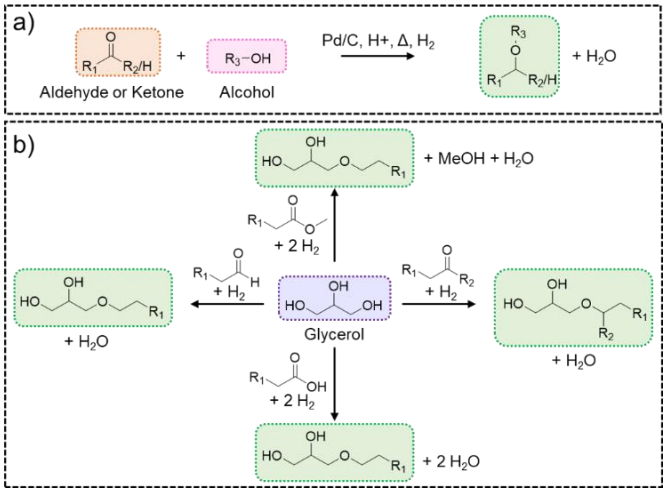

Scheme 4.2. a) Reductive etherification of carbonyl compounds with alcohols, b) Reductive etherification of glycerol with aldehydes, ketones, carboxylic acids, and fatty acid methyl esters.

The heterogeneously catalyzed reductive etherification of aldehydes and ketones with an alcohol allows for flexibility in the choice of both reactants, enabling the utilization of biomass-derived alcohols with carbon chain branches produced via the Guerbet reaction, as well as carbonyl compounds obtained from a variety of biomass sources, as shown in Scheme 4.1. This method is therefore suitable for the selective synthesis of symmetrical or asymmetrical primary or secondary ethers. Reductive etherification of carbonyl compounds can also be performed with polyols such as glycerol,[181–183] to produce surfactants, fuel additives, and other value-added products. Drawbacks of the reductive etherification synthesis involve the requirement of hydrogen, and the use of precious metal catalysts. In addition, there are some limitations to the scope of aldehydes for the synthesis; for example, the carbonyl group of an aromatic aldehyde can reduce rapidly, thereby reducing the extent of etherification.[25]

Work in our group has recently demonstrated that a wide variety of ethers suitable for use as fuels and lubricants can be synthesized from biomass-derived platform molecules.[22] Representative ethers prepared with high yields are shown in Table 4.6. These reactions were carried out at 393 K using a combination of Pd/C and H_2, and silica-supported 4-ethylbenzenesulfonic acid (EBSA/SiO_2). In order to utilize Guerbet alcohols, four equivalents of aldehyde or ketone were required per equivalent of alcohol.[22] Amberlyst 15 was also an effective acid catalyst for this reaction. Unlike direct etherification, this method enabled the use of substituted alcohols and Guerbet alcohols, since dehydration of the alcohols to olefins is not observed. Thus, carbonyl compounds and alcohols can be selected independently to produce either symmetrical or asymmetrical ethers.

Table 4.6. Conversion of biomass-derived carbonyl compounds and alcohols to ethers.[22]

Entry	Carbonyl (C)	Alcohol (A)	Mol C:A	Ether	%Yield / (% Conv. of Limiting Substrate)
1	2-heptanone	butanol	1:4	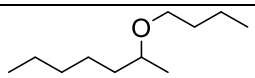	88 / (100)
2	2-ethyl-hexanal	butanol	1:4	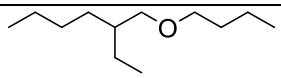	85 / (100)
3	2-heptanone	2-decyl-tetradecanol	4:1	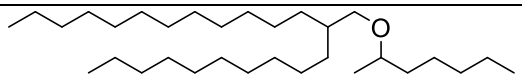	91 / (100)
4	butanal	2-decyl-tetradecanol	4:1	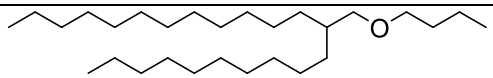	88 / (97)
5	isobutanal	2-decyl-tetradecanol	4:1	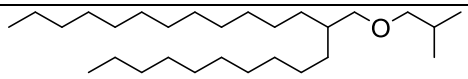	86 / (100)
6	cyclopentanone	2-decyl-tetradecanol	4:1	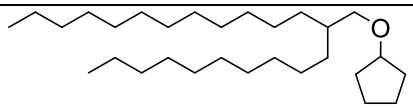	87 / (100)
7	8-pentadecanone	2-hexyl-decanol	4:1	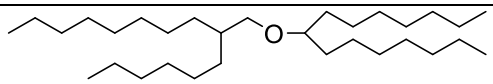	88 / (93)
8	octanal	2-decyl-tetradecanol	4:1	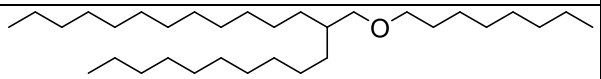	59 / (94)
9	2-ethyl-hexanal	2-decyl-tetradecanol	4:1	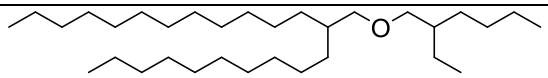	51 / (79)

Reagents and conditions: carbonyl compound (2 or 8 mmol), alcohol (2 or 8 mmol), 5% Pd/C (2.5 mol%), EBSA/SiO_2 (entries 1-2: 2.5 mol%, entries 3,6,7: 10 mol%, entries 4,5,8,9: 5 mol%), 393 K, 150 psi H_2, 5 h.

The mechanism of reductive etherification is not known, but it has been proposed to proceed via hemiacetal or acetal intermediates, as shown in Scheme 4.3.[22,25,180] The first step is the acid-catalyzed activation of the carbonyl group, which is followed by addition of an alcohol to form the hemiacetal or acetal intermediate. These intermediates can undergo hydrogenolysis to form ether directly, or undergo a two-step process of acid-catalyzed dehydration or loss of alcohol followed by hydrogenation over Pd/C.

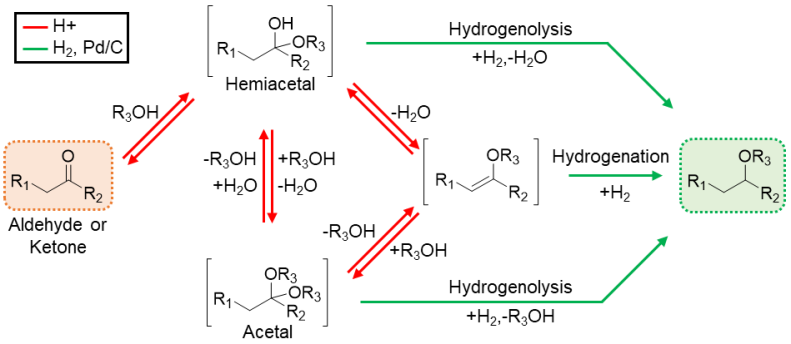

Scheme 4.3. Reaction pathway for the reductive etherification of aldehydes or ketones with alcohols proposed by Fujii et al.[180]

In addition to the synthesis of lubricant-range ethers from biomass-derived alcohols, reductive etherification has been employed for the synthesis of glycerol ethers, as shown in Scheme 4.2b. The Lemaire group has prepared glycerol ethers selectively via the reductive etherification of glycerol with aldehydes,[182] ketones,[182] carboxylic acids[183], methyl esters, and triglycerides.[181] These reactions were performed with a combination of carbon-supported palladium, H_2, and an acid catalyst.[181–183]

The mechanism for glycerol etherification with a carboxylic acid in the presence of molecular hydrogen proposed by the Lemaire group is shown in Scheme 4.4. The major product is shown in green. Minor products involve the ether formed from the middle hydroxyl group, as well as the unreduced ester. The proposed mechanism for etherification of glycerol with the methyl ester proceeds similarly except that the hydroxy group is replaced with a methoxy group.[181] The same group has also demonstrated that glycerol ethers can be produced from the reductive etherification of triglycerides directly with glycerol in a two-step process.[181] First, glycerol and triolein are esterified using 10 wt% BaO/Al_2O_3 at 473 K, followed by reduction in 50 bar H_2, with 10 wt% Amberlyst 15, and 1 mol% Pd/C at 393 K, resulting in an isolated yield of 34% of the mono-ether.[181]

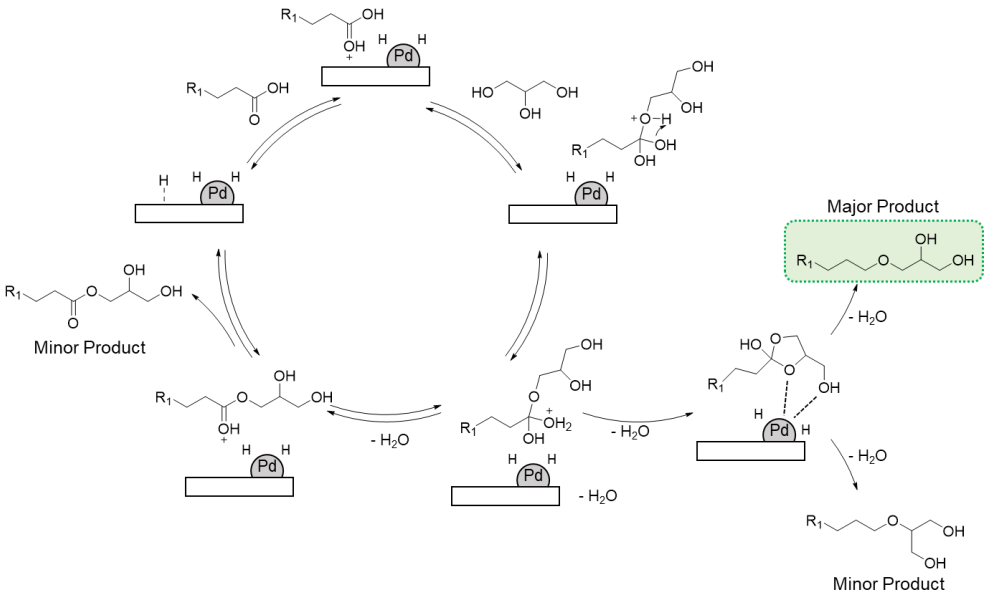

Scheme 4.4. Mechanism of glycerol etherification with carboxylic acid (adapted from ref.[183])

iii. Synthesis of Ethers from Furanics via Direct and Reductive Etherification

Furfural and other furanic compounds have emerged as a class of useful platform molecules that can be readily produced from biomass via the dehydration of sugars derived from cellulose and hemicellulose or synthesized directly from biomass feedstocks.[69,151,184,185] Ethers obtained from these platform molecules, such as alkoxymethyl furfural, can be used as biofuels and specialty chemicals.[151,186,187] Both direct and reductive etherification have been employed to upgrade these synthons to furanyl ethers. Etherification of furans with alcohols presents challenges similar to those for the direct etherification of alcohols in terms of activity and selectivity. Undesired side reactions such as the unimolecular and bimolecular dehydration of alcohols make the task of synthesizing asymmetrical ethers challenging. In addition, there is a tradeoff between reaction rate and selectivity for producing ethers, as increasing temperature improves total product yield but decreases selectivity for direct etherification.[53] Several recent efforts by our group and others to produce ethers from both direct and reductive etherification of furfural, furfuryl alcohol, and 5-hydroxyl-methyl furfural (HMF) are shown in the Scheme 4.5. Below, we discuss recent efforts to synthesize furanyl ethers via direct etherification of furanyl alcohols with linear alcohols, reductive etherification of furans with alcohols, and transfer hydrogenation/etherification reactions.

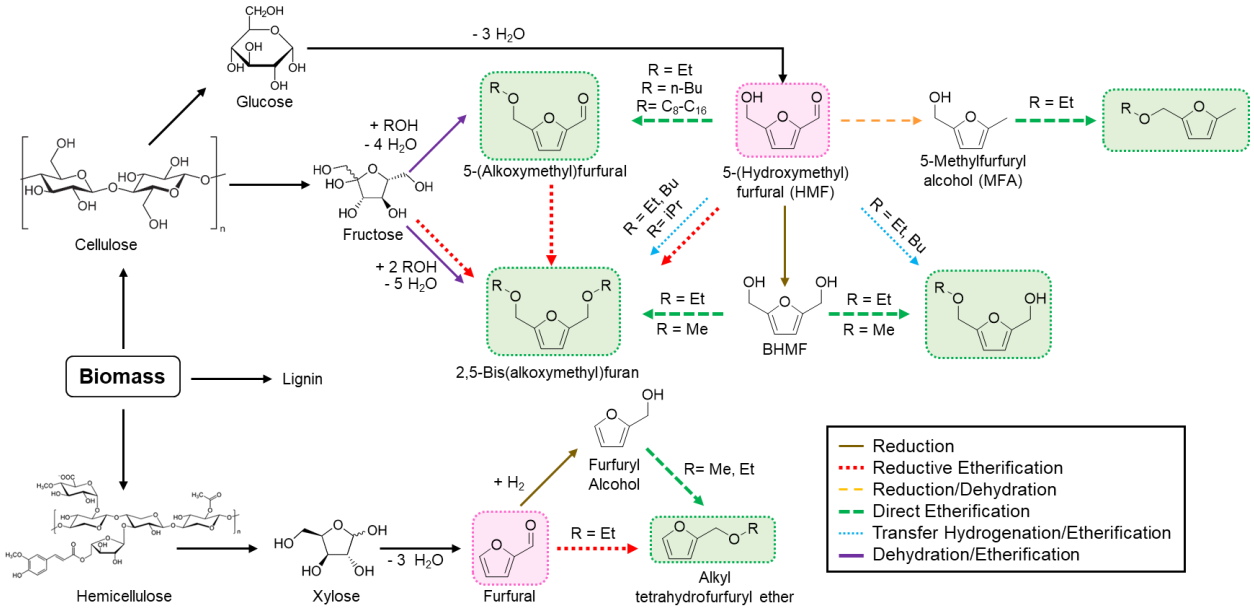

Scheme 4.5. Synthesis of furanyl ethers via direct and reductive etherification of biomass-derived platform molecules.

a) Direct Etherification of Ethanol and HMF

The direct etherification of furfuryl alcohol, HMF, and 2,5-bis(hydroxymethyl)furan (BHMF) with linear alcohols is represented in Scheme 4.5 by the dashed green lines. One reaction of particular interest is the direct etherification of HMF with ethanol to produce 5-(ethoxymethyl)furan-2-carbaldehyde (EMF) and ethyl levulinate (EL).[53,188–192] Both products can serve as platform molecules for the synthesis of fuels and, hence, understanding which reaction conditions favor either EMF or EL production would enable the proper choice of reaction conditions to make one of these two products. Table 4.7 summarizes the effectiveness of solid-

acid catalysts for selective production of EMF or EL and compares the yields with those obtained using sulfuric acid.

In a study of the etherification of HMF with ethanol, Lanzafame et al. suggested that the presence of Brønsted versus Lewis acid sites on the catalyst surface are required to selectively produce EMF or EL. They achieved EMF yields of 76% and EL yields of 23% at 100 % conversion of HMF for the direct etherification of HMF with ethanol over Z-SBA-15 for 5 hours at 413 K.[188] Under the same reaction conditions but using Amberlyst 15 as the catalyst, they observed a >99% yield of EL at 100% conversion of HMF.[188] In fact, they found that purely Brønsted-acidic catalysts, such as H_2SO_4, Amberlyst 15, and Al-MCM-41 (Si/Al = 25), favored formation of EL. However, introduction of Lewis acid sites, such as Zr^{4+} into SBA-15 (Z-SBA-15) or extra-framework isolated Al^{3+} sites in Al-MCM-41 (Si/Al = 50), resulted in higher selectivity to EMF.[188]

Table 4.7. Direct etherification of HMF with ethanol over acid catalysts.

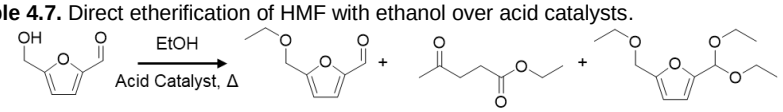

5-hydroxymethyl-furfural **(HMF)** | 5-(ethoxymethyl) furan-2-carbaldehyde **(EMF)** | ethyl levulinate **(EL)** | 5-(ethoxymethyl)-furfural diethylacetal **(EMFDEA)**

Catalyst	Temp. [K]	Time [h]	HMF:ROH [mol]*	HMF Conv. [%]	EMF yield [%]	EL yield [%]	EMFDEA yield [%]	DE yield [%]	Ref.
Z-SBA-15	413	5	~1:23	100	76	23		-	188
Al-MCM-41 (Si/Al 50)	413	5	~1:23	100	68	10		13	188
SZ-SBA-15	413	5	~1:23	100	62	35		-	188
Al-MCM-41 (Si/Al 25)	413	5	~1:23	100	37	47		12	188
Amberlyst 15	413	5	~1:23	100	-	>99		-	188
SBA-15	413	5	~1:23	75	-	-		54	188
Al-MCM-41 (Si/Al 75)	413	5	~1:23	61	-	-		19	188
H_2SO_4	413	5	~1:23	100	3	96		-	188
H_2SO_4 (5 mol%)	348	24	~1:43		81	16			53
Dowex DR2030 (5 mol%)	348	24	~1:43		57	8	33		53
Amberlyst 15 (5 mol%)	348	24	~1:43		55	8	31		53
Dowex50WX8 (5 mol%)	348	24	~1:43		45	9	28		53
Silica sulfuric acid (5 mol%)	348	24	~1:43		36	7	25		53
Amberlite IR120 (5 mol%)	348	24	~1:43		33	7	14		53
NKG-9	343	24	~1:86	100	82.8				189
HY-Zeolite	343	24	~1:86	10	8.5				189
Al-TUD-1 (Si/Al 21)	413	24	~1:57	97	70	11	3		192
Al-TUD-1(4)-at (acid treated)	413	42	~1:57	88	81	6			192
H-ZSM-5	413	24	~1:139	~100	~80	~5			190
H-MOR	413	24	~1:139	~100	~80	~5			190
SO_3H-SBA-15-D	413	24	~1:139	~100	~10	~75			190
Amberlyst 15	363	2	~1:10	25.5	62.5	5.2			191
$H_4SiW_{12}O_{40}$	363	2	~1:10	89.4	85.3	5.4			191
40 wt.% HSiW/MCM-41	363	2	~1:10	80.1	85.8	4.6			191

HMF: 5-hydroxymethylfurfural; EMF: 5-(ethoxymethyl)furan-2-carbaldehyde; EL: ethyl 4-oxopentanoate or ethyl levulinate; DE: 1,1-dietoxy ethane, EMFDEA: 5-(ethoxymethyl)- furfural diethylacetal. *Ethanol is used as both the reactant and solvent.

Our group and others have shown that high selectivities towards EMF can be achieved using the Brønsted acid catalyst Amberlyst 15. We observed EMF yields of over 55% from the etherification of HMF and ethanol at 348 K for 24 h.[53] Similarly, Che et al. have observed EMF yields of over 62% for the etherification of HMF and ethanol at 363 K for 2 h.[191] Ether formation is favored at lower temperatures, which means that in order to produce EMF in high yields, longer reaction times and lower temperatures are preferred, and under these conditions, Lewis acid sites are not needed to produce EMF selectively. Amberlyst 15 is an excellent candidate for carrying

out reactions at lower temperatures, because it is thermally stable up to 393 K, and does not degrade like the sulfonated functionalized ion-exchange resin NKG-9, which was selective for EMF synthesis from HMF and ethanol but decomposed during the reaction.[189]

In addition to ethanol, direct etherification of HMF over solid acid catalysts has been achieved with other alcohols, such as butanol[53,193] and C_8-C_{16} alcohols.[131,193] For example, Iborra et al. have investigated the cross-etherification of C_8-C_{18} n-alcohols with HMF to produce asymmetrical ethers for applications as biodegradable surfactants over zeolites H-BEA, HY, H-MOR, H-MFI, ITQ-2, and MCM-41 at 373 K. This work identified H-BEA as an effective catalyst, enabling the attainment of ether yields over 92%.[131] HMF can also undergo self-etherification to produce 5,5′-oxy(bis-methylene)-2-furaldehyde (OBMF), a useful precursor for the synthesis of crown ethers, polyurathanes, polyamides, and other polymers.[194] Sn-montmorillonite gave almost complete conversion of HMF with 98% selectivity to OBMF using non-polar aprotic dicholoroethane as a solvent at 373 K.[194]

b) Direct Etherification of Furfural and Methyl Furfural with *Ethanol*

The direct etherification of furfural with ethanol or methanol to produce alkyl-tetra-hydrofurfuryl ether can also be achieved over solid acid catalysts. Cao et al. have demonstrated that H-MFI (Si/Al 25) was effective in the etherification of furfuryl alcohol with methanol and ethanol, obtaining selectivities to methyl furfural ether (MFE) and ethyl furfuryl ether (EFE) of 58.9% and 44.8%, respectively at 298 K for 24 h using methanol or ethanol as the solvent.[195]

Methyl furfuryl alcohol (MFA) can be produced from HMF via selective hydrogenation over a Ru–MoO_x/C catalyst.[196] The etherification of MFA with ethanol to produce 2-(ethoxymethyl)-5-methylfuran (EMMF) was achieved over Amberlyst 15. Recent work in our group has demonstrated EMMF selectivities and yields of over 98% over Amberlyst 15 at 298 K.[197] Amberlyst 15 was also effective for the direct etherification of other alcohols such as butanol and other furans such as BHMF. It was proposed that the high selectivity towards asymmetrical ethers is achieved through the formation of a solvation shell of polar C_1-C_4 alcohols that form around the active site of the catalyst, enhancing the cross-coupling reaction, shown in Figure 4.6.[197]

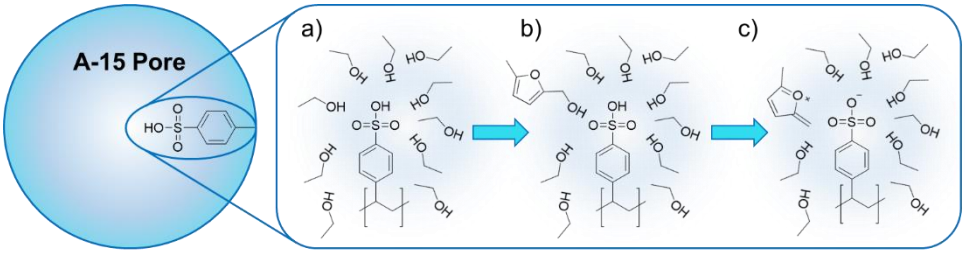

Figure 4.6. Formation of the reactive intermediate in a solvation shell inside a pore of Amberlyst 15 for the etherification of methyl furfural with ethanol (adapted from ref [197]).

c) *Direct Etherification of BHMF*

Amberlyst 15 and zeolites are effective for the direct etherification of furan compounds with alcohols. For the direct etherification of BHMF with ethanol, yields of up to 80% 2,5-bis(ethoxymethyl)furan and 6% (5-(ethoxymethyl)furan-2-yl)methanol were achieved using 5

mol% catalyst loading of Amberlyst 15, at 313 K for 16 h.[53] Etherification of BMMF and BHMF with methanol is also highly selective over zeolites. Fang et al. achieved ether selectivities of over 95% over 1.5% Sn-ZSM-5 at 338 K.[198] The authors suggest that the main and side reactions, such as furan ring opening and polymerization, are dictated by pore structure as well as synergistic effects between Brønsted and Lewis acidity.[198]

d) Reductive Etherification of HMF, Furfural, Alkoxy-Methyl-Furfural, and Levulinic Acid with Alcohols

The cross-etherification of alcohols is limited by the tendency for branched alcohols, such as isopropanol, to undergo unimolecular dehydration, as discussed in Section 4.V.i. One way to suppress this side reaction and improve the selectivity to cross-etherification products is to employ reductive etherification. Some examples of reductive etherification routes to producing ethers from furans are illustrated in Scheme 4.5 by the dotted red lines. Work in our group has employed reductive etherification for the production of 2,5-bis-(alkoxymethyl)furan via the reaction of HMF with ethanol and butanol. Yields of the di-ether (2,5,-bis(ethoxymethyl)furan)) of up to 59%, with 7% of the mono-ether (5-(ethoxymethyl)furan-2-yl)methanol),) and 1% 2-(diethoxymethyl)-5-(ethoxymethyl)furan, were produced using 5 mol% Amberlyst 15, 1 mol% Pt/alumina, at 348 K for 24 h in the presence of 200 psi H_2.[53] Wu et al. have demonstrated that Pd supported on TiO_2, Al_2O_2, SiO_2, and active carbon are also effective for the reductive etherification of furfural with ethanol at 333 K with 0.3 MPa of H_2.[199] Yields of up to 81% of furfuryl ethyl ether (FEE) were obtained over 0.7 wt% Pd/C with minor formation of 2-(diethoxymethyl)furan (4%), furfuryl alcohol (10%), and tetrahydrofurfuryl alcohol (3%).[199] The authors suggested that palladium hydride, formed *in situ*, catalyzes the formation of the key intermediate, 2-(diethoxymethyl)furan.[199] They also suggested that the key to achieving a high yield of ether is the balance between the proton-donating ability and hydrogenolysis activity of palladium hydride, which requires tuning of the Pd loading, hydrogen pressure, and reaction temperature.[199]

Reductive etherification of alcohols with levulinic acid or ethyl levulinate can also be employed for the synthesis of sustainable non-VOC solvents or biofuels.[200,201] Recent efforts have demonstrated that methanol, ethanol, n-butanol, and n-heptanol can undergo reductive etherification with levulinic acid to produce alkyl 4-alkoxypentanoates (4-alkoxyvalerates) in 54−77% yield under hydrogen at 473 – 493 K and 1000 psig in the presence of a Pd/C catalyst.[200] The addition of acidity has also shown to improve the yield and selectivity of ethyl-4-ethoxypentanoate (EEP) by reductive etherification of ethanol with ethyl levulinate at 413 K, as introducing zeolite beta as a co-catalyst with Pd/SiO_2-Carbon enabled the attainment of EEP yields of 93% at 100% conversion of ethyl levulinate.[201]

e) Etherification via Transfer Hydrogenation for the Synthesis of Furanyl Ethers

Transfer hydrogenation etherification has also emerged as a method of synthesizing furanyl ethers. A few illustrations of this means of HMF etherification are presented in Scheme 4.5 by the dotted blue lines. In this case, the alcohol serves as both the solvent, reactant, and hydrogen transfer agent. Jae et al. have demonstrated that Lewis acidic Sn-BEA and Zr-BEA are effective catalysts for the transfer hydrogenation and etherification of HMF with 2-propanol and 2-butanol at 453 K. Yields of over 80% of 2,5,-bis(isopropoxylmethyl)furan were reported.[202] Vlachos et al. proposed a mechanism and reaction pathway for the formation of 2,5-bis(alkoxymethyl)furan from HMF via direct etherification and etherification via transfer hydrogenation using isopropanol.[202] This

reaction pathway is shown more generally for alcohols in Scheme 4.6. HMF is first converted to BHMF via transfer hydrogenation by an alcohol. The BHMF then undergoes direct etherification with another alcohol molecule to produce the mono-ether, and a second etherification with another alcohol molecule to produce the di-ether.[202] The proposed rate limiting step is the Meerwein-Ponndorf-Verley (MPV) conversion of HMF to BHMF via hydrogen transfer from the alcohol. Roman-Leshkov and coworkers have also identified Lewis acid zeolites as effective catalysts for the coupled transfer hydrogenation and etherification of HMF with ethanol and butanol at 393 K for 24 h and pressures of 791 kPa in a 100 mL stainless steel Parr reactor.[133] The authors found that Sn-BEA showed the highest stability and selectivity for etherification, whereas Hf-BEA and Zr-BEA appeared to be more active for the MPV reduction. Hard Lewis-acid centers, such as Zn and Sn, were found to be particularly effective in stabilizing the transition state of the rate-limiting hydride transfer step, whereas the weaker Lewis acid centers, such as Ti and Ta were less effective in catalyzing hydrogen transfer.[133] Primary alcohols are less likely to donate a hydrogen, as 2-butanol is more effective than 1-butanol.[133] Thus for the etherification of substituted alcohols with furans, hydrogen transfer reductive etherification is an attractive option. Still, it is important to note that etherification via transfer reductive hydrogenation is typically done in a batch reactor to support the hydrogen transfer step, which can limit the process scalability and increase the concentration of water in the vessel, thus inhibiting both the transfer hydrogenation and etherification reactions.[133]

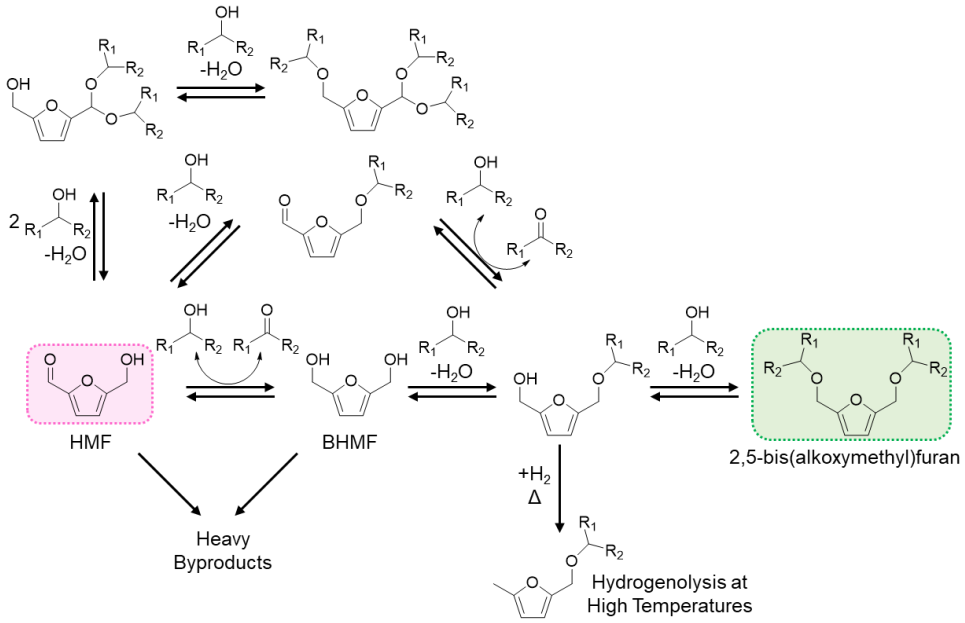

Scheme 4.6. Reaction of sequential catalytic transfer hydrogenation and etherification of HMF to 2,5-bis(alkoxymethyl)furan with alcohol (ethanol, 1-butanol, isopropanol) catalyzed by Sn-Beta (adapted from ref. [202]).

iv. Etherification by Alcohol Addition to an Olefin

Branched ethers produced by the addition of an alcohol to an olefin, such as methyl-*tert*-butyl ether (MTBE), ethyl-*tert*-butyl ether (ETBE), *tert*-amyl methyl ether (TAME), and *tert*-amyl-ethyl ether (TAEE), are useful fuel additives that can be generated from biomass-derived molecules. During the direct etherification of *tert*-butanol with linear alcohols, *tert*-butanol tends to favor dehydration to isobutene, producing water, thereby reducing ether selectivity. The reaction

of an alcohol and an olefin to yield an ether is stoichiometric; however, there are many challenges to the synthesis of ethers by the addition of an alcohol to an olefin. These include reactor design, side product formation, and product inhibition. This section discusses these challenges and identifies how the yield of the desired ether products can be improved.

One key challenge in the reaction of olefins with alcohols is the fact that for gaseous olefins, such as isobutene, the reaction cannot be performed in a single phase. For example, the formation of methyl *tert*-butyl ether is often completed in a two-step process: isobutanol is first dehydrated over a silica-alumina catalyst at 498 K, then reacted with isobutene over Amberlyst 15 at 323 K, achieving a yield of MTBE and MIBE of approximately 28% with a MTBE:MIBE ratio of 11.7:1.[203] Not only is the ether selectivity fairly low, but the second step involves either bubbling a gas through liquid, which introduces mass transfer limitations, or operating at elevated pressure in order to keep all reactants in the liquid phase.[204]

The formation of side products is also a key concern, since isomerization and dimerization of olefins, as well as alcohol dehydration, adversely affect selectivity to the desired ethers. Scheme 4.7 provides an overview of the reaction pathway and side products formed from the addition of primary alcohols to linear olefins. In the presence of an acid catalyst, olefins can undergo oligomerization, producing higher carbon-number products that can further oligomerize and contribute to coke formation and, hence, catalyst deactivation. In addition, alcohols can undergo unimolecular dehydration to form olefins or direct etherification to form symmetrical ethers. When olefins are reacted with glycerol or polyols, the polymerization of the alcohols to poly-ethers is also a concern. As shown in Scheme 4.7, primary olefins can readily isomerize to form secondary olefins,[204] which can also react with alcohol to produce a variety of ether products depending on which side of the double bond the alcohol adds to. Karinen et al. have found that as the temperature increases from 333 to 353 K, the ratio of olefin isomerization to etherification increases for reactions of methanol, ethanol, 1-propanol, 1-butanol, 2-butanol, and isobutanol with 2-methyl-1-butene and 2,4,4-trimethyl-1-pentene over Amberlyst 15.[204] Other authors have suggested that isobutene dimerization over Amberlyst 35 and Purolite CT275 increases with increasing temperature and increasing olefin to alcohol ratio.[205] For side reactions involving alcohol dehydration, the production of water presents additional challenges. Water can readily react with 1,1-disubstituted olefins to form tertiary alcohol,[17,204,206] and thereby inhibit active sites on the catalyst, decreasing rates of both isomerization and etherification.[127,204,207]

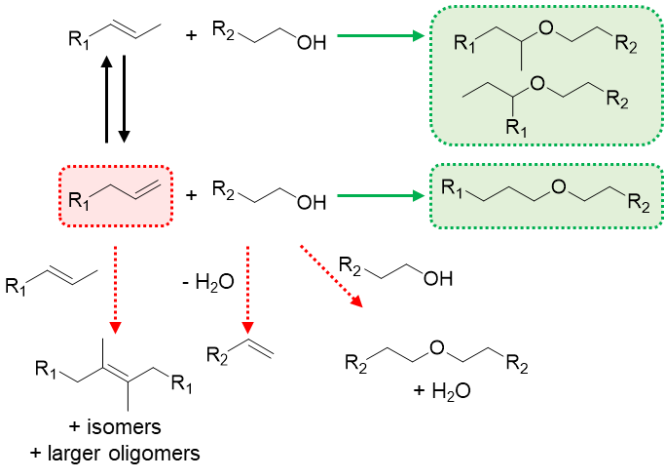

Scheme 4.7. Reaction pathway and side product formation for the etherification of primary alcohols with linear olefins.

The challenges noted above can be surmounted in several ways in order to control product selectivity. These include the choice of catalyst, the ratio of olefins to alcohols, the choice of alcohol and olefin structures, the temperature, and water removal. Scheme 4.8 shows some sample reactions of olefins with alcohols to produce useful ether products. Amberlyst 35 is an effective catalyst for producing asymmetrical ethers from a variety of alcohols and olefins.[146,207,208] As shown in Scheme 4.8a, glycerol can be reacted with isobutene to form mono-, di-, and tri-*tert*-butyl ethers. Klepacova et al. have reported yields of di- and tri- ethers from glycerol of up to 89% at 100% conversion of glycerol at 333 K,[207] and demonstrated that Amberlyst 35 is highly selective for the etherification of isobutene with ethylene glycol compared with para-toluene sulfonic acid and large-pore zeolites H-Y and H-BEA.[209] Karinen et al. have found that for the etherification of glycerol with isobutene over Amberlyst 35, optimal selectivity towards ethers was achieved with an isobutene to glycerol molar ratio of 3:1 at 353 K.[208] By controlling the reaction conditions, it is possible to tune the distribution of ethers to match desired fuel blends, thus avoiding costly separations. As mentioned in Section 4.III, di- and tri-*tert*-butyl glyceryl ethers are preferred for diesel blends due to their solubility in diesel fuel and their properties such as viscosity and cloud points.[143–146] Klepacova et al. found that the highest yields of di- and tri-*tert*-butyl glyceryl ethers were achieved over Amberlyst 35.[209] While glycerol conversion was highest over zeolite HBEA, the reaction to form tri-*tert*-butyl glycerol ether was sterically hindered, thus the selectivity was low.[209]

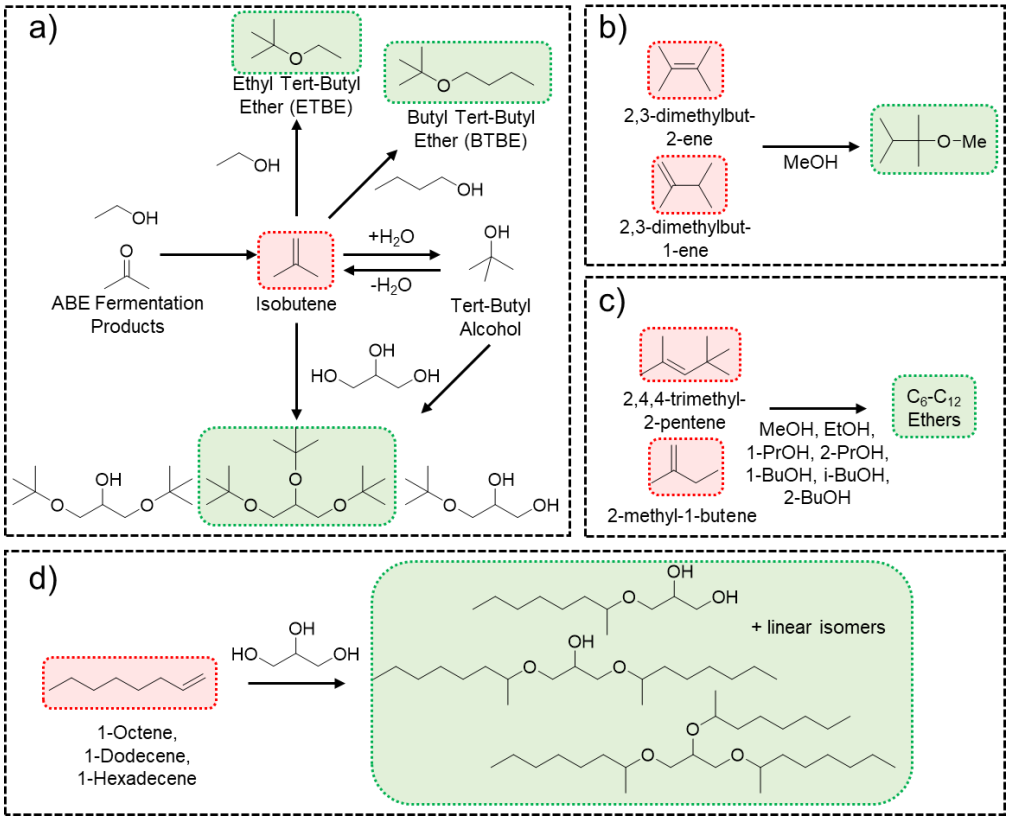

Scheme 4.8. Scope of ether formation reactions via alcohol addition to olefins catalyzed by Amberlyst 35 and other catalysts.

The reaction of isobutene with ethanol or butanol produces ethyl-*tert*-butyl ether (ETBE) and butyl-*tert*-butyl ether (BTBE), respectively, as shown in Scheme 4.8a. Tejero et al. found

Amberlyst 35 to be the most effective catalyst for this reaction compared to Amberlyst 16, Amberlyst 39, Amberlyst 46, Amberlyst 70, and Purolite CT-275, at temperatures between 315 and 353 K.[210] Amberlyst 35 was also effective for the etherification of 2-methyl-1-butene and 2,4,4-trimethyl-1-pentene with various C_1-C_4 alcohols between 333 – 353 K in the liquid phase (Scheme 4.8c)[204] and for the etherification of C_8-olefins with methanol in the liquid phase between 323 – 363 K.[206]

Badia et al. suggest that Amberlyst 35 is the most promising catalyst because of its strong acidity and rigid polymer backbone, which enhance the reaction rate.[210] However, according to Ruppert et al., catalyst hydrophilicity and pore structure are the most critical catalyst properties for achieving high ether selectivity.[211] While Bajus et al. suggest that H-BEA is not effective for etherification reactions of olefins and alcohols, Ruppert et al. have reported H-BEA to be more selective for the etherification of glycerol and other glycols with 1-octene, 1-dodecene, and 1-hexadene compared to Amberlyst 70, p-TSA, H-Y, USY, and H-MFI. Using H-BEA, selectivities towards mono- and di-octyl ethers from glycols such as ethylene glycol and 1,2-propylene glycol of up to 85-95% were achieved at glycol conversions between 15-20% at temperatures between 393 – 413 K.[211] Silica-supported sulfated zirconia, Amberlyst 16W, and Amberlyst 15 have also been employed as catalysts for the reactions of C_6 olefins with methanol (Scheme 4.8b)[212], etherification of isoamylenes (2-methyl-1-butene, and 2-methyl-2-butene) with methanol, ethanol, and n-propanol (Scheme 4.8c),[127] and isobutene with butanol (Scheme 4.8a),[213] respectively, for temperatures between 333 and 353 K. While zeolites introduce pore volume constraints, they are thermally stable above 423 K, unlike Amberlyst 35 and Amberlyst 16. Still, the majority of alcohol additions to olefins are performed between 323 and 363 K, which is well within the range of thermal stability of resin catalysts. The catalysts that are effective for the etherification of olefins with alcohols contain large pore volumes or no pores, and have high acid capacities, suggesting that Amberlyst 35 is a promising candidate for these reactions.

The ratio of alcohol to olefin strongly affects the kinetics of the reaction. Hatchings et al. have observed that the kinetics of etherification varies with the ratio of reactants.[214] For the reaction of isobutene with methanol or n-butanol over Amberlyst 15, at lower isobutene to alcohol ratios, the rate of etherification is zero order in alcohol and first order in olefin, whereas at higher alcohol to isobutene ratios, the reaction is first order in alcohol and zero order in olefin. These observations suggest that when the surface is saturated with alcohol, the rate-limiting step is the protonation of the olefin by the solvated proton, and when the surface is saturated with olefins coordinated to the sulfonic acid groups, the rate limiting step is the interaction of the olefin with the alcohol.[214]

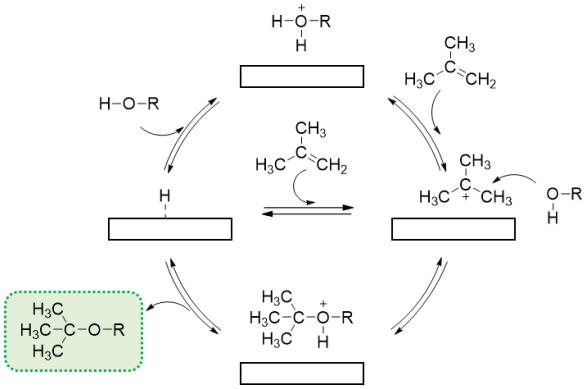

Scheme 4.9. Proposed mechanism for the etherification of isobutene with linear alcohols (top pathway shows how alcohol can be protonated and then donate a hydrogen to the olefin).

Scheme 4.9 shows a proposed mechanism for the reaction of isobutene with an alcohol and demonstrates how solvated alcohols can assist in the protonation of the olefin. In the general mechanism suggested by Tretbar et al., the olefin is first protonated by the acid site, leaving a stabilized carbocation intermediate, which then accepts electrons from the oxygen of the alcohol, forming a protonated ether, which, in turn, desorbs in the final step to form the asymmetrical ether.[213] The upper pathway in Scheme 4.9 shows how the alcohol can be protonated by the acid site and then proceed to readily donate an acidic hydrogen to the olefin. For this mechanism, the rate-limiting step would be protonation of the olefin, resulting in a first order dependence of the rate of etherification on the olefin concentration. This conclusion is consistent with the observation that the reaction is first order in olefin and zero order in alcohol at low isobutene to alcohol ratios.[127,203,214]

The alcohol structure also affects the mechanism for the addition of an alcohol to an olefin. Ancillotti and Fattore have suggested that when isobutene is reacted with higher alcohols, the reactivity order is related to the alcohol basicity, which dictates the proton transfer ability of the ROH_2^+.[215] Therefore, in the case where the alcohol to olefin ratio is greater than or equal to one, the alcohol acts as a solvent. Karinen et al. have shown that etherification and dehydration rates increase with decreasing alcohol polarity and with increasing carbon number of the alcohol, owing to the acidity and Mulliken charges of the oxygen atom of the alcohol.[204] Hatchings et al. and Ancillotti et al. also point out that the higher reactivity of n-butanol over methanol for etherification of tertiary olefins over Amberlyst 15 reflects the higher acidity of the proton on n-butanol than on methanol.[214,216] The authors suggest that the excess of alcohol breaks up the network of hydrogen-bonded sulfonic acid groups, which aids in solvating and, hence, dissociating the proton.[214] By contrast, Linnekoski et al. found that methanol, ethanol, and 1-propanol affect the rate of olefin isomerization but not the etherification rate for alcohol addition to isoamylenes.[127] This trend was explained by the fact that 2-methyl-1-butene isomerizes to 2-methyl-2-butene more rapidly in the presence of more acidic protons caused by more basic alcohols. The more substituted olefin, 2-methyl-2-butene, is more stable and thus less reactive for etherification, so the effects of increased acid strength cancel each other out, resulting in no net change in the etherification rate. The solvation effects of alcohols are consistent with the mechanism proposed in Scheme 4.9, in which the rate-limiting step for etherification is the protonation of the olefin.

In addition to the choice of alcohol, the choice of olefin also contributes to the reaction kinetics. The more volatile the olefin, the more pressure must be applied to maintain a liquid phase reaction. Generally, the longer the chain length, the lower the volatility. The selection of isomer also affects the reaction rate, because the olefin isomers which are thermodynamically favored at equilibrium have a lower reactivity for etherification. Selecting less substituted olefins can increase etherification rates, although isomerization is likely to occur. Karinen and Krause found that etherification rates of olefins with methanol were lower for olefins with longer carbon chains (C_8) compared to shorter chains (C_5).[206] In addition, they found that the equilibrium between 2,4,4-trimethyl-1-pentene and 2,4,4-trimethyl-2-pentene was affected by steric hindrance, which is another concern when selecting an olefin for this reaction.[206]

Temperature has a clear effect on ether selectivity. As discussed earlier, the optimal temperatures for etherification of olefins with alcohols is between 323 and 363 K.[127,204,206,207,209,210,212,213] The tradeoffs between catalyst activity and selectivity are critical in optimizing for ether formation. In a prospective study by Soto et al., the equilibrium conversion, selectivity, and yield was optimized using a combination of experimental and numerical multi-objective optimization in order to determine conditions most favorable for the liquid phase

etherification of isobutene and isoamylene by addition of ethanol over Amberlyst 35.[17] This study concluded that the optimal experimental conditions for maximizing the simultaneous production of ETBE and TAEE occurred for molar alcohol to olefin ratios of 0.9, C_4 to C_5 olefins ratios of 0.5, and at a temperature of 323 K.[17]

In summary, the reaction of alcohols with olefins produces asymmetrical ethers with a high degree of branching for use as fuel additives. Under the right conditions, high yields of mono- di- and tri- ethers of glycerol with olefins as well as cross coupling of mono-alcohols with olefins can be achieved. While this method of producing ethers could be employed to produce symmetrical linear ethers, the tendency for olefins to undergo isomerization and oligomerization suggests that direct etherification of alcohols is more appropriate for obtaining high selectivities towards linear symmetrical ethers. Thus, this reaction is best employed when the olefin is highly substituted and the desired product is an asymmetrical ether.

VI. The Role of Cooperative Brønsted and Lewis Acidity in Selective Ether Synthesis

Recent studies of alcohol etherification and dehydration over solid acids have indicated that by tuning the strength and ratio of Brønsted and Lewis acid sites on the surface of the catalyst, the selectivity of the reaction can be adjusted. As mentioned in Section 4.V.i, our group has proposed that cooperative effects between Brønsted and Lewis acid sites on tungstated zirconia promote the bimolecular etherification of dodecanol to form di-dodecyl ether.[99] Padovan and Hammond have suggested that bifunctional Brønsted and Lewis acidic zeolites facilitate the production of butoxymethyl furan via the etherification of furfural and 2-butanol.[217] The authors found that a bifunctional H-BEA containing 2 wt% Sn and 0.5 wt% Al gave high ether selectivity, >75%, and exhibited excellent stability. By contrast, monofunctional analogues or physical mixtures of the analogues were less selective and stable.[217] Fang et al. also found that Sn-MFI was effective for the etherification of 2,5-bis(hydroxymethyl)furan (BHMF) with methanol to produce 2,5-Bis(methoxymethyl)furan (BMMF), achieving a selectivity of 95%. The authors found that BMMF formation increased with increasing Lewis acidity of the catalyst.[198]

Several studies have shown that the ratio of Brønsted to Lewis acid sites on the surface of a catalyst can be tuned to adjust the product distribution for glycerol dehydration reactions. Wang et al. studied the dehydration of glycerol to acrolein over Al/H-ZSM5 zeolite catalysts, and suggested that a cooperative effect between Brønsted and Lewis acid sites on the surface of the catalyst is responsible for the high acrolein selectivity. [218] Foo et al. studied the role of Lewis and Brønsted acid sites in the dehydration of glycerol over niobia, and concluded that a higher ratio of Brønsted acid sites to Lewis acid sites results in higher acrolein selectivity, whereas a larger ratio of Lewis acid sites to Brønsted acid sites results in higher selectivity towards hydroxyacetone.[84] Cooperative effects between Brønsted and Lewis acid sites on Sn-Beta have also been proposed for ethanol dehydration. For example, Bukowski et al. have proposed a concerted transition state involving both the Lewis acidic Sn center and an adjacent weakly Brønsted-acidic framework silanol group.[170]

Because there is precedent for the role of Brønsted and Lewis acidity in controlling etherification and dehydration selectivity over metal oxides, the investigation of tuning Brønsted and Lewis acid sites by varying the ratio of Brønsted to Lewis acid sites, changing the strength of Lewis acid centers by varying the metal cations, and changing the density of Brønsted acid sites, is a promising avenue for future improvement of ether selectivity that is not afforded by Brønsted acidic polymeric resins.

VII. Conclusions and Outlook

We have shown that ethers suitable for use as fuels, lubricants, and specialty chemicals can be synthesized from a variety of biomass-derived platform molecules through direct and reductive etherification of alcohols, aldehydes, ketones, esters, carboxylic acids, and olefins. The best strategy for synthesizing ethers from biomass-derived compounds using heterogeneous catalysts depends on the structure of the reactants and the properties of the catalyst. In this chapter, we have outlined the advantages and disadvantages to various methods of producing ethers from renewable sources. Here we summarize the recommended synthesis routes for producing a particular type of ethers from a defined set of reactants.

Symmetrical ethers can be formed from linear alcohols via direct etherification over a solid acid, using the reactant alcohol as the solvent, at low temperatures, and with minimal side product formation. If there are carbon chain branches on the alcohol, direct etherification is still viable as long as the branches are at least three carbons away from the hydroxyl group of the alcohol. If mixtures of symmetrical and asymmetrical linear ethers are desired, direct etherification of a mixture of linear alcohols is a viable synthetic route. However, if purely asymmetrical ethers are desired, we recommend reductive etherification of an alcohol and an aldehyde or ketone in the presence of a solid acid catalyst and a hydrogenation catalyst, such as Pd/C. This method enables selective synthesis of asymmetrical or symmetrical ethers from alcohols with a significantly larger range of structures including branched alcohols, such as those produced from the Guerbet reaction, to create lubricant-range molecules, as well as 2° and 3° alcohols for use as diesel and gasoline additives. Reductive etherification can also be used to prepare ethers via the reaction of alcohols with esters and carboxylic acids, and both direct and reductive etherification can also be employed for the valorization of glycerol and polyols for the synthesis of fuel additives and specialty chemicals.

Fuel additives can also be produced via direct, reductive, and transfer hydrogenation etherification of furfural and furans derived from biomass. For these methods, we discussed the reaction pathways and conditions for selective synthesis of the desired ethers based upon recent developments in the literature. Amberlyst 15 and zeolites stand out as selective catalysts for the direct etherification of ethanol with hydroxymethyl furfural. Amberlyst 15 is also an effective catalyst for the etherification of furfural or methyl furfural with ethanol and for the direct etherification of BHMF with alcohols. Low temperatures and longer reaction times are preferred for these reactions. Reductive etherification of furans enables enhanced selectivity towards cross-etherification by limiting homocoupling of alcohols and can be achieved using a combination of an acid catalyst, Pd/C, and H_2 for reduction. For the etherification of substituted alcohols with furans, transfer hydrogenation etherification is also a viable option, as the alcohol can be used as both the reducing agent and the reactant, eliminating the need to supply molecular hydrogen.

The addition of an alcohol to an olefin is another method of producing ethers. The selectivity to ether via this reaction depends on avoidance of alcohol dehydration. This can be achieved by operating at temperatures between 323 and 363 K and using Amberlyst 35 as a catalyst. This synthesis method is most effective for the etherification of alcohols with highly substituted olefins, such as the synthesis of ethyl-*tert*-butyl ether.

Brønsted acidic resins with large pores that swell in the presence of solvent such as Amberlyst 70 are effective in promoting etherification of alcohols by increasing the concentration of alcohol around the active site. A high local concentration of alcohol can also be achieved using bifunctional catalysts that contain proximate adsorption sites for alcohols, such as the Brønsted and Lewis acid sites on tungstated zirconia. Future directions in employing tandem catalysts,

tuning pore sizes, and identifying the site requirements for side reactions could enable finer enhancements of selectivity for both direct and reductive etherification reactions. Another promising approach, particularly for the synthesis of asymmetrical ethers via direct etherification, is the use of so-called "heterogenized" homogeneous acid catalysts. For example, the homogeneous cationic ruthenium−hydride complex $[(C_6H_6)(PCy_3)(CO)RuH]^+BF_4^-$ is known to catalyze the selective etherification of two different alcohols to form asymmetrical substituted ethers with a large scope of substrates and without the need for reactive reagents or protecting groups.[219] Developing heterogeneous catalysts that enable selective asymmetrical ether synthesis without the need for reductive etherification could lower costs associated with operating under hydrogen pressure, and would allow more flexibility in the choice of alcohol substrates.

The removal of water is also a major consideration in the synthesis of ethers, as water inhibits active sites for etherification, thus lowering the etherification rate and selectivity. Investigation into water removal with membranes and reactive distillation with recirculation is a physical method of improving ether yields. Further investigation into tuning feed ratios for direct and reductive etherification may also elucidate pathways towards producing blends of ethers for fuel and lubricant applications. Moving forward, investigation of multi-step processes for synthesizing ethers directly from biomass will be necessary to provide further insights into developing industrially-relevant processes for synthesizing renewable ethers. Overall, these recent efforts to synthesize ethers from renewable sources using sustainable heterogeneous catalysis provide a vast scope of pathways towards utilizing biomass-derived platform molecules and have the potential to enable the production of fuels, lubricants, and specialty chemicals which can replace petroleum-derived products at low cost and with reduced adverse environmental effects.

5. Ethanol Oxidation Selectivity over Ag and Au on Li_2O/Al_2O_3 and Al_2O_3-Supported Catalysts

I. Abstract

Previous accounts by Lippits and Nieuwenhuys reported ethylene oxide selectivities of >95% from the direct conversion of ethanol over Ag, Au, and Cu nanoparticles on Li_2O/Al_2O_3.[220,221] In contrast, a recent report by Silbaugh et al. observed no ethylene oxide under the same reaction conditions.[222] Here, the effect of catalyst support, Li_2O loading, and various nanoparticle synthesis procedures were explored in order to provide further clarity on this discrepancy, indicating that the primary product of ethanol oxidation over these catalysts is acetaldehyde, not ethylene oxide.

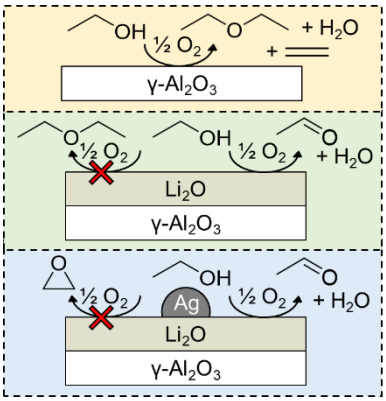

Figure 5.1. Graphical abstract for Chapter 5.

II. Introduction

Two compelling research papers published by Lippits and Nieuwenhuys reported high ethylene oxide selectivities from the direct conversion of ethanol over Ag, Au, and Cu nanoparticles on Li_2O/Al_2O_3,[220,221] which motivated further investigation of the oxidation of ethanol over a series of Ag and Au catalysts. The implications of the direct conversion of ethanol to ethylene oxide are extraordinary, as ethanol could be used as a sustainably-derived platform chemical to produce ethylene oxide, which is a high-value precursor for many polymers and specialty chemicals. After a recent publication from Silbaugh et al. reported that Ag, Au, and Cu on Li_2O/Al_2O_3 catalysts did not produce ethylene oxide from ethanol oxidation over the same reaction conditions,[222] we were motivated to provide further explanations for the discrepancy in selectivities observed for the oxidation of ethanol.

Since the original Lippits and Nieuwenhuys publications in 2010, there have to our knowledge been no additional reports of ethylene oxide production directly from ethanol over any heterogeneous catalyst. In industry, ethylene oxide has been reported to be produced from ethanol, but it is produced via a two-step process in which ethylene is the intermediate, such as the process employed by the Scientific Design Company.[223] There were several key claims of the study by Lippits and Nieuwenhuys. First, ethylene oxide was produced directly from ethanol without an ethylene intermediate, as evidenced from the fact that no ethylene oxide was detected when ethylene was fed over the catalyst. Second, for Ag-based catalysts, both Li_2O and O_2 are necessary for selective ethylene oxide formation. And third, CeO_x and Li_2O suppress ether formation from ethanol by neutralizing acid sites on Al_2O_3. They reported selectivities towards ethylene oxide over 95% over $Ag/Li_2O/Al_2O_3$, $Au/Li_2O/Al_2O_3$, and $Cu/Li_2O/Al_2O_3$ at 200 °C in the presence of O_2.

According to experimental thermodynamic data, the Gibbs free energy of formation for the reaction of ethanol plus ½ O_2 to form ethylene oxide and water is -70.5 kJ mol^{-1} at 298 K and -42 kJ mol^{-1} at 500 K. The Gibbs free energy of formation for the reaction of ethanol plus ½ O_2 to produce acetaldehyde and water is -190.3 kJ mol^{-1} at 298 K and -166.2 kJ mol^{-1} at 500 K. In the absence of oxygen, the reaction of ethanol to produce ethylene oxide and H_2 has ΔG_{rxns} of +158.1 kJ mol^{-1} and +187 kJ mol^{-1} at 298 K and 500 K, respectively.[157] The production of water drives both reactions in the presence of oxygen and indicates that both the formation of ethylene oxide and acetaldehyde are downhill in Gibbs free energy. Still, the formation of acetaldehyde is thermodynamically preferred over the formation of ethylene oxide. With this in mind, we synthesized and tested a series of Ag and Au catalysts for the ethanol oxidation reaction under the same reaction conditions as those previously reported, and tested additional nanoparticle synthesis methods, supports, and promoters.

III. Experimental

i. Catalyst Synthesis and Characterization

$Ag/Li_2O/Al_2O_3$ and $Au/Li_2O/Al_2O_3$ catalysts were synthesized using previously reported methods.[220,221] $Li_2O/\gamma\text{-}Al_2O_3$ was synthesized via incipient wetness impregnation of a solution of $LiNO_3$ on commercial $\gamma\text{-}Al_2O_3$. The powder was treated in air at 350 °C for 4 h by ramping at a rate of 2 °C min^{-1}. $Ag/Li_2O/Al_2O_3$ catalysts were prepared either via deposition-precipitation (DP) or incipient wetness impregnation (IWI). For the DP method, a slurry of nanopure H_2O, urea, and $AgNO_3$ was allowed to stir at 80 °C. As the urea decomposes, Ag nanoparticles are deposited on the surface of the catalyst. The catalyst was then filtered and rinsed with nanopure H_2O and dried at 110 °C overnight. For IWI of the silver nanoparticles, the catalyst support was impregnated with $AgNO_3$ and treated in air at 600 °C for 3 h at a heating rate of 2 °C min^{-1}. Au nanoparticles were deposited on Li_2O/Al_2O_3 via deposition-precipitation of $HAuCl_4$. Prior to the start of the reaction, Ag catalyst were pretreated for 2 h at 400 °C in 40 mL min^{-1} He. Additional details for catalyst synthesis are provided in Table 5.2.

ii. Ethanol Oxidation Reactions

Gas-phase reactions were performed in a 6.35 mm OD quartz tube with an expanded section (~12.7 mm OD, ~20 mm length) packed with quartz wool above and below the catalyst. Reactions were carried out in 15 kPa air (Praxair, Ultra Zero Grade) using Helium (Praxair, 5.0 Ultra High Purity) as a carrier gas. Liquid-phase ethanol was injected via a Cole Palmer 74900 Series syringe pump into the reactor with lines heated to >94 °C to vaporize the ethanol before reaching the reactor. Experiments were carried out at atmospheric pressure, at 200 °C, with a total flow rate of 40 mL min^{-1}. Reaction products were analyzed using an Agilent 6890N chromatograph containing a (5%-phenyl)-methylpolysiloxane capillary column (Agilent, HP-5) connected to a flame ionization detector. The temperature program for the GC column began at -10 °C, then ramped to 30 °C at 3 °C min^{-1}, then ramped to 60 °C at 20 °C min^{-1}, which enabled the ability to distinguish between ethylene oxide and acetaldehyde. Retention times and response factors were obtained either by injecting solutions of products via the syringe pump, or by flowing standard gas mixtures into the reactor via a mass flow controller. Ethylene oxide (50 mg mL^{-1} in EtOH), acetaldehyde (50 wt% in EtOH), and ethyl acetate (99.8%) were obtained from Sigma Aldrich, and standard gas (3.01% methane, 1.5% ethylene, 1.5% ethane, 1% propene, 1.01% propane, 0.745% cis-2-butene, 0.748% trans-2-butene, 0.75% butane, 0.6% n-pentane in He), 1% Ar in He (CSG), ammonia (99.995%), and He (5.0 UHP) was obtained from Praxair.

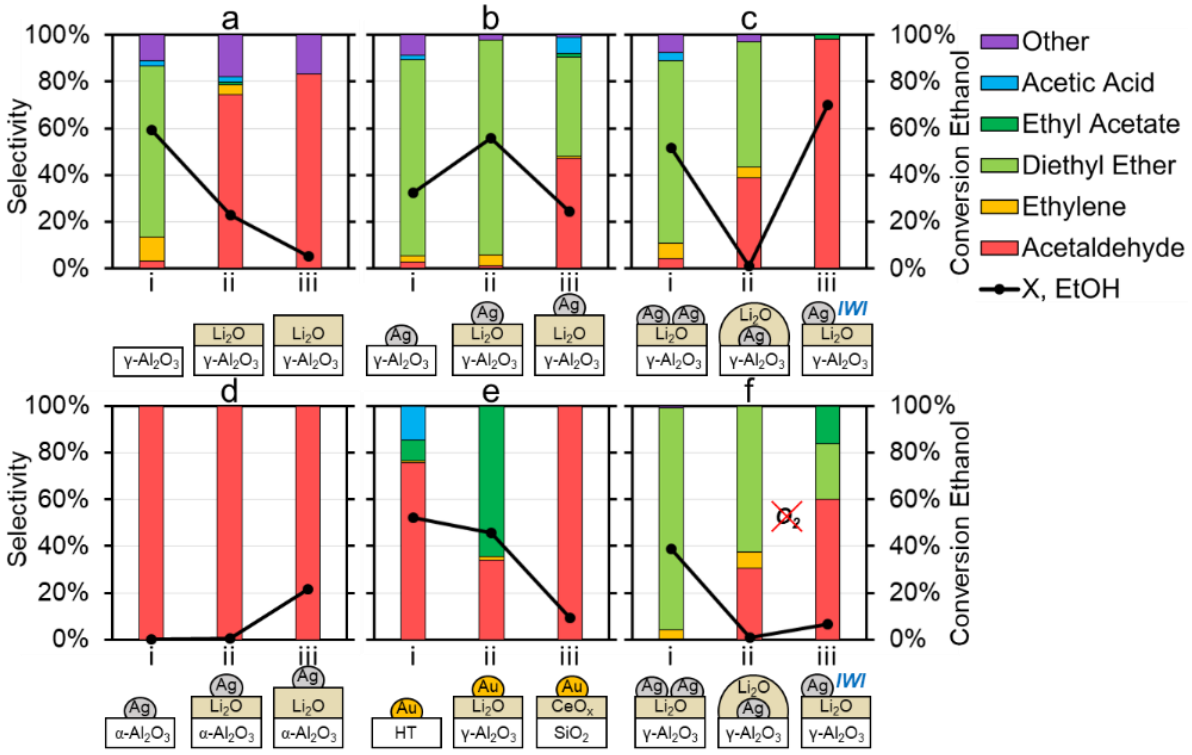

Figure 5.2. a) Effect of Li_2O loading on γ-Al_2O_3 on reaction selectivity i) no Li_2O, ii) Li:Al 1:15, iii) Li:Al 1:7, b) Effect of Li_2O loading on Ag/Li_2O/γ-Al_2O_3 catalysts with Ag:Al 1:75, i) no Li_2O, ii) Li:Al 1:15, iii) Li:Al 1:7, c) i) Ag/Li_2O/γ-Al_2O_3 with Li:Al 1:15 and Ag:Al 1:25, ii) Ag/Li_2O/γ-Al_2O_3 prepared with Li_2O IWI after Ag DP, iii) IWI of Ag onto Ag/Li_2O/Al_2O_3 with Li:Al 1:15 and Ag:Al 1:75, d) Effect of Li_2O loading on α-Al_2O_3 catalysts with Ag:Al 1:75, i) no Li_2O, ii) Li:Al 1:15, iii) Li:Al 1:7, e) Au nanoparticle catalysts, i) Au/HT, ii) Au/Li_2O/Al_2O_3 Li:Al 1:15, Au:Al 1:75, iii) Au/CeO_x/SiO_2, f) Reactions of catalysts in c) in the absence of air. Reaction conditions: 200 mg catalyst, 3 kPa EtOH, 15 kPa air (40 mL min^{-1} total flow in He), 200 °C.

IV. Results and Discussion

The key results of the oxidation reactions of ethanol over the various catalysts at 200 °C are summarized in Figure 5.2a-f. From Figure 5.2a, it is clear that as lithium oxide loading on γ-Al_2O_3 is increased, etherification is suppressed, acetaldehyde formation predominates, and catalyst activity decreases. While the Li_2O does suppress acid sites necessary for etherification and dehydration, it does not give way to ethylene oxide formation. From Figure 5.2b, as the weight loading of Li_2O is increased for Ag/Li_2O/Al_2O_3 catalysts, ether formation is also suppressed, giving way to acetaldehyde formation. The only catalyst that showed trace amounts of product at the proper retention time for ethylene oxide was the Ag/Al_2O_3 catalyst, but the quantity is insufficient for accurate characterization. It is likely that any trace amounts of ethylene oxide formed were a result of ethanol dehydration to ethylene on acidic sites on alumina, followed by ethylene epoxidation, which is known to occur over Ag/Al_2O_3.[224,225]

Upon increasing the $AgNO_3$ concentration for deposition-precipitation, etherification becomes more predominant, as seen in the first entry of Figure 5.2c. This could be due to the $AgNO_3$ solution dissolving the lithium oxide during deposition-precipitation. In order to test this, two alternative methods of catalyst synthesis were performed, where the Ag nanoparticles were deposited onto the alumina first, followed by incipient wetness impregnation of lithium oxide, and where silver nanoparticles were deposited via incipient wetness impregnation onto the Li_2O/Al_2O_3

catalyst, both shown in Figure 5.2c. For both alternative methods, ether formation is suppressed, indicating that the deposition precipitation method could result in degradation of the lithium oxide layer. The $Ag/Li_2O/\gamma\text{-}Al_2O_3$ catalyst prepared via incipient wetness impregnation of $AgNO_3$ was most active and selective for the formation of acetaldehyde.

Because the primary product after acidity has been suppressed is acetaldehyde, this poses the question of whether ethylene oxide is forming on the surface of the catalyst and is rapidly isomerizing to acetaldehyde. According to reports in the literature, low surface area alpha alumina is inert for the isomerization of acetaldehyde to ethylene oxide.[226] Thus, a series of $Ag/Li_2O/Al_2O_3$ catalysts were synthesized on a low surface area $\alpha\text{-}Al_2O_3$ support, and the results are shown in Figure 5.2d. From this Figure, it is clear that the only product formed is acetaldehyde, and the activity of the catalysts is significantly lower than the $\gamma\text{-}Al_2O_3$-supported catalysts. A series of gold catalysts were also tested for ethanol oxidation reactions, yielding acetaldehyde and ethyl acetate as the primary products, as shown in Figure 5.2e. The reactions in Figure 5.2c were repeated in the absence of air and are shown in Figure 5.2f, in which catalytic activity and acetaldehyde selectivity both decrease. Additional reactions in the absence of oxygen are provided in Table 5.3.

A comparison of the results from this work and previously reported selectivities for ethanol oxidation over Ag and Au on Li_2O/Al_2O_3 are shown in Table 5.1. In agreement with Silbaugh et al. we observed no formation of ethylene oxide over either $Ag/Li_2O/Al_2O_3$ or $Au/Li_2O/Al_2O_3$ under the same reaction conditions, contrary to the observations of Lippits and Nieuwenhuys. The selectivity distributions and catalyst activities from this work match closely with those identified by Silbaugh et al., except for the reaction of ethanol over the $Ag/Li_2O/Al_2O_3$ catalysts, in which we observed the formation of ether as well, possibly as a result of residual acid sites on the alumina. Other studies have also shown that $AgLi\text{–}Al_2O_3$ catalysts containing different phases of alumina are selective for the oxidative dehydrogenation of ethanol.[227]

While it is possible that the synthesis methods of Lippits and Nieuwenhuys yielded different catalysts which were indeed active for ethylene oxide formation, it is more likely that acetaldehyde was misidentified as ethylene oxide. If the selectivities were switched for their results, it would match more closely with the results of this work and of Silbaugh et al. Due to the similar mass fragments for acetaldehyde and ethylene oxide, it is unlikely that the m/z ratios of the two could be distinguished using mass spectrometry. The GC retention times for ethylene oxide and acetaldehyde are fairly close, and under certain column program temperatures, may overlap. In addition, while the formation of glycol upon bubbling the product through NaOH would be indicative of the presence of ethylene oxide, the methods were not clearly stated in the Lippits and Nieuwenhuy's manuscripts, thus the glycol may also have been misidentified. Finally, it was noted that the authors did not observe any ethylene oxide when flowing ethylene over the catalysts, but seeing as alumina and silica-supported Ag and Au catalysts have been established as ethylene epoxidation catalysts,[224,225,228] it is surprising that no ethylene epoxidation occurred.

Table 5.1. Comparison of Selectivities Reported for Ethanol Oxidation in the Literature

Catalyst	Ref.	X, EtOH	Selectivity			
			Acetaldehyde	Ethyl Acetate	Ethylene oxide	Other
$Ag/Li_2O/\gamma\text{-}Al_2O_3$	This Work	25	50	0	0	50
	[220]	58	4	0	96	0
	[222]	15	>99	0	0	<1
	[227]	68	>99	0	0	0
$Au/Li_2O/\gamma\text{-}Al_2O_3$	This Work	46	84	16	0	0
	[221]	80	0	0	95	5
	[222]	35	80	15	0	5

Reaction Conditions: 200 °C, GHSV 2500 h^{-1}, $EtOH/O_2$ mixture 1:1 mol

V. Conclusions

The compelling reaction of the direct conversion of ethanol to ethylene oxide over Ag and Au nanoparticles on Li_2O/Al_2O_3 may indeed be too good to be true. Upon reproducing the reaction conditions from Lippits and Nieuwenhuys, it was found that the primary ethanol oxidation product is acetaldehyde, in contradiction to their studies and in agreement with recent reports from Silbaugh et al. Additional alumina supported catalysts were also found to be ineffective in producing ethylene oxide from ethanol. While Lippits and Nieuwenhuys claimed that oxygen aids in ethylene oxide production, here we see that oxygen aids in acetaldehyde formation.

The process of producing ethylene oxide from ethylene has been well-established in the literature and in industrial processes, and it has been proposed that on Ag-based catalysts, oxametallacycle intermediates are responsible for the pathway to form ethylene oxide.[229,230] In order to successfully produce ethylene oxide directly from ethanol, it would be necessary to abstract a hydrogen from the β-C of the ethanol, form a CO bond, and abstract a hydrogen from the –OH group. Breaking both the β-C-H bond and the CO bond would lead to unimolecular dehydration to form ethylene and water. Breaking both the α-C-H bond and the –OH bond would result in acetaldehyde formation. If it were possible to convert ethanol directly into ethylene oxide through an oxametallacycle intermediate, the oxygen would likely need to be provided by the alcohol and not from the oxygen supplied in the feed, otherwise an ethylene intermediate would likely be formed. Thus, the challenge of reproducibly forming ethylene oxide directly from ethanol remains, although further understanding of ethanol conversion to other products like acetaldehyde and acetic acid can aid in defining possible pathways to utilize this sustainably-derived resource.

VI. Supporting information

i. Catalyst Properties and Synthesis Methods

Table 5.2. Synthesis of Catalysts.

Ent	Catalyst Name	Support	NP	Preparation Method of NP	Preparation Method of Li_2O	Target Li:Al
1	$Li_2O/\gamma\text{-}Al_2O_3$ Li:Al 1:15	$\gamma\text{-}Al_2O_3$	N/A	N/A	IWI of $\gamma\text{-}Al_2O_3$	1:15
2	$Li_2O/\gamma\text{-}Al_2O_3$ Li:Al 1:7	$\gamma\text{-}Al_2O_3$	N/A	N/A	IWI of $\gamma\text{-}Al_2O_3$	1:7
3	$Ag/Li_2O/\gamma\text{-}Al_2O_3$-DP Li:Al 1:15, Ag:Al 1:75	$\gamma\text{-}Al_2O_3$	Ag	DP	IWI of $\gamma\text{-}Al_2O_3$	1:15
4	$Ag/Li_2O/\gamma\text{-}Al_2O_3$-DP Li:Al 1:7, Ag:Al 1:75	$\gamma\text{-}Al_2O_3$	Ag	DP	IWI of $\gamma\text{-}Al_2O_3$	1:7
5	$Ag/\gamma\text{-}Al_2O_3$-DP Ag:Al 1:75	$\gamma\text{-}Al_2O_3$	Ag	DP	N/A	N/A
6	$Ag/Li_2O/\gamma\text{-}Al_2O_3$-DP Li:Al 1:15, Ag:Al 1:25	$\gamma\text{-}Al_2O_3$	Ag	DP	IWI of $\gamma\text{-}Al_2O_3$	1:15
7	$Ag/Li_2O/\gamma\text{-}Al_2O_3$-DP Li1 Li:Al 1:15, Ag:Al 1:75	$\gamma\text{-}Al_2O_3$	Ag	DP	IWI of $Ag/\gamma\text{-}Al_2O$	1:15
8	$Ag/Li_2O/\gamma\text{-}Al_2O_3$-IWI Li:Al 1:15, Ag:Al 1:75	$\gamma\text{-}Al_2O_3$	Ag	IWI	IWI of $\gamma\text{-}Al_2O_3$	1:15
9	$Ag/\alpha\text{-}Al_2O_3$-DP Ag:Al 1:75	$\alpha\text{-}Al_2O_3$	Ag	DP	N/A	N/A
10	$Ag/Li_2O/\alpha\text{-}Al_2O_3$-DP Li:Al 1:15, Ag:Al 1:75	$\alpha\text{-}Al_2O_3$	Ag	DP	IWI of $\alpha\text{-}Al_2O_3$	1:15
11	$Ag/Li_2O/\alpha\text{-}Al_2O_3$-IWI Li:Al 1:15, Ag:Al 1:75	$\alpha\text{-}Al_2O_3$	Ag	IWI	IWI of $\alpha\text{-}Al_2O_3$	1:15
12	$Au/Li_2O/\gamma\text{-}Al_2O_3$	$\gamma\text{-}Al_2O_3$	Au	DP	IWI of $\gamma\text{-}Al_2O_3$	1:15
13	1%Au/HT	Hydrotalcite	Au		N/A	N/A
14	$Au/CeO_x/SiO_2$	SiO_2	Au			N/A
Abbreviations: DP: Deposition-precipitation, IWI: Incipient Wetness Impregnation						

ii. Catalyst Screening for Ethanol Oxidation Selectivities With and Without Air

Table 5.3. Reactions in the Presence and Absence of Air.

Catalyst						Selectivity [mol%]					
	PM[a]	Target Li:Al	Target Ag:Al /Au:Al	kPa O_2	Ethy-lene	Acetal-dehyde	Diethyl ether	Ethyl Acetate	Acetic Acid	Other	X, EtOH
γ-Al_2O_3	0	0	0	3	11%	3%	74%	0%	2%	11%	59%
γ-Al_2O_3	0	0	0	0	7%	0%	94%	0%	0%	0%	74%
Li_2O/γ-Al_2O_3 Li:Al 1:15	0	1:15	0	3	4%	75%	0%	1%	2%	18%	23%
Li_2O/γ-Al_2O_3 Li:Al 1:15	0	1:15	0	0	10%	61%	0%	9%	0%	21%	6%
Li_2O/γ-Al_2O_3 Li:Al 1:7	0	1:7	0	3	0%	83%	0%	0%	0%	17%	5%
Li_2O/γ-Al_2O_3 Li:Al 1:7	0	1:7	0	0	0%	74%	0%	0%	0%	26%	0%
Ag/γ-Al_2O_3 Ag:Al 1:75	DP	0	1:75	3	3%	3%	86%	0%	2%	9%	33%
Ag/γ-Al_2O_3 Ag:Al 1:75	DP	0	1:75	0	2%	2%	93%	0%	0%	4%	25%
Ag/Li_2O/γ-Al_2O_3	DP	1:15	1:75	3	5%	1%	92%	0%	0%	2%	56%
Ag/Li_2O/γ-Al_2O_3	DP	1:7	1:75	3	1%	47%	42%	2%	7%	1%	24%
Ag/Li_2O/γ-Al_2O_3	DP	1:7	1:75	0	2%	7%	90%	1%	0%	0%	20%
Ag/Li_2O/γ-Al_2O_3	DP	1:15	1:25	3	7%	4%	79%	0%	3%	8%	52%
Ag/Li_2O/γ-Al_2O_3	DP	1:15	1:25	0	4%	0%	95%	0%	0%	1%	39%
Ag/Li_2O/γ-Al_2O_3, Ag first	DP	1:15	1:75	3	5%	39%	54%	0%	0%	3%	1%
Ag/Li_2O/γ-Al_2O_3, Ag first	DP	1:15	1:75	0	7%	31%	63%	0%	0%	0%	1%
Ag/Li_2O/γ-Al_2O_3	IWI	1:15	1:75	3	0%	98%	0%	2%	0%	0%	70%
Ag/Li_2O/γ-Al_2O_3	IWI	1:15	1:75	0	0%	60%	24%	16%	0%	0%	7%
Ag/α-Al_2O_3 Ag:Al 1:75	DP	0	1:75	3	0%	100%	0%	0%	0%	0%	0%
Ag/α-Al_2O_3 Ag:Al 1:75	DP	0	1:75	0	0%	100%	0%	0%	0%	0%	0%
Ag/Li_2O/α-Al_2O_3	DP	1:15	1:75	3	0%	100%	0%	0%	0%	0%	0%
Ag/Li_2O/α-Al_2O_3	DP	1:15	1:75	0	0%	100%	0%	0%	0%	0%	0%
Ag/Li_2O/α-Al_2O_3	IWI	1:15	1:75	3	0%	100%	0%	0%	0%	0%	21%
Ag/Li_2O/α-Al_2O_3	IWI	1:15	1:75	0	0%	100%	0%	0%	0%	0%	2%
1%Au/HT		0		3	0%	94%	0%	2%	4%	0%	52%
1%Au/HT		0		0	0%	82%	0%	18%	0%	0%	14%
Au/Li_2O/γ-Al_2O_3		1:15	1:75	3	0%	84%	0%	16%	0%	0%	46%
Au/Li_2O/γ-Al_2O_3		1:15	1:75	0	6%	78%	0%	5%	3%	9%	21%
Au/Li_2O/γ-Al_2O_3*		1:15	1:75	3	67%	28%	0%	0%	0%	6%	100%
Au/Li_2O/γ-Al_2O_3*		1:15	1:75	0	91%	4%	0%	0%	0%	6%	100%
Au/CeO_x/SiO_2		0		3	0%	100%	0%	0%	0%	0%	9%
Au/CeO_x/SiO_2		0		0	0%	100%	0%	0%	0%	0%	1%

Reaction Conditions: 200 mg catalyst, 3 kPa EtOH, 15 kPa air (40 mL min^{-1} total flow in He), 200 °C, * 400 °C, [a]PM: Nanoparticle Preparation Method.

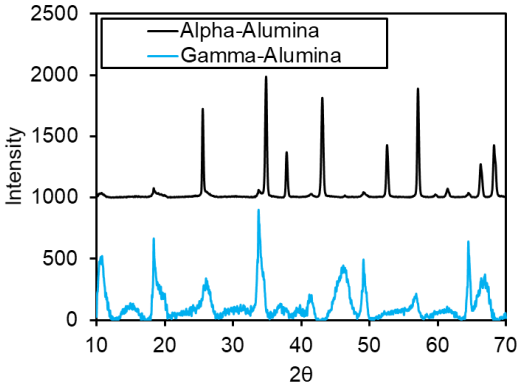

Figure 5.3. XRD of α-alumina prepared through high temperature calcination of γ-alumina. XRD reveals clear alpha phase of alumina after calcination of γ-Al_2O_3 at 1200 °C for 24 hours.

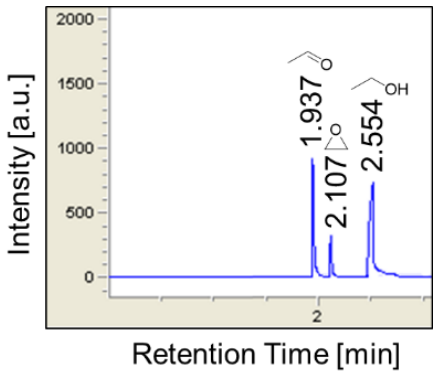

Figure 5.4. GC Retention times for acetaldehyde (1.937), ethylene oxide (2.107), and ethanol (2.554), demonstrating that acetaldehyde and ethylene oxide can be separated in the GC column.

6. Mechanism and Kinetics of the Conversion of Ethanol and Acetone to Isobutene over $Zn_xZr_yO_z$

I. Abstract

Isobutene is a specialty chemical used in the production of fuel additives, polymers, and other high-value products. While normally produced by steam cracking of petroleum naphtha, there is increasing interest in identifying routes to isobutene from biomass-derived compounds, such as ethanol and acetone. Recent work has shown that zinc-zirconium mixed oxides are effective and selective catalysts for producing isobutene from ethanol. We report here investigations of the mechanism and kinetics of the acetone and ethanol conversion to isobutene with the aim of elucidating the reaction pathway, the roles of active acidic and basic sites, and the role of water in promoting stability and selectivity. Zinc-zirconium mixed oxide catalysts with varying zinc loadings were synthesized and characterized with XRD, Raman, BET, CO_2-TPD, NH_3-TPD, and DRIFTS IR of adsorbed pyridine. The observed reaction kinetics suggest that the reaction of ethanol to isobutene proceeds via a five-step sequence. Ethanol first undergoes dehydrogenation to acetaldehyde, which is then oxidized to acetic acid. This product undergoes ketonization to produce acetone, which dimerizes to form diacetone alcohol. The latter product either decomposes directly to isobutene and acetic acid or produces these products by dehydration to mesityl oxide and subsequent hydrolysis. The acetic acid formed undergoes ketonization to produce additional acetone. We find that dispersion of zinc oxide on zirconia produces a balance between Lewis acidic and basic sites that prevent the loss of ethanol via dehydration to ethylene and promote the cascade reactions of ethanol and acetone to isobutene.

II. Introduction

Isobutene is a valuable platform molecule used for the synthesis of polymers, such as butyl rubber, and other polymer precursors, such as methyl methacrylate, methacrolein, and acrylics.[231] Ethers such as methyl-tert-butyl ether (MTBE) and ethyl-tert-butyl ether (ETBE), high-octane additives for gasoline, can be produced by reaction of isobutene with an alcohol.[232,233] The principal source of isobutene today is steam cracking of naphtha, dehydration of fossil-derived tert-butanol, or dehydrogenation of petroleum-derived isobutane.[234] Isobutene can also be produced via the reaction of CO and H_2, obtained by steam reforming of methane, over a zirconia-based catalyst in process known as isosynthesis.[235–238] Growing concern with the rise in atmospheric CO_2 levels caused by the consumption of petroleum-derived sources of carbon has motivated exploration of renewable sources of carbon to meet the increasing global demand for fuels and specialty chemicals.[1] Fermentation of monosaccharides to produce renewable isobutene has been demonstrated, although the yields and cost are not yet competitive with fossil-based production of isobutene.[156]

Ethanol and acetone are attractive starting points for the synthesis of isobutene, since both can be produced by the fermentation of biomass-derived sugars.[11,12,239] Recent work by Sun et al. has demonstrated that ethanol and acetone can be converted into isobutene with high selectivity over zinc-zirconia mixed oxide catalysts.[42,43,240] The authors identified $Zn_1Zr_{10}O_z$ as a selective and stable catalyst for the production of isobutene from ethanol and acetone in the gas phase at 723 K with a steam-to-carbon molar ratio of 5. The conversion of acetone to isobutene was thought to proceed via the adsorption of acetone on a Lewis-acidic Zr atom, followed by hydrogen extraction by a basic oxygen to form an adsorbed enolate, which then attacks a second acetone to

form diacetone alcohol. This product then either decomposes to form isobutene and acetic acid or dehydrates to form mesityl oxide, which then hydrolyzes to produce isobutene and acetic acid.[43] Subsequent work by Li et al. showed that diacetone alcohol, mesityl oxide, phorone, and isophorone are potential intermediates in the conversion of acetone to isobutene over $Zn_xZr_yO_z$.[241] Crisci et al. have also reported that isobutene yields of up to 50% could be obtained by reacting acetic acid over an amorphous binary metal oxide ($Zn_2Zr_8O_z$) at 723 K.[242] We note that while potential intermediates have been identified for the reaction of acetone to isobutene over $Zn_xZr_yO_z$, the mechanism is not yet clearly defined. For the reaction of ethanol to isobutene, neither the reaction pathway nor the active sites necessary for each step in the reaction pathway are known.

Sun et al. suggest that a balance between acid and base sites on $Zn_xZr_yO_z$ is responsible for the effective cascade reaction of bioethanol and acetone to isobutene.[42] The authors observed a selectivity to isobutene of over 88% from acetone at 723 K in the presence of water over $Zn_1Zr_{10}O_z$.[43] By contrast, ZrO_2 exhibited a significantly lower selectivity to isobutene (~13%) for the reaction of acetone, with methane and CO_2 (~60% and ~27%, respectively) appearing as the principal products. It was suggested that the zinc oxide present on the surface passivates the strong Brønsted acidity of the zirconia and introduces basicity, preventing decomposition of acetone as well as suppressing ethanol dehydration to ethylene for the ethanol to isobutene reaction. These authors also found that the selectivity towards isobutene from acetone over pure ZnO was approximately the same (~80%) as that observed over $Zn_1Zr_{10}O_z$ for an acetone conversion of ~28%. While the comparison of ZrO_2 and $Zn_1Zr_{10}O_z$ suggests that basicity is necessary for the reactions of ethanol and acetone to isobutene, the role of the zirconia support remains unclear. Because only a small difference in isobutene selectivity is observed for the reaction of acetone over ZnO compared to $Zn_1Zr_{10}O_z$ at the same conversion, it is unclear what role the balance between acid and base properties of the catalyst plays in the acetone to isobutene reaction.

The role of Brønsted acid sites in the synthesis of isobutene has also been considered. Herrmann and Iglesia have recently reported the selective conversion of acetone to isobutene and acetic acid over Brønsted-acidic aluminosilicates, and proposed a radical-mediated pathway for the formation of isobutene via an equilibrated pool of C_6 intermediates; however, the catalyst underwent rapid deactivation due to side product formation over the Brønsted-acid sites, which produced coke.[243] Hutchings et al. have also observed catalyst deactivation for the reaction of acetone to isobutene over Brønsted-acidic zeolites BEA and ZSM-5.[244] Ponomareva et al. have suggested that Brønsted acid sites on cesium-modified mordenite and MCM-41 were preferable for the synthesis of isobutene from acetone, although these authors also observed catalyst deactivation due to coking.[245] Sun et al. and Liu et al. have suggested that weak Brønsted-acid sites are responsible for isobutene formation, but strong Brønsted-acid sites catalyze coke formation and that the absence of Brønsted acidity prevents side reactions.[43,240] Crisci et al. have noted that Brønsted-acid sites may be required to promote the hydrolysis of mesityl oxide to isobutene and that ZnO is unable to catalyze the formation of isobutene from acetic acid.[242]

Therefore, examination of the literature does not fully address the question of which active sites are necessary for isobutene formation from ethanol and acetone. While the dispersion of ZnO on zirconia provides basicity and suppresses ethanol dehydration, it is unclear whether zirconia simply provides a high surface area support or whether the interaction of the dispersed ZnO with the support produces additional or stronger Lewis acidity, or aids in the formation of oxygen vacancies that promote the dissociation of water. The aim of this work was to develop a detailed understanding of the sequence of reactions involved in the conversion of ethanol and acetone to isobutene over $Zn_xZr_yO_z$. This effort involved identifying the stable reaction intermediates and the

types of sites required to promote each phase of the reaction sequence. To this end, we synthesized and characterized a series of $Zn_xZr_yO_z$ catalysts with varying acidity and basicity and used these materials in a systematic study of the roles of acid and base sites for each step in the reaction pathway. The presentation of our results starts by detailing the catalyst characterization. We then develop a picture for the overall reaction pathway involved in the conversion of ethanol and acetone to isobutene over $Zn_xZr_yO_z$. Next, we propose a mechanism for each step in the reaction pathway that is consistent with the experimental data, catalyst characteristics, and a thorough review of the existing literature. Finally, we discuss the role of water in promoting isobutene formation and preventing catalyst deactivation, as well as the role of the mesityl oxide intermediate.

III. Materials and Methods

i. Materials

All chemicals obtained commercially were used without further purification. The following compounds were obtained from Sigma Aldrich: ethanol (>99.5%), 4-hydroxy-4-methyl-2-pentanone (diaceone alcohol, 99%), mesityl oxide (90%, remainder 4-methyl-4-penten-2-one), acetaldehyde solution (50 wt% in ethanol), acetone (>99.5 %), acetic acid (>99%), diethyl ether (>99%), and ethyl acetate (99.8%). Acetone d-6 (99.9%) and deuterium oxide (99.9%) were obtained from Cambridge Isotope Laboratories. Standard gas (3.01% methane, 1.5% ethylene, 1.5% ethane, 1% propene, 1.01% propane, 0.745% cis-2-butene, 0.748% trans-2-butene, 0.75% butane, 0.6% n-pentane in He), 1% Ar in He (CSG), ammonia (99.995%), and He (5.0 UHP) were obtained from Praxair. Isobutene gas (99%) was obtained from Sigma-Aldrich. Nanopure water was obtained via a MilliQ water purification system. Zinc oxide (99.9995% metals basis) was obtained from Puratronic.

ii. Synthesis of zirconia and zinc zirconia mixed oxide

Porous amorphous zirconia, and the zinc-zirconia mixed oxides were synthesized using modifications of previously reported methods.[43,73,99,159,246] Amorphous zirconium oxyhydroxide ($ZrO_x(OH)_{4-2x}$) was formed by adding ammonium hydroxide (Spectrum, 28–30%) dropwise to a stirred solution of 0.5M zirconyl chloride octahydrate (Sigma Aldrich, 98%) at 298 K. The precipitate was filtered and rinsed with 10% ammonium hydroxide and dried at 383 K for 24 h. The zinc zirconia mixed oxides were prepared via incipient wetness impregnation of amorphous zirconium oxyhydroxide with an aqueous solution of zinc nitrate hexa-hydrate (Alpha Aesar, 99%) in a mortar with varying concentrations of zinc nitrate corresponding to the target Zn weight loadings. The wetted support was ground with a pestle in the mortar. After impregnation, the catalyst was dried at 383 K for 0.3 h, and then heated in air at 3 K min^{-1} to a temperature of 673 K and held at this temperature for 2 h, and then heated further to 823 K at a rate of 5 K min^{-1} and held at this temperature for 3 h, after which it was cooled to room temperature. Monoclinic zirconia was prepared using the same calcination procedure but in the absence of the zinc precursor.

iii. Catalyst Characterization

Powder X-ray diffraction (XRD) patterns for ZnO, ZrO_2, and the $Zn_xZr_yO_z$ catalysts were taken with a Bruker D8 GADDS diffractometer equipped with a Cu-Kα source (40 kV, 40 mA). Raman spectra were obtained with a LabRAM HR Horiba Scientific Raman spectrometer equipped with a 532 nm^{-1} laser. BET surface areas were calculated from nitrogen adsorption

isotherms acquired with a Micrometrics Gemini VII Surface Area and Porosity instrument after being degassed overnight at 393 K with a Micrometrics VacPrep 061. Scanning electron microscopy images of $Zn_xZr_yO_z$ (2.2 wt% Zn) were acquired with an FEI Quanta FEG 250 scanning electron microscope (SEM) equipped with a Bruker Quantax energy dispersive spectrometer (EDS). ICP Elemental analysis was performed by Galbraith Laboratories, Inc. to determine Zn and Zr loadings.

The identification of Brønsted- and Lewis-acid sites was determined from IR spectra of adsorbed pyridine. Spectra were acquired using a Thermo Scientific Nicolet 6700 Fourier Transform Infrared Spectrometer (FT-IR) equipped with a Diffuse Reflectance Infrared Fourier Transform Spectroscopy (DRIFTS) cell. A mixture of catalyst (50 mg) diluted with KBr (250 mg) was added to the DRIFTS cell and pre-treated at 573 K for 2 h under 50 mL min^{-1} helium. DRIFTS scans for ZnO were repeated in the presence and absence of KBr diluent. Background scans of the catalysts were taken at 393 K, 423 K, 473 K, 523 K, and 573 K. Pyridine (2 µL) was introduced into the He flow at 323 K, and spectral data was taken after stabilization of adsorbed pyridine at 323 K. The temperature was then raised to measure the amount of pyridine that remained adsorbed at 373 K, 393 K, 423 K, 473 K, 523 K, and 573 K. Spectral intensities were calculated using the Kubelka-Munk function.

The density of acid sites was measured by ammonia temperature-programmed desorption (NH_3-TPD).[247] NH_3-TPD profiles of the ZnO, ZrO_2, and $Zn_xZr_yO_z$ samples were acquired using a gas-phase flow reactor with an outlet flowing to a mass spectrometer (MKS, Cirrus). Samples (~200 mg) were loaded into a quartz reactor and plugged on either end with quartz wool. A thermocouple was placed above the catalyst bed. Samples were first heated at 5 K min^{-1} to a temperature of 723 K and held for 0.5 h in a flow of 50 mL min^{-1} He (Praxair, UHP). The reactor was then cooled to 323 K and the He flow was increased to 250 mL min^{-1}, and 1% Ar in He (Praxair, CSG) was introduced at 50 mL min^{-1}. The catalyst was saturated with NH_3 by flowing 5 mL min^{-1} of NH_3 for 0.5 h. After stopping the flow of NH_3, 300 mL min^{-1} of He was passed over the catalyst bed overnight to remove any physisorbed NH_3 from the catalyst surface. The temperature-programmed desorption was carried out in 50 mL min^{-1} of 1% Ar in He as the temperature was ramped from 323 to 973 K at a ramp rate of 5 K min^{-1}. The desorbed NH_3 coming out of the outlet flow was directed to mass spectrometer for quantification. Standards with known concentrations of NH_3 were taken before and after each TPD measurement to account for any drift during the course of the experiment. Ar was used as an internal standard for quantification. The quantity of acid sites on the catalyst surface corresponds to the amount of NH_3 desorbed from the catalyst during the TPD.

The density of basic sites was measured by temperature-programmed desorption of CO_2 (CO_2-TPD) using a Micrometrics Auto Chem II 2920 instrument equipped with a thermal conductivity detector. The catalyst samples were pretreated under He flow at 873 K for 3 h, then cooled to 313 K. CO_2 was then introduced at 313 K for 0.5 h at 30 mL min^{-1}, then purged with He at 313 K for 0.5 h to remove any physisorbed species from the surface. The temperature-programmed desorption of CO_2 was then performed in 50 mL min^{-1} He using a temperature ramp rate of 5 K min^{-1} up to a temperature of 1073 K.

iv. Reactions

Gas-phase reactions were performed in a gas phase flow reactor. The catalyst was placed in a 6.35 mm-OD quartz tube with an expanded section (~12.7 mm OD, ~20 mm length) packed with quartz wool above and below the catalyst. The reactor temperature was maintained using a tube furnace equipped with an Omega temperature controller and K-type thermocouple. Prior to

each reaction, the catalyst was treated in 40 mL min^{-1} He for 2 h at 723 K at a ramp rate of 10 K min^{-1}.

Reactions were performed using helium (Praxair, 5.0 Ultra High Purity) as a carrier gas. Liquid-phase reactants (ethanol, acetaldehyde/ethanol solution, acetic acid, acetone, diacetone alcohol, mesityl oxide, and nanopure water) were injected via a Cole Palmer 74900 Series syringe pump into the reactor with lines heated to >367 K to vaporize the liquids before reaching the reactor. Experiments were carried out at atmospheric pressure, between 573 and 823 K, with total flow rates ranging from 10 to 300 mL min^{-1} in a balance of helium. Reaction products were analyzed using an Agilent 6890N gas chromatograph (GC) containing a (5%-phenyl)-methylpolysiloxane capillary column (Agilent, HP-5) connected to a flame ionization detector. The temperature program for the GC column began at 263 K (cooled with liquid N_2), then ramped to 283 K at 3 K min^{-1}, then ramped to 353 K at 33 K min^{-1}, held at 353 K for 1 min, then ramped to 363 K at 33 K min^{-1} and held at 363 K for 1 min. Retention times and response factors were obtained either by injecting solutions of products via the syringe pump, or by flowing standard gas mixtures into the reactor via a mass flow controller. Concentrations of CO_2 were estimated based on the stoichiometry in Table 6.2, closing carbon balances to within ± 5%. Response factors for higher olefins C_9+ produced in the absence of water were estimated using the effective carbon number method.[248]

IV. Results and Discussion

i. Catalyst Characterization

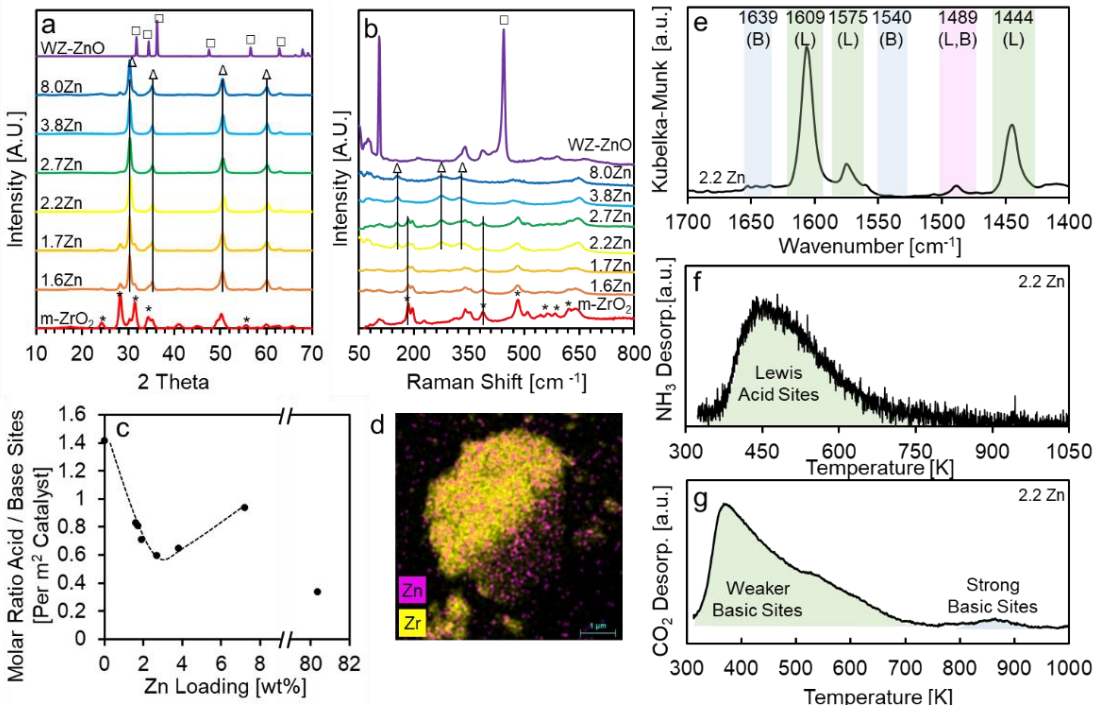

Figure 6.1. a) X-ray diffraction patterns of ZnO, ZrO_2, and $Zn_xZr_yO_z$ catlaysts with varying weight loadings of Zn (1.6 wt% - 8.0 wt%), b) Raman spectra of catalysts; Abbreviations: wurtzite (WZ), monoclinic (m); Symbols: wurtzite phase (squares), tetragonal zirconia (triangles), monoclinic zirconia (stars), c) Weight loading of Zn versus molar ratio of total Lewis acid to base sites, d) SEM EDX of $Zn_xZr_yO_z$ 2.2 wt% Zn, e) Representative DRIFTS spectrum of the adsorption of pyridine onto $Zn_xZr_yO_z$ 2.2 wt% Zn at 393 K (intensities normalized by the Kubelka-Munk function), f) NH_3-TPD profile of $Zn_xZr_yO_z$ 2.2 wt% Zn, g) CO_2-TPD profile of $Zn_xZr_yO_z$ 2.2 wt% Zn.

Table 6.1. Summary of Catalyst Characterization					
Catalyst	Wt% Zn[1]	BET Surface Area (m^2 g^{-1})	Acid Sites Present	Basicity[2] (µmol CO_2/m^2)	Acidity[3] (µmol NH_3/m^2)
WZ-ZnO	80.3	3.6	Lewis	4.78	1.9
$Zn_xZr_yO_z$	8.0	53.3	Lewis	2.81	2.6
$Zn_xZr_yO_z$	3.8	46.1	Lewis	2.43	1.8
$Zn_xZr_yO_z$	2.7	48.1	Lewis	2.51	1.5
$Zn_xZr_yO_z$	2.2	51.0	Lewis	3.21	2.6
$Zn_xZr_yO_z$	1.7	49.5	Lewis	2.75	2.2
$Zn_xZr_yO_z$	1.6	48.1	Lewis	2.65	2.2
m-ZrO_2	0	55.7	Lewis	1.83	2.6
[1] Weight percent zinc measured by ICP by Galbriath, [2] Measured from CO_2 TPD, [3] Measured from NH_3 TPD					

To probe the relationship between Lewis acidity and basicity and catalytic activity for the ethanol to isobutene reaction, $Zn_xZr_yO_z$ catalysts with varying weight loadings of Zn were synthesized and characterized using a variety of structural and surface characterization techniques. This series of catalysts were then employed to identify the effects of acidity and basicity on the kinetics and mechanism of the ethanol and acetone to isobutene reactions. The Zn weight loadings, BET surface areas, identification and quantification of acid sites, and quantification of basic sites are summarized in Table 6.1. Apart from the low-surface area ZnO, the weight loading of Zn had a minimal effect on the surface area of the catalysts, which were all within the range of 46-56 m^2 g^{-1}. The measured weight loadings of Zn in the bulk measured by ICP closely matched the targeted amounts of Zn added to the support via incipient wetness impregnation (Figure 6.13).

X-Ray diffraction (XRD) and Raman spectroscopy were used as complimentary techniques to determine surface phase transformations of the zirconia support with increasing zinc loading. The XRD patterns and Raman spectra are shown in Figure 6.1a and Figure 6.1b. The XRD patterns in Figure 6.1a show that the dominant phase of the pure zirconia is monoclinic, as evidenced by the peaks at 2θ angles of 24°, 28°, 32°, and 56°,[63,67,249] which are denoted by the stars. As the Zn loading increases, prominent peaks at 2θ angles of 30°, 35°, 50°, and 59° appear, denoted by the triangles, that are characteristic of tetragonal zirconia.[67,72,250] The pure bulk ZnO exhibits clear peaks at 2θ angles of 32°, 34°, 37°, 47°, 57°, 64°, 67°, 68°, and 69°, denoted by the squares, that are characteristic of wurtzite (WZ).[251,252] The wurtzite phase is not observed for $Zn_xZr_yO_z$, suggesting that clusters of bulk ZnO are not present on the surface of these catalysts. As the weight loading of Zn approaches a theoretical monolayer coverage of zinc oxide over the zirconia (occurring at molar ratio of Zn:Zr ~1:50 for particles 5 µm in diameter), the crystal structure of the zirconia changes from monoclinic to tetragonal. This suggests that as the Zn incorporates into the structure of the oxide, the tetragonal phase of zirconia is stabilized. We have previously observed this stabilizing effect for tungstated zirconia; as tungsten oxide is added to the surface of zirconia, the Zr-O-W interactions stabilize the tetragonal zirconia phase and inhibit the sintering of zirconia to the more thermodynamically stable monoclinic phase.[99] Similarly, the absence of the wurtzite phase suggests that Zr-O-Zn interactions are present instead of clusters of ZnO.

Because the weight loadings of Zn are fairly low, XRD may not be sufficient to identify the presence or absence of the wurtzite phase of ZnO; therefore, Raman spectra of the series of catalysts were acquired to provide further evidence for the absence of wurtzite ZnO, as shown in Figure 6.1b. Raman spectroscopy is sensitive to the wurtzite phase of ZnO, as evidenced by the strong band at approximately 430 cm^{-1}.[251,253] Consistent with the observation by XRD, the monoclinic phase of zirconia gives way to the tetragonal phase as Zn is added to the zirconia, as evidenced by the fact that the Raman bands at 181, 377, 472, 556, 616, and 634 cm^{-1} (monoclinic) decrease as Zn loading increases, and the bands at 149, 269, and 312 cm^{-1} (tetragonal) increase as

Zn loading increases.[75,254,255] No evidence for a band at 430 cm^{-1} was observed for any of the $Zn_xZr_yO_z$ catalysts, further indicating the absence of ZnO on the catalyst surface. SEM-EDX characterization of the $Zn_xZr_yO_z$ with 2.2 wt% Zn further suggest that the Zn is well dispersed on the surface of the catalyst, as shown in Figure 6.1d. The trends in XRD patterns and Raman spectra are in good agreement with the work of Baylon et al., who found that with increasing Zn loading, the fraction of tetragonal versus monoclinic zirconia in $Zn_xZr_yO_z$ increases, and that ZnO is not present.[254] These authors also found that intermediate weight loadings of Zn facilitated the formation of Zn-O-Zr moieties with balanced acid-base properties that facilitate cascade aldolization and self-deoxygenation reactions of acetone and methyl ethyl ketone.[254]

A combination of diffuse reflectance infrared spectroscopy of adsorbed pyridine (DRIFTS-py), ammonia temperature-programmed desorption (NH_3-TPD), and CO_2 temperature-programmed desorption (CO_2-TPD) were used to identify and quantify the acid and base sites on the catlaysts. A representative DRIFTS spectrum for the adsorption of pyridine onto the $Zn_xZr_yO_z$ catlayst with 2.2 wt% Zn at 393 K is shown in Figure 6.1e. Bands at 1609 cm^{-1}, 1575 cm^{-1}, and 1444 cm^{-1} are characteristic of pyridine adsorbed on Lewis acid sites; however, the absence of bands at 1639 cm^{-1} and 1540 cm^{-1}, corresponding to the pyridinium ion, suggests that there are no Brønsted acid sites present.[67,80] DRIFTS-py spectra for ZnO, ZrO_2, and $Zn_xZr_yO_z$ samples with Zn weight loadings of 1.6% – 8.0% are shown in Figure 6.14. For each of these catlaysts, Lewis acid sites were observed but none of the catlaysts contained Brønsted acid sites. The relative strength of Lewis acid sites can be compared by plotting the percent of pyridine remaining on the surface as a function of temperature from the DRIFTs experiments or by comparing the peak NH_3 desorption temperature from NH_3-TPD experiments. From Figure 6.15, it is observed that the percent desorption of pyridine as function of temperature does not differ significantly between $Zn_xZr_yO_z$ (2.2 wt% Zn) and ZrO_2. Comparison with ZnO is difficult due to its low surface area, resulting in a low signal, where the bands associated with pyridine adsorption onto Lewis acid sites are only observed at low temperatures.

NH_3-TPD was used to quantify the concentration of acid sites. The μmol NH_3/m^2 determined from NH_3-TPD spectra are summarized in Table 6.1. A representative NH_3-TPD profile for the $Zn_xZr_yO_z$ catlayst with 2.2 wt% Zn is shown in Figure 6.1f. The shaded green region represents NH_3 desorption from weak to moderate Lewis acid sites. The NH_3-TPD profiles for the full series of catalysts are shown in Figure 6.16a. Interestingly, the distribution of acid site strengths were similar for the series of $Zn_xZr_yO_z$ catalysts and ZrO_2, with peak for NH_3 desorption occuring in the temperature range of approximatley 433-473 K (Figure 6.17). For the ZnO, however, the maximum NH_3 desorption occurs at approximately 504 K (Figure 6.17), suggesting that the Lewis acid sites, although lower in concentration, are slightly higher in strength. A higher temperture NH_3 desorption peak was not observed for any of the catalysts, as shown in Figure 6.16a, further suggesting that the concentration of Brønsted acid sites is insignificant. While no Brønsted acid sites were observed for these *ex-situ* characterization techniques of the $Zn_xZr_yO_z$ prepared via incipient wetness impregnation, it is possible that the dissociation of water under reaction conditions produces protons which act as Brønsted acid sites, a subject that will be discussed in Section 6.IV.iii and Section 6.IV.iv.

The basic sites on the catalyst surface were quantified by temperature-programmed desoprtion of CO_2, as shown in Table 6.1. A representative CO_2-TPD plot is shown in Figure 6.1g over $Zn_xZr_yO_z$ (2.2 wt% Zn) and the remainder of the plots are given in Figure 6.16b. Two peaks are observed in the CO_2-TPD profile, a strong peak with a maximum CO_2 desorption around 375 K with a broad shoulder around 520 K, and a small CO_2 desoprtion peak at around 865 K. Sun et

al. have assigned the low temperature peak to the desoprtion of weakly adsorbed CO_2 on the Lewis-basic oxygen atoms of the hydroxyl groups on ZrO_2, and the high temperature peak to CO_2 adsorbed on strong Lewis acid base pairs (Zr^{4+}-O^{2-}).[42] Consistent with the results of Sun et al., our CO_2-TPD results did not reveal a peak corresponding to weakly adsorbed CO_2 for ZnO, which exhibits only a single peak at approximately 700 K, attributed to an absence of hydroxyl groups.[42]

In summary, characterization of $Zn_xZr_yO_z$ shows that this material consists of highly-dispersed zinc oxide on the surface of tetragonal zirconia, with no evidence for ZnO nanoparticles. The surface of $Zn_xZr_yO_z$ contains a balance between moderately Lewis acidic and basic sites. As shown in Figure 6.1c, varying the weight loading of Zn tunes the ratio of Lewis acid to base sites on $Zn_xZr_yO_z$. This figure also shows that monoclinic zirconia has a significantly higher Lewis acid to base ratio and that zinc oxide has a significantly lower Lewis acid to base ratio than $Zn_xZr_yO_z$. While the differences in the ratios of Lewis acid to base sites are subtle for $Zn_xZr_yO_z$ with varying Zn loadings, there are still differences in the acid to base ratios. Evidence for these differences will be discussed in Section 6.IV.iii and Section 6.IV.iv in the context of our studies of the reactions of ethanol and acetone to isobutene.

ii. Proposed Reaction Pathway for Ethanol to Isobutene

In this section, we will propose a reaction pathway for the conversion of ethanol to isobutene. Evidence supporting this pathway and the site requirements for each step will be presented in Section 6.IV.iii. The overall proposed reaction pathway for the conversion of ethanol to isobutene is shown by Scheme 6.1.

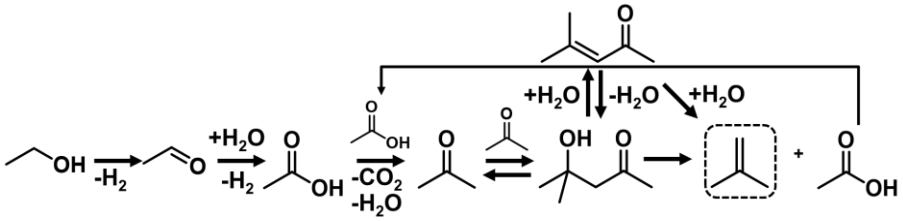

Scheme 6.1. Proposed reaction pathway for the conversion of ethanol to isobutene.

The first step in the proposed reaction pathway is the dehydrogenation of ethanol to produce acetaldehyde, followed by oxidation to produce acetic acid. Two equivalent moles of acetic acid then undergo ketonization to produce one mole each of acetone, CO_2, and H_2O. Two moles of acetone then dimerize to produce diacetone alcohol, which undergoes direct decomposition to produce isobutene and acetic acid or, alternatively, undergoes reversible unimolecular dehydration to produce mesityl oxide followed by hydrolysis to isobutene and acetic acid. The acetic acid produced in this last step undergoes further ketonization to produce more acetone, which then reacts further to produce isobutene.

Table 6.2. Reaction Stoichiometry and Free energies of formation for ethanol, acetic acid, acetone, and mesityl oxide conversion to isobutene.

Overall Reaction	Maximum Theoretical Carbon Selectivity towards Isobutene [%]	$\Delta G_{rxn,\ 723}$ K* [kJ mol^{-1}]
3 EtOH + H_2O → 2 CO_2 + 6 H_2 + C_4H_8	66.7	-235.9
3 CH_3COOH → C_4H_8 + 2 CO_2 + 2 H_2O	66.7	-228.1
3 CH_3COCH_3 → 2 C_4H_8 + CO_2 + H_2O	88.9	-76.1
3 $C_6H_{10}O$ + H_2O → 4 C_4H_8 + 2 CO_2	88.9	-266.0
* Gibbs free energies of formation calculated from DFT, computational details provided in the Supporting Information.		

Scheme 6.1 shows that acetic acid, acetone, and mesityl oxide are reaction intermediates. The data shown in Table 6.2 present the Gibbs free energies of reaction for forming isobutene from ethanol and each of the reaction intermediates listed. The Gibbs free energies were calculated using density functional theory for the reaction temperature of 723 K. Also shown in this table are the maximum carbon selectivities for forming isobutene from each starting compound. Computational details on the calculations are given in Figure 6.18.

The effect of spacetime, defined as the inverse of the weight hourly space velocity ($WHSV^{-1}$), on product distribution for the gas phase conversion of ethanol to isobutene reaction was investigated over $Zn_xZr_yO_z$ (2.2 wt% Zn). These studies were conducted at 723 K with a steam to carbon molar ratio of 5, as these reaction conditions showed the optimal selectivity towards isobutene. As the temperature increases, the rate of isobutene formation from acetone increases up to 723 K, at which point the catalysts begin to deactivate. Isobutene selectivity also increases with increasing steam to carbon ratio, but the rate drops above a S/C of 5 (see Figure 6.19 and Figure 6.20). It is worth noting that at lower temperatures (698 K), higher selectivities towards desired products along the ethanol to isobutene reaction pathway (acetaldehyde, acetone, and isobutene) can be achieved (see Figure 6.21), but due to higher rates at 723 K, this temperature was selected for observation of reaction intermediates.

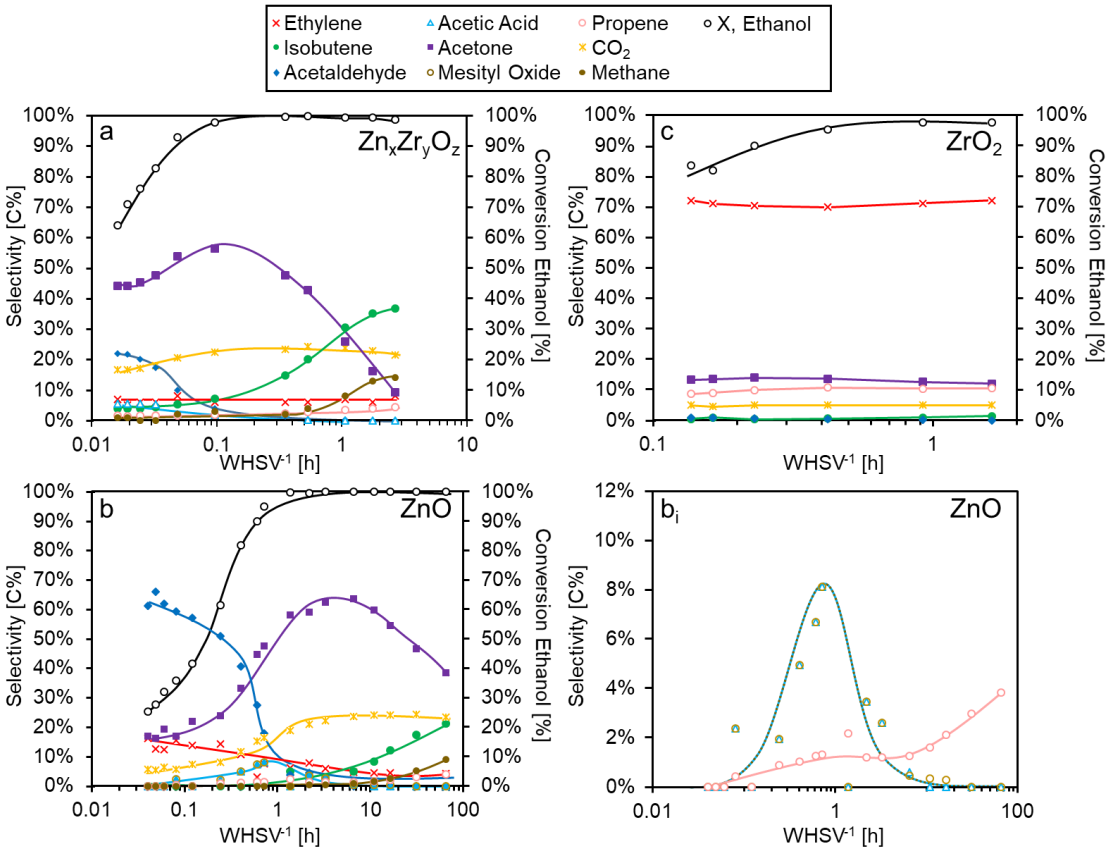

Figure 6.2. Effect of spacetime on ethanol conversion and product selectivity over a) $Zn_xZr_yO_z$ (2.2 wt % Zn), b) bulk wurtzite ZnO, b_i) bulk wurtzite ZnO (scale enlarged), and c) monoclinic ZrO_2. Reaction Conditions 723 K, atmospheric pressure, 20-300 mL min^{-1} He, a) 4 mg $Zn_xZr_yO_z$ (2.2 wt% Zn), S/C 5, 0.16 kPa EtOH, 11.4 kPa H_2O, b) 311 mg ZnO, S/C 5, 0.21 kPa EtOH, 11.4 kPa H_2O, c) 22.4 mg ZrO_2, S/C 2, 0.7 kPa EtOH, 30 kPa H_2O. WHSV is defined as the mass flow of reactants divided by the mass of catalyst (g h^{-1} g^{-1}). Lines are meant to guide the eye.

Figure 6.2a shows that as the spacetime increases, the conversion of ethanol over $Zn_xZr_yO_z$ (2.2 wt% Zn) increases. At low spacetimes, the principal products are acetaldehyde and acetone, as well as CO_2. Smaller amounts of acetic acid and ethylene are also observed. As the spacetime is increased, the selectivity to acetone reaches a maximum, whereas the selectivity to isobutene begins to rise monotonically, suggesting that acetone is an intermediate in the formation of isobutene. The selectivity to ethylene is invariant with spacetime, suggesting that this product is produced via a pathway that is not involved in the conversion of ethanol to isobutene, e.g., by direct ethanol dehydration. Trace amounts of propene (pink, circle) can also be observed, and increase with increasing conversion of ethanol. The formation of propene likely comes from the dehydration of isopropanol, which is produced from the reduction of acetone. We note that propene formation from ethanol over $AgCeO_2/ZrO_2$[256] and Y_2O_3-CeO_2[257] has been reported, and it has been proposed that the acetone is reduced to propanol by hydrogen transfer from ethanol via the Meerwein–Ponndorf–Verley (MPV) mechanism (see Scheme 6.6). The formation of methane as a result of acetone decomposition also increases as spacetime is increased.

Figure 6.2b shows the effect of spacetime on the product selectivity for the reaction of ethanol to isobutene over zinc oxide. The trends in the intermediates produced in the reaction appear to be similar to those for $Zn_xZr_yO_z$ in Figure 6.2a; acetaldehyde and acetone are observed as intermediates, and the selectivity to isobutene, propene, and methane steadily increase with increasing spacetime. However, to achieve the same conversion of ethanol and product yields over ZnO as those over $Zn_xZr_yO_z$, an order of magnitude higher spacetime is required for ZnO. Other differences are observed, including a clear peak in the selectivity towards acetic acid and mesityl oxide at lower spacetimes over ZnO than $Zn_xZr_yO_z$, (see Figure 6.2b$_i$).

As shown in Figure 6.2c, the reaction of ethanol over ZrO_2 indicates that the major product is ethylene, resulting from the unimolecular dehydration of ethanol. Some acetone is formed, but only trace amounts of isobutene are produced and the selectivity to this product does not change significantly with increasing spacetime. The high selectivity to ethylene over ZrO_2 even in the presence of water is not surprising, as zirconia is known to catalyze the unimolecular dehydration of alcohols.[87,258] Because of the subtler differences in the reaction intermediates observed over $Zn_xZr_yO_z$ (2.2 wt% Zn) compared to ZnO, we will place more of a focus on comparing reactions over these two catalysts in subsequent sections.

iii. Ethanol Conversion to Acetone

In this section, we focus on the steps involved in the conversion of ethanol to acetone, a critical intermediate in producing isobutene. We use a combination of experimental evidence and information taken from the literature to propose a mechanism for each of the following steps: ethanol dehydrogenation to acetaldehyde, acetaldehyde oxidation to acetic acid, and ketonization of acetic acid to acetone. The elementary processes involved in the conversion of acetone to isobutene are discussed in 6.IV.iv.

a) Ethanol Dehydrogenation to Acetaldehyde

The proposed first step in the reaction of ethanol to isobutene is the dehydrogenation of ethanol to produce acetaldehyde and H_2. The observation of a maximum in the rate of acetaldehyde production over $Zn_xZr_yO_z$ (2.2 wt% Zn) at low ethanol conversions, seen in Figure 6.2a, suggests that acetaldehyde is an intermediate in the reaction pathway. Additional information on the role of the acid-base properties of the catalyst on the dehydrogenation of ethanol to acetaldehyde and the

competing reaction, ethanol dehydration, were obtained by measuring the ethanol conversion and product selectivities for ZrO_2, $Zn_xZr_yO_z$, and ZnO at 698 K, as shown in Figure 6.3.

Acetaldehyde is observed for all the $Zn_xZr_yO_z$ catalysts and over bulk ZnO, as shown in Figure 6.3a. Some acetaldehyde can also be observed for the reaction of ethanol over ZrO_2, although the selectivity is minimal. Because the basicity and acidity of the catalysts change with weight loading of Zn, the ethanol conversion and the product selectivities can be correlated with the ratio of Lewis acidity and basicity quantified by NH_3-TPD and CO_2-TPD, respectively. As shown in Figure 6.3b, the conversion of ethanol decreases as the ratio of Lewis acidity to basicity increases. Ethanol dehydration is greatly suppressed by the addition of Zn to zirconia, as evidenced by minimum in ethylene selectivity for the catalysts with intermediate ratios of acid to base sites (red line and square points). However, the ethylene selectivity increases slightly over the most basic catalyst (ZnO). The selectivity to acetone is also highest for $Zn_xZr_yO_z$ for the sample containing 2.2 wt% Zn. There is a clear relationship between the rate of ethanol consumption and basicity (Figure 6.22b) but not acidity (Figure 6.22a), further suggesting that ethanol dehydrogenation to acetaldehyde is base-catalyzed. From the relationship between the Lewis acid/base ratio and the reaction selectivity it becomes clear that minimizing ethylene production requires an optimal ratio of Lewis acid to base sites which can be achieved with $Zn_xZr_yO_z$. We also found that ethanol dehydration increases in the absence of water over $Zn_xZr_yO_z$, as shown in Figure 6.4 and Figure 6.23. The combination of strong Lewis basicity introduced by dispersing Zn on the catalyst surface and the inhibition of dehydration by water are thus expected to be responsible for promoting the ethanol dehydrogenation over $Zn_xZr_yO_z$ and ZnO.

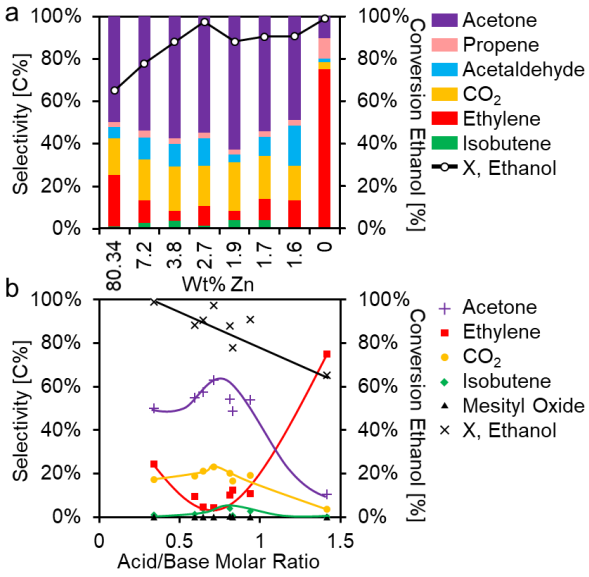

Figure 6.3. a) Conversion and selectivity of ethanol conversion over ZnO, ZrO_2, and $Zn_xZr_yO_z$ catalysts as a function of Zn loading, and b) selectivity as a function of acid/base molar ratio normalized by catalyst surface area. Reaction conditions: 698 K, 1 kPa EtOH, S/C 4, 50 mL min^{-1} He, spacetime normalized by BET surface area.

Prior studies have shown that ethanol dehydrogenation is Lewis base-catalyzed and inhibited by water,[36,259] whereas the ethanol dehydration is catalyzed by Brønsted or Lewis acidity,[31,32,35,260] and inhibited by water.[31,32] Of particular note for the present studies, Vohs and Barteau suggested that over the (0001)-Zn surface of ZnO, ethanol and 1-propanol dehydration

and dehydrogenation share a common intermediate, an ethoxide, formed by dissociative adsorption of ethanol onto the catalyst surface.[261]

Based upon our experimental results and proposed mechanisms for ethanol dehydrogenation in the literature, we propose the mechanism for the Lewis/Brønsted-base catalyzed dehydrogenation of ethanol to produce acetaldehyde over the zinc zirconia mixed oxide catalysts shown in Scheme 6.2. Although the surface contains Zn-O-Zr moieties, the surface is drawn as ZnO for simplicity because it is estimated that the surface coverage of ZnO exceeds one monolayer for the mixed oxide catalysts. The first step is the dissociative adsorption of ethanol onto the catalyst surface. This is followed by the rate limiting base-catalyzed abstraction of hydrogen, breaking a C-H bond to form a bound alkoxide intermediate. The alkoxide then desorbs to produce acetaldehyde, leaving hydrogen on the surface. The hydrogen can then leave as H_2 or as water via a Mars-Van-Krevelen (MVK) mechanism, leaving an oxygen vacancy on the surface, which is replenished by water which dissociates on the surface. While acetaldehyde is observed as a product at low spacetimes, it is not observed at higher conversions, suggesting that it remains adsorbed on the surface in the form of an alkoxide, which is later oxidized to produce acetic acid.

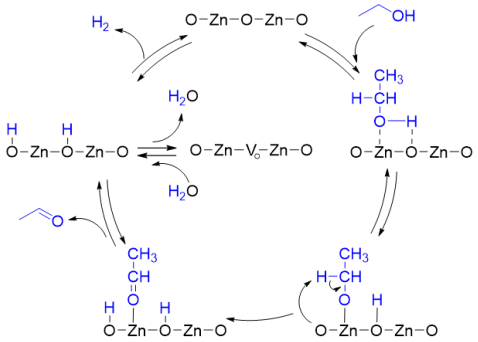

Scheme 6.2. Proposed mechanism for the dehydrogenation of ethanol over $Zn_xZr_yO_z$.

b) Oxidation of Acetaldehyde to Acetic Acid

The next step in the proposed reaction pathway for the formation of isobutene from ethanol is oxidation of acetaldehyde (or an adsorbed alkoxide) to produce acetic acid (or a surface acetate species). Acetic acid is observed as an intermediate at low spacetimes over ZnO (Figure 6.2b$_i$) but is not observed for the reaction of ethanol over $Zn_xZr_yO_z$ (Figure 6.2a). This is likely due to the rapid ketonization of acetic acid to produce acetone over $Zn_xZr_yO_z$, as discussed further in Section 6.IV.iii.c). To deduce the reaction pathway for the oxidation of acetaldehyde to acetic acid over $Zn_xZr_yO_z$, we compared the reaction of ethanol and mixtures of ethanol and acetaldehyde over $Zn_xZr_yO_z$ and ZnO in the presence and absence of water. Mixtures of ethanol and acetaldehyde (50 wt%) were used to ensure that the reactants were introduced in the liquid phase before vaporizing in the feed line to the reactor. Key results for these reactions are shown in Figure 6.4, and the reaction conditions for the entries are given in Table 6.3.

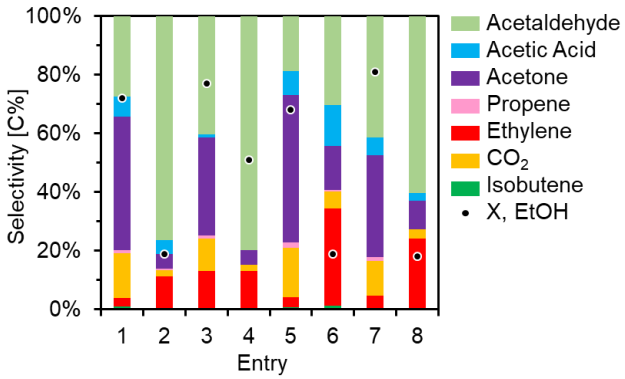

Figure 6.4. Reactions of ethanol and acetaldehyde over ZnO and $Zn_xZr_yO_z$. Reaction conditions given in Table 6.3. For carbon selectivity calculations, acetaldehyde is considered a product, despite being co-fed in Entries 4-8.

Table 6.3. Reaction Conditions for Figure 6.4.

Entry	Substrate	Catalyst	Catalyst Mass [mg]	Substrate Partial Pressure [kPa]	Partial Pressure H_2O [kPa]
1	Ethanol	$Zn_xZr_yO_z$ 2.2 wt% Zn	4.8	0.16	13
2	Ethanol	$Zn_xZr_yO_z$ 2.2 wt% Zn	4.8	0.16	0
3	Ethanol	ZnO	58	0.19	13
4	Ethanol	ZnO	58	0.19	0
5	Ethanol / Acetaldehyde	$Zn_xZr_yO_z$ 2.2 wt% Zn	4.8	0.11 / 0.03	13
6	Ethanol / Acetaldehyde	$Zn_xZr_yO_z$ 2.2 wt% Zn	4.8	0.11 / 0.03	0
7	Ethanol / Acetaldehyde	ZnO	60.1	0.1 / 0.03	13
8	Ethanol / Acetaldehyde	ZnO	60.1	0.1 / 0.03	0
Additional Reaction Conditions for Entries 1-8: 723 K, 150 mL min^{-1} He, atmospheric pressure.					

Water is necessary to promote the reactions of ethanol and ethanol/acetaldehyde mixtures over both $Zn_xZr_yO_z$ and ZnO, as evidenced by the significantly lower conversions observed in the absence of water (entries 2, 4, 6, and 8) compared to the presence of water (entries 1, 3, 5, and 7). The conversions shown in entries 2, 4, 6, and 8 correspond to initial conversion and selectivity, because both $Zn_xZr_yO_z$ and ZnO both rapidly deactivated in the absence of water (see Figure 6.24a and Figure 6.24b).

As discussed in Section 6.IV.iii.a), the ethanol selectivity to ethylene is higher over ZnO than $Zn_xZr_yO_z$ (2.2 wt% Zn) in the presence of water, as shown by entries 1 and 3 in Figure 6.4. Over $Zn_xZr_yO_z$, the selectivity towards ethylene is relatively unchanged when acetaldehyde is co-fed with ethanol in the presence of water (entry 5 compared to entry 1). However, over ZnO, the selectivity to ethylene is lower when acetaldehyde is co-fed (entry 7 compared to entry 3). This suggests that the production of ethylene over ZnO comes from the dehydration of ethanol.

The selectivity to acetic acid is generally higher when acetaldehyde (entries 5-8) is co-fed with ethanol, suggesting that acetaldehyde is an intermediate in acetic acid formation. Slightly higher amounts of acetic acid are observed over $Zn_xZr_yO_z$ (entries 1, 2, 5, 6) compared to ZnO (entries 3, 4, 7, 8), suggesting that the oxidation of acetaldehyde is promoted by balanced acid/base sites. Ethyl acetate was not observed for any of the reactions, suggesting that the oxidation of acetaldehyde over $Zn_xZr_yO_z$ and ZnO occurs via hydroxyl addition to acetaldehyde as opposed to the decomposition of ethyl acetate, as proposed for the formation of acetone from ethanol over Y_2O_3-CeO_2.[257]

It has been proposed that acetaldehyde oxidation to acetic acid occurs via direct participation of surface hydroxyl groups from adsorbed water over Sc/In_2O_3[257] and ZnO-CaO.[262] Rahman et al. found that water inhibits the aldolization of acetaldehyde to crotonaldehyde over

ZnO, favoring instead the oxidation of acetaldehyde to acetic acid, which undergoes ketonization to produce acetone.[263] Silva Calpa et al. have shown that the addition of Zn to monoclinic zirconia produces defect sites in the form of oxygen vacancies that improve the redox properties of the catalyst and promote the dissociation of water on the surface.[264] In a subsequent study of the conversion of ethanol to acetone over $Zn_xZr_{1-x}O_{2-y}$, the authors suggested that acetaldehyde reacts with the oxygen of the solid solution to produce vacancies on the catalyst surface, which then undergo ketonization to acetone and CO_2, followed by the dissociation of water over vacancy sites to re-oxidize the surface.[265] Other studies have shown that oxygen vacancies are able to promote the dissociation of water to produce surface hydroxyl groups over ceria[266] and zirconia.[267] In addition, theoretical investigations of the partial dissociation of H_2O over ZnO (1011) have concluded that the hydrogen bonding of water aids in water dissociation; therefore the greater the surface coverage of water, the greater the water dissociation.[268]

Based upon our experimental evidence indicating that water is critical for the oxidation of acetaldehyde and that balanced Lewis acid/base sites promote the oxidation of acetaldehyde, and the published evidence for the role of water dissociation in the oxidation of acetaldehyde,[257,262–269] we propose a mechanism for the oxidation of acetaldehyde shown in Scheme 6.3. Acetaldehyde first adsorbs onto a Lewis acid site and water dissociates onto the catalyst surface over oxygen vacancies. This is followed by the addition of the hydroxyl group to the carbonyl carbon, and then base-catalyzed hydrogen abstraction, leading to formation of the carbon oxygen double bond to produce bound acetic acid, which can either desorb or remain on the surface to undergo ketonization in the next step.

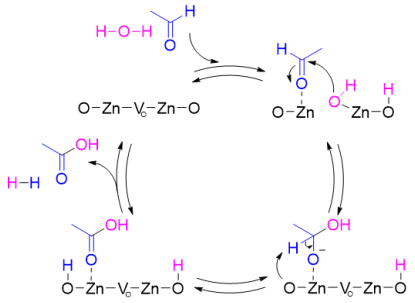

Scheme 6.3. Proposed mechanism for the oxidation of acetaldehyde over $Zn_xZr_yO_z$.

c) Ketonization of Acetic Acid to Acetone

The next step in the proposed reaction pathway is the ketonization of acetic acid to produce acetone. As shown earlier in Figure 6.2b$_i$, at low spacetimes, the reaction of ethanol over ZnO yields a small amount of acetic acid, which is generated and then consumed as the spacetime increases. In contrast, as shown in Figure 6.2a, no significant amounts of acetic acid can be observed for the reaction of ethanol over $Zn_xZr_yO_z$ (2.2 wt% Zn). This suggests that acetic acid reacts more rapidly over $Zn_xZr_yO_z$ than over ZnO, indicating that ketonization requires a higher concentration of Lewis acid sites. To further probe the reactivity of acetic acid, we studied the reaction of acetic acid over ZnO and $Zn_xZr_yO_z$ (2.2 wt% Zn) in the presence and absence of water.

The reaction of acetic acid to produce isobutene over $Zn_xZr_yO_z$ (2.2 wt% Zn) is stable for over 5 h at 723 K for a steam-to-carbon ratio of 5.4, as shown in Figure 6.25. Interestingly, in contrast to the literature,[242] we found that bulk ZnO is also capable of catalyzing the ketonization of acetic acid to acetone and subsequent isobutene formation at 723 K, and remains stable even

though the reaction is much slower than over $Zn_xZr_yO_z$. The two leftmost entries in Figure 6.5 show a comparison of $Zn_xZr_yO_z$ (2.2 wt% Zn) and bulk ZnO for the reaction of acetic acid in the presence of water at 723 K under the same reaction conditions and normalized by the surface area of the catalyst. The conversion of acetic acid is greater over the mixed oxide catalyst, and the rate of isobutene formation is over 3 times greater over the $Zn_xZr_yO_z$ compared to ZnO ($4.11 \cdot 10^{-5}$ mol h^{-1} m^{-2} versus $1.25 \cdot 10^{-5}$ mol h^{-1} m^{-2}, respectively). As shown in the three rightmost entries of Figure 6.5, the selectivity to isobutene can be increased over ZnO as the spacetime, and thus conversion of acetic acid, is increased. To reach the same rate of isobutene formation over ZnO as that observed over the mixed oxide catalyst, the spacetime needs to be increased by approximately a factor of 4. Still, the reaction pathway and intermediates appear to be the same over ZnO as they are over $Zn_xZr_yO_z$, although as the conversion is increased, the selectivity to methane over ZnO also increases.

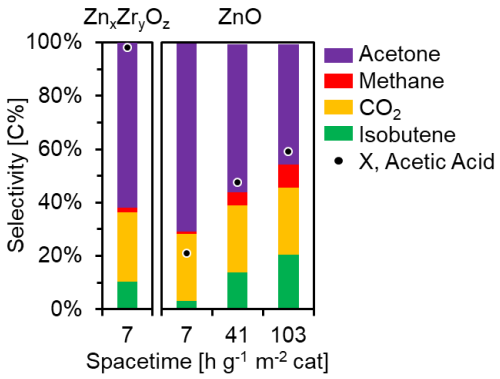

Figure 6.5. Reactions of acetic acid and water over $Zn_xZr_yO_z$ and ZnO at varying spacetimes. Reaction conditions: Left: 22.3 mg $Zn_xZr_yO_z$ 2.2 wt% Zn, 723 K, 0.16 kPa acetic acid, 11.4 kPa H_2O, S/C 5.4; Right: 319 mg ZnO, 723 K, 0.18 kPa acetic acid, 13 kPa H_2O, S/C 5.7.

In the absence of water, the rate of acetic acid consumption over both ZnO and $Zn_xZr_yO_z$ decreases rapidly due to catalyst deactivation. As shown in Figure 6.26a and Figure 6.26b, the initial rate of isobutene formation is high, but the catalyst begins to immediately deactivate and produce significant amounts of acetic anhydride, as well as small amounts of methane. This suggests that water, while inhibiting active sites for acetic acid adsorption, inhibits undesired acetone decomposition to methane and bimolecular dehydration of acetic acid to produce acetic anhydride. Furthermore, at a constant steam-to-carbon ratio, there is an increase in the rate of isobutene formation and selectivity with increasing acetic acid partial pressure (see Figure 6.27), suggesting that the surface is not saturated with acetic acid. The clear differences in the reaction rates of acetic acid over ZnO and $Zn_xZr_yO_z$ suggest that the balanced acid-base pairs on $Zn_xZr_yO_z$ are more effective for the ketonization step than the strong Lewis base-weak Lewis acid pairs on bulk ZnO.

Previous studies have suggested that Lewis acid/base pairs promote ketonization of acetic acid over $Zn_xZr_yO_z$ prepared via sol-gel synthesis,[242] and that the acid-base properties of the catalyst or coordination vacancies play a critical role in catalyzing the ketonization reaction over metal oxides.[41] Wang and Iglesia have suggested that the rate limiting step for the ketonization of C_2-C_4 carboxylic acids over TiO_2 and ZrO_2 is C-C bond formation between 1-hydroxy enolate species and co-adsorbed acids bound at neighboring acid-base pairs saturated with active monodentate carboxylates.[270] Gumidyala et al. also proposed that C-C coupling is the rate limiting step for acid-catalyzed ketonization of acetic acid over H-ZSM5, and that water inhibits the

reaction rate but improves catalyst stability.[271] Gangadharan et al. have suggested that water promotes propanal ketonization and inhibits aldol condensation over ceria modified zirconia ($Ce_xZr_{1-x}O_2$) by increasing the concentration of surface –OH groups that enhance the formation of surface carboxylates with the aldehyde.[272] A DFT study of the ketonization of acetic acid over tetragonal zirconia reported by Tosoni et al. has also highlighted the beneficial role of oxygen vacancies and reduced Zr^{3+} centers for the ketonization reaction, which proceeds via adsorption of acetic acid followed by formation of an enolate and an acylic intermediate, which react together to form the beta-keto acid.[273]

Based upon our experimental observations and the precedent for Lewis acid-base catalyzed ketonization in the literature, we propose the following mechanism for the ketonization of acetic acid to produce acetone and CO_2 over $Zn_xZr_yO_z$, shown in Scheme 6.4. First, two acetic acid molecules adsorb onto acid-base pairs, with the basic oxygen interacting with the hydrogen on the hydroxyl group and the Lewis acidic Zn interacting with the carbonyl oxygen. Next, a basic oxygen abstracts a hydrogen from the methyl group, producing a carbanion, which then attacks the carbonyl group of the second acetic acid to form a C-C bond in the rate limiting step to produce an adsorbed dimer. From there, subsequent dehydration and C-C bond cleavage produce CO_2 and acetone. The importance of Lewis acidity is clear in the rate limiting step, as the Zn must be sufficiently acidic to active the adsorbed acetic acid. We also point out that acetic acid ketonization reactions are typically carried out at lower temperatures (~503-603 K)[270,271] as opposed to 723 K, further suggesting that water is necessary to prevent side reactions that may occur more readily at higher temperatures. The desorption of acetone in the final step is reversible, because although significant amounts of acetone are observed for this reaction, the dimerization of acetone requires the adsorption of acetone on the catalyst surface.

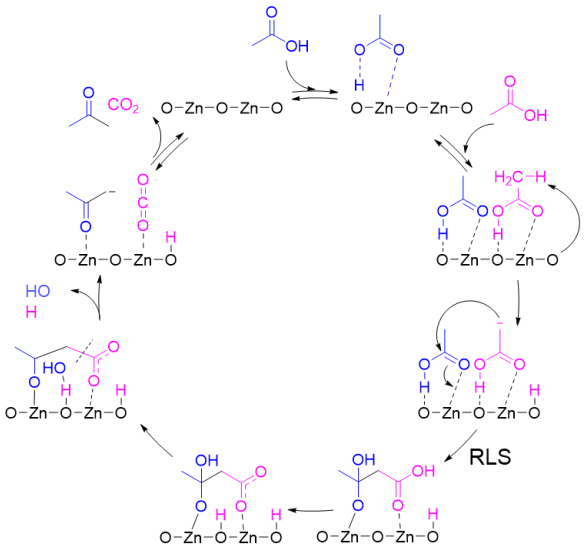

Scheme 6.4. Proposed mechanism for the ketonization of acetic acid over $Zn_xZr_yO_z$.

iv. Conversion of Acetone to Isobutene

As demonstrated in Section 6.IV.iii, acetone is a critical intermediate in the cascade of reactions leading from ethanol to isobutene. The mechanism for the conversion of acetone to isobutene is difficult to probe, as intermediates such as diacetone alcohol are unstable, and it is unclear whether mesityl oxide is an intermediate in this reaction pathway and what role water plays in promoting the decomposition of C_6 intermediates to isobutene and acetic acid. In this section,

we discuss the condensation of acetone to diacetone alcohol and investigate the role of mesityl oxide in the conversion of acetone to isobutene. We then propose a reaction mechanism and use it to develop a rate expression for the conversion of acetone to isobutene.

a) Acetone Condensation to Diacetone Alcohol

The first step in the proposed reaction pathway for the conversion of acetone to isobutene is the dimerization of acetone to produce diacetone alcohol. The product distribution observed upon feeding diacetone alcohol to the reactor is nearly identical to that observed when acetone is the feed. In fact, upon introduction into the reactor via a syringe pump through heated lines (~367 K), the diacetone alcohol is already completely converted to acetone before reaching the catalyst bed, suggesting that this reaction step is reversible, and that equilibrium lies strongly to the left. This is consistent with the calculated gas phase free energy (+110.8 kJ mol^{-1}), which indicates that the reaction of acetone to diacetone alcohol is strongly disfavored (Figure 6.18). Studies in the literature indicate that both Brønsted acid sites and Lewis acid-base pairs can facilitate the activation of acetone.[274–277] Therefore, we assume that acid-base sites on the surface of $Zn_xZr_yO_z$ are responsible for promoting the dimerization of acetone to diacetone alcohol.

b) Reaction of Mesityl Oxide to Isobutene

Mesityl oxide is observed as a secondary product at low conversions for the reaction of ethanol and acetone to isobutene over bulk ZnO, and at low conversions for the reaction of acetone to isobutene over both ZnO and $Zn_xZr_yO_z$ (2.2wt% Zn) (see Figure 6.2b_i and Figure 6.19). However, the role of mesityl oxide as an intermediate is unclear. As observed from the infrared spectra of adsorbed pyridine and the NH_3 TPD spectrum of $Zn_xZr_yO_z$, significant quantities of Brønsted acid sites were not identified, suggesting that unless temporary weak Brønsted acid sites are generated from water during the reaction, the mechanism of isobutene formation does not involve Brønsted acid-catalyzed cleavage of mesityl oxide. To better understand the role of mesityl oxide in the conversion of acetone to isobutene, the reaction of mesityl oxide to isobutene was investigated over both $Zn_xZr_yO_z$ (2.2 wt% Zn) and ZnO.

Figure 6.6 shows the product distribution for reactions of mesityl oxide (90%, remainder 4-metylpent-4-en-2-one) over $Zn_xZr_yO_z$ (2.2 wt% Zn) and ZnO at two different spacetimes (Table 6.4, entries 1-2, and 4-5, respectively) and in the absence of water (Table 6.4, entries 3 and 6). As shown in Figure 6.6 and Table 6.4, entries 1-2 and 5-6, both isobutene and acetone are formed. This indicates that the acetone to diacetone alcohol to mesityl oxide pathway is reversible under reaction conditions. Therefore, it is inconclusive whether the reaction to form isobutene proceeds via hydrolysis of mesityl oxide or whether the mesityl oxide is only a side product. As spacetime is increased for the reaction of mesityl oxide and water over $Zn_xZr_yO_z$ (Table 6.4, entries 1 to 2) and ZnO (Table 6.4, entries 4 to 5), the selectivity to isobutene and the conversion of mesityl oxide increase, and the selectivity to acetone decreases, suggesting that acetone is an intermediate in the formation of isobutene from mesityl oxide and water. As spacetime is increased, there is an increase in the formation of other side products, such as isophorone and higher C_{9+} compounds, resulting from the condensation of mesityl oxide with acetone. These products are not observed for the reaction of acetone and water over these catalysts under the same reaction conditions and steam-to-carbon ratios, suggesting that mesityl oxide is an intermediate for the formation of side products. ln contrast to the reaction of acetone to isobutene, both $Zn_xZr_yO_z$ and ZnO deactivate over the course of a few hours, even in the presence of water, as shown in Figure 6.28a and Figure

6.28b. In the absence of water, the activity of the catalysts decreased rapidly after approximately 15 min time on stream, as shown by entries 3 and 6 in Table 6.4. Evidence for coke formation could be observed by the formation of high carbon number products (C_{9+}), as well as visual observation of black deposits on the catalyst after the reaction.

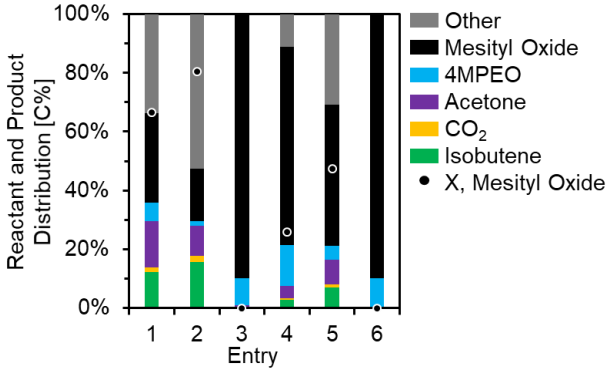

Figure 6.6. Product distribution for the reaction of mesityl oxide over $Zn_xZr_yO_z$ (2.2 wt% Zn) and ZnO at varying spacetimes and in the presence and absence of water. Reaction conditions given in Table 6.4.

Table 6.4. Reaction Conditions for Figure 6.6.

Entry	Catalyst	Catalyst Mass [mg]	Spacetime [hr g cat^{-1} m^{-2}]	Partial Pressure H_2O [kPa]
1	$Zn_xZr_yO_z$ 2.2 wt% Zn	4.9	1.7	13
2	$Zn_xZr_yO_z$ 2.2 wt% Zn	4.9	21.8	13
3	$Zn_xZr_yO_z$ 2.2 wt% Zn	4.9	1.7	0
4	ZnO	60.8	1.5	13
5	ZnO	60.8	17.8	13
6	ZnO	60.8	1.5	0

Additional Reaction Conditions: 723 K, 0.012 kPa initial 4-methylpent-4-en-2-one, 0.12 kPa initial Mesityl Oxide, 150 mL min^{-1} He (entries 1,3-4,6), 11.8 mL min^{-1} He (entry 2), 12.4 mL min^{-1} He (entry 5). Entries 1,2,4,5 S/C 6.3. Entries 3 and 6 taken after 15 minutes time on stream.

The initial feed for the mesityl oxide experiments contains an equilibrated mixture of mesityl oxide with 10 mol% of the isomer 4-methylpent-4-en-2-one (4MPEO). At low spacetimes for the reaction of mesityl oxide over $Zn_xZr_yO_z$ and ZnO in the presence of water, the percentage of 4MPEO relative to mesityl oxide increases to 17 mol % (entries 1 and 4). At higher spacetimes, however, the percentage of 4MPEO drops to 8 mol % and 9 mol% over $Zn_xZr_yO_z$ and ZnO, respectively. In the absence of water, the activity of both catalysts is almost completely negligible, and the relative percent of 4MPEO is close to that in the feed (9 mol % and 10 mol% 4MPEO for $Zn_xZr_yO_z$ and ZnO, respectively). The increase in the relative partial pressure of 4MPEO at low spacetimes suggests that mesityl oxide may undergo isomerization or that mesityl oxide is consumed faster than 4MPEO.

From these data, we conclude that over $Zn_xZr_yO_z$ and ZnO, the conversion of two molecules of acetone to produce mesityl oxide and water is reversible under reaction conditions, that increasing spacetime leads to increasing conversion of mesityl oxide, and that the mechanism of catalyst deactivation comes from the formation of condensation products which further oligomerize and contribute to coke formation. Because of the reversible nature of the acetone to mesityl oxide reaction, it remains inconclusive whether mesityl oxide is a necessary intermediate for the formation of isobutene. To further probe the acetone to isobutene reaction, additional rate measurements and isotopic labeling experiments were performed.

c) Kinetic Isotope Effects for the Reaction of Acetone to Isobutene

The kinetic isotope effect for the reaction of acetone to isobutene was measured for both $Zn_xZr_yO_z$ and ZnO to identify the rate-limiting step. A reaction temperature of 623 K was selected so that rates of both mesityl oxide and isobutene formation could be measured at low conversions and with negligible catalyst deactivation. The results of the kinetic isotope effect measurements are shown in Table 6.5. In agreement with Sun et al. we did not observe a significant kinetic isotope effect for the formation of isobutene from acetone over $Zn_xZr_yO_z$.[43]

We also measured kinetic isotope effects for the formation of isobutene from acetone over ZnO and did not observe a kinetic isotope effect. These findings indicate that C-H bond cleavage is not involved in the rate-limiting step for the reaction of acetone to isobutene over either $Zn_xZr_yO_z$ or ZnO and suggest that the rate-limiting step for isobutene formation is not the dehydration of diacetone alcohol to produce mesityl oxide. We propose, instead, that it must be either C-C bond formation occurring during acetone coupling to form diacetone alcohol or the decomposition of diacetone alcohol, which does not involve the breaking of C-H or O-H bonds. The formation of mesityl oxide was also not significantly affected by deuteration of either acetone or water over either $Zn_xZr_yO_z$ or ZnO, confirming that unimolecular dehydration of diacetone alcohol is not rate-limiting for the dominant pathway towards forming either mesityl oxide or isobutene.

The slight kinetic isotope effect for isobutene formation over ZnO in the presence of acetone-d_6 and D_2O and for mesityl oxide formation in the presence of acetone-d_6 may be due to minor pathways towards isobutene and mesityl oxide formation that are limited by activation of water or C-H bond cleavage; however, because these kinetic isotope effects are small and nearly within error, we suggest that the rate limiting step for the dominant pathway for isobutene formation is either C-C coupling or decomposition of diacetone alcohol and that C-C coupling is the rate limiting step for the dominant pathway for mesityl oxide formation.

Table 6.5. Kinetic Isotope Effect Experiments for Acetone Conversion to Isobutene and Mesityl Oxide

Reactants	Observed KIE Isobutene (k_H/k_D)		Observed KIE Mesityl Oxide (k_H/k_D)	
	$Zn_xZr_yO_z$ (2.2 wt% Zn)	ZnO	$Zn_xZr_yO_z$ (2.2 wt% Zn)	ZnO
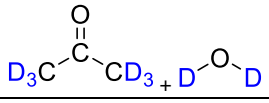	0.96 ± 0.20	1.34 ± 0.10	1.11 ± 0.10	1.11 ± 0.10
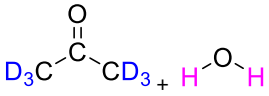	1.02 ± 0.29	1.12 ± 0.11	1.20 ± 0.11	1.07 ± 0.10
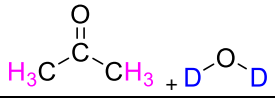	1.01 ± 0.10	1.14 ± 0.10	1.08 ± 0.10	1.18 ± 0.10

Reaction conditions: 623 K, 1 kPa acetone/d_6-acetone, 15 kPa H_2O/D_2O, WHSV 2.2 h^{-1}, 50 mL min^{-1} He, 1 atm.

d) Roles of Acidity and Basicity on the Conversion of Acetone to Isobutene

The kinetic isotope experiments do not reveal whether the mechanism of acetone to isobutene is different over $Zn_xZr_yO_z$ and ZnO. Further investigation into the nature of the active sties for this reaction were probed by measuring the effect of acidity and basicity on the reaction selectivity for the acetone to isobutene reactions. As demonstrated previously, the acid-base properties of the $Zn_xZr_yO_z$ can be tuned by adjusting the weight loading of Zn on the surface. The effect of Zn loading on the selectivity and activity for the acetone to isobutene reaction is shown

in Figure 6.7a, in which 0 wt% Zn corresponds to pure monoclinic zirconia, and 80.3 wt% Zn corresponds to bulk zinc oxide.

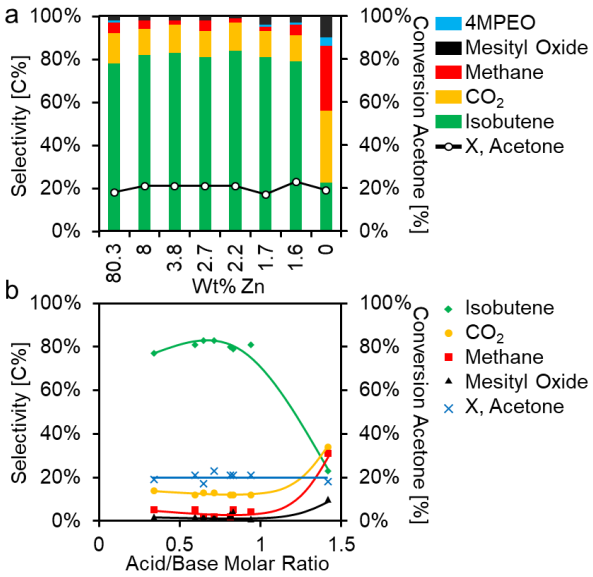

Figure 6.7. a) Conversion of acetone to isobutene as a function of weight loading normalized by surface area of catalyst. b) Conversion and selectivity for the acetone to isobutene reaction as a function of acid/base ratio. Reaction conditions: 698 K, 0.5 kPa acetone, 30 kPa H_2O, S/C 8.2, 50 mL min^{-1} He, 1 m^2 catalyst

Interestingly, above a Zn loading of 1.6 wt%, the selectivity to isobutene remains relatively unchanged, exhibiting nearly theoretical isobutene selectivities (~80%), with some minor formation of methane and trace amounts of mesityl oxide. In contrast to the reaction of ethanol to isobutene, no propene was observed, further suggesting that alcohols are required in the feed to serve as reducing agents for the MPV reduction of acetone. The conversions for these catalysts are relatively consistent despite the differences in acidity and basicity. To assess the effects of catalyst acid-base properties on the selectivity of the acetone to isobutene reaction, the conversion and selectivity towards isobutene, methane, and mesityl oxide were plotted versus the total basicity measured from CO_2-TPD, the total acidity measured via NH_3-TPD, and the acid/base ratio. These graphs are shown in Figure 6.29a, Figure 6.29b, and Figure 6.7b, respectively. Figure 6.7b clearly shows that the most acidic catalyst (ZrO_2) exhibits higher methane formation, suggesting that the addition of Zn suppresses the decomposition of acetone to methane by introducing basicity. Apart from the highly acidic ZrO_2, which exhibits a lower isobutene selectivity, there is no clear correlation between catalyst acidity and basicity, and the observed trends in product selectivity (Figure 6.29a and Figure 6.29b). However, by plotting product selectivity versus the molar ratio of acid to base sites for each of the catalysts tested **(**Figure 6.7b**)**, the subtler effects of acid/base ratios on selectivity can be observed for $Zn_xZr_yO_z$. The 2.2 wt% Zn catalyst exhibits a slightly higher isobutene selectivity and the lowest selectivity towards side products (methane, mesityl oxide, etc.) compared to catalysts with other weight loadings of Zn. This catalyst has an acid/base molar ratio of approximately 0.71. XRD and Raman surface characterization revealed that at a Zn weight loading of 2.2%, nearly all the zirconia has transitioned from the monoclinic to the tetragonal phase (Figure 6.1a and Figure 6.1b), suggesting that the surface contains a sufficient coverage of Zn to stabilize the tetragonal phase but does not yet form bulk ZnO clusters. As mentioned in Section 6.IV.i, this suggests that the Zn-O-Zr interactions are more predominant at

this intermediate Zn weight loading, suggesting that these moieties are beneficial for promoting the reaction of acetone to isobutene. By plotting the acid/base ratio versus isobutene selectivity for the acetone to isobutene reaction, we can conclude that the formation of isobutene from acetone requires a balance of Lewis acid and base sites.

e) Kinetics of the Acetone to Isobutene Reaction

To gain further insight into the mechanism and kinetics of acetone conversion to isobutene, a series of experiments were performed under conditions of differential conversion (< 7%) in which the effects of temperature, water partial pressure, and acetone partial pressure on the rates of formation of isobutene and mesityl oxide were measured.

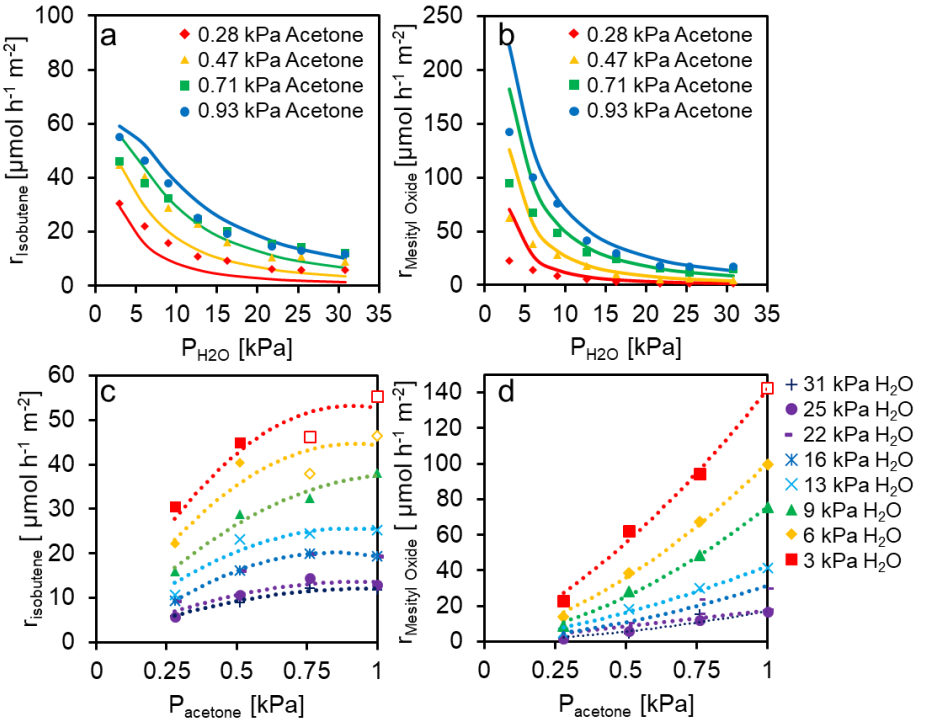

Figure 6.8. a) Effect of water partial pressure on rates of isobutene formation, b) effect of water partial pressure on rates of mesityl oxide formation, c) effect of acetone partial pressure on rates of isobutene formation, d) effect of acetone partial pressure on rates of mesityl oxide formation. Reaction conditions: 623 K, Atmospheric pressure, 5.5 mg $Zn_xZr_yO_z$ (2.2 wt% Zn), 50 mL min^{-1} He. Solid lines represent fit to the kinetic model given by Equation 6.2. Dashed lines are intended to guide the eye. Hollow data points refer to initial rates after which the catalyst rapidly deactivates.

Figure 6.8 shows the effects of water and acetone partial pressure on the rates of isobutene and mesityl oxide formation over $Zn_xZr_yO_z$ (2.2 wt% Zn) at 623 K. As evidenced by Figure 6.8a and Figure 6.8b, water inhibits both isobutene and mesityl oxide formation; however, water is necessary to prevent deactivation, which occurs when the steam-to-carbon ratio drops below 5. Figure 6.8c and Figure 6.8d show that the rate of isobutene formation lies between zero and first order in acetone partial pressure and the rate of mesityl oxide formation is between first and second order in acetone partial pressure. This suggests a mechanism in which mesityl oxide formation is limited by the surface reaction of two molecules of acetone, and the isobutene formation reaction is both promoted and inhibited by acetone on the surface.

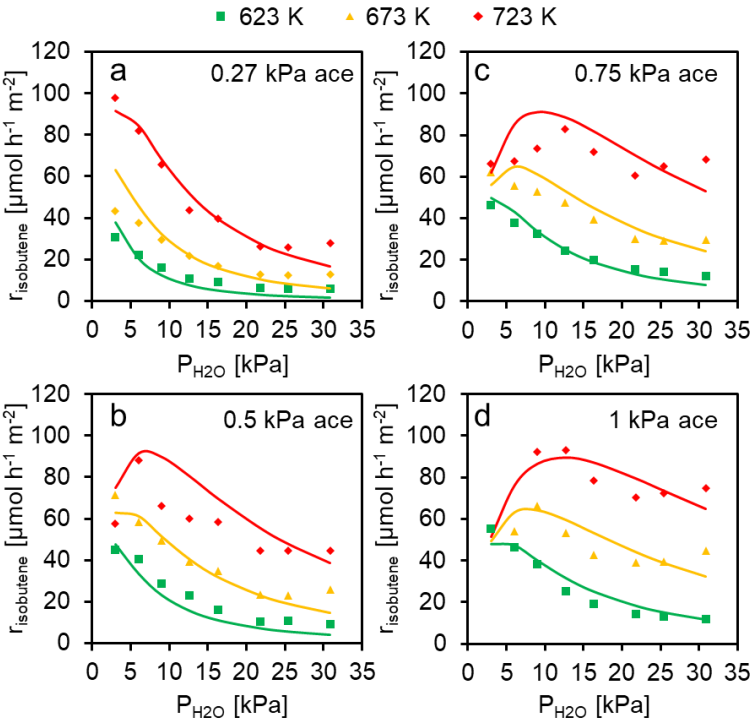

Figure 6.9. Rate of isobutene formation as function of temperature and pressure of reactants. Reaction conditions: Atmospheric pressure, 5.5 mg $Zn_xZr_yO_z$ (2.2 wt% Zn), 50 mL min^{-1} He, $X_{acetone}$ <7%, a) 0.27 kPa acetone, b) 0.5 kPa acetone, c) 0.75 kPa acetone, d) 1 kPa acetone. Solid line is fit to kinetic model given by Equation 6.2.

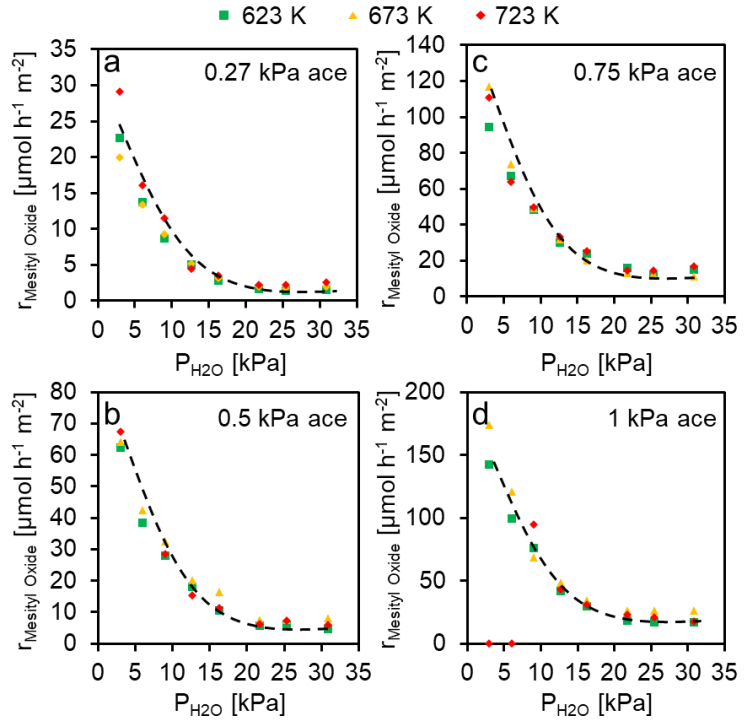

Figure 6.10. Rate of mesityl oxide formation as function of temperature and pressure of reactants. Reaction conditions: Atmospheric pressure, 5.5 mg $Zn_xZr_yO_z$ (2.2 wt% Zn), 50 mL min^{-1} He, $X_{acetone}$ <7%, a) 0.27 kPa acetone, b) 0.5 kPa acetone, c) 0.75 kPa acetone, d) 1 kPa acetone. Dashed lines are to guide the eye.

To further probe the kinetics of the conversion of acetone to isobutene, the initial rates of isobutene and mesityl oxide formation as a function of acetone and water partial pressure were measured at 673 K and 723 K, as shown in Figure 6.9 and Figure 6.10. Figure 6.9 shows that rate of isobutene formation increases with increasing temperature. As the temperature increases, the inhibiting effects of water are less prominent, suggesting that the competitive adsorption of acetone and water on active sites lies in favor of acetone at higher temperatures. Figure 6.10 shows that while the rate of mesityl oxide formation increases with increasing partial pressure of acetone, the rate of mesityl oxide formation at a given partial pressure of acetone and water is nearly independent of the temperature between 623 and 723 K. Figure 6.11 shows the ratio of isobutene to mesityl oxide formed as a function of acetone and water partial pressure at 623, 673, and 723 K. The selectivity towards isobutene increases with increasing water partial pressure and decreases with increasing acetone partial pressure, demonstrating that water inhibits mesityl oxide formation more than isobutene formation. The selectivity towards isobutene relative to mesityl oxide also increases as temperature increases, because the rates of mesityl oxide formation are relatively unaffected by temperature but the activation energy for isobutene formation is positive.

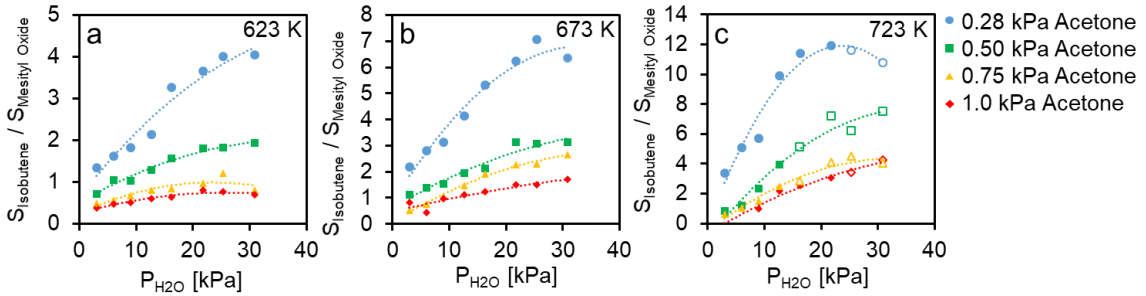

Figure 6.11. Selectivity ratio of isobutene to mesityl oxide (carbon %) as a function of temperature and partial pressure of reactants. Reaction conditions: Atmospheric pressure, 5.5 mg $Zn_xZr_yO_z$ (2.2 wt% Zn), 50 mL min^{-1} He, $X_{acetone}$ <7%, a) 623K, b) 673 K, c) 723 K. Hollow data points represent initial rates measured for conditions which resulted in catalyst deactivation. Dashed lines are intended to guide the eye.

f) Proposed Mechanism and Kinetic Model for Acetone Conversion to Isobutene

Based on the measured kinetics and the proposed roles of acid and base sites for the reactions of acetone, diacetone alcohol, and mesityl oxide to isobutene, we propose the mechanism for the conversion of acetone to isobutene shown in Scheme 6.5. The first is the upper pathway shown in this scheme. Water adsorbs dissociatively and forms a temporary Brønsted acidic proton which protonates the hydroxyl group of the adsorbed diacetone alcohol. Next, in a concerted step, the hydroxyl group that came from water adds to the carbonyl group while the C-C bond is broken to form isobutene, water, and acetic acid. In the second pathway, a variant of the first, diacetone alcohol adds a proton produced by heterolytic dissociation of water, and then undergoes dehydration, leaving behind a carbocation intermediate. The next step is then addition of a hydroxyl group, produced by the heterolytic dissociation of water, to the carbonyl group, followed by C-C bond cleavage to produce isobutene and acetic acid. The third pathway involves Lewis-acid catalyzed dehydration of diacetone alcohol to form mesityl oxide, which either desorbs from the surface or abstracts a hydrogen from the catalyst surface to produce the carbocation intermediate in the middle pathway. This intermediate then forms isobutene and acetic acid by addition of a hydroxyl group and cleavage of the C-C bond. In each of these three cases, the key transition state involves a partial bond between the hydroxyl group and the carbonyl, the breaking of a C-C bond, the formation of a C=C double bond, and a partial positive charge on the most

substituted carbon. The acetic acid formed then undergoes further ketonization to produce more surface acetone, water, and CO_2.

Two different rate expressions for the reaction kinetics were developed and fit to the experimental data. Equation 6.1 was derived for the case in which the rate-limiting step is C-C coupling of acetone to produce diacetone alcohol (labeled "a" on Scheme 6.5) and Equation 6.2 was derived for the case in which rate limiting step is the decomposition of the C_6 intermediate (either protonated diacetone alcohol or a C_6 carbocation intermediate) to produce isobutene and acetic acid (labeled "b" or "c" on Scheme 6.5). The step marked "d" on Scheme 6.5 was not considered as a rate limiting step for isobutene formation because no significant kinetic isotope effect was observed for deuterated acetone.

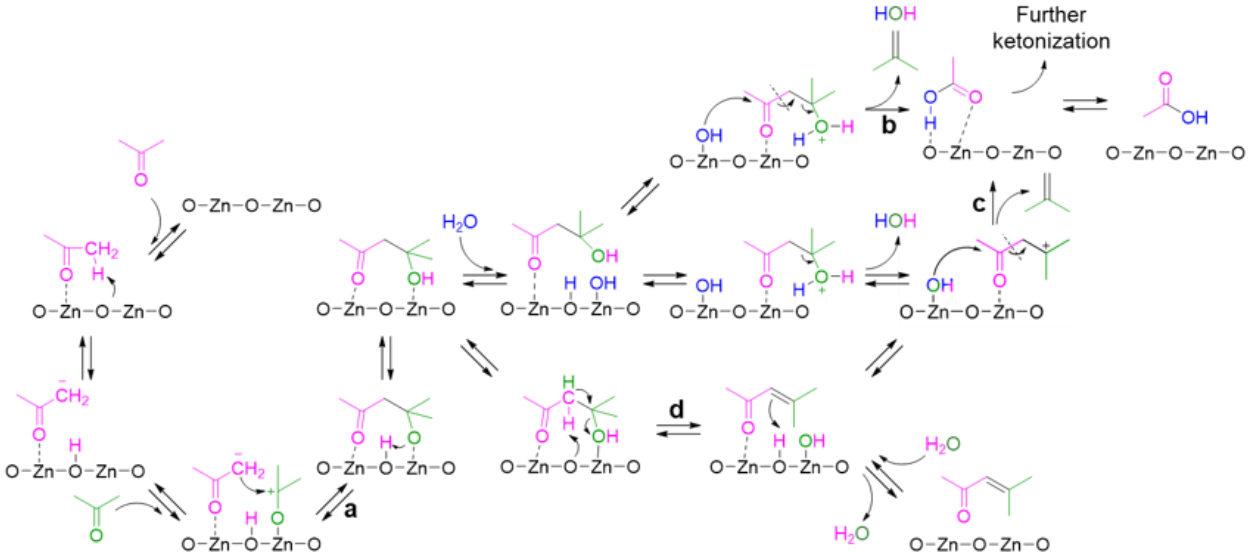

Scheme 6.5. Proposed mechanism for the conversion of acetone to isobutene and acetic acid.

The full derivations of these rate expressions based upon the elementary steps, assumptions, and site balances, as well as descriptions of the rate constants, are given in Section 6.VI.ii. In Equations 6.1 and 6.2, given below, P_A and P_{H2O} are the partial pressures of acetone and water, respectively; k_1 and k_{-1} are the forward and reverse rate constants for the coupling of acetone to diacetone alcohol; K_A and K_{H2O} are the equilibrium constants for the adsorption of acetone and water onto active sites, respectively; k_2 is the rate constant for the dehydration of diacetone alcohol to produce mesityl oxide; and k_3 is the rate constant for the decomposition of diacetone alcohol to produce isobutene and acetic acid.

$$r_{isobutene} = \frac{k_1 K_A^2 P_A^2 - k_{-1}\left(\frac{k_1 K_A^2 P_A^2}{(k_{-1} + k_2 + k_3 P_{H2O})}\right)}{(K_A P_A + K_{H2O} P_{H2O})^2} \qquad 6.1$$

$$r_{isobutene} = \frac{\frac{k_1 K_A^2 P_A^2 k_3 K_{H2O} P_{H2O}}{(k_{-1} + k_2 + k_3 P_{H2O})}}{(K_A P_A + K_{H2O} P_{H2O})^3} \qquad 6.2$$

These equations were derived with the following assumptions: the adsorption and desorption of acetone, water, and mesityl oxide are quasi-equilibrated; ketonization of acetic acid is rapid; the pseudo-steady state approximation can be applied to the rate of formation of diacetone

alcohol; the surface is saturated with acetone and water; and the concentration of mesityl oxide is negligible (as rates of mesityl oxide formation become zero upon extrapolating to zero conversion). It should also be noted that the rate expression derived from Equation 6.1 would be the same if mesityl oxide were an intermediate for isobutene formation, because C-C bond formation would still be rate limiting.

The measured rate data were fit to Equations 6.1 and 6.2 by adjusting the rate parameters to minimize the sum of least squares of the residuals. The form of Equation 6.2 is a more accurate representation of the data, as evidenced by the parity plots in shown in Figure 6.12, suggesting that the rate limiting step for isobutene formation is the decomposition of diacetone alcohol. The model for the case in which the rate of isobutene formation is limited by C-C coupling of diacetone alcohol fits well at low acetone partial pressures and low temperatures but breaks down at high temperatures and high partial pressures of acetone. This could be explained by the fact that while water inhibits the reaction by occupying active sites, it is necessary to prevent deactivation and promote the decomposition of diacetone alcohol by providing surface hydroxyl groups and Brønsted acidic protons. This promoting role of water is not captured in the first model. The rate parameters obtained from the fit of the rate data to Equation 6.2 are given in Table 6.6, and the Arrhenius plots are given in Figure 6.30. The apparent activation energy for isobutene formation is calculated to be 160 ± 19 kJ mol^{-1}.

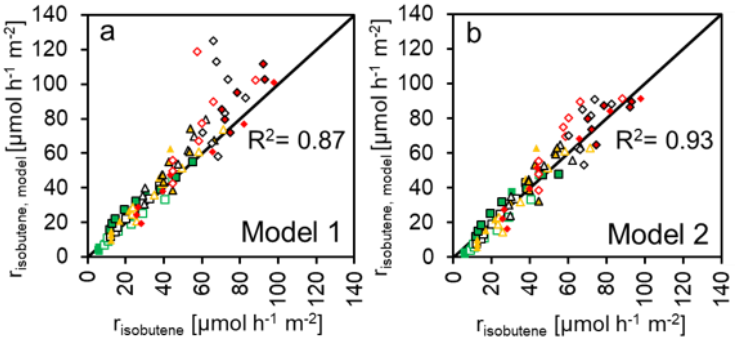

Figure 6.12. Parity plots for the rate of isobutene formation for a) Model 1 based upon Equation 6.1, and b) Model 2 based upon Equation 6.2.

Based upon measurements of the reaction kinetics, the measured kinetic isotope effects, and the effect of the acid/base ratio on the kinetics of the acetone to isobutene conversion, we conclude that the acetone to isobutene reaction proceeds via C-C coupling to produce diaceteone alcohol, followed by protonation and concerted –OH addition and β-scission to produce isobutene and acetic acid, which undergoes further condensation to produce acetone. Isobutene may also form via dehydration to mesityl oxide followed by hydrolysis of the addition product. In both cases the key transition state for isobutene formation from the C_6 compound involves the addition of a surface hydroxyl group to the carbonyl group as the C-C bond is broken. We also conclude that the role of water for the conversion of acetone to isobutene is to prevent deactivation, inhibit acetone decomposition to methane and CO_2, and dissociate to produce temporary Brønsted acid sites and hydroxyl groups that participate in the decomposition of the C_6 intermediates. The addition of water shifts the equilibrium towards diacetone alcohol and away from mesityl oxide, thereby preventing side product formation and limiting the coupling of mesityl oxide with acetone to produce C_9 compounds, such as isophorone and mesitylene, which contribute to coke formation.

V. Conclusions

In this study, we comprehensively studied the reaction pathway, mechanism, and roles of acid and base sites for the reactions of ethanol and acetone to isobutene over $Zn_xZr_yO_z$. Characterization of $Zn_xZr_yO_z$ revealed that the acid-base properties of this catalyst can be tuned by varying the Zn loading. The ethanol to isobutene reaction was found to proceed via ethanol dehydrogenation to acetaldehyde, oxidation to acetic acid, ketonization to acetone, then reversible condensation to produce diacetone alcohol followed by either dehydration to mesityl oxide or hydrolysis to produce isobutene and acetic acid, which undergoes further ketonization. Acetone was found to be a critical intermediate in the ethanol to isobutene pathway. Mechanisms consistent with measurements of the kinetics, roles of acid and base sites, and previous work in the literature were presented for each of the steps leading up to acetone formation from ethanol.

Reactions of mesityl oxide and diacetone alcohol show that the acetone to diacetone alcohol to mesityl oxide reaction step is reversible under reaction conditions. Kinetic isotope effects revealed that the rate-limiting step for converting acetone to isobutene is either the coupling of acetone to diacetone alcohol or the decomposition of diacetone alcohol. Modeling the effects of water and acetone partial pressure on the rate of isobutene formation over $Zn_xZr_yO_z$ suggests that the rate-limiting step is the decomposition of diacetone alcohol. While water inhibits the rate of isobutene formation, it is necessary to hydrate the surface to oxidize acetaldehyde to produce acetic acid; inhibit unimolecular dehydration of ethanol, acetic acid, and diacetone alcohol; prevent oligomerization of condensation products which lead to coke formation and thus deactivation; and promote the decomposition of C_6 intermediates to produce isobutene.

The addition of Zn to ZrO_2 introduces basicity without passivating the Lewis acidity, preventing unimolecular dehydration of ethanol and decomposition of acetone to methane and CO_2. The zirconia support promotes the reaction of ethanol and acetone to isobutene by increasing the surface area and dispersion of zinc, lowering the strong basicity of the zinc oxide, and forming Zn-O-Zr moieties with the optimal ratio and strength of Lewis acid and Brønsted/Lewis basic sites and with excellent redox properties.

Our studies reported in Section 6.IV.iii indicate that successful conversion of ethanol to acetone over $Zn_xZr_yO_z$ requires avoidance of ethanol dehydration. This reaction can be minimized at 698 K using a S/C = 5 and high spacetimes to promote the cascade reaction. In Section 6.IV.iv, it was demonstrated that optimal yields of isobutene from acetone over $Zn_xZr_yO_z$ can be achieved at 723 K with a S/C = 5, under which conditions the activity is high and the temperature is high enough to limit mesityl oxide formation, but low enough to prevent acetone decomposition to methane and CO_2 as well as the formation of C_9 condensation products which lead to coke formation. Ultimately, a 2-step process in which ethanol is first converted to acetone at 698 K followed by acetone conversion to isobutene at 723 K could be employed to optimize yields of isobutene from ethanol.

VI. Supporting Information

i. Supplemental Schemes, Figures, and Tables

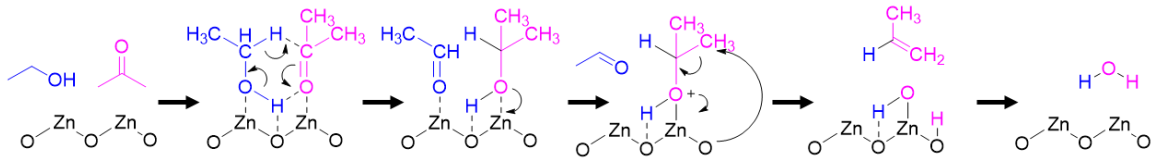

Scheme 6.6. Production of propene from ethanol and acetone via MPV reduction of acetone to produce isopropanol, followed by dehydration to produce propene.

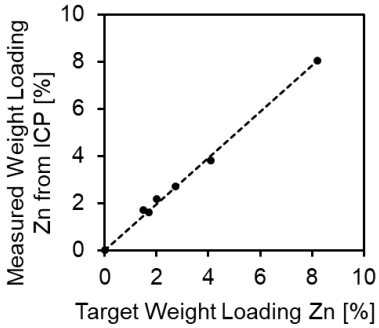

Figure 6.13. Target weight loading of Zn for incipient wetness impregnation method versus measured weight loading from ICP conducted by Galbriath Laboratories.

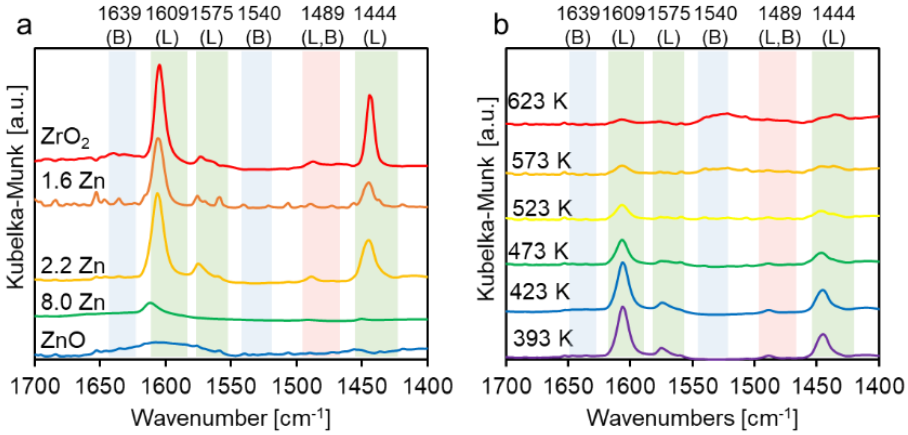

Figure 6.14. a) DRIFTS-py at 393 K for ZnO, ZrO_2, and $Zn_xZr_yO_z$ with varying weight loadings of Zn. Catalysts diluted with KBr (250 mg KBr, 50 mg catalyst) except for ZnO which was not diluted by KBr, b) DRIFTS- py as a function of temperature over $Zn_xZr_yO_z$ (2.2 wt% Zn).

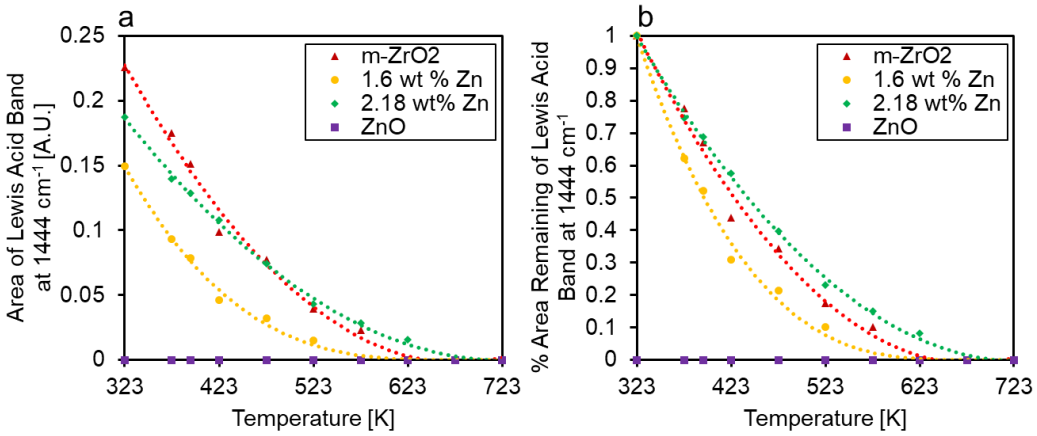

Figure 6.15. a) Area of band at 1444 cm^{-1} measured from DRIFTS spectra of adsorbed pyridine over selected catalysts as a function of temperature, b) percent area of band at 1444 cm^{-1} remaining after increasing the temperature for monoclinic zirconia, $Zn_xZr_yO_z$ with Zn weight loadings of 1.6 and 2.18, and bulk zinc oxide. Pyridine was introduced at 323 K.

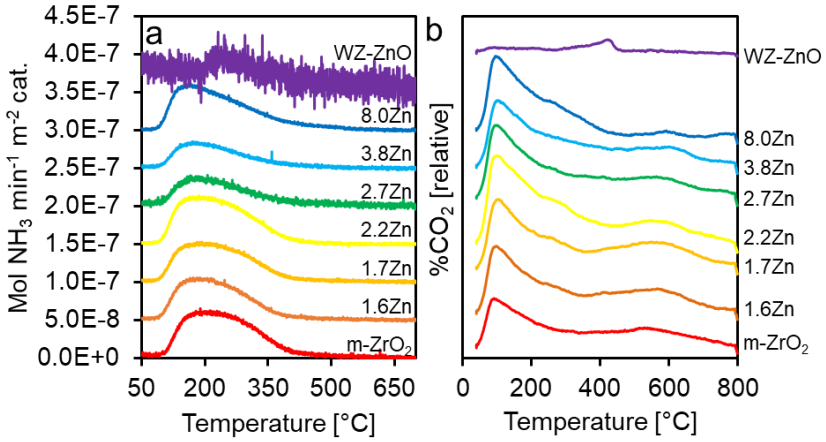

Figure 6.16. a) NH_3-TPD profiles of catalysts, b) CO_2-TPD profiles of catalysts.

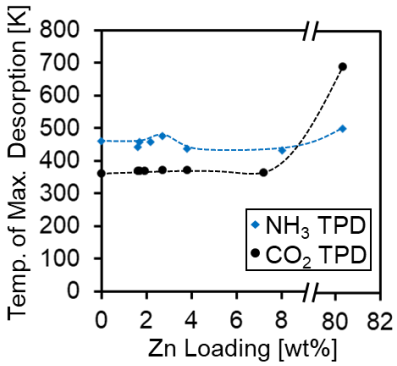

Figure 6.17. Temperature of maximum desorption of NH_3 (blue diamond) and CO_2 (black circle) during temperature-programmed-desorption (TPD) experiments for ZrO_2, ZnO, and the $Zn_xZr_yO_z$ catalysts.

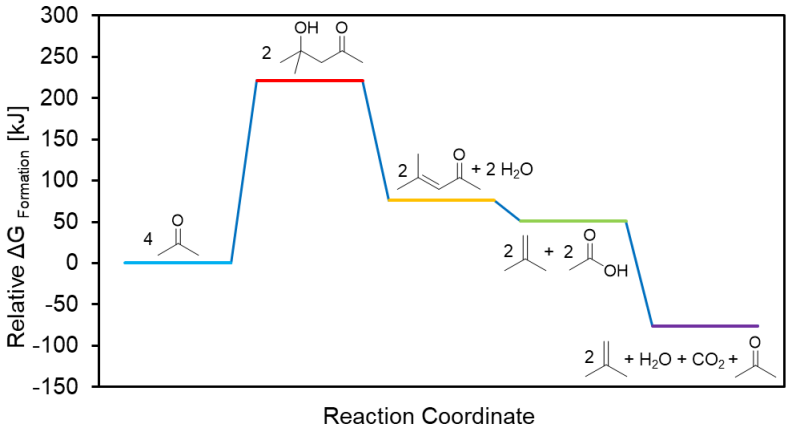

Figure 6.18. Gas phase free energies of formation calculated from DFT. Values are normalized relative to acetone and are expressed on a basis of kJ per number of moles shown by the stoichiometry for each intermediate step.

Details for Qchem Calculations: Geometry minimization: exchange omega B97X-D, basis 6-31G**, Frequency calculation: exchange omega B97X-D, basis 6-31G**, Single point energy: exchange omega B97X-D, basis 6-311++G(3df,3pd).

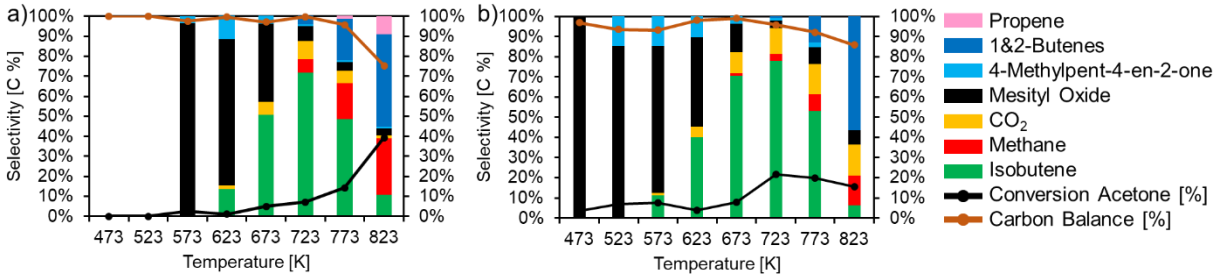

Figure 6.19. Effect of temperature on the acetone to isobutene reaction. Reaction Conditions: 0.4 kPa acetone, 17.8 kPa H_2O, S/C 8, 50 mL min^{-1} He, a) 283.5 mg ZnO, b) 20.5 mg $Zn_xZr_yO_z$ (2.2 wt% Zn). Catalyst deactivation for both catalysts began at 773 K, data recorded is from initial rate.

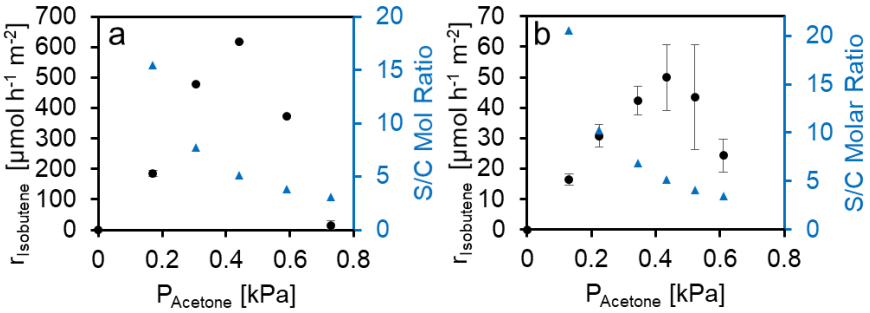

Figure 6.20. Effect of steam to carbon ratio on reaction rates for the acetone to isobutene reaction over a) $Zn_xZr_yO_z$ (2.2 wt% Zn) and b) ZnO (61.4 mg). Reaction conditions: 723 K, 150 mL min^{-1} He with a) 15 kPa H_2O and b) 13 kPa H_2O.

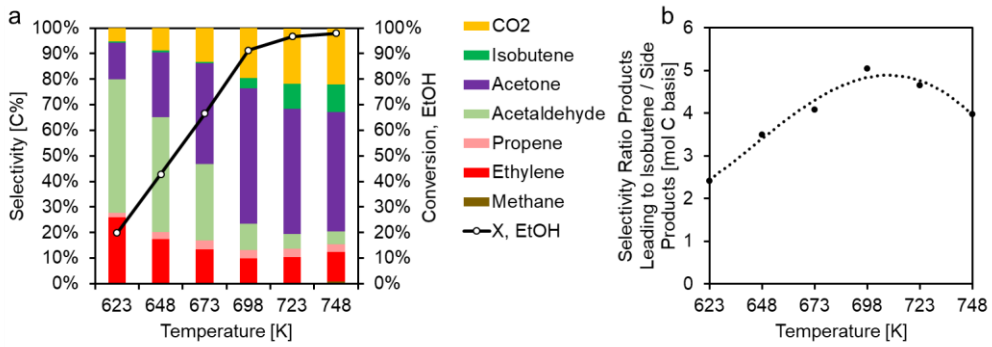

Figure 6.21. a) Effect of temperature on the ethanol to isobutene reaction over $Zn_xZr_yO_z$ (2.2 wt% Zn). Reaction Conditions: 0.1 kPa acetone, 30 kPa H_2O, 50 mL min^{-1} He, atmospheric pressure, b) Selectivity ratio of productive products leading to isobutene (acetaldehyde, acetone, and isobutene) over undesired side products (methane, ethylene, and propene), demonstrating that 698 K is the ideal temperature for maximizing the productive cascade reaction.

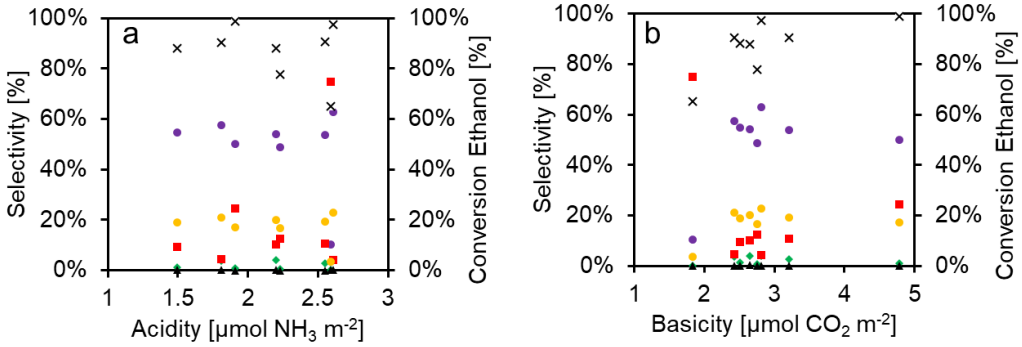

Figure 6.22. a) Effect of acidity (measured by NH_3-TPD) on the selectivity for the ethanol to isobutene reaction, b) effect of basicity (measured by CO_2-TPD) on the ethanol to isobutene reaction. Reaction conditions: 698 K, 1 kPa EtOH, S/C 4, 50 mL min^{-1} He, WHSV 0.7, spacetime normalized by BET surface area.

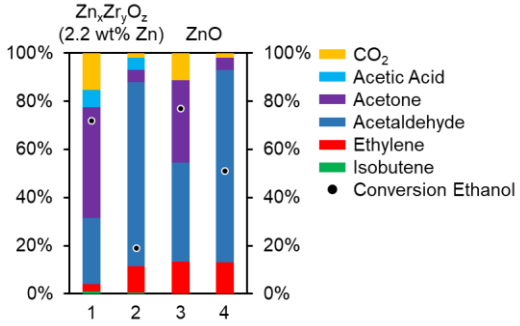

Figure 6.23. Ethanol reactions over $Zn_xZr_yO_z$ (2.2 wt% Zn) and ZnO in the presence and absence of water. Entries 1, 2: $Zn_xZr_yO_z$ (2.2 wt% Zn) 4.8 mg, entries 3, 4: 58 mg ZnO, 0.2 kPa acetone, entries 1, 3: 13 kPa H_2O, entries 2, 4: 0 kPa H_2O, 150 mL min^{-1} He, 723 K. As observed by entries 1 and 2, in the absence water, the selectivity towards ethylene (red) increases over $Zn_xZr_yO_z$ (2.2 wt% Zn) and the conversion dramatically decreases. Over ZnO (entries 3 and 4), the absence of water also decreases the conversion and significantly decreases the conversion of acetaldehyde to acetone.

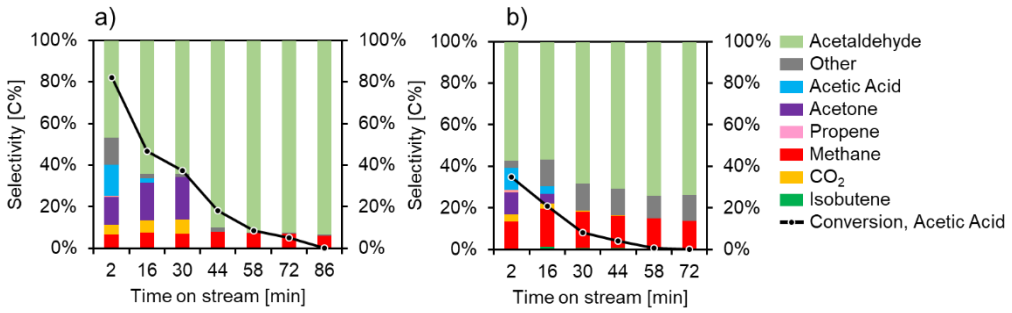

Figure 6.24. Reactions of ethanol and acetaldehyde mixtures in the absence of water over a) ZnO (60.1 mg), and b) $Zn_xZr_yO_z$ 2.2 wt% Zn (4.8 mg). Reaction conditions: 0.11 kPa EtOH, 0.03 kPa acetaldehyde, 723 K, 150 mL min^{-1} He, atmospheric pressure.

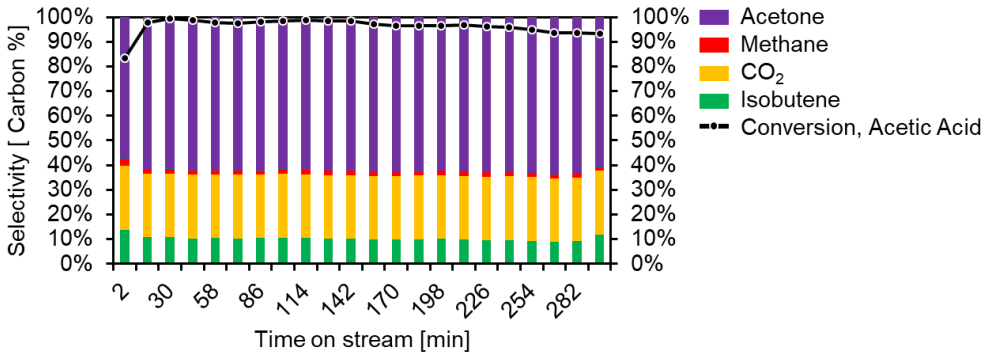

Figure 6.25. Effect of time on stream for the reaction of acetic acid to isobutene at 723 K. Reaction conditions: 22.3 mg $Zn_xZr_yO_z$ 2.2 wt% Zn, 150 mL min^{-1} He, 0.21 kPa acetic acid, 11.4 kPa H_2O, S/C 5.4. Reaction was stable for over 5 h.

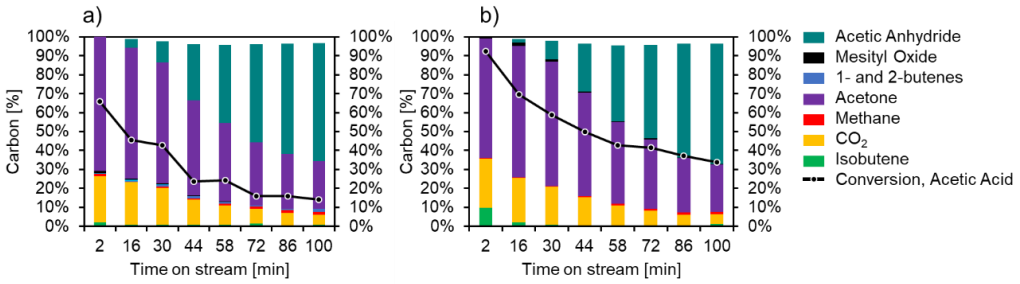

Figure 6.26. Reactions of acetic acid in the absence of water over a) ZnO and b) $Zn_xZr_yO_z$ 2.2 wt% Zn. Reaction conditions: a) 723 K, 0.22 kPa acetic acid, 60.1 mg catalyst, 150 mL min^{-1} He; b) 723 K, 0.26 kPa acetic acid, 4.9 mg catalyst, 150 mL min^{-1} He.

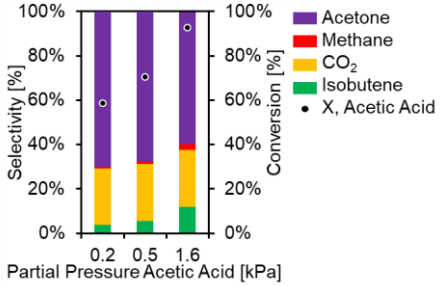

Figure 6.27. Effect of partial pressure for the reaction of acetic acid to produce isobutene over $Zn_xZr_yO_z$ 2.2 wt% Zn. Reaction conditions: 723 K, 20.8 mg $Zn_xZr_yO_z$ 2.2 wt% Zn, 15-150 mL min^{-1} He, S/C 5.

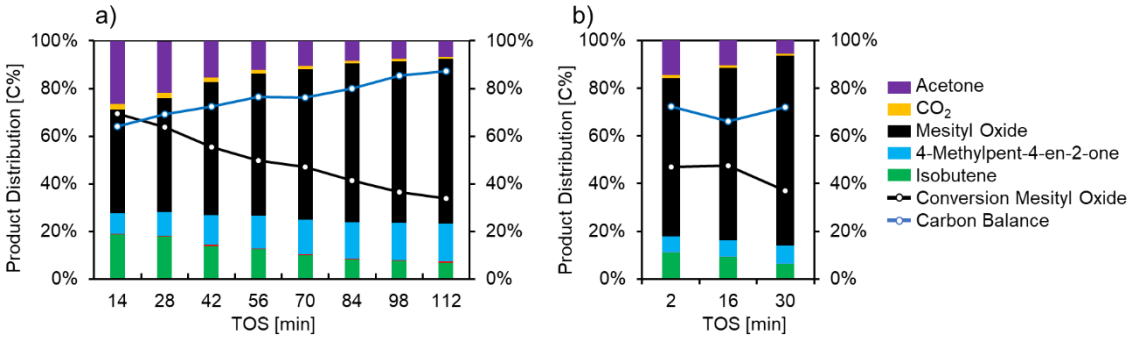

Figure 6.28. Deactivation of catalysts for the reaction of mesityl oxide and water over a) 4.8 mg $Zn_xZr_yO_z$ 2.2 wt% Zn and b) 60.8 mg ZnO. Reaction Conditions: 723 K, 150 mL min^{-1} He, S/C 6.3, 13 kPa H_2O, 0.012 kPa initial 4-methylpent-4-en-2-one, 0.12 kPa initial Mesityl Oxide.

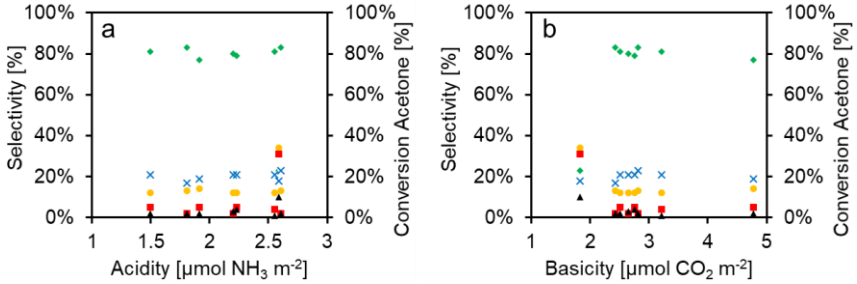

Figure 6.29. Conversion and selectivity for the acetone to isobutene reaction as a function of a) acidity [µmol NH_3 m^{-2}] and b) basicity [µmol CO_2 m^{-2}]. Reaction conditions: 698 K,0.5 kPa acetone, 30 kPa H_2O, S/C 8.2, 50 mL min^{-1} He, 1 m^2 catalyst.

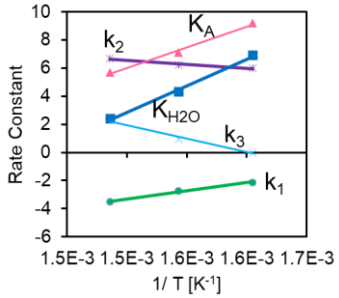

Figure 6.30. Arrhenius plots for rate constants given in Table 6.6.

Table 6.6. Kinetic Parameters from Model 2.

T [K]	k_1 [µmol h^{-1} m^{-2}]	k_2 [µmol h^{-1} m^{-2}]	k_3 [µmol h^{-1} m^{-2} kPa^{-1}]	K_A [kPa^{-1}]	k_{H2O} [kPa^{-1}]	k_{-1} [µmol h^{-1} m^{-2}]
623	0.12	400	1	9000	1000	1000
648	0.065	500	2.6	1200	75	1000
673	0.03	800	10	300	11	1000
Apparent E_A [kJ mol^{-1}]	-96 ± 8	48 ± 11	160 ± 19			
Apparent ln[A]	-21 ± 2	15 ± 2	31 ± 4			
ΔH_{ads} [kJ mol^{-1}]				-238 ± 20	-315 ± 20	
ΔS [kJ mol^{-1} K^{-1}]				0.3 ± 0.03	0.45 ± 0.03	

ii. Derivation of rate expressions for isobutene formation

The elementary steps for the formation of isobutene from acetone are given by equations S6.1-S6.7, where the partial pressures of the reactants and intermediates are given by: acetone [A], water [H_2O], diacetone alcohol [DAA**], acetic acid [AA*], carbon dioxide [CO_2], isobutene [IB], and mesityl oxide [MO]. The active site, [*] represents a Lewis acid/base pair.

$$[A] + [*] \overset{K_A}{\leftrightarrow} [A*] \text{ Quasi-Equilibrated} \quad \text{S6.1}$$

$$[H_2O] + [*] \overset{K_{H2O}}{\longleftrightarrow} [H_2O*] \text{ Quasi-Equilibrated} \quad \text{S6.2}$$

$$2[A*] \underset{k_{-1}}{\overset{k_1}{\rightleftarrows}} [DAA**] \quad \text{S6.3}$$

$$[DAA**] + [H_2O*] \overset{k_3}{\rightarrow} [IB] + [H_2O*] + [AA*] \quad \text{S6.4}$$

$$2[AA*] \overset{k_4}{\rightarrow} [A*] + [CO_2] + [H_2O*] \text{ fast} \quad \text{S6.5}$$

$$[DAA**] \underset{k_{-2}}{\overset{k_2}{\rightleftarrows}} [MO*] + [H_2O*] \quad \text{S6.6}$$

$$[MO*] \overset{K_{MO}}{\longleftrightarrow} [MO] + [*] \text{ Quasi-Equilibrated} \quad \text{S6.7}$$

Assuming steps in equations S6.1, S6.2, and S6.7 are quasi-equilibrated:

$$[A*] = K_A[A][*] \quad \text{S6.8}$$

$$[H_2O*] = K_{H2O}[H_2O][*] \quad \text{S6.9}$$

$$[MO*] = K_{MO}[MO][*] \quad \text{S6.10}$$

Applying pseudo steady state (PSSH) approximation to [DAA**]:

$$\frac{d[DAA**]}{dt} = k_1[A*]^2 - k_{-1}[DAA**] - k_2[DAA**] + k_{-2}[MO*][H_2O*] - k_3[DAA**][H_2O] \cong 0$$

$$k_{-1}[DAA**] + k_2[DAA**] + k_3[DAA**][H_2O] = k_1[A*]^2 + k_{-2}[MO*][H_2O*]$$

$$[DAA**](k_{-1} + k_2 + k_3[H_2O]) = k_1[A*]^2 + k_{-2}[MO*][H_2O*]$$

$$[DAA**] = \frac{k_1[A*]^2 + k_{-2}[MO*][H_2O*]}{(k_{-1} + k_2 + k_3[H_2O])}$$

$$[DAA**] = \frac{k_1K_A^2[A]^2[*]^2 + k_{-2}K_{MO}K_{H2O}[MO][H_2O][*]^2}{(k_{-1} + k_2 + k_3[H_2O])}$$

Model 1: Assuming rate limiting step for isobutene formation is C-C coupling of acetone:

$$r_{IB} = k_1[A*]^2 - k_{-1}[DAA**]$$

Substitute [DAA**]:

$$r_{IB} = k_1[A*]^2 - k_{-1}\left(\frac{k_1K_A^2[A]^2[*]^2 + k_{-2}K_{MO}K_{H2O}[MO][H_2O][*]^2}{(k_{-1} + k_2 + k_3[H_2O])}\right)$$

$$r_{IB} = k_1 K_A^2 [A]^2 [*]^2 - k_{-1}\left(\frac{k_1 K_A^2 [A]^2 [*]^2 + k_{-2} K_{MO} K_{H2O} [MO][H_2O][*]^2}{(k_{-1} + k_2 + k_3[H_2O])}\right)$$

$$r_{IB} = [*]^2 (k_1 K_A^2 [A]^2 - k_{-1}\left(\frac{k_1 K_A^2 [A]^2 + k_{-2} K_{MO} K_{H2O} [MO][H_2O]}{(k_{-1} + k_2 + k_3[H_2O])}\right)$$

$$\frac{r_{IB}}{[*]^2} = k_1 K_A^2 [A]^2 - k_{-1}\left(\frac{k_1 K_A^2 [A]^2 + k_{-2} K_{MO} K_{H2O} [MO][H_2O]}{(k_{-1} + k_2 + k_3[H_2O])}\right)$$

Site balance:

$$L_1 = [*] + [A*] + [H_2O*] + [MO*]$$

$$L_1 = [*] + K_A[A][*] + K_{H2O}[H_2O][*] + K_{MO}[MO][*]$$

$$L_1 = [*](1 + K_A[A] + K_{H2O}[H_2O] + K_{MO}[MO])$$

$$\frac{L_1}{[*]} = (1 + K_A[A] + K_{H2O}[H_2O] + K_{MO}[MO])$$

Substituting site balance:

$$r_{IB} = \frac{k_1 K_A^2 [A]^2 - k_{-1}\left(\frac{k_1 K_A^2 [A]^2 + k_{-2} K_{MO} K_{H2O} [MO][H_2O]}{(k_{-1} + k_2 + k_3[H_2O])}\right)}{(1 + K_A[A] + K_{H2O}[H_2O] + K_{MO}[MO])^2}$$

Assume low [MO] and sites are saturated with acetone and water:

$$r_{IB} = \frac{k_1 K_A^2 [A]^2 - k_{-1}\left(\frac{k_1 K_A^2 [A]^2}{(k_{-1} + k_2 + k_3[H_2O])}\right)}{(K_A[A] + K_{H2O}[H_2O])^2} \qquad 6.1$$

Model 2: Assuming rate limiting step is the decomposition of diacetone alcohol:

$$r_{IB} = k_3 [DAA**][H_2O*]$$

Substitute [DAA**]:

$$r_{IB} = k_3 K_{H2O}[H_2O][*] \frac{k_1 K_A^2 [A]^2 [*]^2 + k_{-2} K_{MO} K_{H2O} [MO][H_2O][*]^2}{(k_{-1} + k_2 + k_3[H_2O])}$$

$$\frac{r_{IB}}{[*]^3} = k_3 K_{H2O}[H_2O] \frac{k_1 K_A^2 [A]^2 + k_{-2} K_{MO} K_{H2O} [MO][H_2O]}{(k_{-1} + k_2 + k_3[H_2O])}$$

Substitute site balance:

$$r_{IB} = \frac{k_3 K_{H2O}[H_2O] \frac{k_1 K_A^2 [A]^2 + k_{-2} K_{MO} K_{H2O} [MO][H_2O]}{(k_{-1} + k_2 + k_3[H_2O])}}{(1 + K_A[A] + K_{H2O}[H_2O] + K_{MO2}[MO])^3}$$

Assume low [MO] and sites are saturated with acetone and water:

$$r_{IB} = \frac{\frac{k_1 K_A^2 [A]^2 k_3 K_{H2O}[H_2O]}{(k_{-1} + k_2 + k_3[H_2O])}}{(K_A[A] + K_{H2O}[H_2O])^3} \qquad 6.2$$

7. References

(1) Chapman, L. Transport and Climate Change: A Review. *J. Transp. Geogr.* 2007, *15* (5), 354–367.

(2) Cayan, D. R.; Bromirski, P. D.; Hayhoe, K.; Tyree, M.; Dettinger, M. D.; Flick, R. E. Climate Change Projections of Sea Level Extremes along the California Coast. *Clim. Change* 2007, *87* (1 SUPPL), 57–73.

(3) Hanjra, M. A.; Qureshi, M. E. Global Water Crisis and Future Food Security in an Era of Climate Change. *Food Policy* 2010, *35* (5), 365–377.

(4) Brook, B. W.; Sodhi, N. S.; Bradshaw, C. J. A. Synergies among Extinction Drivers under Global Change. *Trends Ecol. Evol.* 2008, *23* (8), 453–460.

(5) Obama, B. The Irreversible Momentum of Clean Energy. *Science (80-.).* 2017, *355* (6321), 126–129.

(6) Huber, G. W.; Iborra, S.; Corma, A. Synthesis of Transportation Fuels from Biomass: Chemistry, Catalysts, and Engineering. *Chem. Rev.* 2006, *106* (9), 4044–4098.

(7) Tuck, C. O.; Perez, E.; Horvath, I. T.; Sheldon, R. A.; Poliakoff, M. Valorization of Biomass : Deriving More Value from Waste. *Science (80-.).* 2012, *337* (August), 695–699.

(8) Alonso, D. M.; Bond, J. Q.; Dumesic, J. A. Catalytic Conversion of Biomass to Biofuels. *Green Chem.* 2010, *12* (9), 1493–1513.

(9) Huber, G. W.; Corma, A. Synergies between Bio- and Oil Refineries for the Production of Fuels from Biomass. *Angew. Chemie - Int. Ed.* 2007, *46* (38), 7184–7201.

(10) Shylesh, S.; Gokhale, A. A.; Ho, C. R.; Bell, A. T. Novel Strategies for the Production of Fuels, Lubricants, and Chemicals from Biomass. *Acc. Chem. Res.* 2017, 1–9.

(11) Qureshi, N.; Blaschek, H. P. Recent Advances in ABE Fermentation: Hyper-Butanol Producing Clostridium Beijerinckii BA101. *J. Ind. Microbiol. Biotechnol.* 2001, *27* (5), 287–291.

(12) Sreekumar, S.; Baer, Z. C.; Pazhamalai, A.; Gunbas, G.; Grippo, A.; Blanch, H. W.; Clark, D. S.; Toste, F. D. Production of an Acetone-Butanol-Ethanol Mixture from Clostridium Acetobutylicum and Its Conversion to High-Value Biofuels. *Nat. Protoc.* 2015, *10* (3), 528–537.

(13) Wu, L.; Moteki, T.; Gokhale, A. A.; Flaherty, D. W.; Toste, F. D. Production of Fuels and Chemicals from Biomass: Condensation Reactions and Beyond. *Chem* 2016, *1* (1), 32–58.

(14) Climent, M. J.; Corma, A.; Iborra, S. Conversion of Biomass Platform Molecules into Fuel Additives and Liquid Hydrocarbon Fuels. *Green Chem.* 2014, *16*, 516–547.

(15) Yee, K. F.; Mohamed, A. R.; Huat, S. A Review on the Evolution of Ethyl Tert -Butyl Ether (ETBE) and Its Future Prospects. *Renew. Sustain. Energy Rev.* 2013, *22*, 604–620.

(16) Pilling, M. J. *Low-Temperature Combustion and Autoignition*; Elsevier, 1997; Vol. 27.

(17) Soto, R.; Fité, C.; Ramírez, E.; Bringué, R.; Cunill, F. Equilibrium Conversion, Selectivity and Yield Optimization of the Simultaneous Liquid-Phase Etherification of Isobutene and Isoamylenes with Ethanol over Amberlyst^{TM} 35. *Fuel Process. Technol.* 2016, *142*, 201–211.

(18) Schifter, I.; González, U.; González-Macías, C. Effects of Ethanol, Ethyl-Tert-Butyl Ether and Dimethyl-Carbonate Blends with Gasoline on SI Engine. *Fuel* 2016, *183*, 253–261.

(19) Nel, R. J. J.; De Klerk, A. Dehydration of C5-C12 Linear 1-Alcohols over η-Alumina to Fuel Ethers. *Ind. Eng. Chem. Res.* 2009, *48* (11), 5230–5238.

(20) Bringué, R.; Ramírez, E.; Tejero, J.; Cunill, F. Influence of Acid Ion-Exchange Resins Morphology in a Swollen State on the Synthesis of Ethyl Octyl Ether from Ethanol and 1-

Octanol. *J. Catal.* 2013, *304*, 7–21.
(21) Truitt, M. J. Condensation of Alcohols for Biofuel Production. US 8845766 B2, September 30, 2014.
(22) Jadhav, D.; Grippo, A. M.; Shylesh, S.; Gokhale, A. A.; Redshaw, J.; Bell, A. T. Production of Biomass-Based Automotive Lubricants via Reductive Etherification. *ChemSusChem* 2017, *10*, 2527–2533.
(23) Yoshida, Y.; Monoi, M. Dialkyl Ether, and Lubricant Base Oil and Lubricating Oil Composition Containing the Same. US 9,365,789 B2, 2016.
(24) Gaudin, P.; Jacquot, R.; Marion, P.; Pouilloux, Y.; Jérôme, F. Acid-Catalyzed Etherification of Glycerol with Long-Alkyl-Chain Alcohols. *ChemSusChem* 2011, *4* (6), 719–722.
(25) Bethmont, V.; Fache, F.; Lemaire, M. An Alternative Catalytic Method to the William's Synthesis of Ethers. *Tetrahedron Lett.* 1995, *36* (24), 4235–4236.
(26) Vanderhaegen, B.; Neven, H.; Daenen, L.; Verstrepen, K. J.; Verachtert, H.; Derdelinckx, G. Furfuryl Ethyl Ether: Important Aging Flavor and a New Marker for the Storage Conditions of Beer. *J. Agric. Food Chem.* 2004, *52* (6), 1661–1668.
(27) Baylon, R. A. L.; Sun, J.; Wang, Y. Conversion of Ethanol to 1 , 3-Butadiene over Na Doped Zn x Zr y O z Mixed Metal Oxides. *Catal. Today* 2016, *259*, 446–452.
(28) Angelici, C.; Weckhuysen, B. M.; Bruijnincx, P. C. a. Chemocatalytic Conversion of Ethanol into Butadiene and Other Bulk Chemicals. *ChemSusChem* 2013, *6* (9), 1595–1614.
(29) Jones, M. D.; Keir, C. G.; Iulio, C. Di; Robertson, R. A. M.; Williams, C. V.; Apperley, D. C. Investigations into the Conversion of Ethanol into 1,3-Butadiene. *Catal. Sci. Technol.* 2011, *1* (2), 267–272.
(30) Makshina, E. V; Janssens, W.; Sels, B. F.; Jacobs, P. A. Catalytic Study of the Conversion of Ethanol into 1,3-Butadiene. *Catal. Today* 2012, *198*, 338–344.
(31) Kang, M.; DeWilde, J. F.; Bhan, A. Kinetics and Mechanism of Alcohol Dehydration on γ-Al2O3: Effects of Carbon Chain Length and Substitution. *ACS Catal.* 2015, *5* (2), 602–612.
(32) DeWilde, J. F.; Chiang, H.; Hickman, D. A.; Ho, C. R.; Bhan, A. Kinetics and Mechanism of Ethanol Dehydration on Y-Al 2O3: The Critical Role of Dimer Inhibition. *ACS Catal.* 2013, *3* (4), 798–807.
(33) Iwamoto, M.; Tanaka, M.; Hirakawa, S.; Mizuno, S.; Kurosawa, M. Pulse and IR Study on the Reaction Pathways for the Conversion of Ethanol to Propene over Scandium-Loaded Indium Oxide Catalysts. *ACS Catal.* 2014, *4* (10), 3463–3469.
(34) Sun, J.; Wang, Y. Recent Advances in Catalytic Conversion of Ethanol to Chemicals. *ACS Catal.* 2014, *4*, 1078–1090.
(35) Eagan, N. M.; Kumbhalkar, M. D.; Buchanan, J. S.; Dumesic, J. A.; Huber, G. W. Chemistries and Processes for the Conversion of Ethanol into Middle-Distillate Fuels. *Nat. Rev. Chem.* 2019, *3* (4), 223–249.
(36) Ho, C. R.; Shylesh, S.; Bell, A. T. Mechanism and Kinetics of Ethanol Coupling to Butanol over Hydroxyapatite. *ACS Catal.* 2015, acscatal.5b02672.
(37) Kozlowski, J. T.; Davis, R. J. Sodium Modification of Zirconia Catalysts for Ethanol Coupling to 1-Butanol. *J. Energy Chem.* 2013, *22* (1), 58–64.
(38) Ho, C. R.; Zheng, S.; Shylesh, S.; Bell, A. T. The Mechanism and Kinetics of Methyl Isobutyl Ketone Synthesis from Acetone over Ion-Exchanged Hydroxyapatite. *J. Catal.* 2018, *365*, 174–183.
(39) Higashio, Y.; Nakayama, T. One-Step Synthesis of Methyl Isobutyl Ketone Catalyzed by Palladium Supported on Niobic Acid. *Catal. Today* 1996, *28* (1–2), 127–131.

(40) Gaddy, J. L. Biological Production of Acetic Acid from Waste Gases with Clostridium Ljungdahlii. U.S. Patent 5807722, 1998.
(41) Pham, T. N.; Sooknoi, T.; Crossley, S. P.; Resasco, D. E. Ketonization of Carboxylic Acids: Mechanisms, Catalysts, and Implications for Biomass Conversion. *ACS Catal.* 2013, *3*, 2456–2473.
(42) Sun, J.; Zhu, K.; Gao, F.; Wang, C.; Liu, J.; Peden, C. H. F.; Wang, Y. Direct Conversion of Bio-Ethanol to Isobutene on Nanosized ZnxZryOz Mixed Oxides with Balanced Acid-Base Sites. *J. Am. Chem. Soc.* 2011, *133*, 11096–11099.
(43) Sun, J.; Baylon, R. A. L.; Liu, C.; Mei, D.; Martin, K. J.; Venkitasubramanian, P.; Wang, Y. Key Roles of Lewis Acid−Base Pairs on ZnxZryOz in Direct Ethanol/Acetone to Isobutene Conversion. *J. Am. Chem. Soc.* 2016, *138*, 507–517.
(44) Balakrishnan, M.; Sacia, E. R.; Sreekumar, S.; Gunbas, G.; Gokhale, A. A.; Scown, C. D.; Toste, F. D.; Bell, A. T. Correction for Balakrishnan et Al., Novel Pathways for Fuels and Lubricants from Biomass Optimized Using Life-Cycle Greenhouse Gas Assessment: Table 1. *Proc. Natl. Acad. Sci.* 2015, *112* (29), 7645–7649.
(45) Carlini, C.; Macinai, A.; Raspolli Galletti, A. M.; Sbrana, G. Selective Synthesis of 2-Ethyl-1-Hexanol from n-Butanol through the Guerbet Reaction by Using Bifunctional Catalysts Based on Copper or Palladium Precursors and Sodium Butoxide. *J. Mol. Catal. A Chem.* 2004, *212* (1–2), 65–70.
(46) Maximov, A. L.; Nekhaev, A. I.; Ramazanov, D. N. Ethers and Acetals, Promising Petrochemicals from Renewable Sources. *Pet. Chem.* 2015, *55* (1), 1–21.
(47) Olah, G. Cleaner Burning and Cetane Enhancing Diesel Fuel Supplements. US Patent 5520710 A, 1996.
(48) Wolfgang Beilfuss, Ralf Gradtke, Wolfgang Siegert, Karl-Heinz Diehl, K. W. Glyceryl Ethers as Preservatives for Cooling Lubricants. US Patent 7268102 B2, 2007.
(49) Leslie R. Rudnick, Ross A. Kremer, D. A. L. Alkylated Diphenyl Ether Lubricants. Patent US 5552071 A, September 1996.
(50) Rudnick, L. R. *Synthetics, Mineral Oils, and Bio-Based Lubricants: Chemistry and Technology, Second Edition*; CRC Press, Taylor and Francis Group: Boca Raton, 2013.
(51) Zolper, T.; Li, Z.; Chen, C.; Jungk, M.; Marks, T.; Chung, Y.-W.; Wang, Q. Lubrication Properties of Polyalphaolefin and Polysiloxane Lubricants: Molecular Structure-Tribology Relationships. *Tribol. Lett.* 2012, *48* (3), 355–365.
(52) Benda, R.; Bullen, J.; Plomer, A. Polyalphaolefins - Base Fluids for High-Performance Lubricants. *J. Synth. Lubr.* 1996, *13* (1), 41–57.
(53) Balakrishnan, M.; Sacia, E. R.; Bell, A. T. Etherification and Reductive Etherification of 5-(Hydroxymethyl)Furfural: 5-(Alkoxymethyl)Furfurals and 2,5-Bis(Alkoxymethyl)Furans as Potential Bio-Diesel Candidates. *Green Chem.* 2012, *14* (6), 1626–1634.
(54) Bringué, R.; Ramírez, E.; Iborra, M.; Tejero, J.; Cunill, F. Kinetics of 1-Hexanol Etherification on Amberlyst 70. *Chem. Eng. J.* 2014, *246*, 71–78.
(55) Bringué, R.; Iborra, M.; Tejero, J.; Izquierdo, J.; Cunill, F.; Fite, C.; Cruz, V. Thermally Stable Ion-Exchange Resins as Catalysts for the Liquid-Phase Dehydration of 1-Pentanol to Di-n-Pentyl Ether (DNPE). *J. Catal.* 2006, *244* (1), 33–42.
(56) Medina, E.; Bringué, R.; Tejero, J.; Iborra, M.; Fité, C. Conversion of 1-Hexanol to Di-n-Hexyl Ether on Acidic Catalysts. *Appl. Catal. A Gen.* 2010, *374* (1–2), 41–47.
(57) Hoek, I.; Nijhuis, T. A.; Stankiewicz, A. I.; Moulijn, J. A. Kinetics of Solid Acid Catalysed Etherification of Symmetrical Primary Alcohols: Zeolite BEA Catalysed Etherification of

1-Octanol. *Appl. Catal. A Gen.* 2004, *266* (1), 109–116.
(58) Arata, K. Solid Superacids. *Adv. Catal.* 1990, *37*, 165–211.
(59) Perot, G.; Guisnet, M. Advantages and Disadvantages of Zeolites as Catalysts in Organic Chemistry. *J. Mol. Catal.* 1990, *61* (2), 173–196.
(60) Hino, M.; Arata, K. Synthesis of Solid Superacid of Tungsten Oxide Supported on Zirconia and Its Catalytic Action for Reactions of Butane and Pentane. *J. Chem. Soc. Chem. Commun.* 1988, No. 18, 1259–1260.
(61) Zhou, W.; Soultanidis, N.; Xu, H.; Wong, M. S.; Neurock, M.; Kiely, C. J.; Wachs, I. E. Nature of Catalytic Active Sites in the Supported WO3/ZrO2 Solid Acid System: A Current Perspective. *ACS Catal.* 2017, *7*, 2181–2198.
(62) Patil, M. K.; Prasad, A. N.; Reddy, B. M. Zirconia-Based Solid Acids: Green and Heterogeneous Catalysts for Organic Synthesis. *Curr. Org. Chem.* 2011, *15* (23), 3961–3985.
(63) López, D. E.; Suwannakarn, K.; Bruce, D. A.; Goodwin, J. G. Esterification and Transesterification on Tungstated Zirconia: Effect of Calcination Temperature. *J. Catal.* 2007, *247* (1), 43–50.
(64) Larsen, G.; Lotero, E.; Petkovic, L. M.; Shobe, D. S. Alcohol Dehydration Reactions over Tungstated Zirconia Catalysts. *J. Catal.* 1997, *169* (1), 67–75.
(65) Macht, J.; Baertsch, C. D.; May-Lozano, M.; Soled, S. L.; Wang, Y.; Iglesia, E. Support Effects on Brønsted Acid Site Densities and Alcohol Dehydration Turnover Rates on Tungsten Oxide Domains. *J. Catal.* 2004, *227* (2), 479–491.
(66) Peng, S.; Okeley, N. M.; Tsai, A.-L.; Wu, G.; Kulmacz, R. J.; Van der Donk, W. A. Synthesis of Isotopically Labeled Arachidonic Acids to Probe the Reaction Mechanism of Prostaglandin H Synthase. *J. Am. Chem. Soc.* 2002, *124* (36), 10785–10796.
(67) Zhao, Y.; Li, W.; Zhang, M.; Tao, K. A Comparison of Surface Acidic Features between Tetragonal and Monoclinic Nanostructured Zirconia. *Catal. Commun.* 2002, *3* (6), 239–245.
(68) Baertsch, C. D.; Soled, S. L.; Iglesia, E. Isotopic and Chemical Titration of Acid Sites in Tungsten Oxide Domains Supported on Zirconia. *J. Phys. Chem. B* 2001, *105* (7), 1320–1330.
(69) Wang, A.; Balsara, N. P.; Bell, A. T. Pervaporation-Assisted Catalytic Conversion of Xylose to Furfural. *Green Chem.* 2016, *18* (14), 4073–4085.
(70) Melero, J. A.; Iglesias, J.; Morales, G. Heterogeneous Acid Catalysts for Biodiesel Production: Current Status and Future Challenges. *Green Chem.* 2009, *11* (9), 1285–1308.
(71) Ginjupalli, S. R.; Mugawar, S.; Rajan N., P.; Kumar Balla, P.; Komandur, V. R. C. Vapour Phase Dehydration of Glycerol to Acrolein over NbOPO4 Catalysts. *J. Chem. Technol. Biotechnol.* 2014, *89* (12), 1890–1897.
(72) Larsen, G.; Lotero, E.; Raghavan, S.; Parra, R. D.; Querini, C. A. A Study of Platinum Supported on Tungstated Zirconia Catalysts. *Appl. Catal. A Gen.* 1996, *139* (1–2), 201–211.
(73) Barton, D. G.; Soled, S. L.; G.D. Meitzner; Fuentes, G. A.; E. Iglesia. Structural and Catalytic Characterization of Solid Acids Based on Zirconia Modified by Tungsten Oxide. *J. Catal.* 1999, *181* (1), 57–72.
(74) Balzer, R.; Drago, V.; Schreiner, W. H.; Probst, L. F. D. Synthesis and Structure-Activity Relationship of a WO 3 Catalyst for the Total Oxidation of BTX. *J. Braz. Chem. Soc.* 2014, *25* (11), 2026–2031.
(75) Li, M.; Feng, Z.; Xiong, G.; Ying, P.; Xin, Q.; Li, C. Phase Transformation in the Surface

Region of Zirconia Detected by UV Raman Spectroscopy. *J. Phys. Chem. B* 2001, *105* (34), 8107–8111.
(76) Kuba, S.; Concepción Heydorn, P.; Grasselli, R. K.; Gates, B. C.; Che, M.; Knözinger, H. Redox Properties of Tungstated Zirconia Catalysts: Relevance to the Activation of n-Alkanes. *Phys. Chem. Chem. Phys.* 2001, *3* (1), 146–154.
(77) Galano, A.; Rodriguez-Gattorno, G.; Torres-García, E. A Combined Theoretical-Experimental Study on the Acidity of WO(x)-ZrO(2) Systems. *Phys. Chem. Chem. Phys.* 2008, *10* (28), 4181–4188.
(78) Shimizu, K.; Venkatraman, T. N.; Song, W. NMR Study of Tungstated Zirconia Catalyst: Acidic Properties of Tungstated Zirconia and Influence of Tungsten Loading. *Appl. Catal. A Gen.* 2002, *225* (1–2), 33–41.
(79) Ross-Medgaarden, E. I.; Knowles, W. V.; Kim, T.; Wong, M. S.; Zhou, W.; Kiely, C. J.; Wachs, I. E. New Insights into the Nature of the Acidic Catalytic Active Sites Present in ZrO2-Supported Tungsten Oxide Catalysts. *J. Catal.* 2008, *256* (1), 108–125.
(80) Kourieh, R.; Bennici, S.; Auroux, A. Acid and Redox Properties of Tungstated Zirconia Catalysts. *React. Kinet. Mech. Catal.* 2012, *105* (1), 101–111.
(81) Emeis, C. A. Determination of Integrated Molar Extinction Coefficients for Infrared Absorption Bands of Pyridine Adsorbed on Solid Acid Catalyts. *J. Catal.* 1993, *141*, 347–354.
(82) Baertsch, C.; Komala, K. T.; Chua, Y.; Iglesia, E. Genesis of Brønsted Acid Sites during Dehydration of 2-Butanol on Tungsten Oxide Catalysts. *J. Catal.* 2002, *205* (1), 44–57.
(83) Knaeble, W.; Iglesia, E. Kinetic and Theoretical Insights into the Mechanism of Alkanol Dehydration on Solid Brønsted Acid Catalysts. *J. Phys. Chem. C* 2016, *120* (6), 3371–3389.
(84) Foo, G. S.; Wei, D.; Sholl, D. S.; Sievers, C. Role of Lewis and Brønsted Acid Sites in the Dehydration of Glycerol over Niobia. *ACS Catal.* 2014, *4* (9), 3180–3192.
(85) Calatayud, M.; Ruppert, A. M.; Weckhuysen, B. M. Theoretical Study on the Role of Surface Basicity and Lewis Acidity on the Etherification of Glycerol over Alkaline Earth Metal Oxides. *Chemistry* 2009, *15* (41), 10864–10870.
(86) Jones, A. J.; Iglesia, E. Kinetic, Spectroscopic, and Theoretical Assessment of Associative and Dissociative Methanol Dehydration Routes in Zeolites. *Angew. Chemie Int. Ed.* 2014, *53* (45), 12177–12181.
(87) Kostestkyy, P.; Yu, J.; Gorte, R. J.; Mpourmpakis, G. Structure–Activity Relationships on Metal-Oxides: Alcohol Dehydration. *Catal. Sci. Technol.* 2014, *4* (11), 3861.
(88) Roy, S.; Mpourmpakis, G.; Hong, D.; Vlachos, D. G.; Bhan, A.; Gorte, R. J. Mechanistic Study of Alcohol Dehydration on γ - Al 2 O 3. *ACS Catal.* 2012, *2*, 1846–1853.
(89) Szymanski, J. T.; Roberts, A. C. The Crystal Structure of Tungsttte, Wo3-H2O. *Can. Mineral.* 1984, *22*, 681–688.
(90) Mootz, D.; Wussow, H. G. Crystal Structures of Pyridine and Pyridine Trihydrate. *J. Chem. Phys.* 1981, *75* (3), 1517–1522.
(91) Sievers, C.; Noda, Y.; Qi, L.; Albuquerque, E. M.; Rioux, R. M.; Scott, S. L. Phenomena Affecting Catalytic Reactions at Solid–Liquid Interfaces. *ACS Catal.* 2016, 8286–8307.
(92) Arteconi, A.; Mazzarini, A.; Di Nicola, G. Emissions from Ethers and Organic Carbonate Fuel Additives: A Review. *Water. Air. Soil Pollut.* 2011, *221* (1–4), 405–423.
(93) Guilera, J.; Ramírez, E.; Fité, C.; Tejero, J.; Cunill, F. Synthesis of Ethyl Hexyl Ether over Acidic Ion-Exchange Resins for Cleaner Diesel Fuel. *Catal. Sci. Technol.* 2015, 2238–2250.
(94) Beilfuss, W.; Gradtke, R.; Siegert, W.; Diehl, K.-H.; Weber, K. Glyceryl Ethers as

Preservatives for Cooling Lubricants. US 7268102 B2, 2007.
(95) Schwartz, T. J.; O'Neill, B. J.; Shanks, B. H.; Dumesic, J. A. Bridging the Chemical and Biological Catalysis Gap: Challenges and Outlooks for Producing Sustainable Chemicals. *ACS Catal.* 2014, *4* (6), 2060–2069.
(96) Sreekumar, S.; Baer, Z. C.; Gross, E.; Padmanaban, S.; Goulas, K.; Gunbas, G.; Alayoglu, S.; Blanch, H. W.; Clark, D. S.; Toste, F. D. Chemocatalytic Upgrading of Tailored Fermentation Products Toward Biodiesel. *ChemSusChem* 2014, *94720*, 1–5.
(97) Anbarasan, P.; Baer, Z. C.; Sreekumar, S.; Gross, E.; Binder, J. B.; Blanch, H. W.; Clark, D. S.; Toste, F. D. Integration of Chemical Catalysis with Extractive Fermentation to Produce Fuels. *Nature* 2012, *491* (7423), 235–239.
(98) Pereira, R. C. C.; Pasa, V. M. D. Effect of Mono-Olefins and Diolefins on the Stability of Automotive Gasoline. *Fuel* 2006, *85* (12–13), 1860–1865.
(99) Rorrer, J.; He, Y.; Toste, F. D.; Bell, A. T. Mechanism and Kinetics of 1-Dodecanol Etherification over Tungstated Zirconia. *J. Catal.* 2017, *354*, 13–23.
(100) Casas, C.; Bringué, R.; Ramírez, E.; Iborra, M.; Tejero, J. Liquid-Phase Dehydration of 1-Octanol, 1-Hexanol and 1-Pentanol to Linear Symmetrical Ethers over Ion Exchange Resins. *Appl. Catal. A Gen.* 2011, *396* (1–2), 129–139.
(101) Guilera, J.; Bringué, R.; Ramírez, E.; Iborra, M.; Tejero, J. Comparison between Ethanol and Diethyl Carbonate as Ethylating Agents for Ethyl Octyl Ether Synthesis over Acidic Ion-Exchange Resins. *Ind. Eng. Chem. Res.* 2012, *51*, 16525–16530.
(102) Down, R. D.; Lehr, J. H. *Environmental Instrumentation and Analysis Handbook*; John Wiley & Sons, 2005; Vol. 22.
(103) Sacia, E. R.; Balakrishnan, M.; Deaner, M. H.; Goulas, K. a.; Toste, F. D.; Bell, A. T. Highly Selective Condensation of Biomass-Derived Methyl Ketones as a Source of Aviation Fuel. *ChemSusChem* 2015, *8* (10), 1726–1736.
(104) Pines, H.; Haag, W. O. Alumina: Catalyst and Support. IX. The Alumina Catalyzed Dehydration of Alcohols. *J. Am. Chem. Soc.* 1961, *83* (13), 2847–2852.
(105) Balakrishnan, M.; Sacia, E. R.; Bell, A. T. Syntheses of Biodiesel Precursors: Sulfonic Acid Catalysts for Condensation of Biomass-Derived Platform Molecules. *ChemSusChem* 2014, *7* (4), 1078–1085.
(106) Price, S. C.; Stuart, A. C.; You, W. Polycyclic Aromatics with Flanking Thiophenes: Tuning Energy Level and Band Gap of Conjugated Polymers for Bulk Heterojunction Photovoltaics. *Macromolecules* 2010, *43* (2), 797–804.
(107) Sutter, M.; Silva, E. Da; Duguet, N.; Raoul, Y.; Métay, E.; Lemaire, M. Glycerol Ether Synthesis: A Bench Test for Green Chemistry Concepts and Technologies. *Chem. Rev.* 2015, *115* (16), 8609–8651.
(108) Rahmat, N.; Abdullah, A. Z.; Mohamed, A. R. Recent Progress on Innovative and Potential Technologies for Glycerol Transformation into Fuel Additives: A Critical Review. *Renew. Sustain. Energy Rev.* 2010, *14* (3), 987–1000.
(109) Okoye, P. U.; Abdullah, A. Z.; Hameed, B. H. A Review on Recent Developments and Progress in the Kinetics and Deactivation of Catalytic Acetylation of Glycerol — A Byproduct of Biodiesel. *Renew. Sustain. Energy Rev.* 2017, *74* (November 2015), 387–401.
(110) Nanda, M. R.; Zhang, Y.; Yuan, Z.; Qin, W.; Ghaziaskar, H. S.; Xu, C. Catalytic Conversion of Glycerol for Sustainable Production of Solketal as a Fuel Additive: A Review. *Renew. Sustain. Energy Rev.* 2016, *56* (1), 1022–1031.
(111) Galadima, A.; Muraza, O. A Review on Glycerol Valorization to Acrolein over Solid Acid

Catalysts. *J. Taiwan Inst. Chem. Eng.* 2016, *67*, 29–44.
(112) Talebian-kiakalaieh, A.; Aishah, N.; Amin, S.; Hezaveh, H. Glycerol for Renewable Acrolein Production by Catalytic Dehydration. *Renew. Sustain. Energy Rev.* 2014, *40*, 28–59.
(113) Katryniok, B.; Paul, S.; Dumeignil, F. Recent Developments in the Field of Catalytic Dehydration of Glycerol to Acrolein. *ACS Catal.* 2013, *3*, 1819–1834.
(114) Katryniok, B.; Belli, V.; Dumeignil, F. Glycerol Dehydration to Acrolein in the Context of New Uses of Glycerol. *Green Chem.* 2010, *12*, 2079–2098.
(115) Katryniok, B.; Paul, S.; Dumeignil, F. Towards the Sustainable Production of Acrolein by Glycerol Dehydration. *ChemSusChem* 2009, *2*, 719–730.
(116) Nanda, M. R.; Yuan, Z.; Qin, W.; Xu, C. C. Recent Advancements in Catalytic Conversion of Glycerol into Propylene Glycol : A Review. *Catal. Rev.* 2016, *58* (3), 309–336.
(117) Hejna, A.; Kosmela, P.; Formela, K.; Piszczyk, Ł.; Haponiuk, J. T. Potential Applications of Crude Glycerol in Polymer Technology – Current State and Perspectives. *Renew. Sustain. Energy Rev.* 2016, *66*, 449–475.
(118) Avhad, M. R.; Marchetti, J. M. Innovation in Solid Heterogeneous Catalysis for the Generation of Economically Viable and Ecofriendly Biodiesel: A Review. *Catal. Rev.* 2016, *58* (2), 157–208.
(119) Martin, A.; Armbruster, U.; Gandarias, I.; Arias, P. L. Review Glycerol Hydrogenolysis into Propanediols Using in Situ Generated Hydrogen – A Critical Review. *Eur. J. Lipid Sci. Technol.* 2013, *115*, 9–27.
(120) Gandarias, I.; Arias, P. L.; Agirrrezabal-Telleria, I. Economic Assessment for the Production of 1 , 2-Propanediol from Bioglycerol Hydrogenolysis Using Molecular Hydrogen or Hydrogen Donor Molecules. *Environ. Prog. Sustain. Energy* 2016, *35* (2), 447–454.
(121) Villa, A.; Dimitratos, N.; Chan-thaw, C. E.; Hammond, C.; Prati, L.; Hutchings, G. J. Glycerol Oxidation Using Gold-Containing Catalysts. *Acc. Chem. Res.* 2015, *48*, 1403–1412.
(122) Cornejo, A.; Barrio, I.; Campoy, M.; Lázaro, J.; Navarrete, B. Oxygenated Fuel Additives from Glycerol Valorization . Main Production Pathways and e Ff Ects on Fuel Properties and Engine Performance : A Critical Review. *Renew. Sustain. Energy Rev.* 2017, *79* (April), 1400–1413.
(123) Bagheri, S.; Julkapli, N. M.; Yehye, W. A. Catalytic Conversion of Biodiesel Derived Raw Glycerol to Value Added Products. *Renew. Sustain. Energy Rev.* 2015, *41*, 113–127.
(124) Sun, D.; Yamada, Y.; Sato, S.; Ueda, W. Applied Catalysis B : Environmental Glycerol Hydrogenolysis into Useful C3 Chemicals. *Appl. Catal. B Environ.* 2016, *193*, 75–92.
(125) Erb, B.; Risto, E.; Wendling, T.; Gooßen, L. J. Reductive Etherification of Fatty Acids or Esters with Alcohols Using Molecular Hydrogen. *ChemSusChem* 2016, *9* (12), 1442–1448.
(126) Venu, H.; Madhavan, V. Influence of Diethyl Ether (DEE) Addition in Ethanol-Biodiesel-Diesel (EBD) and Methanol-Biodiesel-Diesel (MBD) Blends in a Diesel Engine. *Fuel* 2017, *189*, 377–390.
(127) Linnekoski, J. A.; Kiviranta-Pääkkönen, P.; Krause, A. O.; Rihko-Struckmann, L. K. Simultaneous Isomerization and Etherification of Isoamylenes. *Ind. Eng. Chem. Res.* 1999, *38* (12), 4563–4570.
(128) Agirre, I.; Güemez, M. B.; Ugarte, A.; Requies, J.; Barrio, V. L.; Cambra, J. F.; Arias, P. L. Glycerol Acetals as Diesel Additives: Kinetic Study of the Reaction between Glycerol and

Acetaldehyde. *Fuel Process. Technol.* 2013, *116*, 182–188.
(129) Sezer, I. Thermodynamic , Performance and Emission Investigation of a Diesel Engine Running on Dimethyl Ether and Diethyl Ether. *Int. J. Therm. Sci.* 2011, *50*, 1594–1603.
(130) Bringué, R.; Fité, C.; Tejero, J.; Cunill, F. Applied Catalysis A , General Dehydration of 1-Octanol to Di- n -Octyl Ether in Liquid Phase with Simultaneous Water Removal over Ion Exchange Resins : E Ff Ect of Working- State Morphologies. *Appl. Catal. A, Gen.* 2017, *545* (May), 10–16.
(131) Arias, K. S.; Climent, M. J.; Corma, A.; Iborra, S. Biomass-Derived Chemicals: Synthesis of Biodegradable Surfactant Ether Molecules from Hydroxymethylfurfural. *ChemSusChem* 2014, *7* (1), 210–220.
(132) Maria, G. J.; Gruter, H.; F. Dautzenberg. Method for the Synthesis of 5-Hydroxymethylfurfural Ethers and Their Use. US 20110082304A1, 2011.
(133) Lewis, J. D.; Vyver, S. Van De; Crisci, A. J.; Gunther, W. R.; Michaelis, V. K.; Griffin, R. G.; Romµn-leshkov, Y. A Continuous Flow Strategy for the Coupled Transfer Hydrogenation and Etherification of 5- (Hydroxymethyl) Furfural Using Lewis Acid Zeolites. *ChemSusChem* 2014, *7*, 2255–2265.
(134) Salimon, J.; Salih, N.; Yousif, E. Biolubricants : Raw Materials , Chemical Modifications and Environmental Benefits. *Eur. J. Lipid Sci. Technol.* 2010, *112*, 519–530.
(135) Masudi, A.; Muraza, O. Vegetable Oil to Biolubricants: Review on Advanced Porous Catalysts. *Energy & Fuels* 2018, acs.energyfuels.8b02017.
(136) Holmberg, K.; Erdemir, A. Influence of Tribology on Global Energy Consumption, Costs and Emissions. *Friction* 2017, *5* (3), 263–284.
(137) Holmberg, K.; Erdemir, A. The Impact of Tribology on Energy Use and CO 2 Emission Globally and in Combustion Engine and Electric Cars. *Tribol. Int.* 2019, *135* (January), 389–396.
(138) Nagendramma, P.; Kaul, S. Development of Ecofriendly/Biodegradable Lubricants: An Overview. *Renew. Sustain. Energy Rev.* 2012, *16* (1), 764–774.
(139) Fan, Z.; Zhao, Y.; Preda, F.; Clacens, J. M.; Shi, H.; Wang, L.; Feng, X.; De Campo, F. Preparation of Bio-Based Surfactants from Glycerol and Dodecanol by Direct Etherification. *Green Chem.* 2015, *17* (2), 882–892.
(140) Gu, Y.; Azzouzi, A.; Pouilloux, Y.; Jérôme, F.; Barrault, J. Heterogeneously Catalyzed Etherification of Glycerol: New Pathways for Transformation of Glycerol to More Valuable Chemicals. *Green Chem.* 2008, *10* (2), 164.
(141) Haynes, M. P.; Buckley, H. R.; Higgins, M. L.; Pieringer, R. A. Synergism between the Antifungal Agents Amphotericin B and Alkyl Glycerol Ethers. *Antimicrob. Agents Chemother.* 1994, *38* (7), 1523–1529.
(142) On, S.; Effect, T. H. E.; Ethers, G.; Tumour, O. N. Studies on the Effect of Methoxy-Substituted Glycerol Ethers on Tumor Growth and Metastatis Formation. *Br. J. Exp. Pathol.* 1971, *52* (3), 221–230.
(143) García, E.; Laca, M.; Pérez, E.; Garrido, A.; Peinado, J. New Class of Acetal Derived from Glycerin as a Biodiesel Fuel Component. *Energy and Fuels* 2008, *22* (6), 4274–4280.
(144) Noureddini, H.; Dailey, W. R.; Hunt, B. A. PRODUCTION OF ETHERS OF GLYCEROL FROM CRUDE GLYCEROL - THE BY- PRODUCT OF BIODLESEL PRODUCTION. *Chem. Biomol. Eng. Res. Publ.* 1998, *18*.
(145) Melero, J. a.; Vicente, G.; Morales, G.; Paniagua, M.; Moreno, J. M.; Roldán, R.; Ezquerro, a.; Pérez, C. Acid-Catalyzed Etherification of Bio-Glycerol and Isobutylene over Sulfonic

Mesostructured Silicas. *Appl. Catal. A Gen.* 2008, *346* (1–2), 44–51.
(146) Klepáčová, K.; Mravec, D.; Kaszonyi, A.; Bajus, M. Etherification of Glycerol and Ethylene Glycol by Isobutylene. *Appl. Catal. A Gen.* 2007, *328* (1), 1–13.
(147) King, A. E.; Roschen, H. L.; Irwin, W. H. An Accelerated Stability Test Using the Peroxide Value as an Index. *Oil Soap* 1933, *10* (6), 105–109.
(148) Fábos, V.; Koczó, G.; Mehdi, H.; Boda, L.; Horváth, I. T. Bio-Oxygenates and the Peroxide Number: A Safety Issue Alert. *Energy Environ. Sci.* 2009, *2* (7), 767–769.
(149) Wheeldon, I.; Christopher, P.; Blanch, H. Integration of Heterogeneous and Biochemical Catalysis for Production of Fuels and Chemicals from Biomass. *Curr. Opin. Biotechnol.* 2017, No. 45, 127–135.
(150) Goulas, K. A.; Toste, F. D. Combining Microbial Production with Chemical Upgrading. *Curr. Opin. Biotechnol.* 2016, *38*, 47–53.
(151) Lange, J. P.; Van Der Heide, E.; Van Buijtenen, J.; Price, R. Furfural-A Promising Platform for Lignocellulosic Biofuels. *ChemSusChem* 2012, *5* (1), 150–166.
(152) Wang, A.; Balsara, N. P.; Bell, A. T. Continuous Pervaporation-Assisted Furfural Production Catalyzed by $CrCl_3$. *Green Chem.* 2018, *20* (12), 2903–2912.
(153) Dekishima, Y.; Lan, E. I.; Shen, C. R.; Cho, K. M.; Liao, J. C. Extending Carbon Chain Length of 1-Butanol Pathway for 1-Hexanol Synthesis from Glucose by Engineered Escherichia Coli. *J. Am. Chem. Soc.* 2011, *133* (30), 11399–11401.
(154) Sun, D.; Sato, S.; Ueda, W.; Primo, A.; Garcia, H.; Corma, A. Production of C4 and C5 Alcohols from Biomass-Derived Materials. *Green Chem.* 2016, *18* (9), 2579–2597.
(155) Mellmer, M. A.; Gallo, J. M. R.; Martin Alonso, D.; Dumesic, J. A. Selective Production of Levulinic Acid from Furfuryl Alcohol in THF Solvent Systems over H-ZSM-5. *ACS Catal.* 2015, *5* (6), 3354–3359.
(156) Van Leeuwen, B. N. M.; Van Der Wulp, A. M.; Duijnstee, I.; Van Maris, A. J. A.; Straathof, A. J. J. Fermentative Production of Isobutene. *Appl. Microbiol. Biotechnol.* 2012, *93* (4), 1377–1387.
(157) Yaws, C. L. *Yaws' Handbook of Thermodynamic Properties for Hydrocarbons and Chemicals*; Knovel, 2009.
(158) Ribeiro, M.; Pinto, A. C.; Quintella, C. M.; Rocha, G. O.; Teixeira, L. S. G.; Guarieiro, L. N.; Rangel, C.; Veloso, C. C.; Rezende, M. J. C.; Serpa, R.; et al. The Role of Additives for Diesel and Diesel Blended (Ethanol or Biodiesel) Fuels : A Review Nu. *Energy and Fuels* 2007, No. 21, 2433–2445.
(159) Rorrer, J.; Pindi, S.; Toste, D.; Bell, A. T. Effect of Alcohol Structure on the Kinetics of Etherification and Dehydration over Tungstated Zirconia. *ChemSusChem* 2018, *11*, 3104–3111.
(160) Bringué, R.; Tejero, J.; Iborra, M.; Izquierdo, J. F.; Fité, C.; Cunill, F. Water Effect on the Kinetics of 1-Pentanol Dehydration to Di-n-Pentyl Ether (DNPE) on Amberlyst 70. *Top. Catal.* 2007, *45* (1–4), 181–186.
(161) Elliott, J. A.; Hanna, S.; Elliott, A. M. S.; Cooley, G. E. The Swelling Behaviour of Perfluorinated Ionomer Membranes in Ethanol/Water Mixtures. *Polymer (Guildf).* 2001, *42* (5), 2251–2253.
(162) Goncalves, V. L. C.; Pinto, B. P.; Silva, J. C.; Mota, C. J. A. Acetylation of Glycerol Catalyzed by Different Solid Acids. *Catal. Today* 2008, *133–135*, 673–677.
(163) Casas, C.; Guilera, J.; Ramírez, E.; Bringué, R. Reliability of the Synthesis of C 10 – C 16 Linear Ethers from 1-Alkanols over Acidic Ion-Exchange Resins. *Biomass Conv. Bioref.*

2013, No. 3, 27–37.
(164) Walsh, B.; Hyde, J. R.; Licence, P.; Poliakoff, M. The Automation of Continuous Reactions in Supercritical CO2: The Acid-Catalysed Etherification of Short Chain Alcohols. *Green Chem.* 2005, *7* (6), 456–463.
(165) Parrott, A. J.; Bourne, R. a.; Gooden, P. N.; Bevinakatti, H. S.; Poliakoff, M.; Irvine, D. J. The Continuous Acid-Catalysed Etherification of Aliphatic Alcohols Using Stoichiometric Quantities of Dialkyl Carbonates. *Org. Process Res. Dev.* 2010, *14* (6), 1420–1426.
(166) Prymak, I.; Kalevaru, V. N.; Wohlrab, S.; Martin, A. Continuous Synthesis of Diethyl Carbonate from Ethanol and CO2 over Ce-Zr-O Catalysts. *Catal. Sci. Technol.* 2015, *5* (4), 2322–2331.
(167) Dewilde, J. F.; Czopinski, C. J.; Bhan, A. Ethanol Dehydration and Dehydrogenation on γ-Al2O3 : Mechanism of Acetaldehyde Formation. *ACS Catal.* 2014, *4*, 4425–4433.
(168) Christiansen, M. A.; Mpourmpakis, G.; Vlachos, D. G. Density Functional Theory-Computed Mechanisms of Ethylene and Diethyl Ether Formation from Ethanol on ??-Al2O3(100). *ACS Catal.* 2013, *3* (9), 1965–1975.
(169) Yang, D.; Ortuño, M. A.; Bernales, V.; Cramer, C. J.; Gagliardi, L.; Gates, B. C. Structure and Dynamics of Zr6O8Metal-Organic Framework Node Surfaces Probed with Ethanol Dehydration as a Catalytic Test Reaction. *J. Am. Chem. Soc.* 2018, *140* (10), 3751–3759.
(170) Bukowski, B. C.; Bates, J. S.; Gounder, R.; Greeley, J. First Principles, Microkinetic, and Experimental Analysis of Lewis Acid Site Speciation during Ethanol Dehydration on Sn-Beta Zeolites. *J. Catal.* 2018, *365*, 261–276.
(171) Tejero, J.; Fité, C.; Iborra, M.; Izquierdo, J. F.; Bringué, R.; Cunill, F. Dehydration of 1-Pentanol to Di-n-Pentyl Ether Catalyzed by a Microporous Ion-Exchange Resin with Simultaneous Water Removal. *Appl. Catal. A Gen.* 2006, *308*, 223–230.
(172) da Silva, C. R. B.; Gonçalves, V. L. C.; Lachter, E. R.; Mota, C. J. A. Etherification of Glycerol with Benzyl Alcohol Catalyzed by Solid Acids. *J. Braz. Chem. Soc.* 2009, *20* (2), 201–204.
(173) Jaworski, M. A.; Rodríguez Vega, S.; Siri, G. J.; Casella, M. L.; Romero Salvador, A.; Santos López, A. Glycerol Etherification with Benzyl Alcohol over Sulfated Zirconia Catalysts. *Appl. Catal. A Gen.* 2015, *505*, 36–43.
(174) Frusteri, F.; Arena, F.; Bonura, G.; Cannilla, C.; Spadaro, L.; Di Blasi, O. Catalytic Etherification of Glycerol by Tert-Butyl Alcohol to Produce Oxygenated Additives for Diesel Fuel. *Appl. Catal. A Gen.* 2009, *367* (1–2), 77–83.
(175) Frusteri, F.; Frusteri, L.; Cannilla, C.; Bonura, G. Catalytic Etherification of Glycerol to Produce Biofuels over Novel Spherical Silica Supported Hyflon® Catalysts. *Bioresour. Technol.* 2012, *118*, 350–358.
(176) Cannilla, C.; Bonura, G.; Frusteri, L.; Frusteri, F. Glycerol Etherification with TBA: High Yield to Poly-Ethers Using a Membrane Assisted Batch Reactor. *Environ. Sci. Technol.* 2014, *48* (10), 6019–6026.
(177) Cannilla, C.; Bonura, G.; Frusteri, L.; Frusteri, F. Batch Reactor Coupled with Water Permselective Membrane: Study of Glycerol Etherification Reaction with Butanol. *Chem. Eng. J.* 2015, *282*, 187–193.
(178) Pariente, S.; Tanchoux, N.; Fajula, F. Etherification of Glycerol with Ethanol over Solid Acid Catalysts. *Green Chem.* 2009, *11* (8), 1256–1261.
(179) Ruppert, A. M.; Meeldijk, J. D.; Kuipers, B. W. M.; Erné, B. H.; Weckhuysen, B. M. Glycerol Etherification over Highly Active CaO-Based Materials: New Mechanistic

Aspects and Related Colloidal Particle Formation. *Chemistry* 2008, *14* (7), 2016–2024.
(180) Fujii, Y.; Furugaki, H.; Tamura, E.; Yano, S.; Kita, K. A Convenient Catalytic Method for the Synthesis of Ethers from Alcohols and Carbonyl Compounds. *Bull. Chem. Soc. Jpn.* 2005, *78*, 456–463.
(181) Sutter, M.; Dayoub, W.; Métay, E.; Raoul, Y.; Lemaire, M. 1-O-Alkyl (Di)Glycerol Ethers Synthesis from Methyl Esters and Triglycerides by Two Pathways: Catalytic Reductive Alkylation and Transesterification/Reduction. *Green Chem.* 2013, *15* (3), 786.
(182) Shi, Y.; Dayoub, W.; Favre-Réguillon, A.; Chen, G.-R.; Lemaire, M. Straightforward Selective Synthesis of Linear 1-O-Alkyl Glycerol and Di-Glycerol Monoethers. *Tetrahedron Lett.* 2009, *50* (49), 6891–6893.
(183) Sutter, M.; Dayoub, W.; Métay, E.; Raoul, Y.; Lemaire, M. Selective Synthesis of 1-O-Alkyl(Poly)Glycerol Ethers by Catalytic Reductive Alkylation of Carboxylic Acids with a Recyclable Catalytic System. *ChemSusChem* 2012, *5* (12), 2397–2409.
(184) Enslow, K. R.; Bell, A. T. SnCl<inf>4</Inf>-Catalyzed Isomerization/Dehydration of Xylose and Glucose to Furanics in Water. *Catal. Sci. Technol.* 2015, *5* (5), 2839–2847.
(185) Imteyaz Alam, M.; De, S.; Dutta, S.; Saha, B. Solid-Acid and Ionic-Liquid Catalyzed One-Pot Transformation of Biorenewable Substrates into a Platform Chemical and a Promising Biofuel. *RSC Adv.* 2012, *2* (17), 6890–6896.
(186) Alipour, S.; Omidvarborna, H.; Kim, D. S. A Review on Synthesis of Alkoxymethyl Furfural, a Biofuel Candidate. *Renew. Sustain. Energy Rev.* 2017, *71* (January 2016), 908–926.
(187) Ras, E. J.; Maisuls, S.; Haesakkers, P.; Gruter, G. J.; Rothenberg, G. Selective Hydrogenation of 5-Ethoxymethylfurfural over Alumina-Supported Heterogeneous Catalysts. *Adv. Synth. Catal.* 2009, *351* (18), 3175–3185.
(188) Lanzafame, P.; Temi, D. M.; Perathoner, S.; Centi, G.; MacArio, A.; Aloise, A.; Giordano, G. Etherification of 5-Hydroxymethyl-2-Furfural (HMF) with Ethanol to Biodiesel Components Using Mesoporous Solid Acidic Catalysts. *Catal. Today* 2011, *175* (1), 435–441.
(189) Bing, L.; Zhang, Z.; Deng, K. Efficient One-Pot Synthesis of 5-(Ethoxymethyl)Furfural from Fructose Catalyzed by a Novel Solid Catalyst. *Ind. Eng. Chem. Res.* 2012, *51* (47), 15331–15336.
(190) Saravanamurugan, S.; Riisager, A. Solid Acid Catalysed Formation of Ethyl Levulinate and Ethyl Glucopyranoside from Mono- and Disaccharides. *Catal. Commun.* 2012, *17*, 71–75.
(191) Che, P.; Lu, F.; Zhang, J.; Huang, Y.; Nie, X.; Gao, J.; Xu, J. Catalytic Selective Etherification of Hydroxyl Groups in 5-Hydroxymethylfurfural over H4SiW12O40/MCM-41 Nanospheres for Liquid Fuel Production. *Bioresour. Technol.* 2012, *119*, 433–436.
(192) Neves, P.; Antunes, M. M.; Russo, P. A.; Abrantes, J. P.; Lima, S.; Fernandes, A.; Pillinger, M.; Rocha, S. M.; Ribeiro, M. F.; Valente, A. A. Production of Biomass-Derived Furanic Ethers and Levulinate Esters Using Heterogeneous Acid Catalysts. *Green Chem.* 2013, *15* (12), 3367–3376.
(193) Shinde, S.; Rode, C. Cascade Reductive Etherification of Bioderived Aldehydes over Zr-Based Catalysts. *ChemSusChem* 2017, *10* (20), 4090–4101.
(194) Shinde, S.; Rode, C. Selective Self-Etherification of 5-(Hydroxymethyl)Furfural over Sn-Mont Catalyst. *Catal. Commun.* 2017, *88*, 77–80.
(195) Cao, Q.; Guan, J.; Peng, G.; Hou, T.; Zhou, J.; Mu, X. Solid Acid-Catalyzed Conversion of Furfuryl Alcohol to Alkyl Tetrahydrofurfuryl Ether. *Catal. Commun.* 2015, *58*, 76–79.

(196) Yang, Y.; Liu, Q.; Li, D.; Tan, J.; Zhang, Q.; Wang, C.; Ma, L. Selective Hydrodeoxygenation of 5-Hydroxymethylfurfural to 2,5-Dimethylfuran on Ru-MoOx/C Catalysts. *RSC Adv.* 2017, *7*, 16311–16318.
(197) Sacia, E. R.; Balakrishnan, M.; Bell, A. T. Biomass Conversion to Diesel via the Etherification of Furanyl Alcohols Catalyzed by Amberlyst-15. *J. Catal.* 2014, *313*, 70–79.
(198) Fang, W.; Hu, H.; Dong, P.; Ma, Z.; He, Y.; Wang, L.; Zhang, Y. Improvement of Furanic Diether Selectivity by Adjusting Brønsted and Lewis Acidity. *Appl. Catal. A Gen.* 2018, *565* (May), 146–151.
(199) Wang, Y.; Cui, Q.; Guan, Y.; Wu, P. Facile Synthesis of Furfuryl Ethyl Ether in High Yield: Via the Reductive Etherification of Furfural in Ethanol over Pd/C under Mild Conditions. *Green Chem.* 2018, *20* (9), 2110–2117.
(200) Tulchinsky, M. L.; Briggs, J. R. One-Pot Synthesis of Alkyl 4-Alkoxypentanoates by Esterification and Reductive Etherification of Levulinic Acid in Alcoholic Solutions. *ACS Sustain. Chem. Eng.* 2016, *4* (8), 4089–4093.
(201) Qianqian Cui, Yinshuang Long, Yun Wang, Haihong Wu, Yejun Guan, and P. W. A Facile Route toward the Synthesis of Ethyl-4-Ethoxy Pentanoate in High Yield: Reductive Etherification of Ethyl Levulinate in Ethanol on Pd/SiO2-C Catalysts. *ChemSusChem*.
(202) Jae, J.; Mahmoud, E.; Lobo, R. F.; Vlachos, D. G. Cascade of Liquid-Phase Catalytic Transfer Hydrogenation and Etherification of 5-Hydroxymethylfurfural to Potential Biodiesel Components over Lewis Acid Zeolites. *ChemCatChem* 2014, *6*, 508–513.
(203) Nicolaides, C. P.; Stotijn, C. J.; van der Veen, E. R. A.; Visser, M. S. Conversion of Methanol and Isobutanol to MTBE. *Appl. Catal. A, Gen.* 1993, *103* (2), 223–232.
(204) Karinen, R. S.; Linnekoski, J. A.; Krause, A. O. I. Etherification of C5- and C8-Alkenes with C1- to C4-Alcohols. *Catal. Letters* 2001, *76* (1–2), 81–87.
(205) Badia, J. H.; Fité, C.; Bringué, R.; Ramírez, E.; Cunill, F. Byproducts Formation in the Ethyl Tert-Butyl Ether (ETBE) Synthesis Reaction on Macroreticular Acid Ion-Exchange Resins. *Appl. Catal. A Gen.* 2013, *468*, 384–394.
(206) Karinen, R. S.; Krause, A. O. I. Reactivity of Some C8-Alkenes in Etherification with Methanol. *Appl. Catal. A Gen.* 1999, *188* (1–2), 247–256.
(207) Klepáčová, K.; Mravec, D.; Bajus, M. Tert-Butylation of Glycerol Catalysed by Ion-Exchange Resins. *Appl. Catal. A Gen.* 2005, *294* (2), 141–147.
(208) Karinen, R. S.; Krause, A. O. I. New Biocomponents from Glycerol. *Appl. Catal. A Gen.* 2006, *306*, 128–133.
(209) Klepáčová, K.; Mravec, D.; Kaszonyi, A.; Bajus, M. Etherification of Glycerol and Ethylene Glycol by Isobutylene. *Appl. Catal. A Gen.* 2007, *328* (1), 1–13.
(210) Badia, J. H.; Fité, C.; Bringué, R.; Ramírez, E.; Tejero, J. Simultaneous Etherification of Isobutene with Ethanol and 1-Butanol over Ion-Exchange Resins. *Appl. Catal. A Gen.* 2017, *541* (April), 141–150.
(211) Ruppert, A. M.; Parvulescu, A. N.; Arias, M.; Hausoul, P. J. C.; Bruijnincx, P. C. A.; Klein Gebbink, R. J. M.; Weckhuysen, B. M. Synthesis of Long Alkyl Chain Ethers through Direct Etherification of Biomass-Based Alcohols with 1-Octene over Heterogeneous Acid Catalysts. *J. Catal.* 2009, *268* (2), 251–259.
(212) Wang, S.; Guin, J. A. Silica-Supported Sulfated Zirconia: A New Effective Acid Solid for Etherification. *Chem. Commun.* 2000, No. 24, 2499–2500.
(213) Tretbar, M.; Witzel, T.; Hauffe, A.; Junghans, U.; Bulc, A.; Pufky-Heinrich, D. Feasibility Study on the Etherification of Fermentative-Produced Isobutylene to Fully Renewable Ethyl

Tert-Butyl Ether (ETBE). *Catalysts* 2018, *8* (11), 514.
(214) Hatchings, G. J.; Nicolaides, C. P.; Scurrell, M. S. Developments in the Production of Methyl Tert-Butyl Ether. *Catal. Today* 1992, *15* (1), 23–49.
(215) Ancillotti, F.; Fattore, V. Oxygenate Fuels: Market Expansion and Catalytic Aspect of Synthesis. *Fuel Process. Technol.* 1998, *57* (3), 163–194.
(216) Ancillotti, F.; Massi Mauri, M.; Pescarollo, E.; Romagnoni, L. Mechanisms in the Reaction between Olefins and Alcohols Catalyzed by Ion Exchange Resins. *J. Mol. Catal.* 1978, *4* (1), 37–48.
(217) Padovan, D.; Hammond, C. Bifunctional Lewis and Brønsted Acidic Zeolites Permit the Continuous Production of Bio-Renewable Furanic Ethers. *Green Chem.* 2017, No. 19, 2846–2854.
(218) Wang, Z.; Wang, L.; Jiang, Y.; Hunger, M.; Huang, J. Cooperativity of Brønsted and Lewis Acid Sites on Zeolite for Glycerol Dehydration. *ACS Catal.* 2014, *4*, 1144–1147.
(219) Kim, J.; Lee, D.; Kalutharage, N.; Yi, C. S. Selective Catalytic Synthesis of Unsymmetrical Ethers from the Dehydrative Etheri Fi Cation of Two Di Ff Erent Alcohols. *ACS Catal.* 2014, *4*, 3881.
(220) Lippits, M. J.; Nieuwenhuys, B. E. Direct Conversion of Ethanol into Ethylene Oxide on Copper and Silver Nanoparticles: Effect of Addition of CeOx and Li2O. *Catal. Today* 2010, *154* (1–2), 127–132.
(221) Lippits, M. J.; Nieuwenhuys, B. E. Direct Conversion of Ethanol into Ethylene Oxide on Gold-Based Catalysts: Effect of CeOx and Li2O Addition on the Selectivity. *J. Catal.* 2010, *274* (2), 142–149.
(222) Silbaugh, T. L.; Devlaminck, P.; Sofranko, J. A.; Barteau, M. A. Selective Oxidation of Ethanol over Ag, Cu and Au Nanoparticles Supported on Li2O/γ-Al2O3. *J. Catal.* 2018, *364*, 40–47.
(223) Renewable Ethylene Oxide & Glycol.
(224) Jing, X.; Wang, H.; Chen, H.; Huang, J. Biosynthesized Ag/a-Al2O3 Catalyst for Ethylene Epoxidation: The Influence of Silver Precursors. *RSC Adv.* 2014, *4*, 27597–27603.
(225) Rojluechai, S.; Chavadej, S.; Schwank, J. W.; Meeyoo, V. Catalytic Activity of Ethylene Oxidation over Au , Ag and Au – Ag Catalysts : Support Effect. *Catal. Commun.* 2007, *8*, 57–64.
(226) Mao, C.-F.; Vannice, M. A. High Surface Area A-Aluminas III . Oxidation of Ethylene , Ethylene Oxide , and Acetaldehyde over Silver Dispersed on High Surface Area a-Alumina. *Appl. Catal. A Gen.* 1995, *122*, 61–76.
(227) Janlamool, J.; Jongsomjit, B. Oxidative Dehydrogenation of Ethanol over AgLi – Al 2 O 3 Catalysts Containing Different Phases of Alumina. *Catal. Rev.* 2015, *70*, 49–52.
(228) Force, E. L.; Bell, A. T. Infrared Spectra of Adsorbed Species Present During the Oxidation of Ethylene over Silver. *J. Catal.* 1974, *460* (I 975), 440–460.
(229) Linic, S.; Barteau, M. A. Formation of a Stable Surface Oxametallacycle That Produces Ethylene Oxide. *J. Am. Chem. Soc.* 2002, *124* (2), 310–317.
(230) Linic, S.; Barteau, M. A. On the Mechanism of Cs Promotion in Ethylene Epoxidation on Ag. *J. Am. Chem. Soc.* 2004, *126* (26), 8086–8087.
(231) Mascal, M. Chemicals from Biobutanol: Technologies and Markets. *Biofuels, Bioprod. Biorefining* 2012, *6*, 486–493.
(232) Collignon, F.; Mariani, M.; Moreno, S.; Remy, M.; Poncelet, G. Gas Phase Synthesis of MTBE from Methanol and Isobutene over Dealuminated Zeolites. *J. Catal.* 1997, *166* (1),

53–66.
(233) Rorrer, J. E.; Bell, A. T.; Toste, F. D. Synthesis of Biomass-Derived Ethers for Use as Fuels and Lubricants. *ChemSusChem* 2019, *12*, 2835–2858.
(234) Bender, M. An Overview of Industrial Processes for the Production of Olefins - C4 Hydrocarbons. *ChemBioEng Rev.* 2014, *1* (4), 136–147.
(235) Li, Y.; He, D.; Zhu, Q.; Zhang, X.; Xu, B. Effects of Redox Properties and Acid–Base Properties on Isosynthesis over ZrO 2-Based Catalysts. *J. Catal.* 2004, *221*, 584–593.
(236) Erkey, C.; Wang, J.; Postula, W.; Feng, Z.; Philip, C. V.; Akgerman, A.; Anthony, R. G. Isobutylene Production from Synthesis Gas over Zirconia in a Slurry Reactor. *Ind. Eng. Chem. Res.* 1995, *34* (4), 1021–1026.
(237) Tseng, S. C.; Jackson, N. B.; Ekerdt, J. G. Isosynthesis Reactions of CO/H2 over Zirconium Dioxide. *J. Catal.* 1988, *109*, 284–297.
(238) Maruya, K.; Komiya, T.; Hayakawa, T.; Lu, L.; Yashima, M. Active Sites on ZrO2 for the Formation of Isobutene from CO and H2. *J. Mol. Catal. A Chem.* 2000, *159*, 97–102.
(239) Kujawska, A.; Kujawski, J.; Bryjak, M.; Kujawski, W. ABE Fermentation Products Recovery Methods — A Review ABE Fermentation Products Recovery Methods — A Review. *Renew. Sustain. Energy Rev.* 2015, *48* (August 2018), 648–661.
(240) Liu, C.; Sun, J.; Smith, C.; Wang, Y. A Study of Zn x Zr y O z Mixed Oxides for Direct Conversion of Ethanol to Isobutene. *Appl. Catal. A Gen.* 2013, *467*, 91–97.
(241) Li, H.; Sun, J.; Wang, Y. Surface Acetone Reactions on ZnxZryOz: A DRIFTS-MS Study. *Appl. Catal. A Gen.* 2019, *573*, 22–31.
(242) Crisci, A. J.; Dou, H.; Prasomsri, T.; Roman-Leshkov, Y. Cascade Reactions for the Continuous and Selective Production of Isobutene from Bioderived Acetic Acid Over Zinc-Zirconia Catalysts. *ACS Catal.* 2014, *4*, 4196–4200.
(243) Herrmann, S.; Iglesia, E. Selective Conversion of Acetone to Isobutene and Acetic Acid on Aluminosilicates: Kinetic Coupling between Acid-Catalyzed and Radical-Mediated Pathways. *J. Catal.* 2018, *360*, 66–80.
(244) Hutchings, G.; Johnston, P.; Lee, D.; Williams, C. Acetone Conversion to Isobutene in High Selectivity Using Zeolite Catalyst. *Catal. Letters* 1993, *21*, 49–53.
(245) Ponomareva, O. A.; Maerle, A. A.; Rodionova, L. I.; Pavlov, V. S.; Dobryakova, I. V; Belova, M. V; Ivanova, I. I. Production of Isobutylene from Acetone over Micro – Mesoporous Catalysts. *Pet. Chem.* 2016, *56* (3), 271–276.
(246) Biao Zhao, Yong Men, Anni Zhang, JinguoWang, Rong He, Wei An, S. L. Influence of Different Precursors on Isobutene Production from Bio-Ethanol over Bifunctional Zn1Zr10Ox Catalysts. *Appl. Catal. A Gen.* 2018.
(247) Phadke, N. M.; Mynsbrugge, J. Van Der; Mansoor, E.; Getsoian, A. B.; Head-gordon, M.; Bell, A. T. Characterization of Isolated Ga 3+ Cations in Ga/H-MFI Prepared by Vapor-Phase Exchange of H-MFI Zeolite with GaCl3. *ACS Catal.* 2018, *8*, 6106–6126.
(248) Szulejko, J. E.; Kim, Y. H.; Kim, K. H. Method to Predict Gas Chromatographic Response Factors for the Trace-Level Analysis of Volatile Organic Compounds Based on the Effective Carbon Number Concept. *J. Sep. Sci.* 2013, *36* (20), 3356–3365.
(249) Ginjupalli, S. R.; Mugawar, S.; Rajan N., P.; Balla, P. K.; Chary Komandur, V. R. Vapour Phase Dehydration of Glycerol to Acrolein over NbOPO4 Catalysts. *J. Chem. Technol. Biotechnol.* 2014, *89* (12), 1890–1897.
(250) Rao, G. S.; Rajan, N. P.; Pavankumar, V.; Chary, K. V. R. Vapour Phase Dehydration of Glycerol to Acrolein over NbOPO4 Catalysts. *J. Chem. Technol. Biotechnol.* 2014, *89* (12),

1890–1897.
(251) Das, J.; Pradhan, S. K.; Sahu, D. R.; Mishra, D. K.; Sarangi, S. N.; Nayak, B. B.; Verma, S.; Roul, B. K. Micro-Raman and XPS Studies of Pure ZnO Ceramics. *Phys. B Condens. Matter* 2010, *405* (10), 2492–2497.
(252) Dawood, F.; Schaak, R. E. ZnO-Templated Synthesis of Wurtzite-Type ZnS and ZnSe Nanoparticles. *J. Am. Chem. Soc.* 2009, *131*, 424–425.
(253) Rodriguez, J. A.; Wang, X.; Liu, G.; Hanson, J. C.; Hrbek, J.; Peden, C. H. F.; Iglesias-Juez, A.; Fernandez-Garcia, M. Physical and Chemical Properties of Ce1−xZrxO2 Nanoparticles and Ce1−xZrxO 2(111) Surfaces : Synchrotron-Based Studies. *J. Mol. Catal. A Chem.* 2016, *425*, 166–173.
(254) Baylon, R. A. L.; Sun, J.; Kovarik, L.; Engelhard, M.; Li, H.; Winkelman, A. D.; Martin, K. J.; Wang, Y. Structural Identification of ZnxZryOz Catalysts for Cascade Aldolization and Self-Deoxygenation Reactions. *Appl. Catal. B Environ.* 2018, *234*, 337–346.
(255) Li, C.; Li, M. UV Raman Spectroscopic Study on the Phase Transformation of ZrO2, Y2O3-ZrO2 and SO42-/ZrO2. *J. Raman Spectrosc.* 2002, *33* (5), 301–308.
(256) R. V. Matheus, C.; H. Chagas, L.; G. Gonzalez, G.; Falabella S. Aguiar, E.; G. Appel, L. Synthesis of Propene from Ethanol: A Mechanistic Study. *ACS Catal.* 2018, 7667–7678.
(257) Iwamoto, M. Selective Catalytic Conversion of Bio-Ethanol to Propene: A Review of Catalysts and Reaction Pathways. *Catal. Today* 2015, *242* (PB), 243–248.
(258) Xia, W.; Wang, F.; Mu, X.; Chen, K. Remarkably Enhanced Selectivity for Conversion of Ethanol to Propylene over ZrO 2 Catalysts. *Fuel Process. Technol.* 2017, *166*, 140–145.
(259) Chieregato, A.; Ochoa, J. V.; Bandinelli, C.; Fornasari, G.; Cavani, F.; Mella, M. On the Chemistry of Ethanol on Basic Oxides: Revising Mechanisms and Intermediates in the Lebedev and Guerbet Reactions. *ChemSusChem* 2015, *8* (2), 377–388.
(260) Fan, D.; Dai, D. J.; Wu, H. S. Ethylene Formation by Catalytic Dehydration of Ethanol with Industrial Considerations. *Materials (Basel).* 2013, *6* (1), 101–115.
(261) Vohs, J. M.; Barteau, M. A. Dehydration and Dehydrogenation of Ethanol and 1-Propanol on the Polar Surfaces of Zinc Oxide. *Surf. Sci.* 1989, *221*, 590–608.
(262) Nakajima, T.; Tanabe, K.; Yamaguchi, T.; Matsuzaki, I.; Mishima, S. Conversion of Ethanol to Acetone over Zinc Oxide-Calcium Oxide Catalyst. Optimization of Catalyst Preparation and Reaction Conditions and Deduction of Reaction Mechanism. *Appl. Catal.* 1989, *52* (1), 237–248.
(263) Rahman, M. M.; Davidson, S. D.; Sun, J.; Wang, Y. Effect of Water on Ethanol Conversion over ZnO. *Top. Catal.* 2016, *59* (1), 37–45.
(264) Silva-Calpa, L. del R.; Zonetti, P. C.; Rodrigues, C. P.; Alves, O. C.; Appel, L. G.; de Avillez, R. R. The ZnxZr1−xO2−y Solid Solution on M-ZrO2: Creating O Vacancies and Improving the m-ZrO2 Redox Properties. *J. Mol. Catal. A Chem.* 2016, *425*, 166–173.
(265) Silva-calpa, L. R.; Zonetti, P. C.; Oliveira, D. C. De; Avillez, R. R. De; Appel, L. G. Acetone from Ethanol Employing ZnxZr1−xO2−y. *Catal. Today* 2017, *289*, 264–272.
(266) Chen, B.; Ma, Y.; Ding, L.; Xu, L.; Wu, Z.; Yuan, Q.; Huang, W. Reactivity of Hydroxyls and Water on a CeO2(111) Thin Film Surface: The Role of Oxygen Vacancy. *J. Phys. Chem. C* 2013, *117* (11), 5800–5810.
(267) Chenu, E.; Jacobs, G.; Crawford, A. C.; Keogh, R. A.; Patterson, P. M.; Sparks, D. E.; Davis, B. H. Water-Gas Shift: An Examination of Pt Promoted MgO and Tetragonal and Monoclinic ZrO2 by in Situ Drifts. *Appl. Catal. B Environ.* 2005, *59* (1–2), 45–56.
(268) Wang, Y.; Muhler, M.; Wöll, C. Spectroscopic Evidence for the Partial Dissociation of H2O

on ZnO(10$\bar{1}$0). *Phys. Chem. Chem. Phys.* 2006, *8* (13), 1521–1524.
(269) McFarland, E. W.; Metiu, H. Catalysis by Doped Oxides. *Chem. Rev.* 2013, *113* (6), 4391–4427.
(270) Wang, S.; Iglesia, E. Experimental and Theoretical Assessment of the Mechanism and Site Requirements for Ketonization of Carboxylic Acids on Oxides. *J. Catal.* 2017, *345*, 183–206.
(271) Gumidyala, A.; Sooknoi, T.; Crossley, S. Selective Ketonization of Acetic Acid over HZSM-5 : The Importance of Acyl Species and the Influence of Water. *J. Catal.* 2016, *340*, 76–84.
(272) Gangadharan, A.; Shen, M.; Sooknoi, T.; Resasco, D. E.; Mallinson, R. G. Condensation Reactions of Propanal over CexZr 1-XO2 Mixed Oxide Catalysts. *Appl. Catal. A Gen.* 2010, *385* (1–2), 80–91.
(273) Tosoni, S.; Pacchioni, G. Acetic Acid Ketonization on Tetragonal Zirconia : Role of Surface Reduction. *J. Catal.* 2016, *344*, 465–473.
(274) Fu, Y.; Zhang, L.; Yue, B.; Chen, X.; He, H.-Y. Simultaneous Characterization of Solid Acidity and Basicity of Metal Oxide Catalysts via Solid State NMR Technique. *J. Phys. Chem. C* 2018, acs.jpcc.8b06827.
(275) Zaki, M. I.; Hasan, M. A.; Pasupulety, L. Surface Reactions of Acetone on Al2O3, TiO2, ZrO2, and CeO2: IR Spectroscopic Assessment of Impacts of the Surface Acid-Base Properties. *Langmuir* 2001, *17* (3), 768–774.
(276) Biaglow, A. I.; Sepa, J.; Gorte, R. J.; White, D. A 13C NMR Study of the Condensation Chemistry of Acetone and Acetaldehyde Adsorbed at the Brønsted Acid Sites in H-ZSM-5. *J. Catal.* 1995, *151*, 373–384.
(277) Xu, T.; Munson, E. J.; Haw, J. F. Toward a Systematic Chemistry of Organic Reactions in Zeolites: In Situ NMR Studies of Ketones. *J. Am. Chem. Soc.* 1994, *116* (5), 1962–1972.